Adhesion of Lacquers to Tinplate

Thesis submitted for the degree of

Doctor of Philosophy in the University

of Oxford

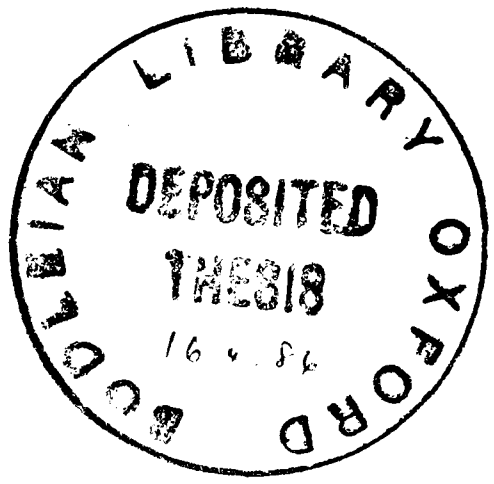

Hilary Term 1985

David G. Dixon

Linacre College

ADHESION OF LACQUERS TO TINPLATE

DAVID G. DIXON

LINACRE COLLEGE

D. Phil.

Hilary Term 1985

Abstract

A set of passivated tinplates coated with organic lacquers as used for internal coatings on cans is examined. Adhesion is measured using a butt-joint test and the results of failure load and percent area lacquer removal analysed in order to grade adhesion performance. Fracture behaviour is determined by the surface structure of the tinplates where a defect distribution common to all types is identified by Weibull analysis as responsible for failure initiation. Differences in fracture behaviour seen in the mechanical test results are revealed by examination of the fracture surfaces using optical microscopy, scanning electron microscopy and X-ray photoelectron spectroscopy. The samples with good lacquer adhesion show a positive relationship between failure load and lacquer removal which is not evident in the samples with poor lacquer adhesion. The latter exhibit weak bonding between the passivation layer and tinplate and on examining those areas of fracture surface where tinplate is revealed the fracture is seen to have propagated at this interface whereas those samples with good adhesion had failed near the lacquer-passivation layer interface within the lacquer.

Passivation layers are characterised using X-ray photoelectron spectroscopy and transmission electron microscopy. Differences in composition relating to specific tin oxides and chromium oxides are correlated with adhesion performance and models for the structure of passivation layers and failure mechanisms are proposed.

Preface

This thesis describes the work carried out by the author in the Department of Metallurgy and Science of Materials, University of Oxford between October 1978 and October 1981. No part of this work has been submitted previously for a degree at this or any other University.

I would like to thank my supervisor, Dr. John Sykes, for his encouragement and useful discussions during this project, Dr. G. Harden, industrial supervisor for provision of materials, XPS facilities and support and also many others at Metal Box including Ms. J. Smith, Mr. J. Walpole and Ms. L. Fellows for technical assistance and helpful discussions.

Thanks are also due to the Science and Engineering Research Council and Metal Box PLC for a CASE studentship and to Professor Sir Peter Hirsch for the provision of laboratory facilities.

Alison Rook typed this thesis and I am indebted to her for her patient and accurate typing.

to my parents

Let me now explain how flimsy is the texture of these films.

Lucretius

"The Nature of the Universe"

c. 50 BC

ADHESION OF LACQUERS TO TINPLATE

C O N T E N T S

		Page
CHAPTER 1	INTRODUCTION	1
	1. TINPLATE	3
	2. LACQUERS	7
	3. ADHESION	11
	i/ MECHANICS OF ADHESION	12
	ii/ ADHESIVE INTERFACES AND JOINTS	15
	4. ADHESION TESTING	23
CHAPTER 2	BACKGROUND	36
	1. The passivation layer	36
	2. Proposed work	42
CHAPTER 3	BUTT-JOINT TEST MEASUREMENTS	47
	1. INTRODUCTION	47
	2. EXPERIMENTAL	48
	3. RESULTS	54
	i/ Butt-joint test	54
	ii/ Fractography and topography	70
	iii/ Weibull statistical analysis	89
	4. ENVIRONMENTAL EFFECTS ON LACQUER ADHESION	108
	5. SUMMARY	110

		Page
CHAPTER 4	X-RAY PHOTOELECTRON SPECTROSCOPY	122
	1. THE TECHNIQUE	122
	i/ X-ray source	123
	ii/ Electron analyser and detector	123
	iii/ Specimen manipulator and UHV system	125
	iv/ Argon ion Etching for Depth profiling	125
	2. INFORMATION FROM XPS	126
	3. QUANTITATIVE ANALYSIS	134
	i/ Physical Modelling	135
	ii/ Elemental Sensitivity	135
	iii/ Comparison with standards	138
	4. EXPERIMENTAL WORK	138
	i/ The tinplate surface	142
	ii/ Fracture surfaces	153
	iii/ Isolated passivation layers	159
	5. SUMMARY OF XPS RESULTS	164
CHAPTER 5	TRANSMISSION ELECTRON MICROSCOPY	203
	1. INTRODUCTION	203
	2. EXPERIMENTAL	207
	3. RESULTS	207
	1. Selected area diffraction analysis and imaging	210
	1.1 Unpassivated tinplate	210
	1.2 300 tinplate	213
	1.3 BS 311 rinplate	216
	1.3a BS 311(C)	216

Page

CHAPTER 5 (continued)

1.3b BS 311(6A) 218

1.3c BS 311(5A) 221

1.4 NS 311 tinplate 221

1.5 KS 311 tinplate 225

4. DISCUSSION 225

CHAPTER 6 DISCUSSION 234

1 Passivation layer structure and composition 234

i/ Chromium in the passivation layer 234

ii/ Tin oxide 239

iii/ Mechanism of formation 241

iv/ Models for passivation layer structure 247

2 Butt-joint tests 250

i/ Interpretation of test data 252

ii/ Fracture surface examination 256

iii/ Correlation of lacquer adhesion performance with sample structure 259

3 Conclusions 268

4 FUTURE WORK 271

APPENDICES 276

CHAPTER 1

INTRODUCTION

Over 10^{10} tinplate containers are manufactured every year, many with internal coatings of organic lacquers to protect the tin against corrosion by the aggressive environment presented by some foodstuffs. The lacquer coating process may precede the manufacture of the can from flat tinplate sheet and high lacquer adhesion is therefore required to withstand the large plastic strains involved in the fabrication, especially of drawn/redrawn two piece cans where a stamped lacquered end is fitted to a one-piece can body produced by repeated drawing of a flat circular sheet. Serious problems arise when lacquer detachment occurs during can manufacture since large areas of debonding cannot easily be repaired and an entire batch of lacquered tinplate may have to be replaced. Figure 1 shows a deep-drawn lacquered can with poor lacquer adhesion. In this example the lacquer is on the outer surface and has become detached during the forming process.

The objective of this work is to investigate lacquer adhesion using a suitable mechanical test, to characterize the surface composition and structure of the tinplate, and to seek a mechanistic understanding of the adhesion behaviour in terms of the nature of the tinplate surface. All tinplates used in the manufacture of cans are given a passivation treatment to reduce tin oxide growth and the lacquer is therefore in contact with this thin passivation film, containing, inter alia, a mixture of tin oxides and chromium oxides. The resulting adhesion properties of a lacquered passivated tinplate will depend on the mechanical properties of the lacquer, passivation

Figure 1. Lacquer debonding on a deep-drawn can (externally lacquered)

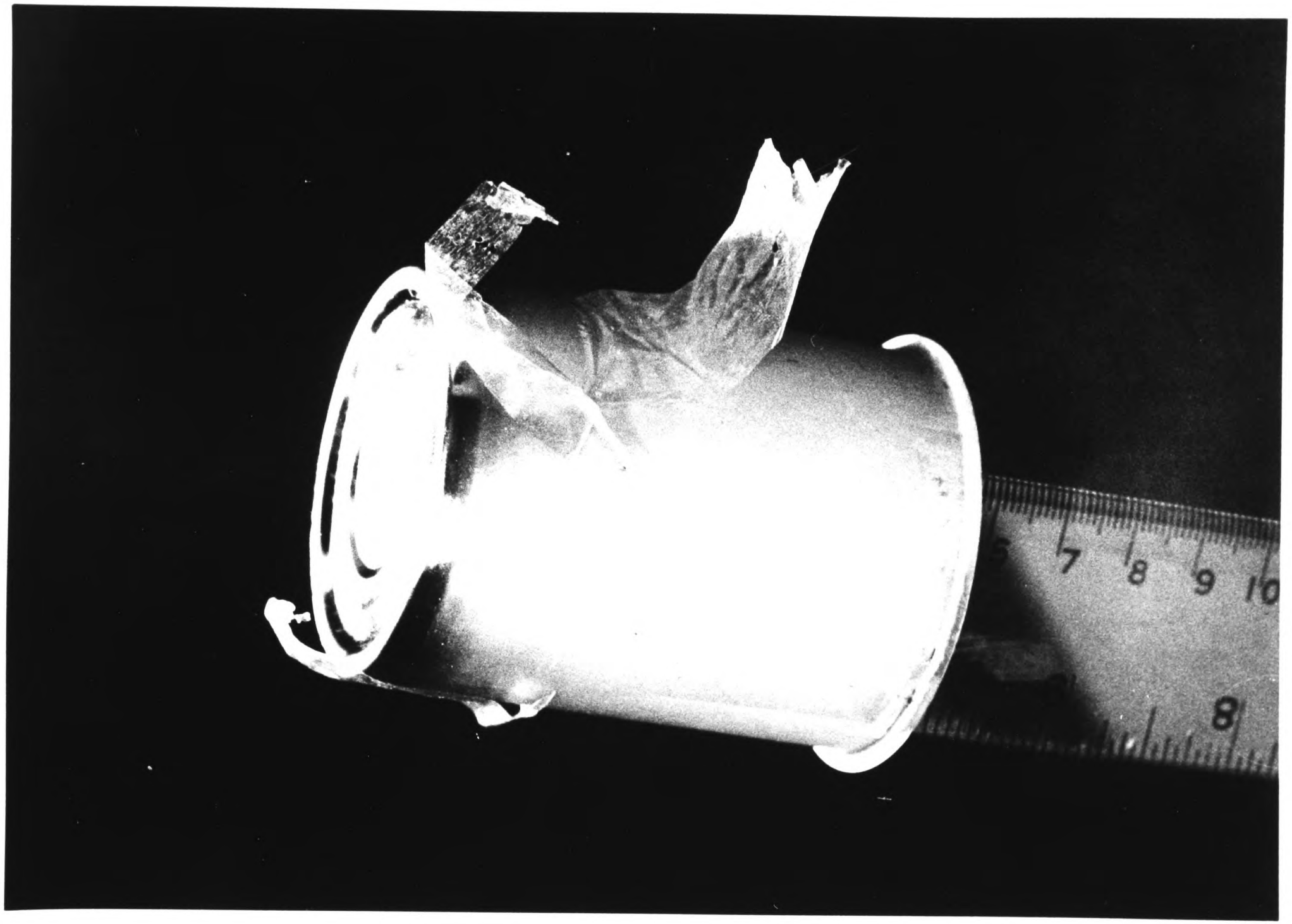

layer and the underlying tinplate and also on the bonding between these individual components. The surface properties of the tinplate are mainly dictated by the passivation layer and by improving the characteristics of this layer it is possible to improve bonding; the main aim of this work will be to correlate the tinplate surface structure and composition with lacquer adhesion performance.

It should be noted that the tinplates investigated in this work, manufactured by British Steel, Nippon Steel and Kawasaki Steel may not be typical of the materials usually produced by them and conclusions concerning their behaviour apply only to these sample sets and cannot be taken to reflect the general behaviour of products from those corporations.

The materials and test methods are described below along with a review of the major theories of adhesion.

1. TINPLATE

Modern tinplate consists of steel sheet with thickness 0.1mm to 0.4 mm which has been electrolytically coated with tin, typically less than 1μm in thickness (older hot-dipped tinplates could have tin coatings almost 1 mm thick in places). The condition of the surfaces controls many important properties such as solderability, appearance, corrosion and lacquer adhesion and has consequently attracted a large body of scientific investigation but the effect of the surface and passivation layer on lacquer adhesion is still not fully explained. Tin is readily oxidised in air and thick tin oxides are known to have a deleterious effect on solderability and lacquer adhesion, so immediately after the electrolytic tinning process the surfaces are passivated.

A schematic section through a piece of lacquered passivated

A SECTION THROUGH LACQUERED TINPLATE (SCHEMATIC)

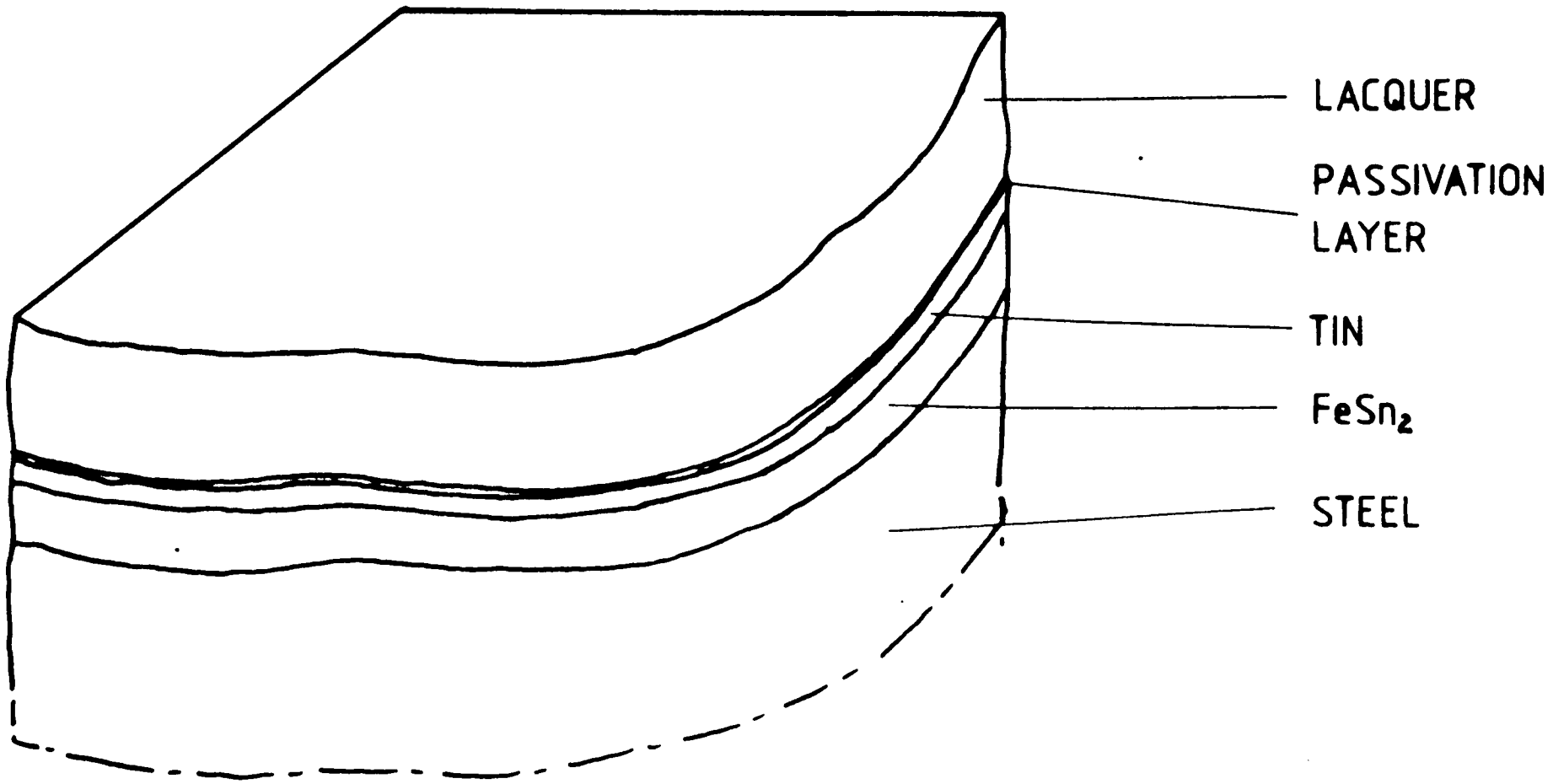

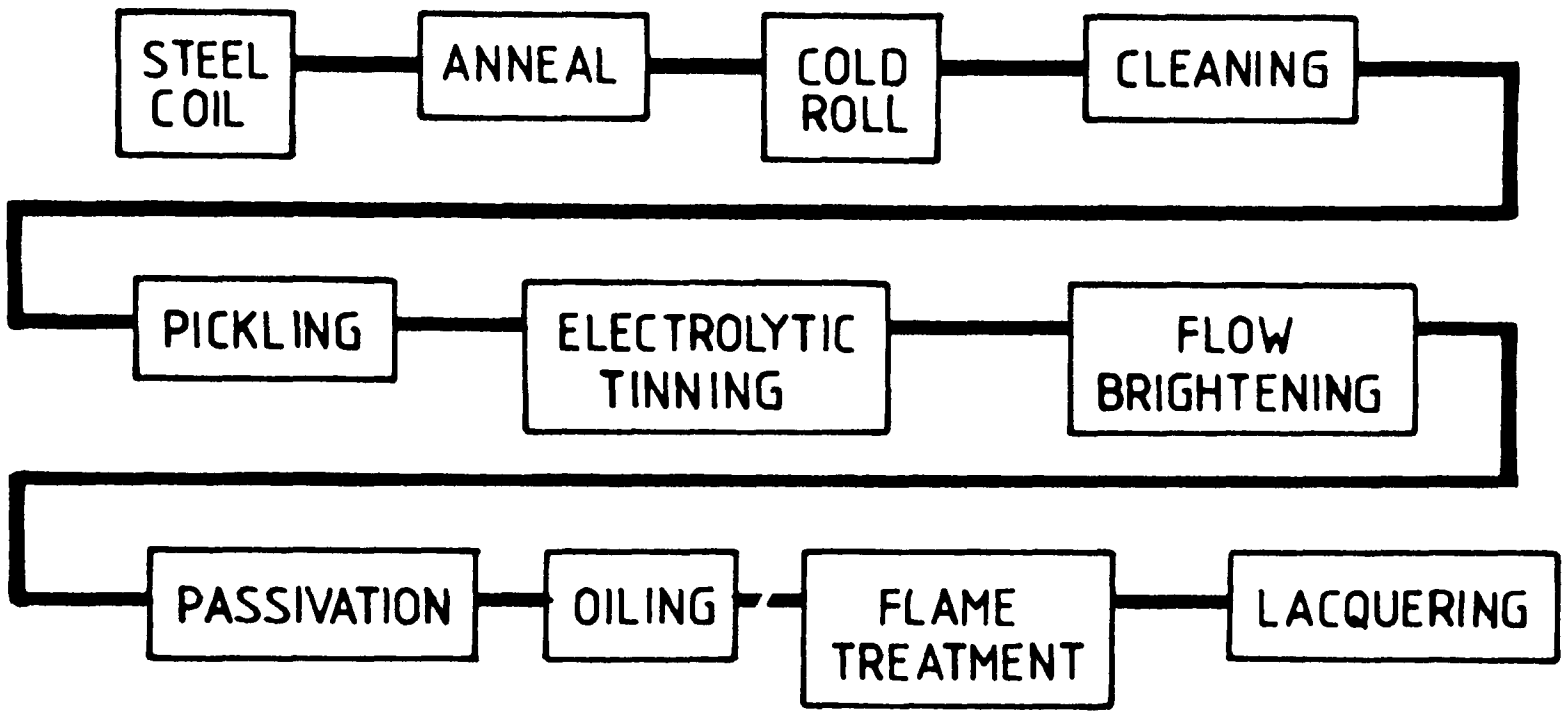

Figure 3. The stages in the production of tinplate. There may be a period of storage after the oiling process.

tinplate is shown in Figure 2. It shows the layered arrangement of materials from the steel base, through the $FeSn_2$ layer, the tin coating, the passivation film and the lacquer coating. The passivation layer in this diagram and throughout this work is taken to include the tin oxides which may be present, having grown either before or after the passivation treatment. The thickness of the passivation layer depends on the type of passivation treatment but is generally of the order of a few nm (Azzeri and Splendorini 1980).

The manufacture of tinplate, starting with a strip of steel which is typically 1 m wide and 5×10^3 m in length is shown schematically in Figure 3. After annealing and rolling the steel is cleaned then pickled in acid to remove oxides before being electrolytically coated with tin. At this stage the tin coating is nodular and matte in appearance so a flow-brightening treatment follows in which the plate is resistively heated to melt the tin and produce a smooth continuous coating. It is during this process that an $FeSn_2$ interlayer forms (usually referred to as the "alloy layer") consisting of a continuous layer of crystallites which may protrude through the tin in places. The tinplate is next quenched, then passivated in a bath containing acidified $Na_2Cr_2O_7$ so that a chromium-rich film is deposited on the surface. If the process comprises only dipping, the tinplate produced is known as type 300 but if treated cathodically a type 311 tinplate is formed. The 300 tinplates are believed to contain only oxidised chromium whereas the 311 types also contain chromium in the metallic form (Azzeri and Splendorini 1980). The passivation process is discussed further in Chapter 6.

Following passivation the tinplate is then oiled to make the handling of individual sheets easier and then stored in the unlacquered state until required for can manufacture.

2. LACQUERS

The interior surfaces of tin cans are coated with polymeric lacquers so that the tinplate is not corroded by the contents of the can. The lacquer may serve as a lubricant during manufacture and also provides aesthetic advantages where consumer and commercial interests are considered.

Lacquer for tinplate must fulfill certain requirements when used for can interiors; these are:

a) flexibility

b) corrosion resistance

c) abrasion resistance

d) non toxicity

and e) good adhesion.

Since the tinplate sheet is often lacquered prior to can manufacture the coating must retain its integrity during the can forming process which may consist of bending (for three-piece cans) or repeated drawing through a die (for two-piece cans). Several lacquer types are available, usually chosen to suit the contents of the can. Application is usually by roller coating at line speeds of up to 600 ft. per minute (Noorlander and Barnes 1981). In this research five types of lacquer commonly found in commercial practice have been employed. Each is diluted with an aromatic solvent such as xylol or an ethylene glycol ether (Askew 1975) for coating and then stoved to drive off the solvent and form a continuous solid film on the tinplate. Curing is by cross-linking for most types but some are thermoplastics. In general, high molecular weight polymers produce better coatings especially if solvents with low evaporation rates are used to assist flowing during the stoving process. The coating varies for different applications from 1.5μm to 10μm; it is usually

applied as a single coat.

The lacquers used in this work are listed below. A list of general properties, applications and coating conditions is given in Table 1 with typical chemical formulae in Figure 4. The formulae are only approximations to the materials used since many variations and additives are found in the practical materials.

i) Oleoresinous

The oldest type of lacquer used for protective coatings on tinplate. Originally, linseed, castor and tung oils were the main constituents and were reacted with natural or synthetic oil-soluble resins. Modern types replace the natural resins with hydrocarbon or phenolic types. Oleoresinous lacquers cure through the uptake of oxygen (Peisach et al 1976) and usually listed as thermoplastic.

ii) Phenolic

This thermosetting lacquer is cured using formaldehyde and an alkali catalyst often with creosols or other substituted phenols (Shetye 1974). It has a high impermeability and can be used in conjunction with epoxides. Applied in low coating thicknesses.

iii) Epoxy

A durable, thermosetting resin, modified by other resins such as urea formaldehyde, polyamide or acrylic (McKirahan and Ludwigsen 1968).

iv) Epoxy-phenolic

The most widely-used lacquer with good chemical resistance. The ratio of epoxide to phenolic can be varied from 5:1 to 1:1 giving a range of lacquer properties (Ley 1967).

v) Organosol

Used where high formability is required; the chemical resistance is lower than for epoxy-phenolic. Organosols are based on poly(vinyl

TABLE 1

LACQUERS - GENERAL PROPERTIES AND APPLICATIONS

Lacquer	Stoving		Type	Flexibility	Typical Use	Chemical Resistance (acids)
Oleoresinous	200-204°C.	10 min.	P	good	fruit	good
Phenolic	200°C.	15 min.	S	poor	meat	good
Epoxy	200°C	15 min.	S	v. good	beverage	v. good
Epoxy-Phenolic	180-200°C.	12-15	S	good	meat, fruit, veg.	v. good
Organosol	180°C.	10 min.	P	v. good	beverage	good

P = thermoplastic

S = thermoset

ⓐ

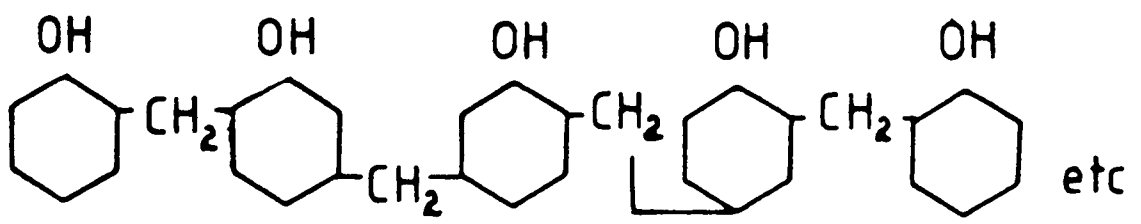

ⓑ

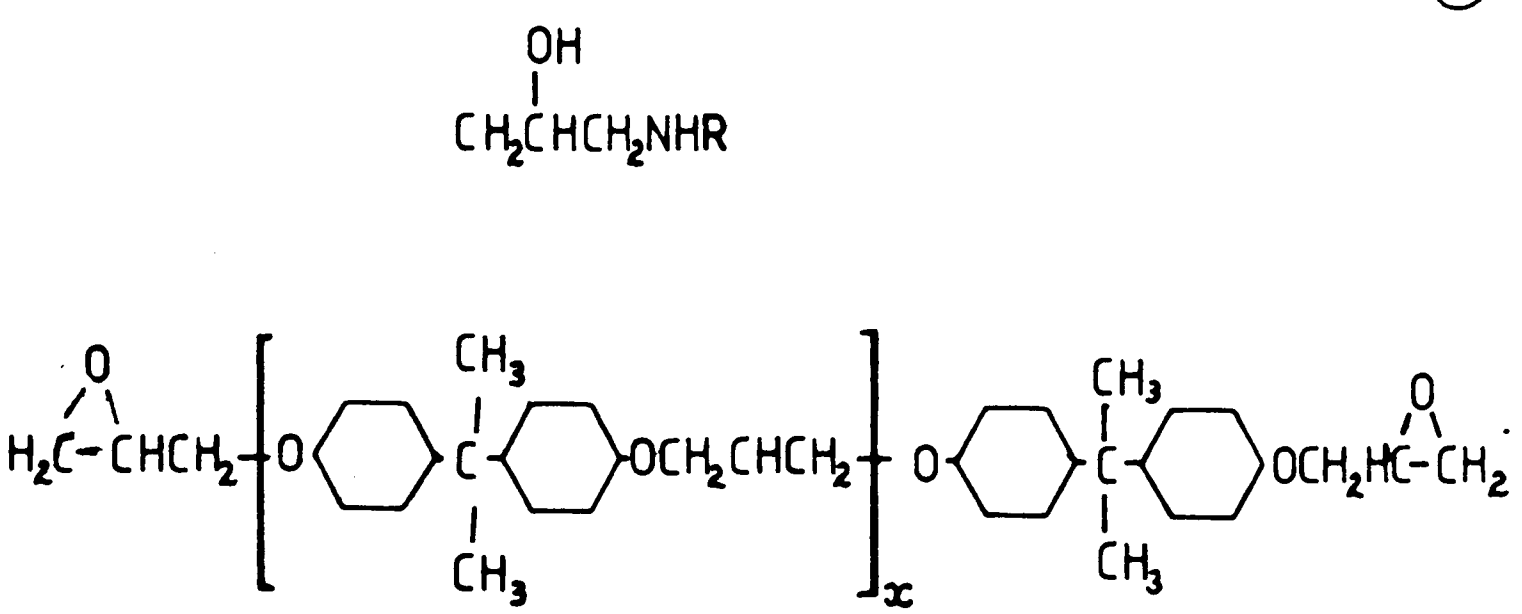

ⓒ

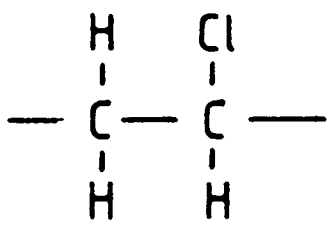

Figure 4. Some chemical formulae of lacquer materials.

a - a phenolic resin

b - epoxies

c - poly(vinyl chloride)

The exact formulae will differ as a result of additives and different formation processes.

chloride) dispersed in an organic vehicle. On stoving the solids fuse to form a continuous thermoplastic coating.

3. ADHESION

The Oxford Dictionary gives the following definition of adhesion:

"The action of sticking (to anything) by physical attraction, viscosity of surface or firm grasping"

and ASTM (1970):

"The state in which two surfaces are held together by interfacial forces which may consist of valence forces or interlocking forces or both".

It is important to define what is meant by adhesion in this work since there are three separate concepts. These are:

i/ Interatomic or intermolecular forces - the energy or force required to separate smooth perfect interfaces.

ii/ Like i/ but including the effects of mechanical keying and defects at the interface.

iii/ Bond strength or adhesive joint strength, discussed by Good (1976).

Category iii is the quantity which is measured by all destructive adhesion tests (which may also measure i and ii) and includes failures which occur away from the bonded interface. This work will measure adhesive joint strength and seek to show the effects of defects or weakly-bonded interfaces in the lacquer tinplate specimens.

Adhesion is a complex phenomenon, depending on many factors such as temperature, testing rate, interface structure and environment. Several theories of adhesion have been advanced (Kinloch 1980) which are appropriate for specific systems or conditions and a summary of these theories is given below:

i/ MECHANISMS OF ADHESION

a) Mechanical Adhesion

This mechanism is concerned with the physical interlocking of prominences on the adhered surface with the adhesive. Sometimes called "hooking adhesion" (Bikerman 1968) it is usually cited as a major mechanism when bonding materials such as wood, textiles or leather which have fibrous surfaces where interpenetration of adhesive can occur (Borroff and Wake 1949). In such fields as carpentry this mechanism is widely regarded as a prime contribution to joint strength but Good (1976) criticizes it as a fundamental mechanism of adhesion.

b) Electrostatic Adhesion

Proposed by Soviet workers (Deryagin and Krotova 1949) this theory relies on the formation of an electrical double layer at an interface which controls adhesion. Based on observations that peel strength is rate-dependent, that the work of peeling is 2 or 3 orders of magnitude greater than required by chemical bonding, and that intense electron emission (with energies in kV) accompanies peeling, the bonded interface was regarded as a capacitor which could therefore be described by an electrostatic treatment. For a parallel plate condenser the energy, W, is given as:

$$W = \tfrac{1}{2}eV = \tfrac{1}{2}CV^2$$

and

$$c = \frac{ka}{4\pi d}$$

hence

$$V^2 = \frac{8\pi W d}{ka}$$

The energy of a capacitor may also be expressed as:

$$W = \frac{2\pi\sigma^2 d}{k}$$

where

W = energy

e = total charge

V = potential difference

c = capacitance

k = dielectric constant

d = plate separation

a = area of plate

σ = surface charge density.

Eliminating d:

$$W = \tfrac{1}{2}V\sigma$$

Deryagin has argued that this energy is equivalent to the work of adhesion measured in peel tests and has produced results showing good agreement between theory and practice.

However, this theory of adhesion has attracted severe criticism from several quarters (Skinner et al 1953, Voyutskii 1963, Schonhorn 1969) and is not, in general, highly regarded in the literature (Allen 1969) since the electrostatic theory of adhesion predicts some adhesion effects which are clearly unrealistic in the light of experimental results. In peel tests a large proportion of the measured energy required to produce debonding is expended in visco-elastic or plastic deformation in the test materials and this quantity should not be included in the interfacial bond strengths predicted by the electrostatic theory.

c) Diffusion Theory

Another theory of essentially Soviet origin (Voyulskii 1963, Vasenin 1969) in which the interdiffusion of adherend and adhesive give rise to adhesion. Applicable to high molecular weight polymers,

this mechanism is likely to occur especially at high temperatures with a high degree of polymer chain mobility but is unlikely to be of importance in bonds containing glass, ceramics or metals at low temperatures. A qualitative description of the adhesion forces produced by such a mechanism can be obtained by considering the number of molecular chains crossing the interface between two polymers, the depth of penetration and the strength of the individual polymer chain. Good agreements between theory and measured adhesion performance for some polymeric systems have been recorded.

d) Adsorption Theory

The adsorption theory of adhesion, as the name implies, is based on the physical forces arising from the intimate contact of two surfaces and is therefore closely allied to the thermodynamic treatment of wetting (Huntsberger 1981, Smith 1980, Mittal 1975); the adsorption theory has been extensively discussed by Eley (1961). Neglecting primary chemical bonds which can be formed across a bonded interface, the main forces of attraction between two phases are due to van der Waal's forces (van der Waal 1873, Langbein 1969) which are due to three separate contributions from:

a) the interaction of permanent dipole moments (Keesom 1915, 1920a, 1920b, 1921)

b) dipole-molecule induction forces (Debye 1920, 1921)

c) molecule-molecule dispersion forces (London 1937).

Schonhorn (1969) has shown that, in theory, van der Waal's forces alone are capable of holding two phases together with a strength that is much greater than the bulk strength of the individual phases if intimate contact is achieved over the whole interface. However, since solid surfaces are rough on a microscopic scale it is necessary for one phase to be liquid in order to achieve

good contact. Moreover, it is important that such a liquid should easily wet the solid surface and avoid air entrapment in cavities etc. and that the solid surface be free of contaminants which may introduce a weak layer. In practice, measured adhesion values depend on many factors and theoretical estimates of bond strengths across interfaces usually give a very poor indication of actual adhesive strength.

The adsorption theory has been treated in depth by Eley (1961) and Wake (1966); the complex considerations of surface thermodynamics and energetics, wetting kinetics and rheological properties are all discussed. In practice the fracture energy, G, is much higher than the surface energy owing to plastic and viscoelastic deformations.

ii/ ADHESIVE INTERFACES AND JOINTS

In the absence of a "Universal Theory of Adhesion" to describe the adhesion forces holding a system together Allen (1969) proposes a combined description of the total adhesive force, ψ:

$$\psi = \alpha \psi_M + \beta \psi_E + \gamma \psi_D + \delta \psi_A + ...\omega \psi_X$$

where

ψ_M = mechanical component of adhesion

ψ_E = electrical component of adhesion

ψ_D = diffusion component of adhesion

ψ_A = adsorption component of adhesion

and α, β, γ, δ are mixing constants.

Whilst this approach includes all the adhesion forces which may hold the system together it is the forces required to produce failure that are of main interest in this work. This description also shows an additive method of combining the components of adhesive force implying no interdependence whereas in some circumstances the effect on adhesion due to one component may be affected by the

magnitude of another component.

In order to measure adhesion for practical purposes it is necessary to destroy the system in some sort of mechanical test, a variety of which are described later. Although non-destructive measurements of interfaces such as infra-red spectroscopy or acoustic microscopy are available it is necessary to measure the strength of a bonded system using a destructive test to induce failure.

The theory of adhesion and adhesive joint failure has lagged behind the development of adhesively-bonded structures (Kinloch 1980) mainly due to the many aspects of science and engineering that must be considered. Modern treatments of adhesion often used a combination of adsorption theory and fracture mechanics to analyse adhesive joint failure although this requires a precise testing method.

It has already been shown that for two phases to achieve intimate contact one of them must be applied in a fluid state and that therefore the wetting equilibrium of such a system should be examined. When a drop of liquid rests in equilibrium on a solid surface the Young equation (1805) is used to relate the contact angle, θ, to the surface free energies:

$$\gamma_{SV} = \gamma_{SL} + \gamma_{LV} \cos\theta$$

where

γ_{SV} is the surface free energy of the solid substrate after vapour adsorption

γ_{SL} is the surface free energy between solid and liquid

γ_{LV} is the surface free energy between liquid and vapour

Note that the surface free energy of the solid in vacuo γ_S may well be much greater than γ_{SV}.

Hence, for complete wetting to occur ($\theta = 0^o$):

$$\gamma_{SV} \geqq \gamma_{SL} + \gamma_{LV}$$

$$\gamma_{S} \geqq \gamma_{SL} + \gamma_{LV} + \pi_{S}$$

where π_S is the equilibrium spreading pressure i.e. the decrease in surface free energy of the solid when immersed in a saturated vapour of the liquid.

Wetting may also occur for the case when $0^o < \theta < 90^o$ if the liquid is forcibly spread over the surface. Indeed, Huntsberger (1981) states that good adhesives are not necessarily those with $\theta = 0^o$. Wetting will take place most easily if the liquid has low γ and the solid a high γ.

Polymers are low energy solids with surface free energies less than $100mJm^{-2}$ (compared with metals and ceramics whose values are typically greater than $500mJm^{-2}$).

Zisman established a means of characterising low energy surfaces using a quantity γ_c, the critical surface tension, an extrapolated value of γ_{LV} at $\theta = 0^o$. Schultz et al (1977) express surface free energy as the sum of polar and dispersion components. The work of adhesion W_A can be related to surface energies of two phases (γ_1 and γ_2) by:

$$W_A = 2\phi(\gamma_1\gamma_2)^{\frac{1}{2}}$$

where ϕ is an interaction parameter (Girifalco and Good 1957) and is expressed as a product of two parameters:

$$\phi = \phi_a\phi_r$$

where ϕ_a accounts for departures from ideality in intermolecular attraction and ϕ_r accounts for departures from regularity in interfacial separation. The quantity W_A is the thermodynamic work required to create two new

surfaces; it does not include loss terms arising from deformation of the surfaces or adherends. Several expressions for W_A are available in the literature (Harkins and Loesner 1950, Fowkes 1972, Huntsberger 1981) and the correlation between W_A and measured bond strength has been widely discussed. Some workers have found a positive relationship between the two (Dahlquist 1970) whilst others have not (Cherry and el Muddarris 1970). Fracture energy, G, is usually much greater (by orders of magnitude) than W_A.

In studies of adhesive failure mechanics for a viscoelastic polymer bonded to a rigid substrate (Gent and Kinloch 1971) a characteristic measure of joint strength, θ, (energy per unit interface) was described and later work (Andrews and Kinloch 1973a,b) separated this parameter into two components, one due to the thermodynamic work of adhesion termed θ_o, the intrinsic failure energy and the second due to energy dissipated viscoelastically in the adhesive, ψ.

$$\theta = \theta_o + \psi$$

Their experimental plots of logθ vs. (log of reduced rate of crack propagation) for various rubber-substrate joints show sets of parallel curves and so they write:

$$\theta = \theta_o F(R)$$

where F(R) is a multiplying factor sensitive to strain rate and temperature.

They show theoretically and experimentally that

$$\psi \propto \theta_o \text{ even though } \psi >> \theta_o$$

arising from the fact that the polymer can only be subjected to stress if the interface is also capable of withstanding stress.

Thus, the failure energy θ ($\equiv$ G) includes the effect of thermodynamic adhesion on measured strength even though W_A may be very

much smaller than θ. θ_o is rate independent, depending on the type and strength of interfacial bonding whereas ψ is dependent on rate and temperature.

Andrews and Kinloch (1973a,b) have also shown that when interfacial failure occurs $\theta_o \approx W_A$ but in cohesive failure $\theta_o >> W_A$. They go on to show:

$$\theta_o = iI + rF_0 + sF_1$$

where i, r and s are the area fractions of interfacial failure, adhesive cohesive failure and substrate cohesive failure and I, F_0 and F_1 are the corresponding failure energies. For strong joints with cohesive failure of the adhesive about 70 to 80% of the value of θ_o was provided by the term rF_0.

a. Effect of substrate

In the case of a purely cohesive failure, well removed from the bonded interface, it is the mechanical properties of the failed bulk phase which determine the strength; for interfacial failure the thermodynamic work of adhesion becomes important and this is dependent upon the characteristics of the bonded surfaces. As shown above, a liquid polymer will most easily wet a high energy surface such as a metal but in the case of passivated tinplate the lacquer is in contact with an oxide layer which is likely to have a lower surface energy. Adsorbed contaminants may seriously lower the surface energy even further (Gledhill et al 1977).

Although the thermodynamic work of adhesion is usually much less than the fracture energy G, Andrews and Kinloch (1973) use a product of W_A and viscoelastic energy to define G, allowing the effect of W_A to be considered in most fracture situations. In interfacial failure the quantity termed by them "intrinsic failure energy" becomes approximately equal to W_A. The same workers show

that the W_A is dependent upon the substrate for the adhesion of a styrene butadiene rubber.

b. Effect of surface topography

Packham (1981) has discussed the effect of surface roughness on the adhesion of polymers to metals. Fibrous oxide surfaces (Sykes 1967) will enhance adhesion by increasing the amount of plastic deformation in the polymer (Bair et al 1971); Reegan and Ilkka (1962) demonstrate a good agreement between the surface roughness of metals and peel strength. In some cases where a polymer is adhering to a fibrous surface and fracture energy is high due to plastic and visco-elastic deformations the adhesion between the polymer and substrate may also be enhanced by mechanical keying.

De Bruyne (1956) has shown that penetration of a liquid into an "ink-pot" re-entrant pit is much more difficult than penetration into pits with perpendicular sides and this process requires a significant time. For example molten polyethylene at 200^{o}C will fill a pore of radius 1μm to a depth of 7μm in 20 minutes (Packham 1970). Incomplete wetting may reduce the contact area of an interface and subsequently reduce adhesion. The defects so produced could also act as stress raisers and initiate failure.

All surfaces are rough on a very fine scale. The effect of surface topography on adhesion has been studied for micrometre-dimension features in many cases but the interface will be more sensitive to flaws than the bulk (Good 1972). Examination of the passivation layers and fracture surfaces will include a consideration of possible defects that could influence fracture behaviour.

At this point, the weak boundary layer concept of Bikerman (1968) should be mentioned. In this thesis, Bikerman considers that true interfacial failure never occurs due to the presence of

a weakening layer located at the bonded interface. This idea has been severely criticized by Good (1972) who rejects its universal applicability but many instances are known where surface contaminants or a diffuse component migrating to an interface can have a deleterious effect on adhesion.

c. Fracture mechanics

The fracture mechanics interpretation of adhesion has been reviewed by Kinloch (1982). These methods are based on the energy-balance approach of Griffith (1920) and Orowan (1948) and the stress-intensity approach of Westergaard (1939) and Irwin (1964). The energy balance method may be summarized for brittle fracture in a brittle continuum with a sharp crack:

$$-\frac{1}{H}\frac{\partial u}{\partial a} \geq 2\gamma$$

where H = width of specimen, u = stored elastic energy, a = crack length and γ = surface free energy.

Since the energy required to cause crack growth in most solids is actually much greater than 2γ due to inelastic deformations the quantity 2γ may be replaced by G, the fracture energy which encompasses all inelastic mechanisms.

The stress intensity approach considers the effect of a loaded sharp crack and uses the quantity K, stress intensity factor such that

$$K = Q\,\sigma(\pi a)^{\frac{1}{2}}$$

where Q is a geometrical factor and σ is applied stress.

Combining the two approaches, for failure conditions in mode I opening:

$$K_{I_C}^2 = \frac{E\,G_c}{1-V^2} \quad \text{for plane strain}$$

The fracture mechanics description requires physical data for the

materials under test. The passivation layer is a ceramic material and as such, will fracture in a brittle manner. The mechanical properties of polymers are more complex, being highly dependent on temperature and test rate. The lacquers used in this work are all flexible (as required for service) but a rapid fracture process in an adhesion test will encourage brittle failure. The mechanics of polymers are treated extensively in the literature (Arridge 1975) and failure mechanisms are discussed in Chapter 6.

The continuum interpretation of fracture mechanics for adhesion has been used by several workers for different test geometries where G is found to be constant for a particular adhesive system (Kinloch 1982, Gent and Kinloch 1971, Kinloch and Shaw 1981). However, this type of analysis requires a precise control over test conditions and accurate knowledge of the flaws in the specimen which are usually introduced by the experimenter to initiate controlled failure. In this work the adhesion of lacquers to passivated tinplates will be studied by using a mechanical test to induce failure. The adhesion of such a system, containing many different components and interfaces is likely to depend on both the intrinsic adhesion across the interfaces and the size, shape and distribution of defects within the sample. Cracks or defects at a weakly-bonded interface will have a greater weakening effect on adhesion than similar flaws in a bulk phase (Good 1972). The effect of defects present in lacquered tinplate specimens will be investigated. If specific interfaces are weakly-bonded or if certain components within the system are weak the propagating crack should reveal these since it will follow the path with the lowest fracture energy.

4. ADHESION TESTING

There are many adhesion tests available (Mittal 1978, Deryagin et al 1978, Bullett and Prosser 1972) but not all are suitable for use with coatings. In some investigations of adhesion it is possible to construct a special adhesively-bonded system with known geometry and carefully controlled conditions such as in the tapered double cantilever beam test (Mostovoy and Ripling 1966). An artifically introduced crack can then initiate a controlled failure.

When measuring the adhesion of thin coatings it is difficult to apply a force to the coating which will induce failure. If the coating possesses a high tensile strength it may be possible partially to remove it and then peel it away. Other alternatives are to bond a test piece on top of the film and load it (as in the butt-joint test) or subject the specimen to high accelerations, bending or stretching. Some of the different test methods include the use of an ultracentrifuge to debond an adhering droplet at up to 15×10^6 gravities (Zimon 1969), ultrasonic methods (Meyer and Rose 1976), torsion testing of bonded, thin-walled cylinders (de Bruyne 1951) and scratch-testing using a variable load.

The full range of test methods will not be reviewed here but several tests, initially used in this work for lacquered tinplate, will be discussed. One of the most commonly used tests for lacquered tinplate is the "Scotch Tape test" in which the lacquer is scored in a cross-hatched pattern and adhesive tape pressed upon it; rapid withdrawal of the tape may then remove sections of the lacquer to yield a semi-quantitative measure of adhesion. A more sophisticated version of the test has been devised (Calder et al 1983) but is not widely used. This method allows an estimate of lacquer adhesion to be rapidly and easily obtained and consequently has gained

general acceptance in the coatings industry. Lacquer adhesion values as measured by the "Scotch Tape test" form the starting point for this work where a comparative set of tinplates with different adhesion properties will be rigorously examined.

Other tests were evaluated before a particular method was chosen for the main testing programme:

i/ The bend test

Lacquered tinplate strips were bent at different rates over a mandrel. At room temperature, all the specimens passed the test with no lacquer detachment; debonding occurred only at liquid nitrogen temperature and this was felt not to be a suitable environment for comparison with factory performance.

ii/ The peel test

This is a widely used test method which has been applied to many different adhesive systems (Kaelble 1959,1962, Bikerman 1961, Chang 1960). The 'T' peel test was used, bonding two strips of lacquered tinplate together and then separating them as shown in Figure 5.

This method was unsuitable for the thick (> 0.20mm) tinplate samples which bent sharply producing severe variations in the rate of debonding and therefore could not be used for the main testing programme which included a range of different tinplates.

iii/ The blister test

Proposed by Dannenberg (1961) this technique has been used successfully for studies of paint adhesion. It has the advantage that a coated substrate may be investigated without the further bonding of test pieces to the coating and introduces an initial crack very near the interface. The crack propagation rate can be controlled and observed during the test.

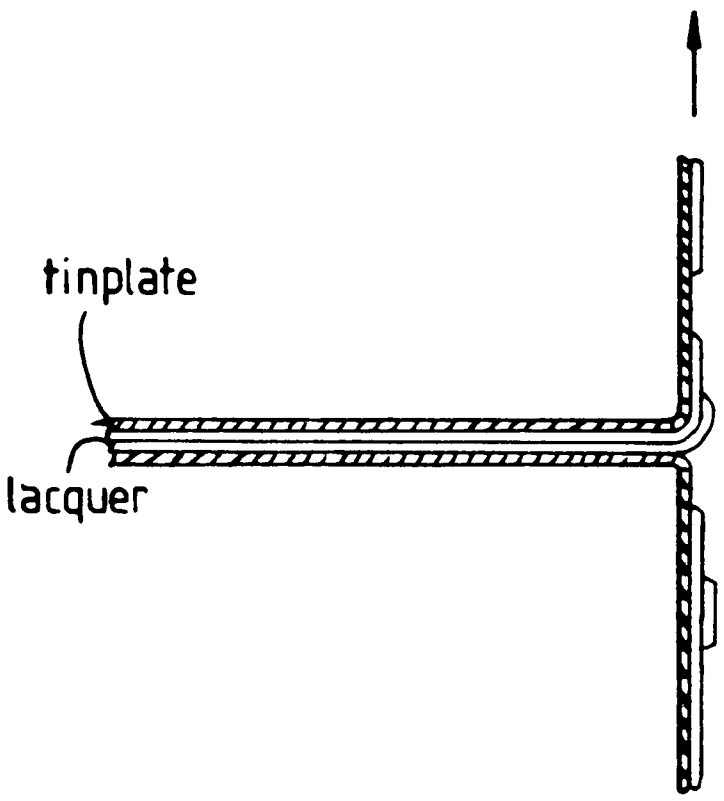

Figure 5. The 'T' peel test applied to lacquered tinplate.

Extra adhesive is not shown.

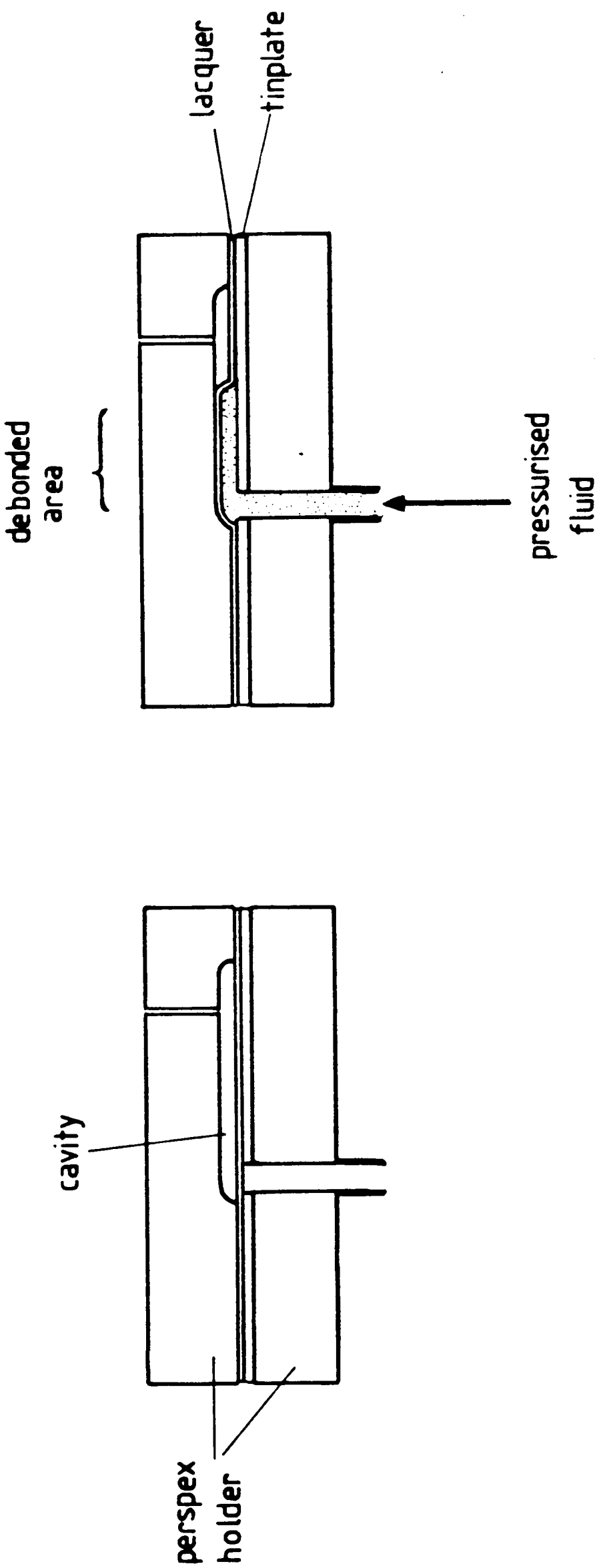

Figure 6. The blister test applied to lacquered tinplate.
In practice bedonding did not occur since the area of unsupported lacquer fractured.

A drawing of the test rig is shown in Figure 5 where a pressurised fluid (compressed air or water in this case) is injected into the specimen at the lacquer-tinplate interface via a hole electrochemically etched through the tinplate. In theory, debonding can be initiated and controlled by the applied pressure but in no instance could this be achieved with lacquered tinplate samples. Fracture of the lacquer always occurred before any debonding. Further refinements such as strengthening the lacquer with a secondary sheet of polymer or reducing the upper cavity depth did not produce blister growth so this method was abandoned since the adhesion of lacquer to the passivated tinplate was too high.

iv/ The butt-joint test

Sometimes known as a "poker-chip" joint, this arrangement provides a convenient method of testing an adhesive system in tension and was chosen as the test method for this work. The test is relatively easy to set up and has been widely used for adhesion studies (Baker 1979, Jennings 1972) including work on lacquered tinplate (Servais et al 1979). The butt-joint test has been used in a similar investigation of the adhesion of a chlorinated rubber to mild steel (Smelt 1979) with some success.

To perform the test, a coupon of lacquered tinplate is bonded between two cylindrical stubs in an alignment jig and then pulled apart in a direction normal to the tinplate surface. Fracture surfaces suitable for fractography are produced and are large enough ($> 1cm^2$) for subsequent XPS analysis. The stress state in a butt-joint has been analysed by several workers, including the case where a void is introduced to act as a stress-raiser (Pirvics 1974).

Taking the simple case of a stressed layer of adhesive in a butt-joint in tensile loading (Figure 7), the stress will vary

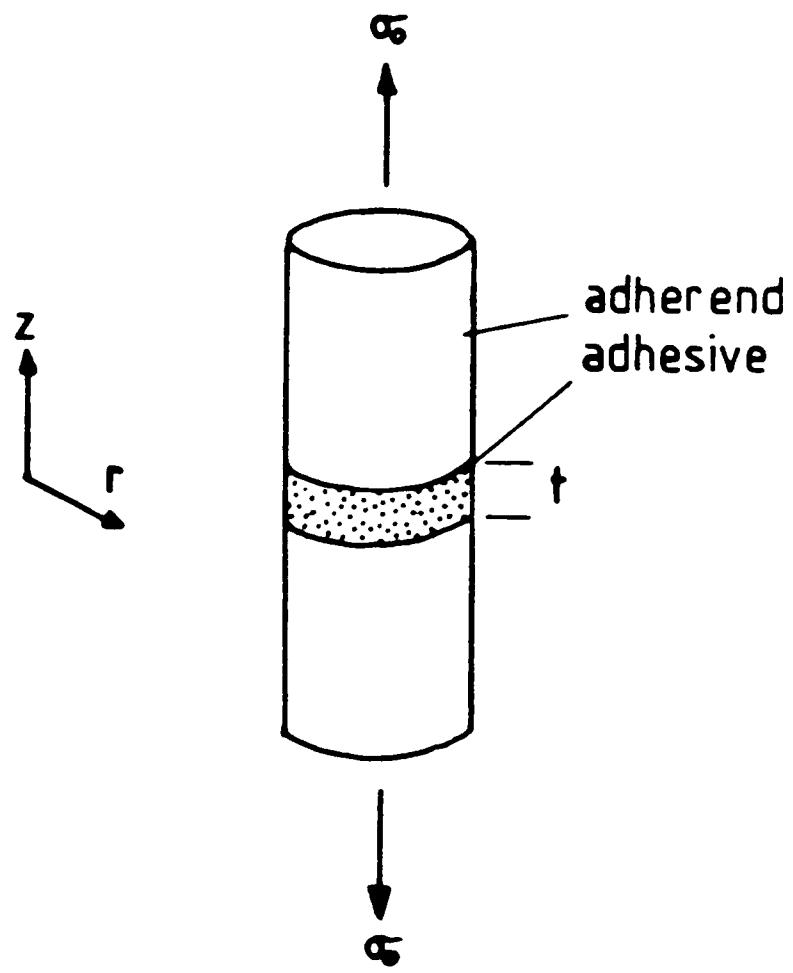

Figure 7. A butt-joint.

For use with lacquered tinplate the lacquer layer is compared with the adhesive in this diagram to determine the stress state in the joint.

throughout the adhesive and most deformation will take place in the adhesive assuming that it has a higher Poisson's ratio and lower shear modulus than the adherend, as is the case for the materials used in this work. Kuenzi and Stevens (1963) have calculated the radial stress, σ_r, and the circumferential stress, σ_θ, in the lacquer layer as:

$$\sigma_r = \sigma_\theta = (\nu_a - \frac{E_a \nu_s}{E_s}) \ (\frac{\sigma_z}{1-\nu_a})$$

where ν_a = the Poisson's rate of adhesive, ν_s = the Poisson's ratio of the adherend, E_a = Young's modulus of adhesive, E_s = Youngs modulus of adherend and σ_z = axial stress.

For an adhesive material with $\nu_a \sim 0.5$, typical of epoxy resins (Smith et al 1974), bonded to an adherend with a much larger modulus such as mild steel (where $E_s/E_a \sim 10^2$):

$$\sigma_r = \sigma_\theta = \sigma_z$$

i.e. most of the adhesive is in a state of hydrostatic stress. Around the circumference of the joint there exists a region of shear stress, τ_{rz}, the magnitude of which depends upon the ratio of joint radius, r, to adhesive thickness, t. Figure 8a shows the radial distribution of shear and tensile stresses in the adhesive for a joint with r/t = 10. Stress distributions are shown for the centre plane of the adhesive layer and the adhesive adherend interface (Alwar and Nagaraja 1976). The effect of varying t, the lacquer (or adhesive) thickness is shown in Figure 8b. If thick layers are used the polymer will bow inwards as the sample is strained and consequently thin lacquers are preferred to reduce this effect. In this work the lacquer and adhesive thickness is so small that the regions of shear stress are limited to a narrow band close to the

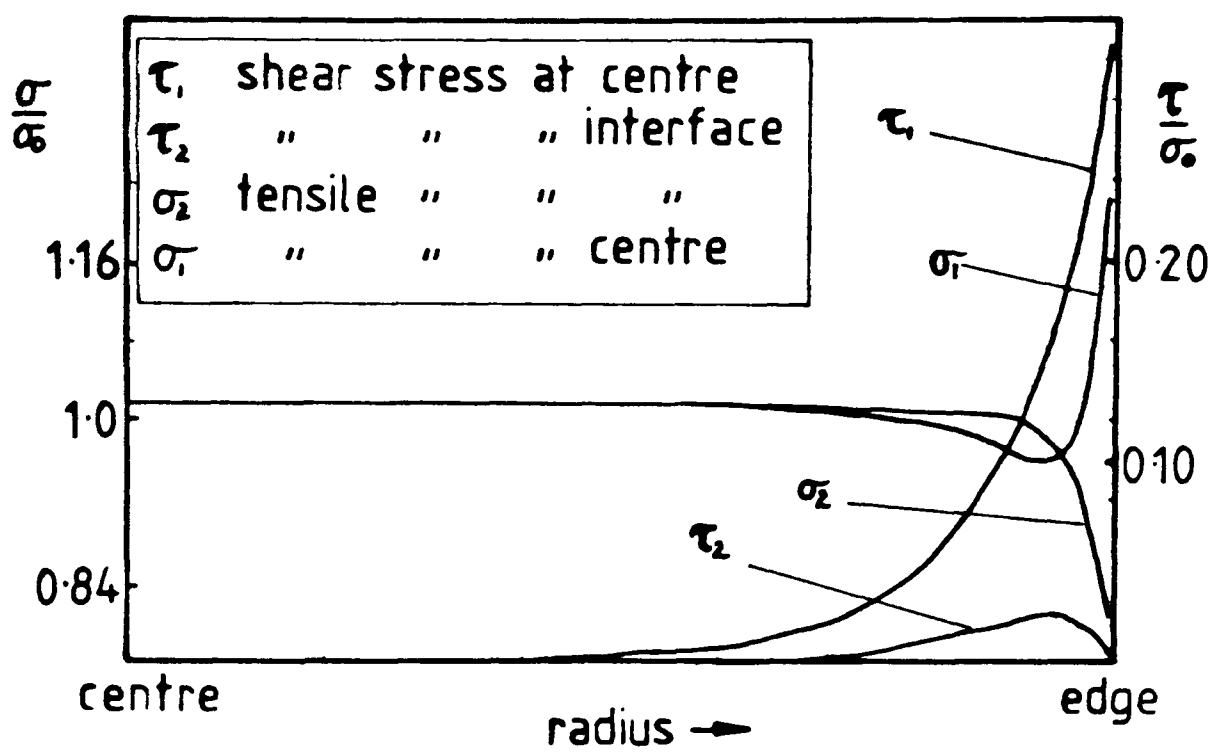

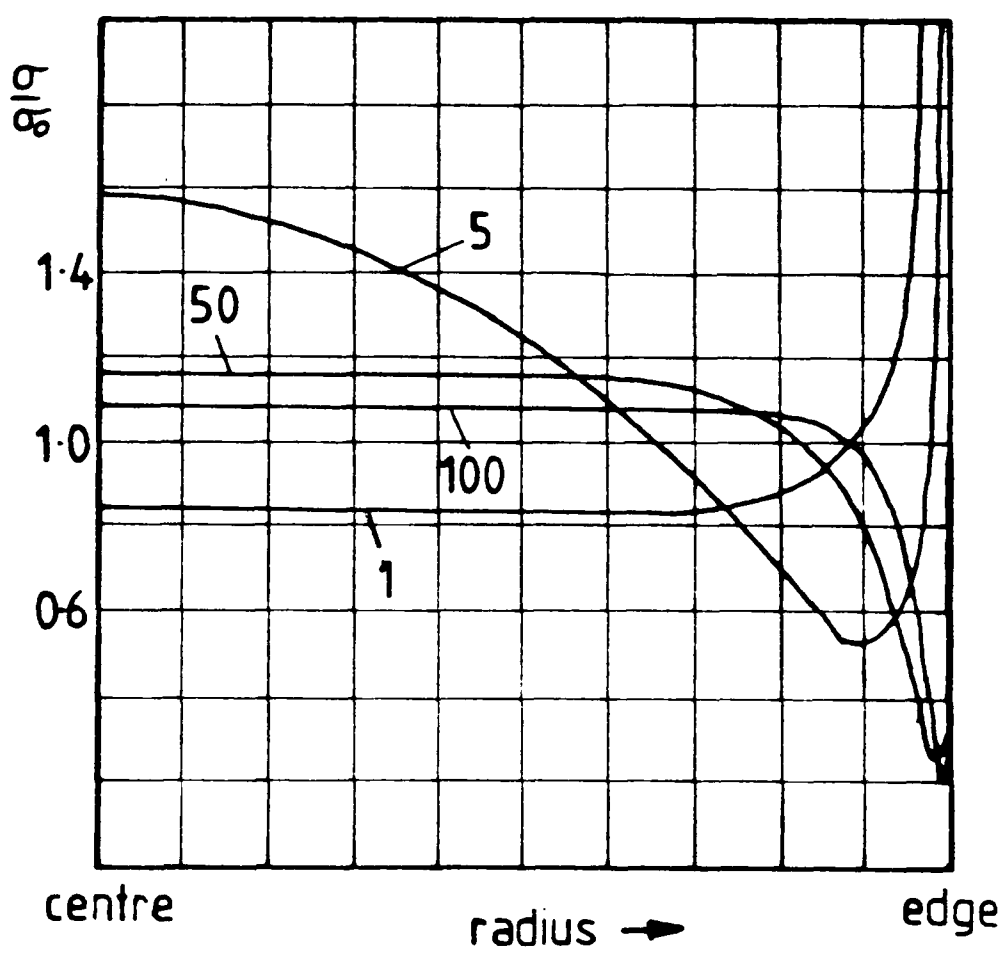

Figure 8. a/ Radial distribution of tensile and shear stresses in the lacquer layer

b/ The effect of altering lacquer thickness on the stresses within a butt-joint.

specimen edges and these stresses can be further reduced by extending the lacquered tinplate beyond the test stubs. Thin glue lines also have the advantages of reducing the statistical likelihood of flaws in the polymer and reducing residual stresses on curing. Edge stress concentrations are also slightly reduced by the presence of a spew fillet of adhesive around the joint (Adams et al 1978). For a simple adherend-adhesive butt-joint, a fracture mechanics failure analysis (Gent 1974) has shown that initiation occurs at the edge stress concentrations. This mode of failure does not often take place when testing lacquered tinplate samples since the complicated surface structure of the tinplate provides flaws which initiate fracture before the stress at the circumference becomes critical.

Bibliography

ASTM D907-70 (1970.

Adams R.D., Coppendale J. and Peppiatt N.A. J. Strain Analysis 13 No. 1 (1978) 1.

Allen K.W. in "Aspects of Adhesion 3" ed. D.J. Alner, Univ. of London Press (1969).

Alwar R.S. and Nagaraja Y.R. J. Adhesion 7 (1976) 279.

Andrews E.H. and Kinloch A.J. Proc. R. Soc. Lond. A332 (1973) 385.

Andrews E.H. and Kinloch A.J. Proc. R. Soc. Lond. A332 (1973) 401.

Andrews E.H. and King N.E. J. Mater. Sci. 11 (1976) 2004.

Arridge R.G.C. "Mechanics of Polymers" Clarendon Press Oxford (1975).

Askew J. Technical Conference Organisation March 1975.

Azzeri N. and Splendorini L. Imballaggio 292 (1980) 65.

Baker F.S. J. Adhesion 10 (1979) 107.

Bair H.E., Matsuoka S., Vadimsky R.D. and Wang T.T. J. Adhesion 3 (1971) 89.

Bikerman J.J. J. Coll. Sci. 2 (1947) 163.

Bikerman J.J. "The Science of Adhesive Joints" 2nd ed. Academic Press New York (1968).

Borroff E.M. and Wake W.C. Trans. Inst. Rubber Ind. 25 (1949) 19.

Bullett T.R. and Prosser J.L. Proc. Org. Coatings 1 (1972) 45.

Calder G.V., Hansen F.C. and Parra A. in "Adhesion aspects of polymer coatings" p. 569 ed. K.L. Mittal, Plenum, New York (1983).

Chang A. Trans. Soc. Rheology 4 (1960) 75.

Cherry B.W. and el Muddarris. J. Adhesion 2 (1970) 42.

Dahlquist C.A. ASTM Spec. Tech. Publ. No. 360 (1964) 36.

Danneberg H. J. Appl. Polymer Sci. 5 (1961) 125.

de Bruyne N.A. in "Adhesion and Adhesives" ed, de Bruyne N.A. and Howink R. Elsevier, London (1951).

de Bruyne N.A. Aero Res. Tech. Notes. Bull. No. 168 (1956).

Debye P. Phys. Zeit. 21 (1920) 178.

Debye P. Phys. Zeit. 22 (1921) 302.

Deryagin B.V. and Krotova N.A. "Adhesion" Moscozs Izd. Akad. Kauk SSSR (1949).

Deryagin B.V., Krotova N.A. and Smilga V.P. "Adhesion of Solids" Studies in Soviet Science, Consultants Bureau, New York (1978).

Eley D.D. "Adhesion" Oxford University Press (1961).

Fowkes F.M. J. Adhesion 4 (1972) 155.

Gent A.N. and Kinloch A.J. J. Polymer Sci. A2 9 (1971) 659.

Gent A.N. J. Polymer Sci. A2 (1974) 283.

Gent A.N. and Kinloch A.J. J. Polymer Sci. A29 (1973) 385.

Girifalco L.A. and Good R.J. J. Phys. Chem. 61 (1957) 904.

Gledhill A., Kinloch A.J. and Shaw S.S. J. Adhesion 9 (1977) 81.

Good R.J. J. Adhesion 4 (1972) 133.

Griffiths A.A. Phil. Trans. R. Soc. A221 (1920) 113.

Harkins W.D. and Loesner E.H. J. Chem. Phys. 18 (1950) 556.

Huntsberger J.R. J. Adhesion 12 (198) 3.

Irwin G.R. Appl. Mat. Res. 3 (1964) 65.

Jennings C.W. J. Adhesion 4 (1972) 25.

Kaelble Trans. Coc, Rheology 3 (1959) 161.

Kaelble Proc. Symp. Adhesion and Cohesion. ed. Weiss, Elsevier, (1961) 74.

Keesom W.H. Proc. K. Ned. Akad. Wetenschap 18 (1915) 636.

Keesom W.H. Proc. K. Ned. Akad. Wetenschap 23 (1920) 939.

Keesom W.H. Proc. K. Ned. Akad. Wetenschap 22 (1921) 129.

Kinloch A.J. J. Mater. Sci. 15 (1980) 2141.

Kinloch A.J. and Shaw S.S. in "Developments in Adhesives - 2" ed. A.J. Kinloch, Applied Science, London (1981).

Kinloch A.J. J. Mater. Sci. 17 (1982) 617.

Kuenzi E.W. and Stevens G.H. US Forest Prod. Lab. Rep. FPL-011 (1963).

Langbein D. J. Adhesion 1 (1969) 237.

Ley J.B. Metal Finishing J. 13 No. 153 (1967) 291.

London F. Trans. Farad. Soc. 33 (1937) 8.

McKirahan R.D. and Ludwigsen R.J. Mater. Protection 7 No. 12 (1968) 29.

Meyer P.A. and Rose J.L. J. Adhesion (1976) 107.

Mittal K.L. in "Adhesion Science and Technology" ed. L.H. Lee, Polymer Science and Technology Series 9A, Plenum, New York (1975).

Mittal K.L. in "Adhesion measurements of Thin Films, Thick Films and Bulk Coatings" ASTM STP 640 (1978).

Mostovoy S. and Ripling E.J. J. Appl. Polymer Sci. 10 (1966) 1351.

Noorlander C. and Barnes W.G. Metal Finishing 79 No. 9 (1981) 21.

Obrzut J.J. Iron Age 225 No. 32 (1982) 61.

Orowan E. Rep. Prog. Phys. 12 (1948) 185.

Packham D.E. Ph.D. thesis, City University, London (1970).

Packham D.E. in "AdhesionAspects of Polymeric Coatings" ed. K.L. Mittal, Plenum Press, New York, (1981) 19.

Peisach M., Wilson V.W. and Szecsei Z. J. Radioanalyt. Chem. 29 (1976) 343.

Pirvics J. J. Adhesion 6 (1974) 207.

Reegan S.C. and Ilkka G.A. "Adhesion of Polyurethanes to Metals" in 'Adhesion and Cohesion' ed. P. Weiss, Elsevier, London (1962).

Schonhorn H. "Adhesion: Fundamentals and Practice" Min. Techn., Maclaren, London (1969).

Schultz J., Tsutsumi K. and Donnet J.B. J. Colloid Interface Sci. 59 (1977) 277.

Servais J.P., Lempereur J., Renard L. and Leroy V. Br. Corr. J. 14 No. 3 (1979).

Shetye S.G. J. Colour Sci. 12 (1974) 1.

Skinner S.M., Savage R.L. and Rutzler J.E. J. Appl. Phys. 24 (1953) 438.

Smelt D.H. D. Phil. thesis, University of Oxford (1979).

Smith A., Wilkinson S.J. and Reynolds W.N. J. Mater. Sci. 9 (1974) 547.

Smith T. J. Adhesion 11 (1980) 243.

Sykes J.M. Ph.D. thesis, University of Cambridge (1967).

van der Waals J.D. Thesis, Leiden (1873).

Vasenin R.M. "Adhesion: Fundamentals and Practice" Min. Techn., Maclaren, London (1969).

Voyutskii S.S. "Autohesion and Adhesion of high Polymers", Interscience, (1963).

Wake W.C. Royal Inst. Chem. Lect. series 4 (1966) 1.

Westergaard H.W. J. Appl. Mech. A6 (1939) 46.

Young T. Trans. R. Soc. 95 (1805) 65.

Zimon A.D. "Adhesion of Dust and Powders", Plenum, New York (1969).

CHAPTER 2

BACKGROUND

The study of tinplate and passivation layers in particular has been pursued over the years using a wide range of analytical techniques in order to understand the surface structure and explain its effects on lacquer adhesion and other properties (Azzeri and Splendorini 1980).

1/ The Passivation layer

Early examinations were based on wet chemical and electrochemical analyses for the estimation of chromium (Hoare et al 1965, Hoare and Britton 1964) and controlled cathodic reduction for measurements of tin oxide (Willey and Kelsey 1958). Britton (1965) subsequently introduced a more rigorous electrochemical test for chromium in which the sample was anodically polarized in disodium phosphate whilst its potential was measured. The potential arrest was interpreted as the oxidation of Cr^{III} to Cr^{VI} leaving some chromium remaining on the tinplate surface. A later work (Rocquet and Aubran 1968) interpreted this as the oxidation of metallic chromium (Cr^{0}) and provoked further investigations (Coad et al 1976, Leroy et al 1976) in which the existence of metallic chromium in the passivation layer, previously doubted, was proved.

Although electrochemical methods are still used as a research tool and for quality control there have been major advances in other surface-analytical techniques since 1965 which offer new insights e.g. photoelectron spectroscopy (XPS), Auger electron spectroscopy (AES) and secondary ion mass spectroscopy (SIMS) which, along with electron microscopy, have all been used to study the passivation layers on tinplates and, in some cases, to infer effects on lacquer adhesion.

Transmission electron microscope (TEM) studies (Albu-Yaron and Smith 1979, Saijo et al 1976) have shown that the passivation layer is not a homogeneous film but comprises discrete crystals of various materials situated in a thinner layer. Britton (1975) using XRF states that the constituents may be intermingled and possible in ill-defined crystal forms and identifies Cr^0 as being left behind on the tinplate after alkali extraction; the alkali-soluble chromium , he proposes, is made up of several different compounds, supporting the work of Salm (1972). In anodic investigations using electrochemical methods and TEM (Britton and Sherlock 1974) SnO_2 and probably SnO are found on tin surfaces treated by the cathodic reduction (311) process.

An estimate of chromium valency in the passivation layer using XPS was attempted (Coad et al 1976, Leroy et al 1976) for 311 type tinplates. Metallic and trivalent chromium were detected and a value of about 10nm for the thickness of the passivation layer was proposed. These works produced results in agreement with those of Rauch and Steinbicker (1975) in suggesting the presence of $Cr(OH)_3$, Cr_2O_3 and Cr^0.

Saijo and co-workers (1976) used a combination of TEM, XPS and electrochemistry to produce a model for passivation layer structure (see Chapter 4) containing discrete layered structures of $Cr(OH)_3$, $CrO_2.nH_2O$, Cr_2O_3 and Cr^0 set in a matrix of SnO_2 and SnO. However, the TEM observations did not account for all the chromium as measured by XPS and electrochemistry which detected Cr^0 as less than 5% of the passivation layer (Coad et al 1976), the rest being in oxidised form. Electrochemical studies (Aubrun and Pennera 1976, Rauch and Steinbicker 1973) tend to yield values of approximately 0.5µg cm^{-2} for Cr^0 which corresponds to an even coverage some 5 monolayers deep. According to Saijo et al (1976) this component is found in discrete particles

as also seen by Albu-Yaron and Smith (1979). Leroy et al (1976) find an even coverage of chromium using secondary ion mass spectroscopy. Taking these results as a whole, the bulk of the evidence suggests that chromium is found both in thinly-dispersed forms and as large (1μm) crystals.

Takano and Watanabe (1976) could not find Cr^0 using TEM except on specially-passivated tinplates and the identification with this technique by Albu-Yaron and Smith on commercial 311 tinplate is unique in the literature.

XPS measurements have concentrated on measurements of Cr^0 and Cr^{3+}; Leroy et al (1976) reported these as well as Cr^{6+} on 311 and 300 type plates but there appear to be no references to the possible presence of Cr^{4+} or the possibility of mixed-valence chromium oxides which contain Cr^{3+} and Cr^{6+}. Servais et al (1976) performed XPS and electrochemical tests and compared results. Previous workers had found that XPS had yielded much lower Cr^0 values than electrochemical results and this inconsistency has been attributed to errors in the latter technique, because alkali stripping had been used to remove chromium oxides before anodic measurements of Cr^0 were made. However, it is likely that the alkali stripping process did not remove all the oxidised forms of chromium which had been subsequently interpreted as metal (Azzeri and Splendorini 1980). Thus, the support for XPS as a quantitative analytical tool in passivation layer examination was strengthened. The same workers performed adhesion tests using a butt-joint tensile test to reveal fractures at a passivation layer interface. Passivation layers were pulled away from the tinplate surface with the lacquer revealing a layer of tin oxide some 2nm thick. This was assumed to have grown during stoving and it was suggested that it had weakened the system allowing lacquer

and passivation layer detachment. They found that similar tests could not be made on tinplates with better lacquer adhesion properties as failure in the sample could not be induced.

In an investigation of the effect of passivation layer structure on lacquer adhesion (Takano and Watanabe 1976) several different passivation layers were examined by TEM and lacquer adhesion by a peel test. Low metallic chromium content was associated with poor adhesion which was also related to high levels of total chromium. Adhesion was also correlated with the nature of the tin oxides; tinplates on which orthorhombic SnO grew performed well in peel tests but tinplates with tetragonal SnO or SnO_2 showed poor lacquer adhesion. Thick tin oxide layers have been shown to lower lacquer adhesion by Horiguchi et al (1984).

TEM can determine the crystal structure of the components of passivation layers and complements XPS, which determines chemical composition. XPS data are often presented in the form of depth profiles achieved by Ar ion etching through the surface (see XPS Chapter 4) although this method leads to many uncertainties and can introduce serious artefacts. Typical depth profiles through passivation layers from the work of Coad et al (1976) and Azzeri et al (1982) are given in Figure 1. Depth profiles will not be presented in this work owing to the artefacts produced by prolonged Ar ion etching. A summary of TEM and XPS results from the literature is given in Table 1. Specific tin and chromium oxides can only be identified with certainty using TEM since there is an overlap of XPS peaks which makes deconvolution difficult. The implications of this are discussed in Chapter 6.

Variations in passivation layer structure with ageing and stoving have received attention by other workers (Albu-Yaron and

Figure 1. XPS depth profiles through 311 passivation layers.

a Coad et al 1976

b Azzeri et al 1982

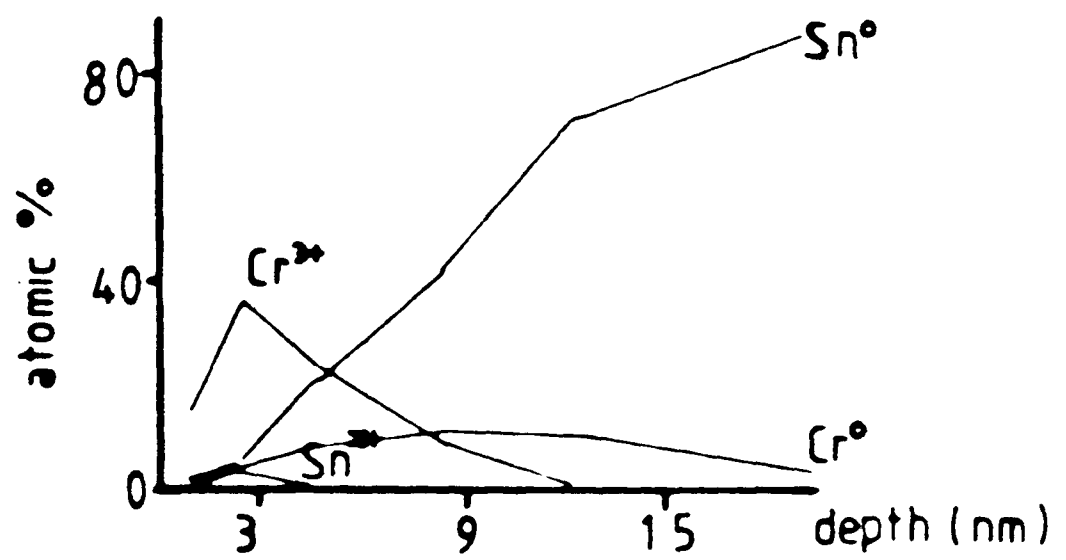

a

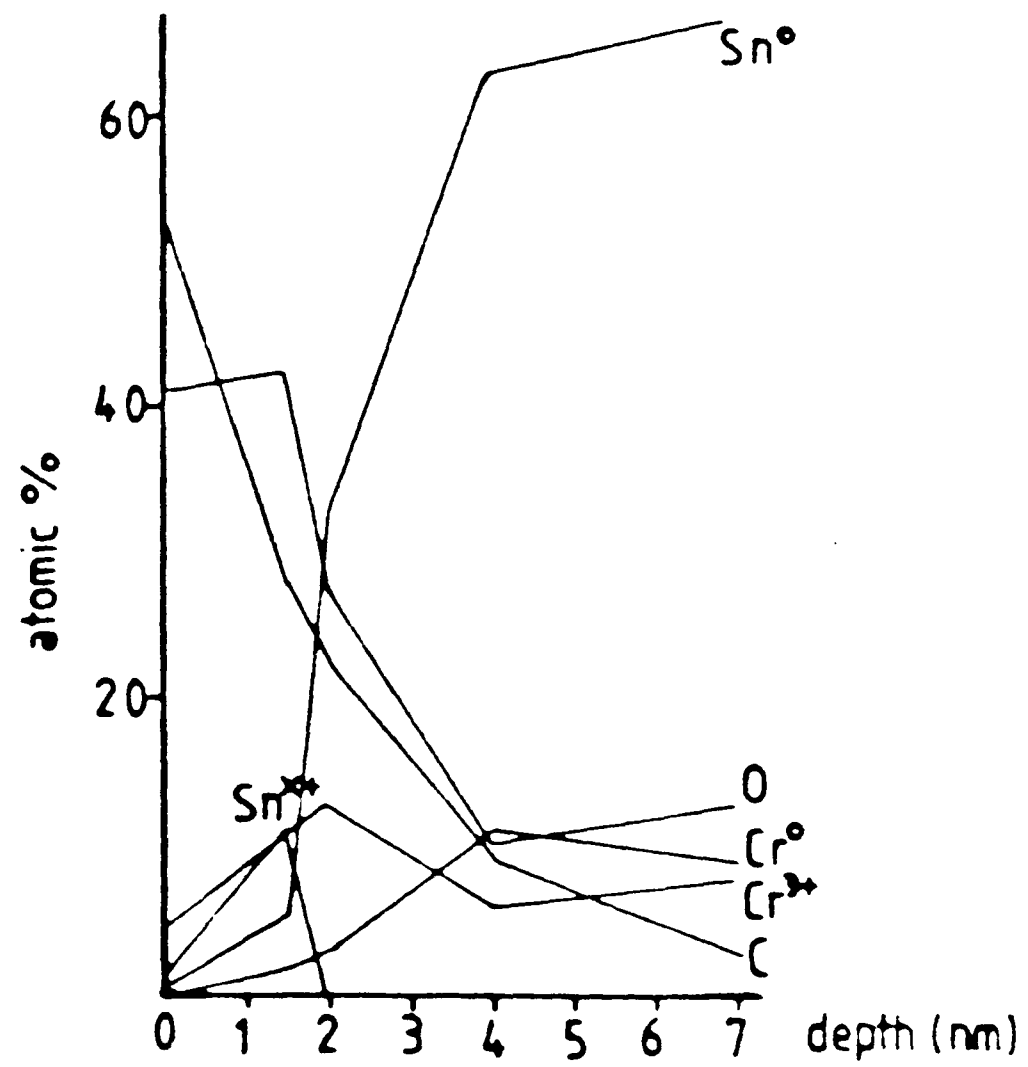

b

TABLE 1

SOME XPS AND TEM RESULTS

FROM EXAMINATIONS OF PASSIVATION LAYERS

ON TINPLATES

Tinplate Type	Method	Composition	Reference
		Cr^0:Cr_{total} Cr_{total}:SnO_x	
311		1:4.89 1:0.2	
311	XPS	1:6 1:0.49	Leroy et al 1976
311		1:2.29 1:0.75	
311		1:2.7 1:0.98	
		Cr^0;Cr^{3+}	
311	XPS	Cr_2O_3	
		Cr^{3+} hydrated	Azzeri et al 1980
		SnO_x	
300	XPS	Cr^{3+}; SnO_x	
		Cr^0; Cr_2O_3	
311	TEM	SnO_2 tetragonal	Albu-Yaron and
		SnO	Smith 1980
		βSn	
311	TEM	SnO tetragonal/orthorhombic	Takano and Watanabe
		SnO_2 " "	1976
311	AES	CrO_3 hydrated	Maeda 1980
		Cr_2O_3	

Grovenor, 1984, Horiguchi et al 1984). The greatest changes in structure occur within a few weeks of manufacture so tinplates which are over one year in age, as used in the experimental work here, will essentially have a stable structure which may then be modified by stoving (after lacquering); such effects are investigated in this work.

The formation of passivation layers is discussed in Chapter 6 and has been investigated in the literature (Carter 1961, Aubrun and Rocquet 1975, Nagel Soepenberg et al 1976).

2/ Proposed Work

Lacquer adhesion has been previously investigated using the butt-joint test (Servais et al 1976), the peel test (Takano and Watanabe 1980) and by deep-drawing lacquered tinplate (Noorlander and Barnes 1981). Comparison between the results from different tests is unreliable since each test imposes different stress conditions on the sample and full details of the substrate and loci of failure are not always reported.

All the adhesion tests in this work are made using a butt-joint method at the same temperature and test rate. Interfacial bonding between the layered structure of lacquered passivated tin-plates will be influenced by a number of factors, including the formation and type of bonds across the interface, the thermodynamic properties of the surfaces (also affected by contaminants and adsorbed water), the topography of the interface and the mechanical properties of the materials in each layer. Defects will also affect both crack initiation and propagation.

The tinplate surfaces will be characterized in terms of composition and structure before bonding and fracture surfaces examined after failure.

The form of the experimental work will therefore be:

i/ Mechanical testing of lacquer adhesion

A set of tinplates with varying lacquer adhesion properties initially defined by Scotch Tape test and factory performance will be examined with a range of lacquers and stoving treatments. Fracture initiation and propagation paths will be determined by fractography and the latter further defined by XPS examination of fracture surfaces.

ii/ Characterization of passivation layers and tinplate surfaces.

A combination of analytical techniques will be used to provide chemical and structural data. X-ray photoelectron spectroscopy (XPS) is a very surface-sensitive method of analysis, measuring the top few monolayers of a solid to yield elemental and chemical bonding information. The area of specimen measured is typically $1cm^2$ and so precludes measurements of spatial distribution but this complementary data can be obtained from transmission electron microscopy (TEM) with a spatial resolution better than 2nm. TEM can also provide structural data from diffracting crystals. Optical and scanning electron microscopy will also be used to observe the topography of tinplates and fracture surfaces.

Thus, it will be possible to characterize the tinplate samples and distinguish variations in their passivation layers and surface topographies.

iii/ Attempt a correlation of i/ with ii/

It is already known from practical experience that certain tinplates possess poor lacquer adhesion, sometimes with a range of different lacquers. A wide range of tinplates, lacquers and stoving conditions will be used and the results of the adhesion tests compared with the tinplate characteristics derived from XPS and TEM. It is intended to produce structural models of the passivation layers and

correlate these with observed lacquer adhesion performance. Models for fracture mechanisms will also be proposed.

Bibliography

Albu-Yaron A. and Smith D.A. Br. Corr. J. 14 No. 3 (1974) 133.

Albu-Yaron A. and Smith D.A. Proc. 2nd Int. Tinplate Conf. (1980) IRTI (London).

Albu-Yaron A. and Grovenor C.R.M. Proc. 3rd Int. Tinplate Conf. (1984) ITRI (London).

Aubrun P. and Rocquet P. J. Electrochem. Soc. 122 (1975) 861.

Aubrun P. and Pennera G.A. Rev. Metall. (Nov. 1976) 745.

Azzeri N. and Splendorini L. Imballaggio 292 (1980) 65.

Azzeri N., Splendorini L., Battistoni C. and Paparazzo E. Surf. Techn. 15 (1982) 255.

Becker J.J. V. Electrochem. Soc. 117 No. 9 (1970) 1211.

Britton S.C. Br. Corr. J. 10 (1975) 2.

Britton S.C. and Hancox J.H. Sheet Metal Ind. 1 (1965) 15.

Britton S.C. and Sherlock J.C. Br. Corr. J. No. 2 (1974) 85.

Carter P.R. J. Electrochem. Soc. 108 No. 8 (1961) 782.

Coad J., Mott B., Harden G, Walpole J. Br. Corr. J. 11 (1976) 219.

Hoare W.E., Hedges E.S., Barry B.T.K. "The technology of tinplate" Arnold (London) 1965.

Horiguchi M., Kurokawa W. and Matsubayashi H. Proc. 3rd Int. Tinplate Conf. (1984) ITRI (London) paper no. 29.

Leroy V., Servais J.P., Habraken L., Belgiurn C.R.M., Renard L., Lempereur J. and Cockerill S.A. Proc. 1st Int. Tinplate Conf. (1976) ITRI (London) 34.

Maeda S., Asai T. and Sawairi T. Proc. 2nd Int. Tinplate Conf. (1980) ITRI (London) paper no. 25.

Nagel Soepenberg E., Vrijburg H.G. and Spruyt A.C. Proc. 1st Int. Tinplate Conf. (1976) ITRI (London) 282.

Noorlander C. and Barnes N.G. Metal Finishing 79 No. 9 (1981) 21.

Rauch S.E. and Steinbicker R.N. J. Electrochem Soc. 120 No. 6 (1973) 735.

Rocquet P. and Aubrun P. Corrosion-Traitments-Protection-Finition 16 No. 5 (1968) 229.

Rocquet P. and Aubrun P. Br. Corr. J. 5 (1970) 193.

Saijo K., Yoshioka O and Oyama T. Tech. Rep. Toyo Kohan Co. Ltd. 23 (1976) 17.

Salm D. BHP Tech. Bull. 16 No. 1 (1972) 2.

Servais J.P., Lempereur J., Renard L. and Leroy V. Br. Corr. J. 14 No. 3 (1979) 126.

Takano H. and Watanabe T. Proc. 2nd Int. Tinplate Conf. (1980) ITRI (London) paper no. 36.

Willey A.R. and Kelsey D.F. Analyt. Chem. 30 (1958) 1804.

CHAPTER 3

BUTT-JOINT TEST MEASUREMENTS

1. INTRODUCTION

The first problem is to chose an adhesion test; many are available but none is perfect for this application. Adhesion test methods have been reviewed and the most promising tried on lacquered tinplate samples. The butt-joint test was chosen in preference to others since it could produce lacquer de-adhesion in a wide range of samples with different lacquer thicknesses, different tinplate thicknesses and different passivation treatments. The blister test could only debond lacquers with very poor adhesion properties; the peel test was not suitable for thick (> 0.2 mm) tinplate samples which were too stiff to deform without introducing sharp bends and erratic peel rates which would make analysis extremely complex; the "Scotch tape test" can only produce semi-quantitative data. The butt-joint is easy to arrange . with controlled geometry and alignment conditions and yields fracture surfaces which are convenient for microscopy and X-ray photoelectron spectroscopy. The butt-joint geometry has also been widely used and several works on the stresses in the joint have been published (Kinloch 1982). The poor adhesion of a lacquer can sometimes be traced to particular stoving conditions or to corrosion but may, on occasions, be attributed to the tinplate itself. Since lacquer adhesion after prolonged exposure to a hostile environment is sure to have different causes to those failures which occur in air at room temperature, this work is concerned with the adhesion of dry lacquer in the mode of failure measured by the butt-joint test (Alwar and Nagaraja 1976, Baker 1979).

The starting point has been a set of different tinplate samples which have been categorised into approximate ranges of adhesion performance as measured by the Scotch tape test (Calder et al. 1983) and in-service behaviour. These are listed in Table 1. The butt-joint test method has been used on these tinplate types with several stoving conditions and a range of lacquers; the results, in the form of failure load and percent area lacquer removal have been treated by statistical methods in order to reveal the effects of a particular tinplate or passivation treatment on lacquer adhesion.

Fractographic analysis of the failed surfaces has been used to identify the direction of fracture propagation and determine possible sites of initiation.

2. EXPERIMENTAL

A range of passivated tinplate samples, known from practical experience to have widely varying lacquer adhesion properties were chosen as a comparative sample set for butt-joint testing. Scotch tape tests showed a degree of correlation between the amount of lacquer removed and tinplate type regardless of the lacquer used for coating, although it is not possible to say whether these samples are typical of the tinplates produced by their manufacturers. These tinplates, listed by manufacturer and passivation treatment were BS 311, NS 311 and KS 311 with "good", "intermediate" and "poor" adhesion properties respectively as measured by the Scotch tape test (see Table 1). In addition a 300 type tinplate (BS 300) with good adhesion properties was tested in order to compare the cathodic dichromate passivation treatment (311) with the dichromate dipping (300) treatment. Both factory-lacquered tinplate and samples coated in the laboratory were tested. Approved stoving conditions were used but some samples were

TABLE 1

Tinplates used in lacquer adhesion tests

Tinplate	Scotch Tape Test result		
	percent lacquer removed		
British Steel 311 (BS)	0	good	*
Nippon Steel 311 (NS)	5	intermediate	*
Kawasaki Steel (311) (KS)	25	poor	*
British Steel 300 Non-passivated (NP)			

* Used as a comparative set for most of this work.

produced by varying the stoving time or stoving in an inert atmosphere to investigate the effect on lacquer adhesion. Typical standard conditions are 10 or 14 minutes at 200°C in air. Inert gas stoving was employed to investigate the effect of tinplate oxidation and was not expected to affect lacquer curing which takes place by cross-linking (except for the oleoresinous lacquers which cure by a reaction with oxygen). Other types of lacquer used were epoxy-phenolic, phenolic and organosol; the lacquer coating thickness was kept constant as far as possible at about 5 μm for most specimens.

Specimens for testing were cut from lacquered tinplate sheet to produce coupons approximately 20 mm square. A typical batch of specimens from one plate would consist of 10 to 20 individual specimens, removed from as small an area of the large sheet as possible so that possible variations in the passivation layer across the sheet could be minimised. The tinplate side was abraded with 600 grit abrasive paper and wiped with methanol but the lacquered side remained unmodified before bonding to the butt-joint stubs. The stubs were prepared by abrading their surfaces after machining to a smooth finish and ultrasonically cleaned in trichloroethylene for 30 minutes. Most of the test pieces were assembled and bonded using a cyanoacrylate adhesive, commercially available as "Loctite Superglue" although initial tests were performed with epoxy adhesive ("Araldite Rapid") which required the stub faces to be machined with 0.5 mm deep grooves. Adhesives were allowed to cure in a alignment jig with a force of 1 kgf holding the stubs together. The assembled test pieces are shown in Figure 1 which depicts the two configurations used for this work. The type 2 specimen was developed to encourage failure in the lacquer or lacquer-tinplate interface by raising the stress on the lacquered side relative to the plain tinplate side. The cut edges of the

TYPE 1

Dimensions in mm

TYPE 2

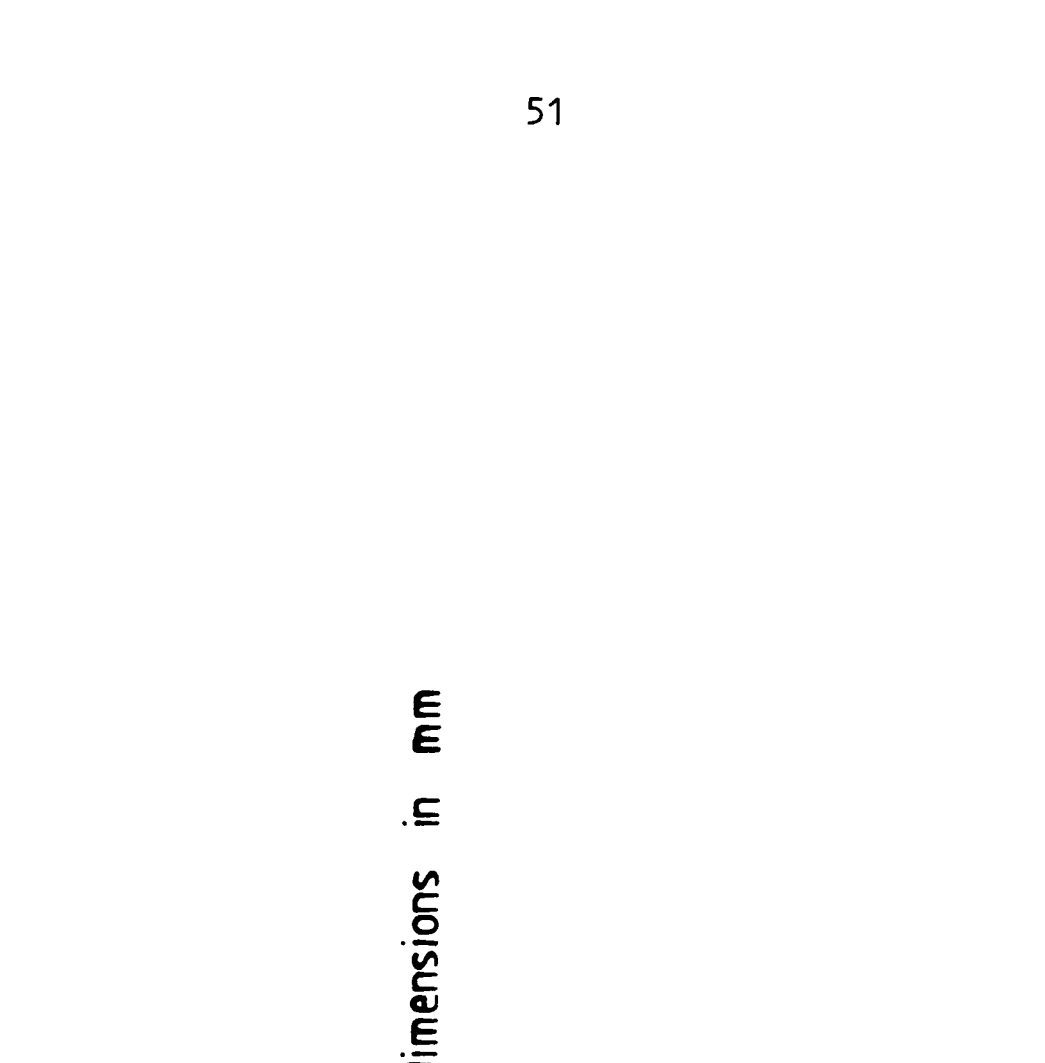

Figure 1. Butt-joint test arrangement

lacquered tinplate were also removed from the bond zone in the second configuration and in some tests with the type 1 configuration. A typical load displacement curve for the butt-joint test is shown in Figure 2 where the maximum load available was 5 kN, corresponding to a stress of 28 MNm^{-2} on the smaller stub face.

Experiments with a solid steel test piece showed that the compliance of the tensile testing apparatus was too high to yield accurate displacement measurements from the load-displacement graph as bond extension in the sample was small compared with the displacement of the machine.

Numerical values of failure load and percent lacquer removal are available from this type of test, the latter measured by placing a transparent grid over the fracture surface and counting the area of exposed tinplate. This approach measures the apparent area of lacquer removal and not necessarily the true area of bare tinplate since there may be thin lacquer layers remaining which, though invisible to the naked eye, can be revealed by microscopy or X-ray photoelectron spectroscopy.

The initial Scotch tape tests point to certain tinplates (especially KS 311) having poor adhesion properties with a variety of lacquers such that the adhesion of lacquer seems to be largely a function of the tinplate itself. This is not to say that lacquer adhesion is unaffected by other factors such as lacquering conditions or that a particular tinplate may not suit a particular lacquer or set of conditions, but that the tinplate surface structure may be a major factor in controlling adhesion.

Since residual stresses in coatings may have a major effect on adhesion, preliminary tests were carried out to determine, in a qualitative way, if these were present in the stoved lacquer layer. A lacquer coating was cut in a straight line and the underlying tin

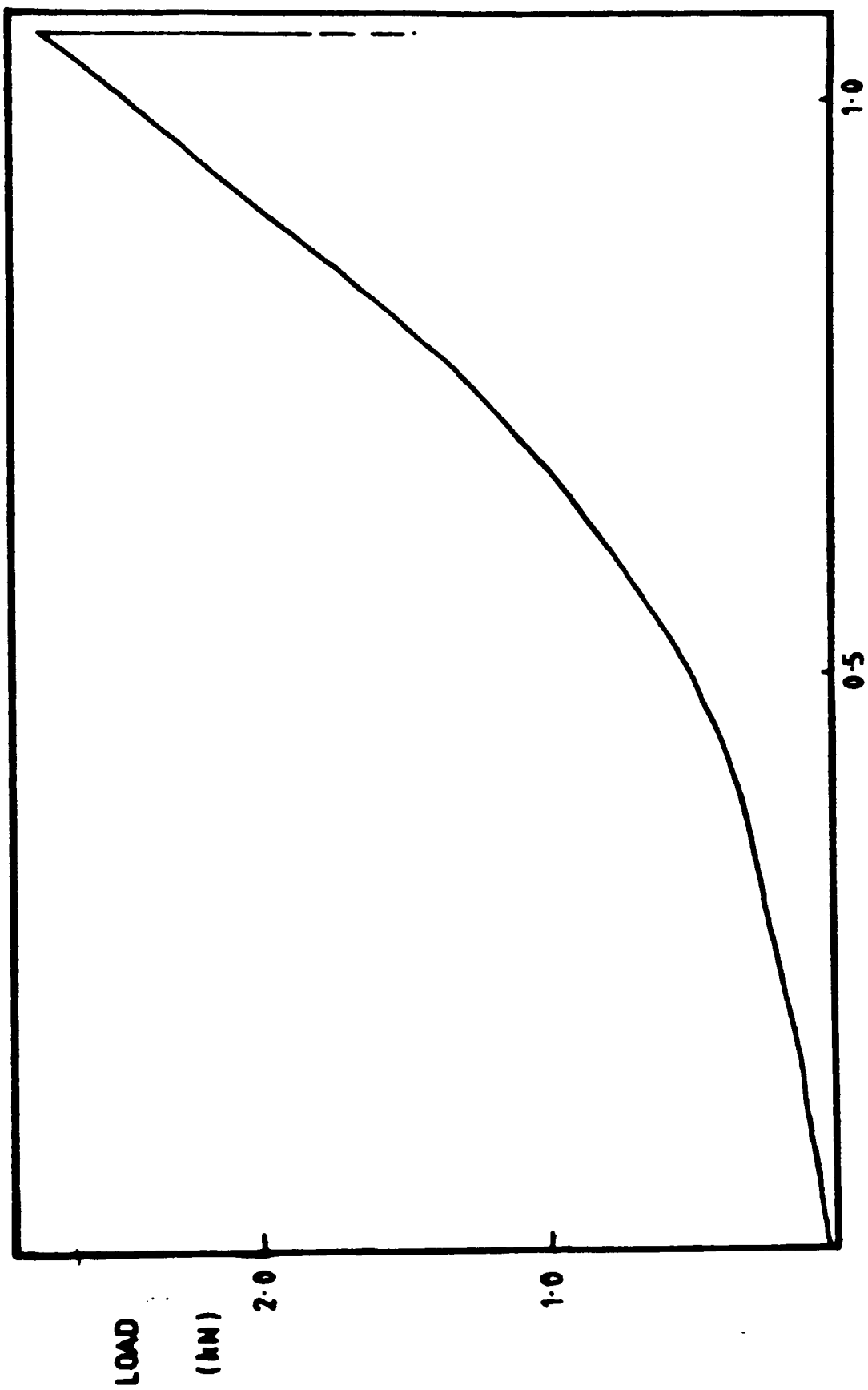

Figure 2. A typical load-displacement curve from a butt-joint test

and steel electrochemically etched to undercut the lacquer. Strong residual stresses in the lacquer would then have warped the free lacquer edges but since no such effect was observed, it was concluded that any stresses formed in the lacquer during stoving had been relieved.

Tensile testing was carried out with a crosshead speed of 0.5 mm min^{-1}, holding the test piece in universal joint grips to ensure alignment.

3. RESULTS

3.1 Butt-joint test

The variables (or'factor levels') investigated were tinplate type, stoving conditions and lacquer type. Table 2 lists the raw data of load to failure in kN and percent lacquer removed. Loads greater than 5 kN could not be measured by the Instron test machine but for the purposes of analysis were taken as 5.1 kN. The sample runs are categorised in Tables 3a and 3b by sample number and factor level where the former comprises data from a number of individual tests from a particular stoved lacquer tinplate. At least 10 specimens were prepared for a sample set but the number of results recorded is in some cases less than this, owing to the tests in which failure occurred in the adhesive rather than in the lacquer-tinplate bond. The failure stress and percent lacquer removal are plotted for each sample in Figures 3 to 6. The values of failure load are correct to ± 0.25 kN (5%) but areal lacquer removal values have errors of ± 10%.

Assessment of these test results on the basis of the means and standard deviations would lead to the conclusion that there is no strong correlation between lacquer adhesion (load to failure or percent

TABLE 2a

Load to failure and lacquer removal

in butt-joint adhesion tests

Sample	No. of obs	Observations (failure load in kN, % lacquer removed)
1	12	(1.5,60), (0.55,12), (0.65,50), (0.85,30), (0.75,65),(2.55,90), (2.7,90),(3.4,90),(2.05,90),(1.5,80), (2.5,-),(1.15,75)
2	10	(0.6,100), (0.7,100),(1.5,100),(1.65,50), (0.9,60),(1.7,60), (1.3,100),(0.8,90),(1.7,95),(1.7,50)
3	8	(3.5,-),(4.0,-),(3.4,-),(3.3,-),(4.5,-),(>5,-)*,(4.2,-), (3.2,-)
4	10	(>5,-)*, (4.2,-),(4.0,-),(3.6,-),(3.6,-),(4.3,-),(4.0,-), (3.6,-),(4.9,-),(3.9,-)
5	8	(1.7,85),(1.2,80),(0.75,45),(1.7,90),(1.35,75), (1.65,85), (1.15,90),(1.1,95)
6	5	(1.0,2),(1.55,20),(1.90,2),(1.4,10),(1.55,4)
7	6	(1.0,15),(1.0,20),(1.3,25),(4.4,85), (0.5,-),(4.9,90)
8	7	(2.95,45),(2.75,40),(1.8,25),(2.1,95),(1.65,20),(2.3,20), (3.45,60)
9	5	(2.05,5), (4.3,10), (1.7,5), (0.7,10), (3.0,10)
10	6	(1.8,20), (1.25,-), (1.25,6), (3.0,25), (3.95,15), (0.9,-)
11	5	(0.65,2), (1.15,2), (1.1,10), (1.3,2), (3.85,2)
12	2	(>2,5)$^{+}$, (>2,25)$^{+}$
13	8	(0.55,100), (0.9,100), (0.55,100), (1.20,95), (1.1,100), (3.1,75), (0.6,100), 1.45,100)
14	5	(0.95,100), (0.3,75), (0.1,100), (0.1,100), (1.95,95)
15	3	(1.55,30), (0.1,90), (0.45,60)
16	6	(3.05,15), (1.95,85), 1.85,85), (0.2,55), (3.1,55), (1.65,55)
17	5	(0.9,55), (1.5,90), (3.0,85), (2.65,25), (2.0,25)

'-' denotes a missing value * value '>'5 taken as 5.1 in the analysi

+ value '>2' taken as missing in the analysis

++ type T butt-joint test specimen

TABLE 2a (continued)

Load to failure and lacquer removal

in butt-joint adhesion tests

Sample	No. of obs	Observations (failure load in kN, % lacquer removed)
18	6	(1.45,-), (1.5,-), (3.15,-), (1.55,-), (1.1,-), (1.55,-)+
19	6	(3.1,-), 3.7,-), (2.6,-), (2.0,-), (3.25,-), (2.7,-)+
20	9	(3.4,-), (2.35,-), (2.80,-), (2.60,-), (2.20,-), (1.95,-)+ (1.90,-), (2.70,-), (1.45,-)
21	12	(2.35,-), (2.70,-), (2.5,-), (>5,-), (>5,-), (2.55,-) (3.70,-), (1.75,-), (3.65,-), (3.00,-), (1.90,-), 1.00,-)
22	5	(1.65,-), (2.30,-), (1.60,-), (1.25,-), (4.00,-)++
23	6	(3.50,-), (4.30,-), >5,-), (4.10,-), (2.85,-), (1.35,-)
24	2	(2.35,5), (2.35,2)+
25	8	(3.40,-), (3.20,-), (>5,-), (>5,-), (3.60,-), (1.60,-) (4.80,-), (>5,-)
26	4	(3.80,-), (2.80,-), (4.30,-), (>5,-)++
27	4	(2.60,-), (3.65,-), (2.05,-), (>%,-)++
28	12	*(>5,-), (>5,-), >5,-), (>5,-), (>5,-), (>5,-), (>5,-), (>5,-) (>5,-), (>5,-), (0.80,-), (4.20,-)
29	4	(1.65,-), (1.2,-), (2.6,-), (2.1,-)++
30	6	(2.60,60), (1.55,10),(0.5,5), (2.80,30), (1.30,10), (3.90,10)
31	5	((1.45,10), (1.10,2), (2.10,10), (2.30,10), (0.80,-)
32	13	*(>5,<5) - all 13
35	6	*(>5,75), (0.55,25), (0.65,50), (0.85,-) (0.30,40), (0.75,60)

'-' denotes a missing value * value '>5' taken as 5.1 in the analysi

+ value '>2' taken as missing in the analysis

++ type I butt-joint test specimen

TABLE 2b

Means and Standard Deviations of data in Table 2a

Sample	Failure load		Percent lacquer removed	
	mean	σn	mean	σn
1	1.68	0.90	66	25
2	1.26	0.43	80	21
3	3.91	0.63	-	-
4	4.12	0.50	-	-
5	1.33	0.32	81	15
6	1.48	0.29	7.6	6.8
7	2.18	1.77	28	31
8	2.42	0.60	44	25
9	2.35	1.22	80	25
10	2.02	1.09	17	70
11	1.61	1.14	3.6	3.2
12	-	-	-	-
13	1.18	0.79	96	8
14	0.68	0.71	94	10
15	0.70	0.62	60	25
16	1.97	0.97	58	24
17	2.01	0.76	56	28
18	1.72	0.66	-	-
19	2.89	0.54	-	-
20	2.37	0.55	-	-
21	2.94	1.21	-	-
22	2.16	0.98	-	-
23	3.53	1.20	-	-
24	-	-	-	-
25	3.99	1.18	-	-
26	4.00	0.83	-	-
27	3.35	1.16	-	-
28	4.67	1.19	-	-
29	1.89	0.52	-	-
30	2.13	1.08	21	19
31	1.55	0.57	8.0	3.5
32	5.1	-	>5	-
35	1.26	1.57	50	17

TABLE 3a

Classification of lacquered tinplate samples

A list of tinplate types, stoving conditions and lacquer types

FACTOR	1	2	3	4	5	6	7	8	9	10	11	12
Tinplate type (T)	NS 311	KS 311	BS 300	BS 311	NP	BS 311(A)	BS 311(B)	H300	NFB 300	BS 311(C)	BS311(D)	BS311(E)
Stoving Conditions (S)	Air std.	Air hot	Air + 13 daystg	Ar	Air pre-stove Ar stove	Air pre-stove Air stove						
Lacquer type (L)	epoxy-phenolic A	organosol	epoxy-phenolic B	phenolic A	phenolic B	oleoresinous	epoxy-phenolic C					

TABLE 3b

The Classification of Individual Sample Sets by Factor Level

Sample No.		1	2	3	4	5	6	7	8	9	10	11	12	13	14	15	16	17
FACTOR	T	1	1	1	2	2	4	4	5	3	3	3	3	3	4	4	2	2
	S	1	4	1	1	1	1	1	1	1	1	2	3	4	1	1	5	6
	L	1	2	1	1	1	1	3	2	3	2	3	3	2	4	4	2	2

Sample No.		18	19	20	21	22	23	24	25	26	27	28	29	30	31	32	35
FACTOR	T	7	7	7	6	7	7	4	6	8	9	6	10	6	11	6	1
	S	1	1	1	1	1	1	1	1	1	1	1	1	1	1	1	1
	L	5	5	5	1	15	5	1	6	6	6	6	5	6	7	6	1

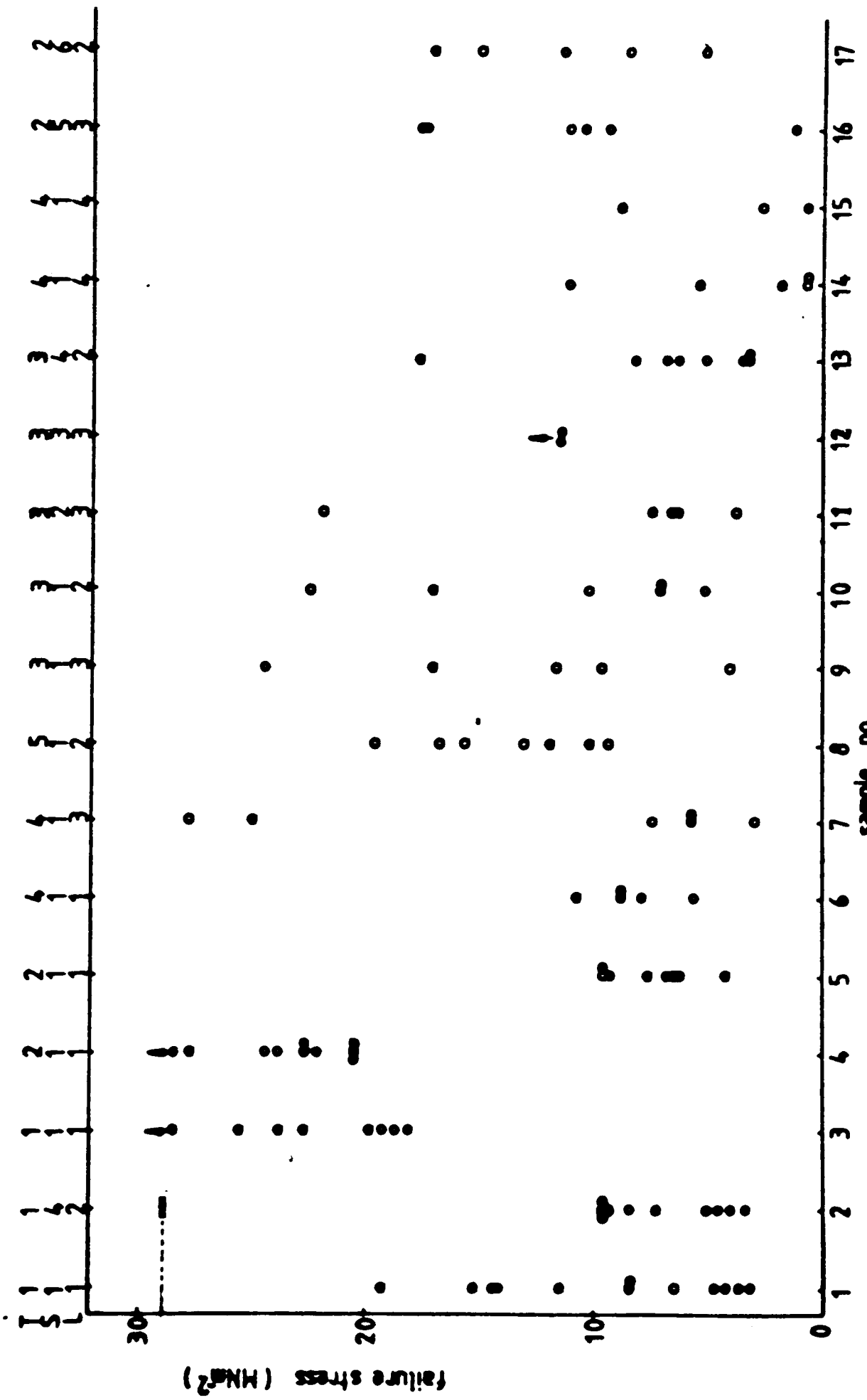

Figure 3. Butt-joint test results. Failure stress. (contd. in Fig. 4)

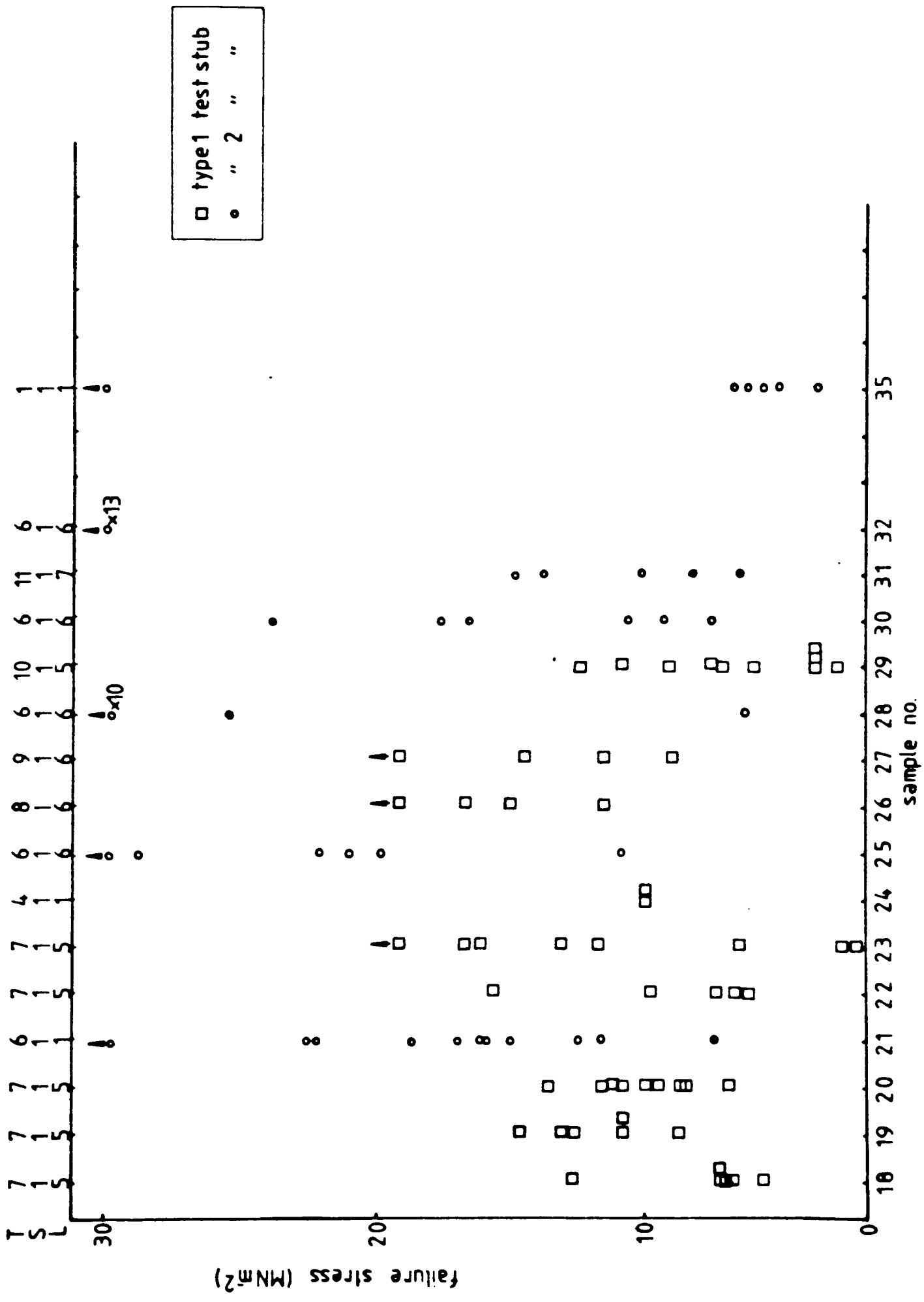

Figure 4. Butt-joint test results. Failure Stress

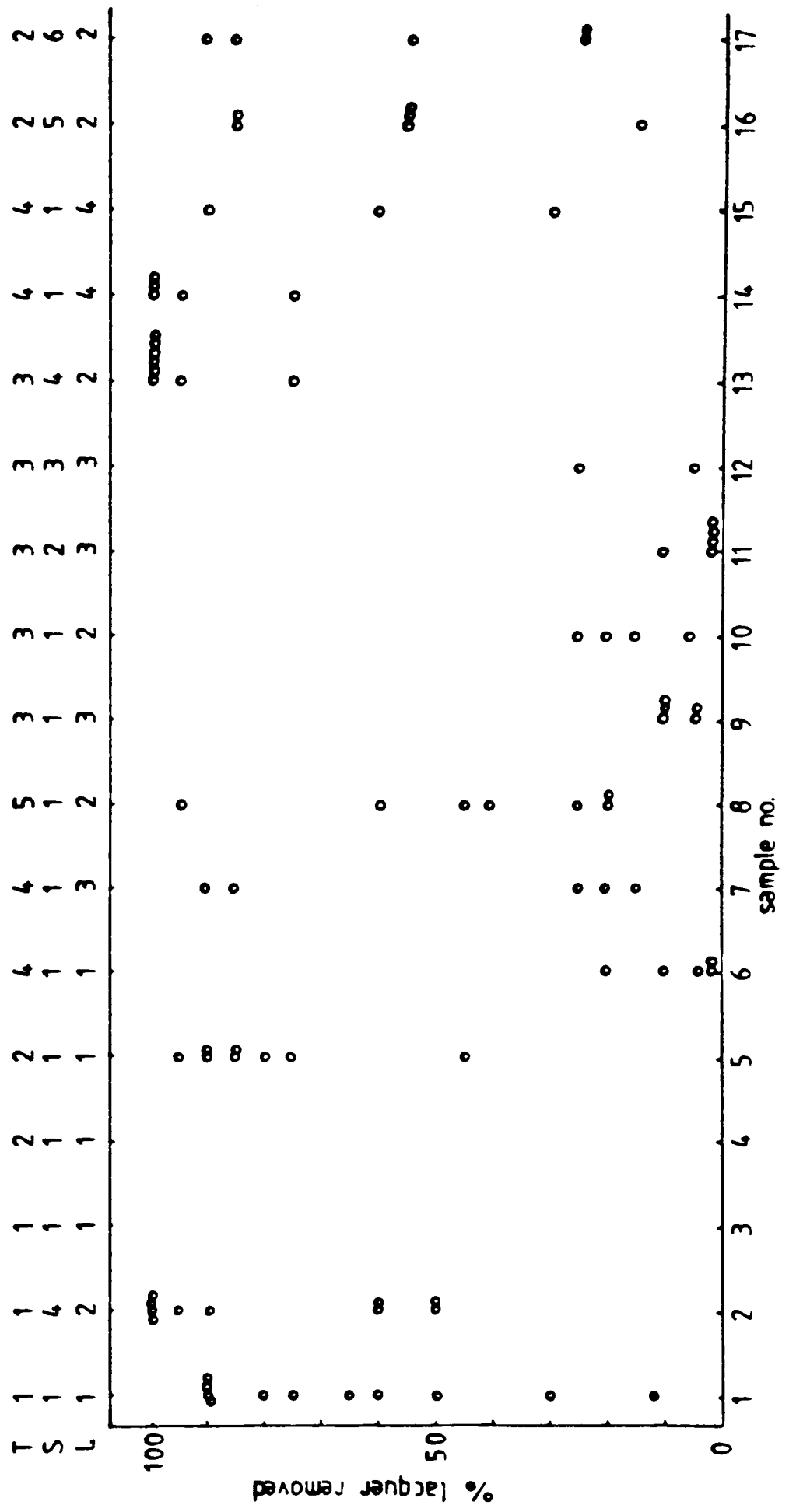

Figure 5. Butt-joint test results. Percent area lacquer removal (contd. in Fig. 6)

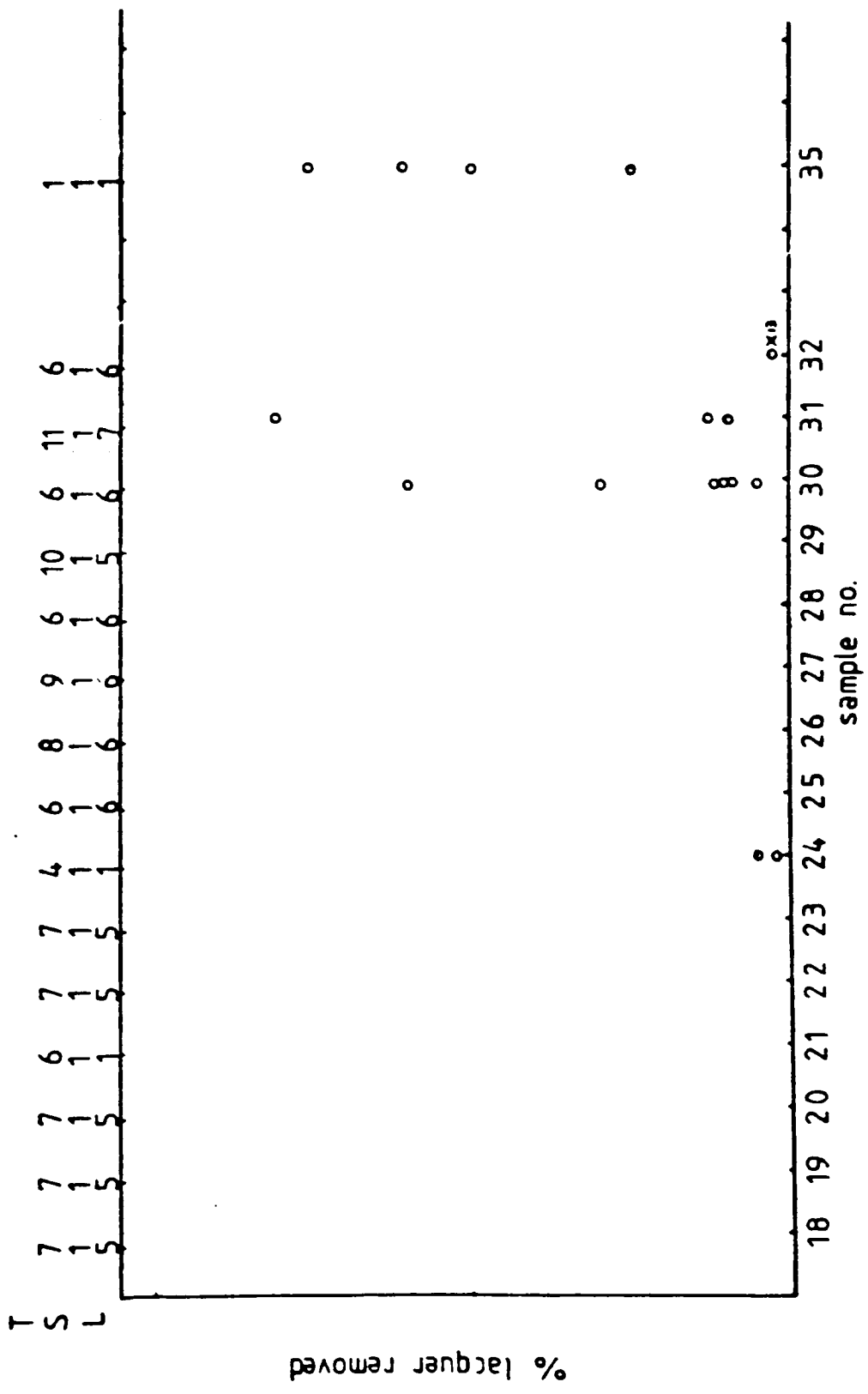

Figure 6. Butt-joint test results. Percent area lacquer removal

lacquer removal) and tinplate type.

These results were analysed by Mr. P.N. Appleby of Metal Box PLC. His report is included as Appendix 1 but his conclusion on fitting the values of failure load and areal lacquer removal to a function of the factor levels is:

"... that the bond strength test is capable of showing up differences between different tinplate samples, particularly with respect to percentage lacquer removed, but that the considerable within-sample variability in the data presents a serious practical drawback to its implementation for all but the crudest comparison."

The above conclusion, based on samples 1-17 forces a more detailed examination of the test results if this particular test is to be used to investigate lacquer adhesion with a view to grading adhesion properties to more subtle levels. The statistical analysis used above is hindered by the wide variability in test results available so further data were collected and the application of a bivariate function of a failure load and percent lacquer removal was investigated. Results from further tests (samples 18-35) were next examined; these include data from the type 1 butt-joint configuration and often omit values of percent lacquer removal as this qualtity was not measured in the earlier tests. For those sample runs which include the lacquer values it may be seen that the KS 311 tinplate, originally classified as having poor adhesion, tends to lose large amounts of lacquer in the test when coated with both epoxy-phenolic and organosol lacquers and that the BS 311 tinplate with nominally "good" adhesion mostly loses less than 30% of its lacquer.

Values of percent lacquer removal are plotted against failure stress in Figures 7 and 8. It can be seen that a correlation exists between the two parameters for some samples

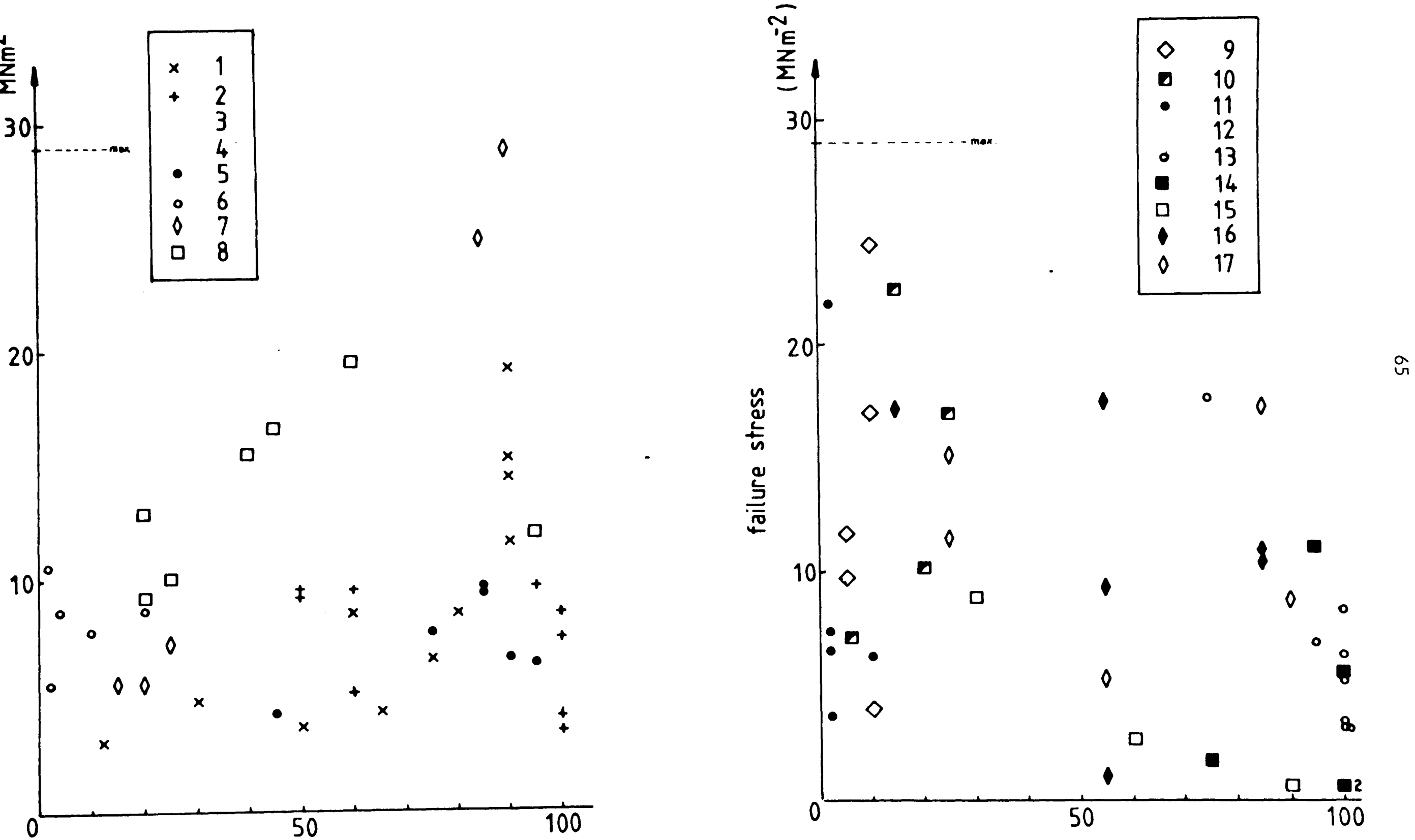

Figure 7. Plots of failure stress vs. percent area lacquer removal

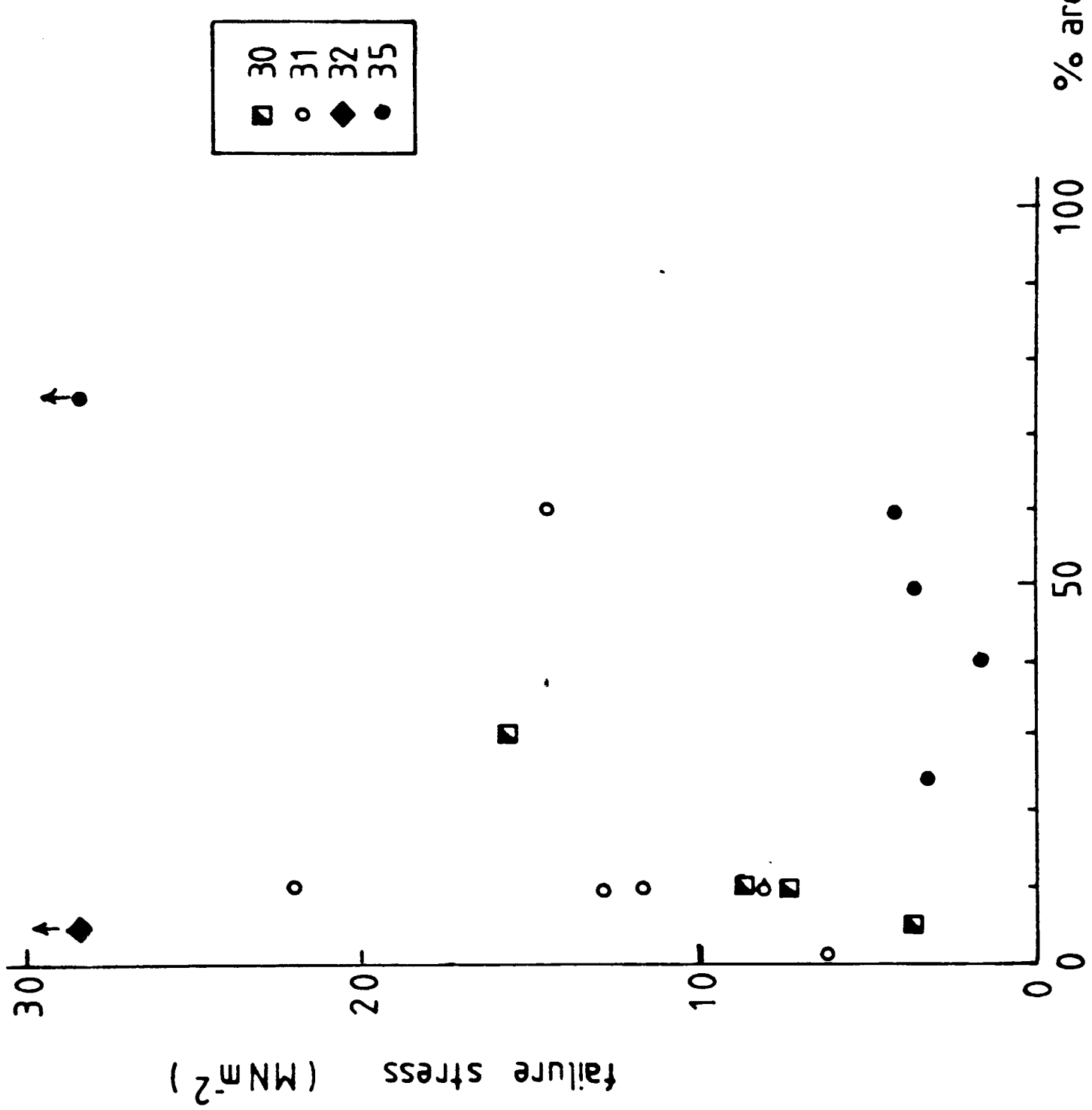

Figure 8. Plots of failure stress vs. percent area lacquer removal

such as 7, 9, 11, 30 and 31, where high failure loads tend to remove large amounts of lacquer. For other samples there is no clear relation between failure stress and percent lacquer removed as demonstrated by sample 16 or sample 14. For sample 15 a negative slope is evident.

Values of percent lacquer removed normalised to failure load are plotted in Figure 9 with their standard deviations. Percent area lacquer removed divided by failure load has been designated the 'area debonding factor' (ADF) and these values are seen to correlate with different tinplate types. BS 311 and BS 300 tinplates generally have low ADF values with small standard deviations despite a wide variation in failure load and lacquer removed. In the case of samples where failure load is not proportional to percent lacquer removal the standard deviations in ADF are, of course, much greater and this group of results includes the NS 311 and KS 311 tinplates which cannot be distinguished by ADF values although they are separated from the BS 311 and BS 300 tinplates on the ADF plot. That the BS 311 and BS 300 tinplates should be differentiated by ADF suggests that these lacquered tinplates fail by a different mechanism to those in which percent lacquer removal is not a function of failure load; this is discussed later. Effects due to stoving conditions are also clearly demonstrated in the ADF plot: BS 300 tinplate lacquered with organosol and stoved in air has a low ADF compared with a similar specimen stoved in argon (samples 10 and 13). Therefore, this type of plot demonstrates a distinct difference in the fracture of lacquered tinplate samples on the basis of tinplate type and stoving conditions. The question that now arises is: "What physical significance (if any) does ADF possess?". As ADF is percent lacquer removed, normalised to failure load it relates to the fracture propagation path in lacquered

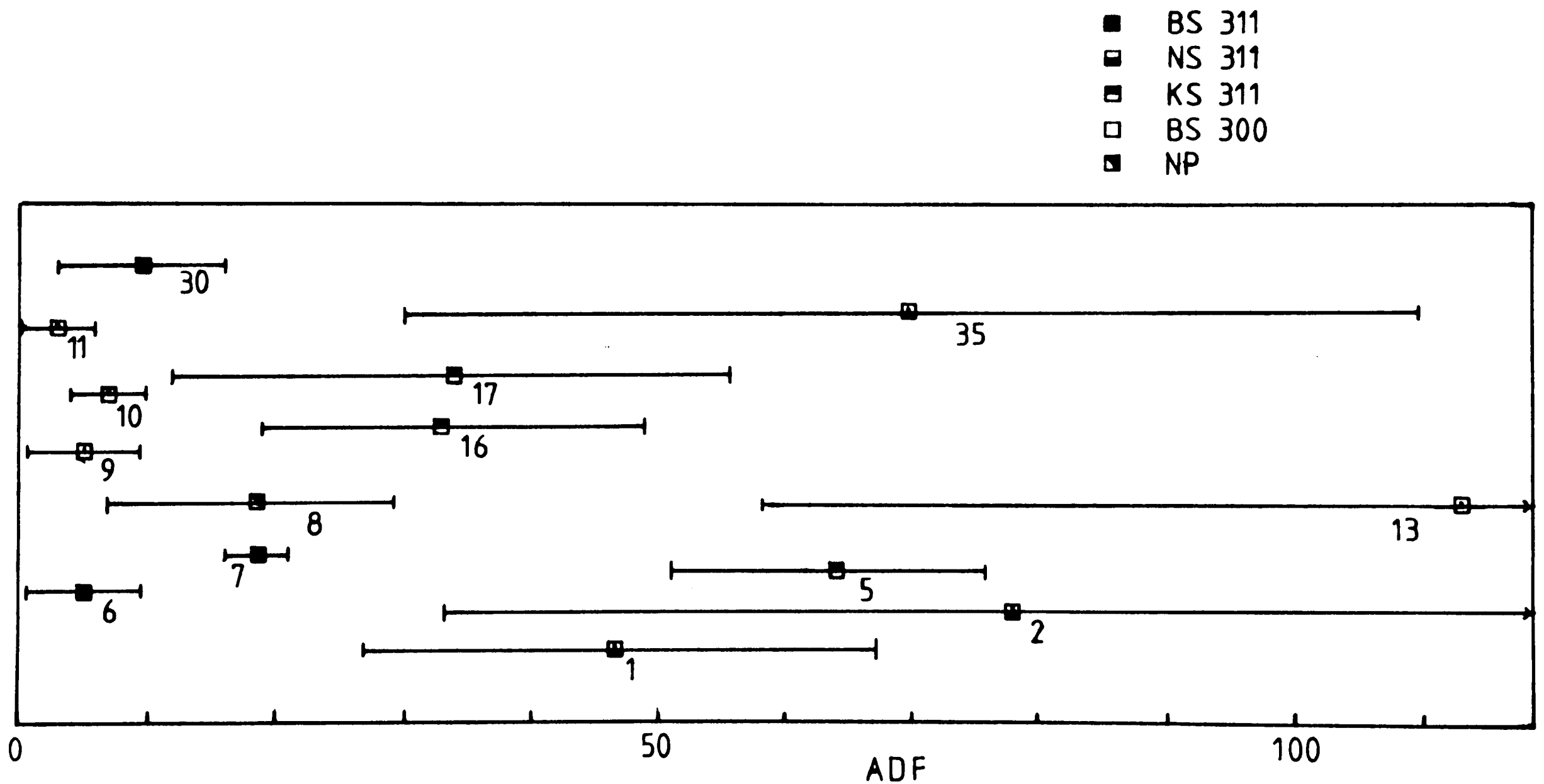

Figure 9. ADF plot (percent area lacquer removal/failure load) showing mean values and standard deviations

TABLE 4

AREA DEBONDING FACTORS

	Area debonding factors (% lacquer removed/failure load	mean	σ_n
1	40.00, 21.82, 76.92, 35.29, 86.67, 35.29, 33.33, 26.47, 43.90, 53.33, 65.2	47.1	20.0
2	166.67, 142.86, 60.67, 30.30, 66.67, 35.29, 76.92, 112.50, 55.88, 29.41	78.3	45.2
5	50.00, 66.67, 60.00, 52.94, 55.55, 51.51, 78.26, 86.36	63.7	12.5
6	2.00, 12.90, 1.05, 7.14, 2.58	5.1	4.4
7	15.25, 20.00, 19.23, 19.31, 18.37	18.4	1.7
8	15.25, 14.54, 13.89, 45.24, 12.12, 8.69, 17.39	18.2	11.3
9	2.44, 2.33, 2.94, 14.29, 3.33	5.1	4.6
10	11.11, 4.80, 8.33, 3.80	7.0	2.9
11	3.08, 1.74, 9.09, 1.34, 0.52	3.2	3.0
13	181.82, 111.11, 181.82, 79.17, 90.91, 24.19, 166.67, 68.97	113.0	54.6
14	105.26, 250.00, 1000, 1000, 48.72	(480.8)	(428.9)
15	19.35, 900, 133.33	(350)	(391)
16	4.92, 43.59, 45.94, (275), 17.74, 33.33	33.3	15.6
17	61.11, 60.00, 28.33, 9.43, 12.50	34.3	22.4
30	23.08, 6.45. 7.69, 10.71, 7.69, 2.56	9.7	6.5
31	6.89, 1.82, 4.76, 4.35	4.5	1.8
35	14.71, 45.45, 76.92, 133.3, 80	70.1	39.5

N.B. Extreme values of ADF in parentheses

is omitted

tinplate as well as fracture initiation. Samples with good adhesion properties will have low ADF values since the properties associated with good adhesion are both high failure load and low lacquer removal. Further examinations of fracture surfaces are required to identify the crack propagation paths, sites of initiation and mechanism of failure as this information will allow the different failure mechanisms to BS 311 and BS 300 compared with NS 311 and KS 311 suggested by ADF to be determined.

It should be noted that the 311 passivation treatment is not a prerequisite for good adhesion and that the unpassivated tinplate sample (sample 8) also possesses an ADF significantly better than some of the tinplates with passivation treatment. The main purpose of a passivation film is to protect the tin from oxidation although it is also required to have good lacquer adhesion properties. It is widely accepted (Albu-Yaron and Smith 1979, Azzeri et al. 1982, Takano and Watanabe 1980) that the passivation layer plays a role in lacquer adhesion and may affect it for better or worse. Despite the "311" categorisation of BS, NS and KS tinplates, it is by no means certain that their passivation films are identical since the electrochemical treatment may vary between different manufacturers (ITRI 1984). The passivation layer structure has been investigated here by X-ray photoelectron spectroscopy and transmission electron microscopy; the larger scale features of the tinplate surfaces and lacquered tinplate fracture surfaces are examined below.

3.2 Fractography and Topography

Typical examples of lacquered tinplate fracture surfaces from the butt-joint test are shown in Figures 10 and 11. The views are of several different tinplate lacquer combinations and illustrate the various types of fracture surface produced from the case of very

Figure 10. Fracture surfaces from the butt-joint test

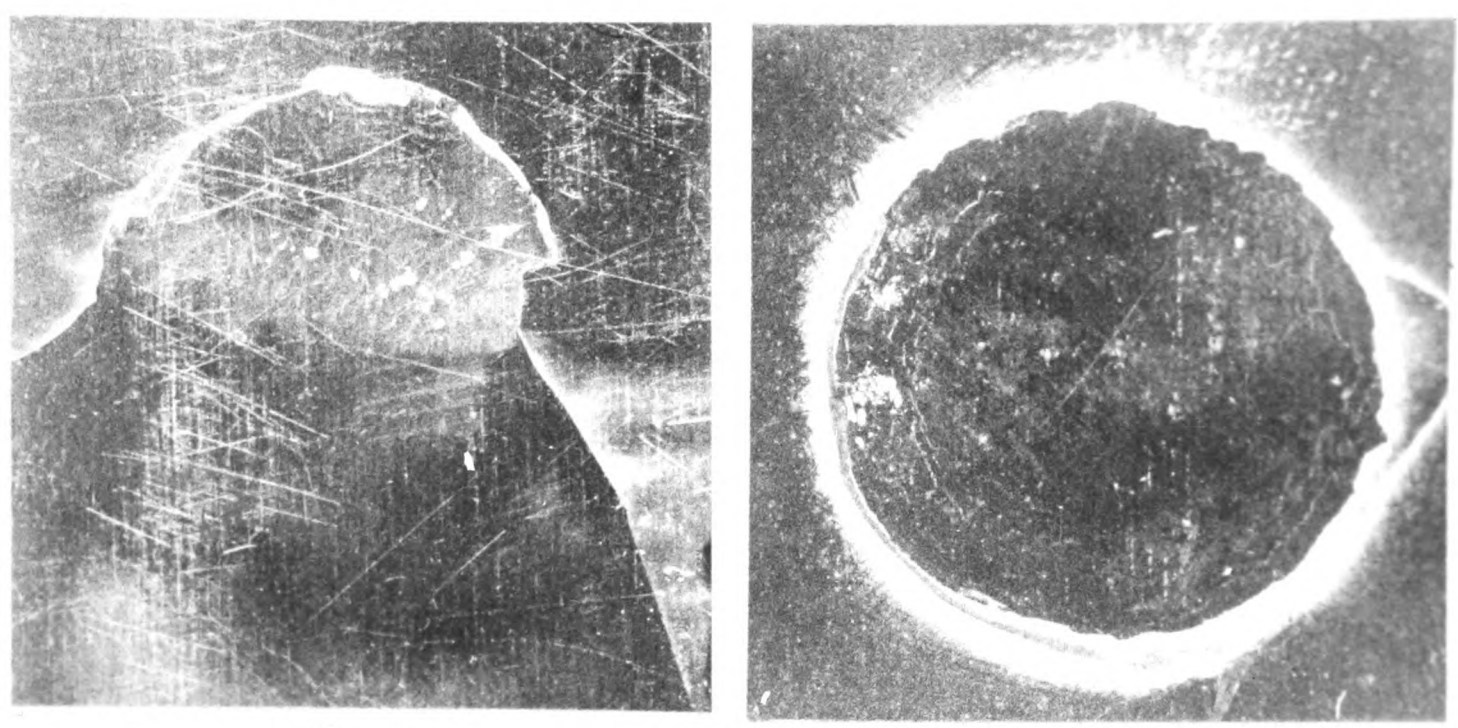
a
1·0 mm
b
c
d

Figure 11. Fracture surfaces from the butt-joint test

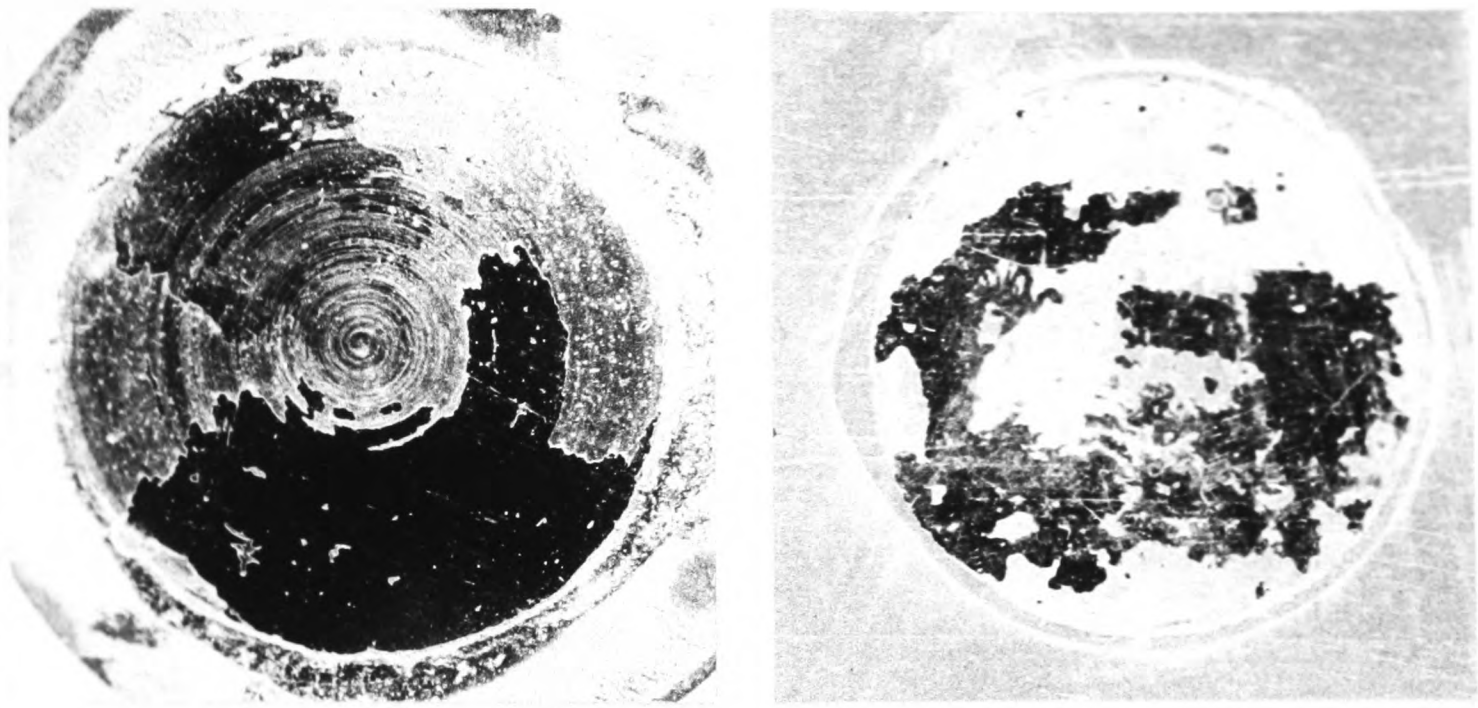

a

1mm

b

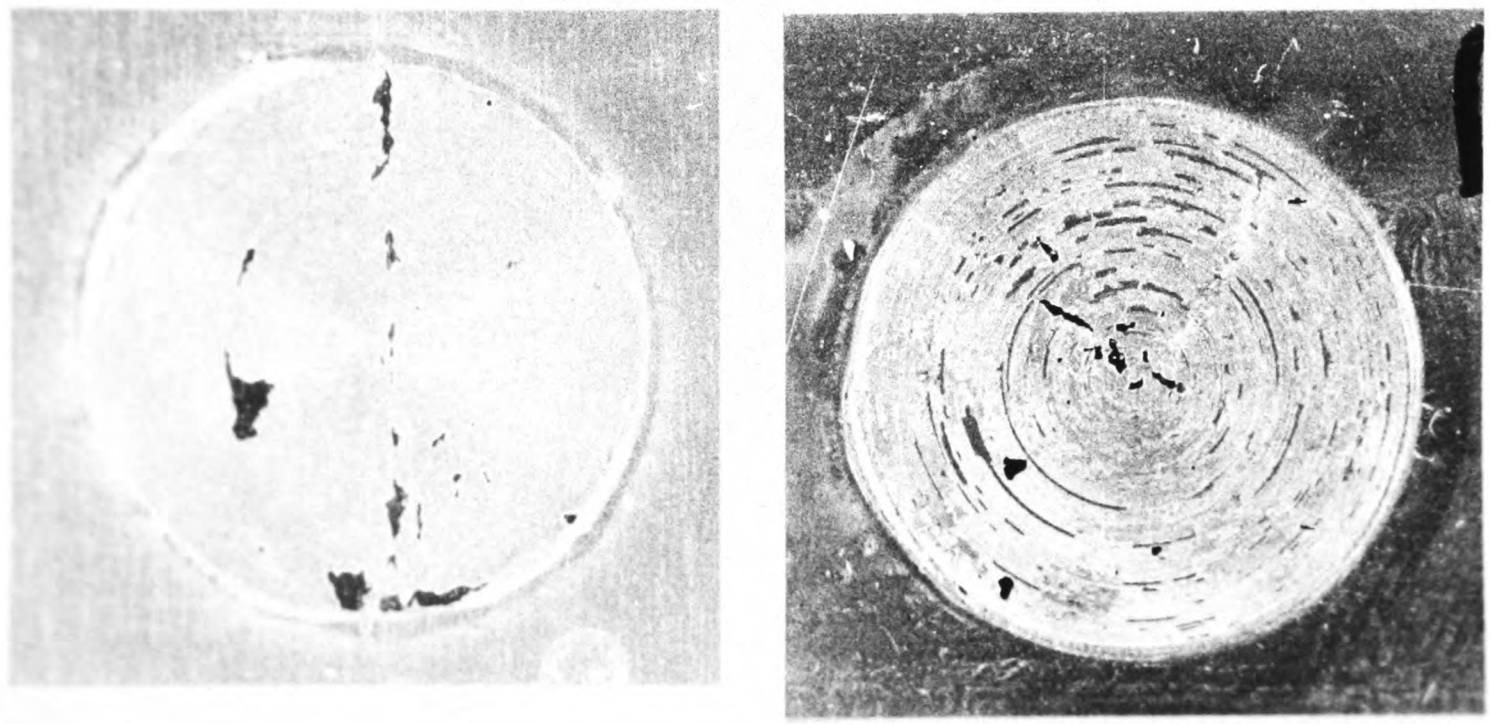

c

d

poor adhesion where lacquer has peeled beyond the bond zone of the butt-joint (Figure 10a) to the case of a sample with very little lacquer debonding (Figure 11d).

The tinplate samples and fracture surfaces have been examined so that each may be characterised in terms of their surface features. Optical microscopy with oblique illumination reveals the large scale topography. Micrographs of BS 311, NS 311, KS 311 and BS 300 are shown in Figure 12 (a to d respectively). The roughly linear surface features are due to the texture of the base steel strips which are made by cold-rolling. This is also shown quantitatively by profilometer traces in Figure 13. The profilometer draws a sharp needle across the specimen surface and draws a magnified trace of the needle tip displacement. Figure 13 reveals that the BS 311 tinplate has smoother and shallower ridges across the rolling direction than either KS 311 or NS 311 but this is not suspected of having a gross effect on lacquer adhesion; on the one hand, rougher surfaces might be expected to increase adhesion by mechanical keying or, on the other hand, reduce it by preventing the lacquer, when first applied, from penetrating the deeper valleys and result in air entrapment. The latter effect is unlikely since the "valleys" are tens of microns wide and a search for such a phenomenon by optical microscopy and electron microscopy of fracture surfaces did not reveal a single example. Packham (1983) had proposed that air entrapped at a polymer-metal interface would actually increase adhesion but he has investigated air bubbles with larger dimensions than those postulated here.

Between the tin and the steel there is a layer of $FeSn_2$ crystallites, usually referred to as the "alloy layer" which is produced during the heating in the flow-brightening process. The $FeSn_2$ crystallites are typically 1 μm long and 0.1 μm wide and are found closely-packed

Figure 12. Optical micrographs of tinplate surfaces.

Oblique illumination

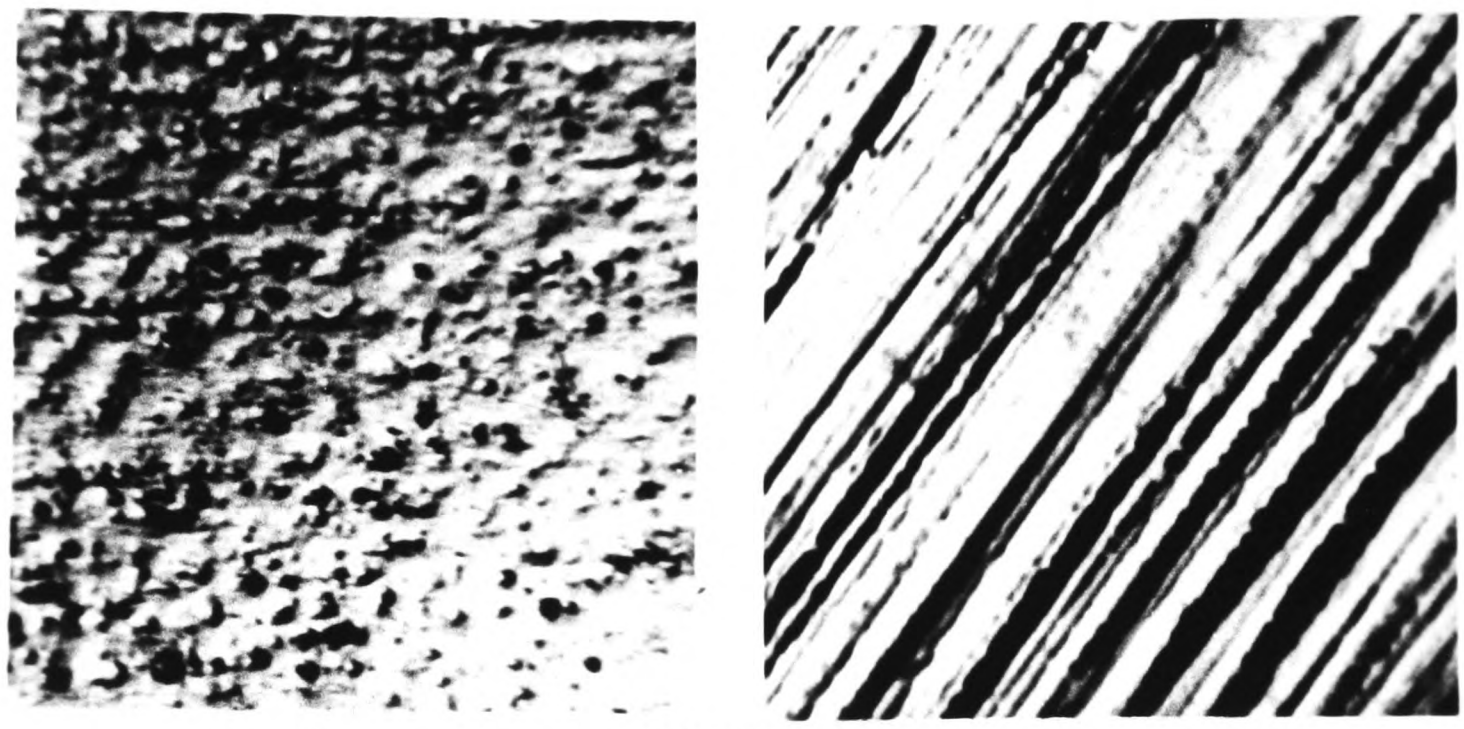
a
0·1 mm
b
d
c

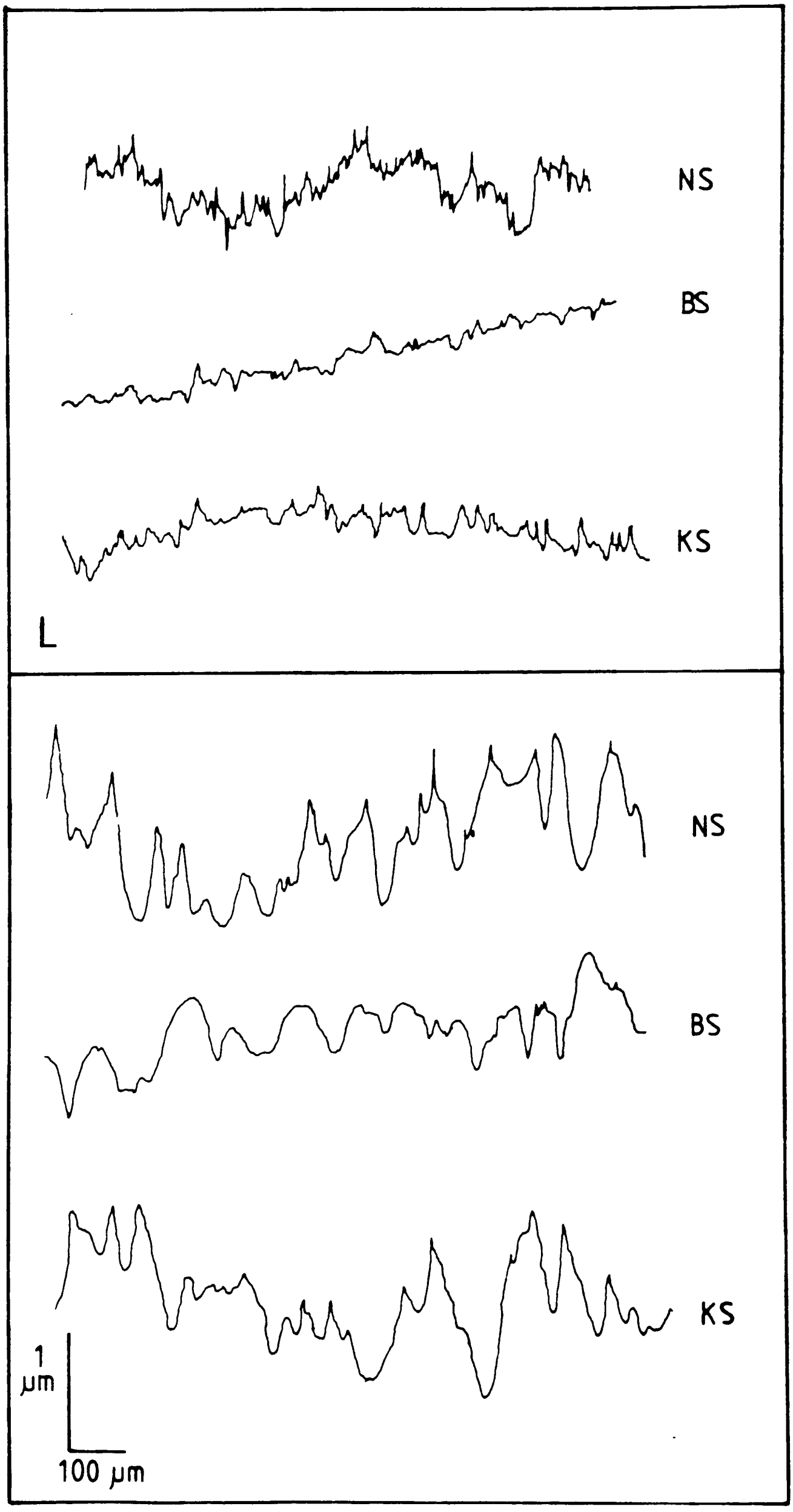

Figure 13. Profilometer traces across the rollink direction for BS311, NS311 and KS311 tinplates.

on the steel surface when the tin is removed by a chemical etch. The development of the alloy layer during flow-brightening is shown in Figure 14. Samples of tinplate were subjected to different durations of flow-brightening and then etched with iodine in methanol solution to remove the tin; scanning electron micrographs are shown where flow-brightening time increases from zero (a) through the normal treatment (c) to a longer than normal treatment (d). The BS, NS and KS tinplates all possessed alloy structures similar to Figure 14c where the different orientations of crystallite groups is due to their growth on grains of different orientations in the polycrystalline steel substrate (Barry and MacKay 1972). The cubic grain in Figure 14c is a tin iodide crystal and results from the etching process. If individual $FeSn_2$ grains protrude through the tin surface or if whole regions are exposed by corrosion or extreme flow-brightening these will affect the surface structure of the tinplate as experienced by a lacquer coat and may affect adhesion. Such regions on fracture surfaces are examined to see if they have influenced the fracture paths.

Neither the $FeSn_2$ layer nor the large scale topography of the tinplates examined reveal differences which are expected to account for the differences in lacquer adhesion between the sample sets. Scanning electron micrographs of the fracture surfaces, however, reveal striking differences between the BS 311 and the NS 311/KS 311 tinplates. Regions where the lacquer has been removed from the tinplate surface are shown in Figure 16 for KS 311 (a) and BS 311 (b) where the marker bars indicate 2 μm. Further areas for BS 311 are shown in Figure 15.

These specimens have organosol lacquer coatings but similar observations hold true for other lacquer types.

Figure 14. Scanning electron micrographs showing the development of the $FeSn_2$ layer with increasing flow-brightening time.

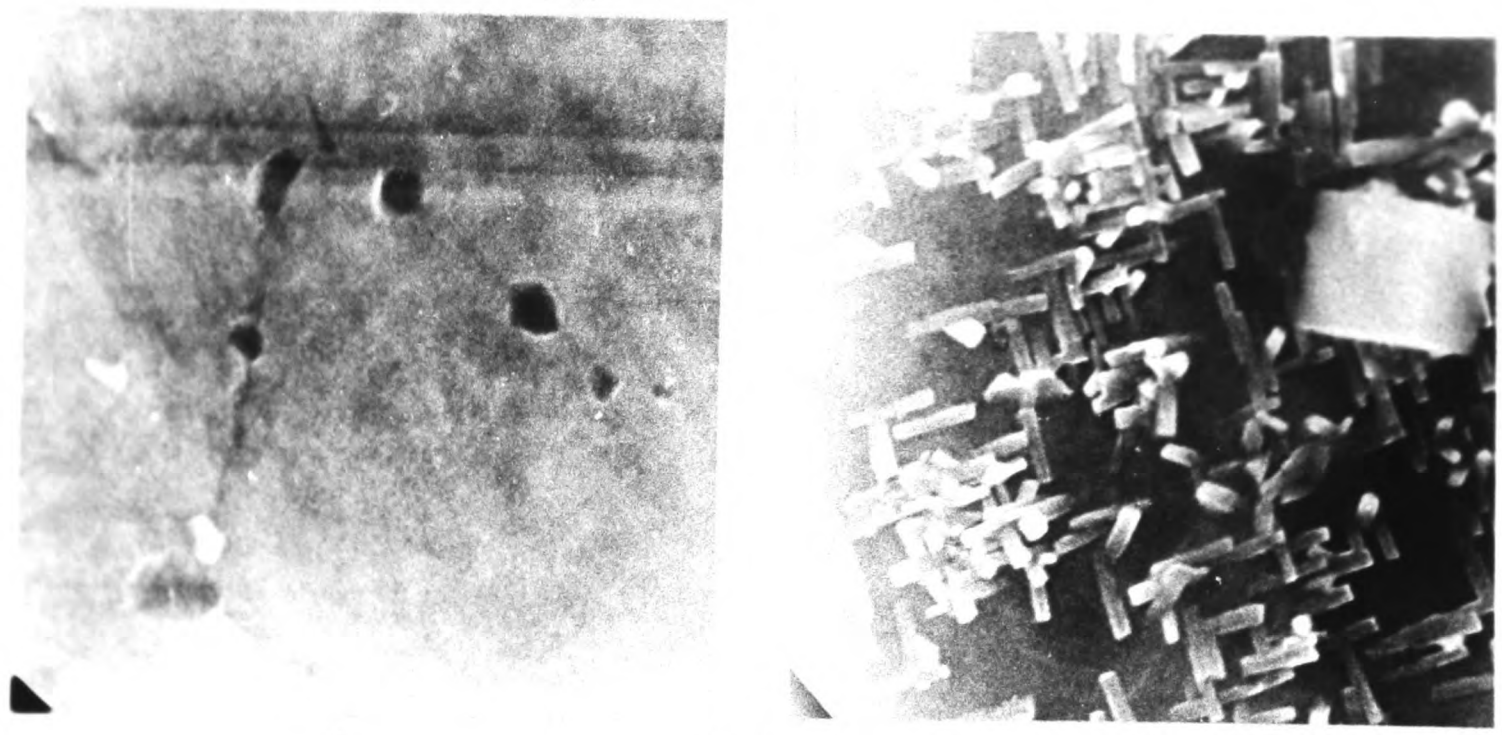
a
1 μm
b
c
d

Figure 15. Scanning Electron micrographs of fracture surfaces. BS 311 sample. a and c, lacquer islands. b, lacquer edge, d, thin lacquer layer.

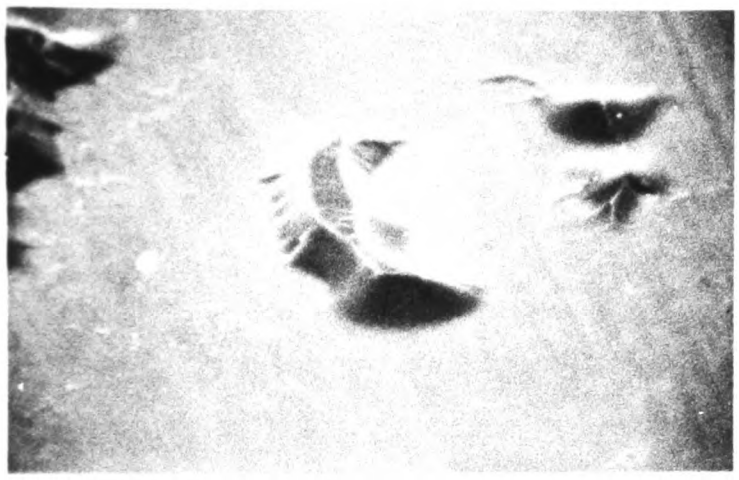

50 μm a

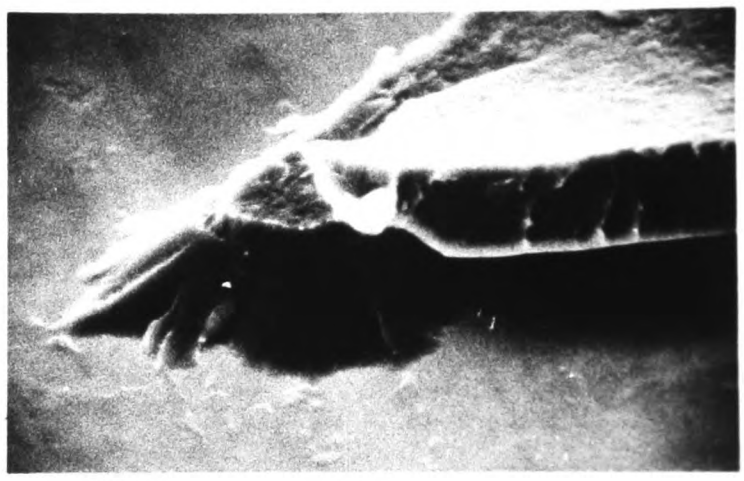

10 μm b

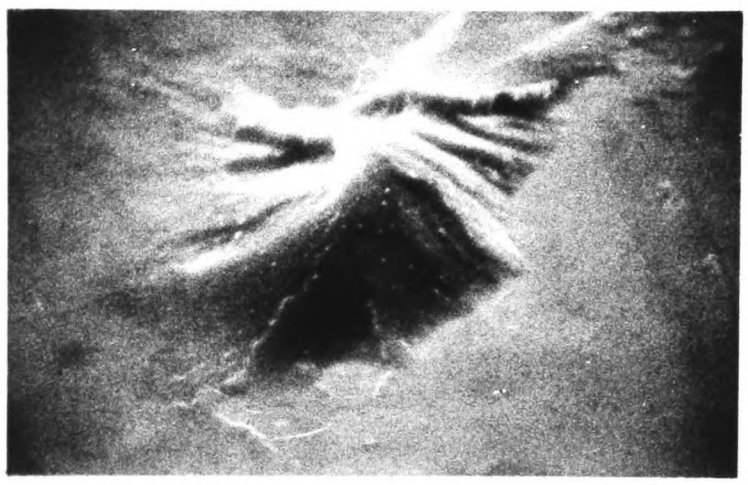

10 μm c

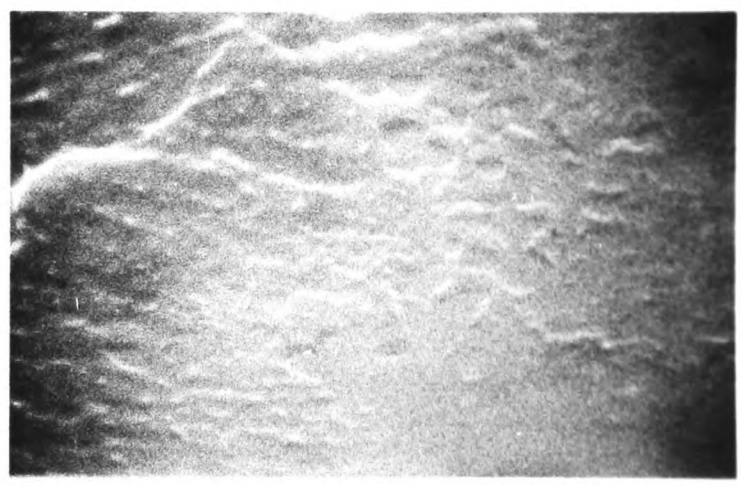

1 μm d

The regions of lacquer remaining on the surfaces of NS 311 and KS 311 tinplates were left as large sections with a definite demarcation between the bare tinplate and the fractured edges of lacquer which exhibited clear fracture markings typical of brittle failure. The BS 311 fracture surfaces were different, with the remaining lacquer in the form of well-separated "islands" (Figures 15a, c). The edges of the remaining lacquer on BS 311 were less steep than those seen on NS and KS tinplates, often spreading out to form a very thin layer of lacquer which extended for several mm beyond the apparent edge of the fractured lacquer edge. This thin layer of lacquer was not visible with the naked eye but is shown in a scanning electron micrograph (Figure 15d). Optical microscopy (Figure 17) shows this more clearly and also shows up fracture markings caused by the propagating crack better than a secondary electron image.

For lacquered BS 311 tinplate, the crack tends to propagate more through the lacquer than is the case for KS 311 and NS 311 tinplates. The fracture is not totally cohesive, however, with regions of bare tinplate visible on the failed surfaces. Common features of the BS 311 fracture surfaces, especially on samples with less than 20% apparent lacquer removal, are roughly circular areas of bare tinplate approximately 0.2 mm in diameter surrounded by a thin lacquer film. The definition of "bare" here is for no lacquer to be detected by optical or electron microscopy. In every case there is a defect at the centre of each area. These defects are typically 1 μm or 2 μm wide and are angular, steep-sided pits in the tin coat (Figure 18) in which is visible the $FeSn_2$ layer; they are quite distinct from other regions on the tinplate where the $FeSn_2$ layer has grown through the tin during flow-brightening and which do not appear to affect the fracture path or correspond to areas of lacquer removal. The angular

Figure 16. Scanning electron micrographs of fracture surfaces.

a/ KS 311, b/ ØS 311

bar = 2 µm

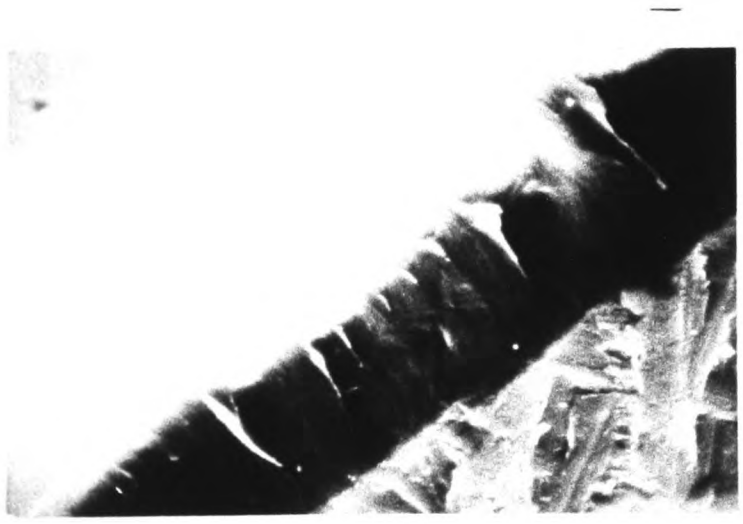

b

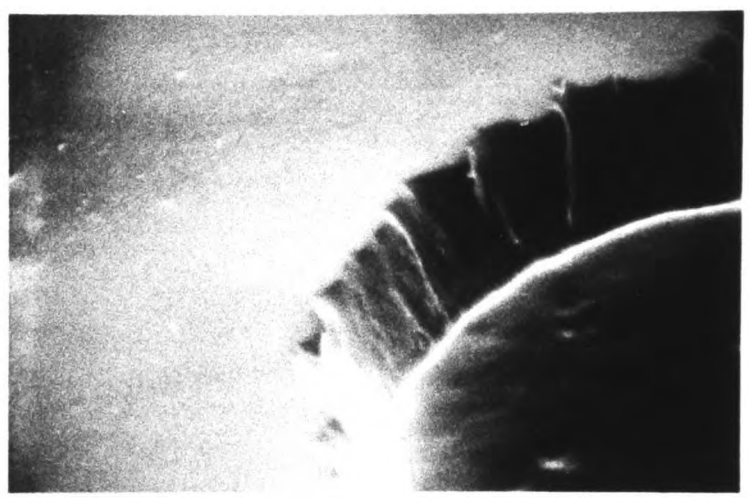

a

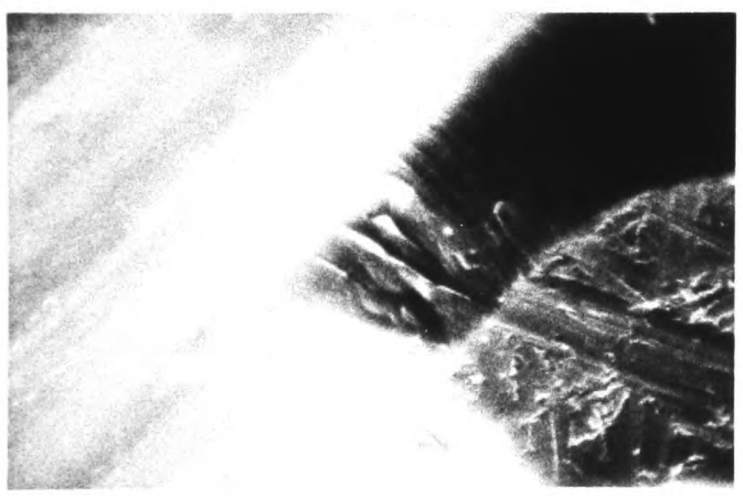

Figure 17. Optical micrographs of BS 311 fracture surfaces.

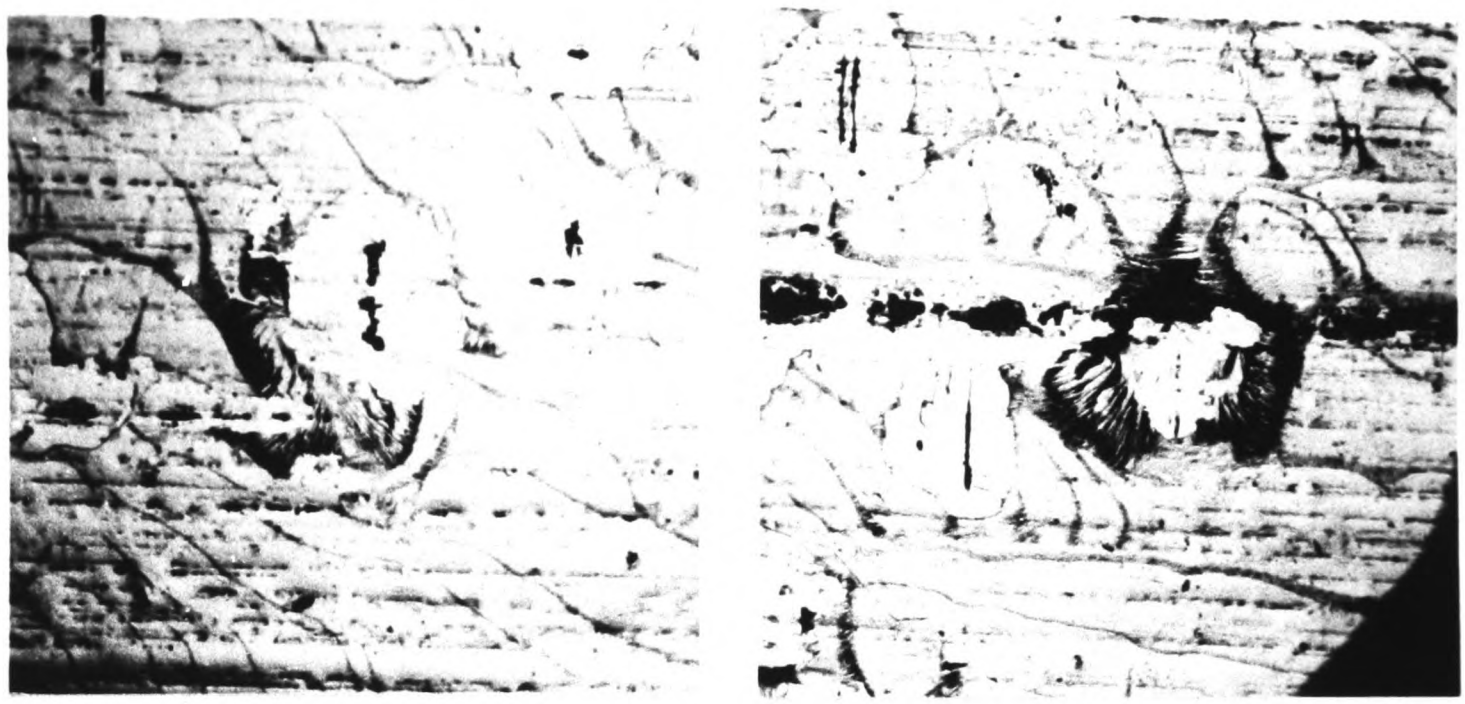

a

0·1 mm

b

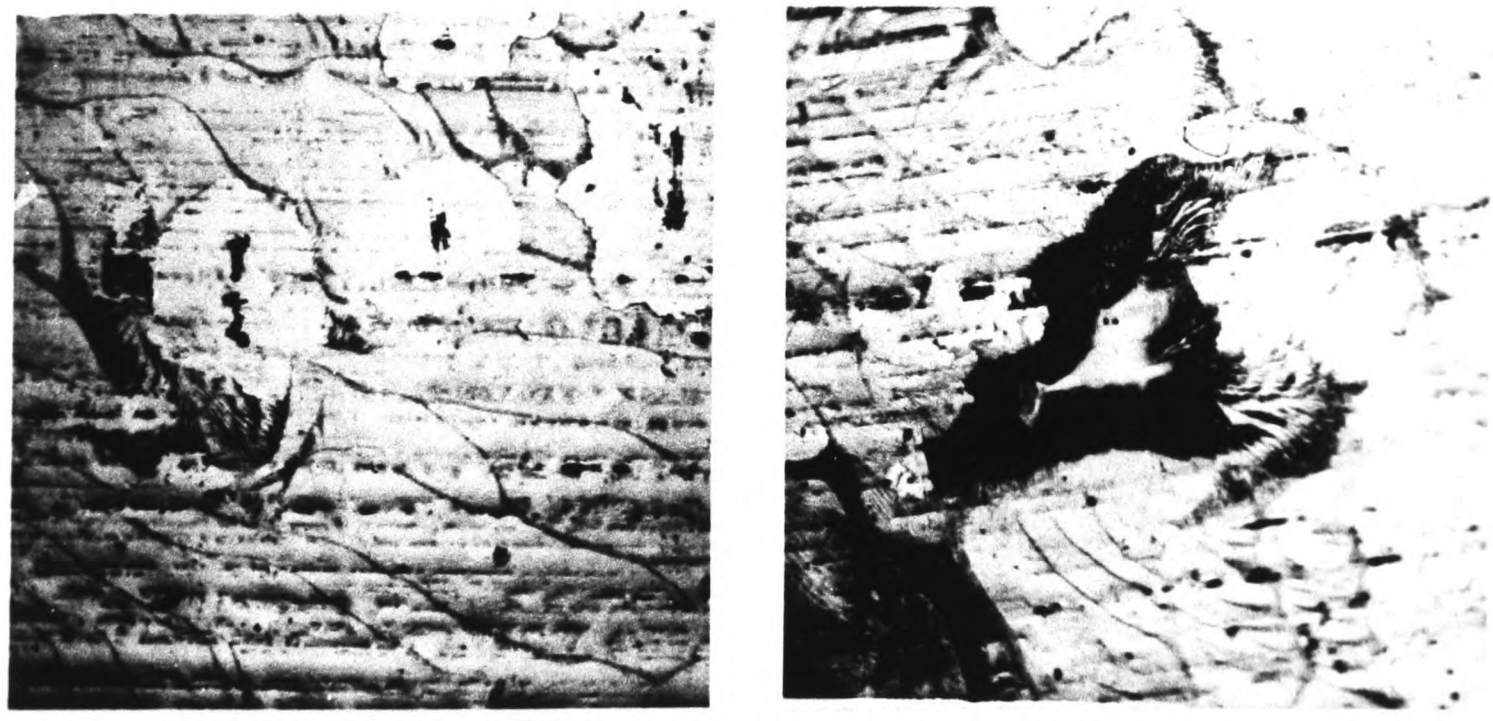

c

d

defects are visible on stoved and unstoved tinplates of all types before and after lacquering and also on unpassivated tinplates. They can also be observed under the thin lacquer layers on fracture surfaces but, in every example observed in this work, one of these defects is found at the centre of every circular debonded zone. In total, some 10 BS 311 samples were examined, each of which possessed over 50 of the circular lacquer debonded zones; BS 311 fracture surfaces with high levels of lacquer removal did not exhibit them.

The fracture markings on the failed specimens may be used to identify the direction of crack propagation (Kies et al 1950, Andrews 1968, Chau and Li 1982, Atsuda and Turner 1982, Kinloch and Young 1983). As the failure of a butt-joint test is a catastrophic process, the initiation point should be located to see if it lies in the passivation layer, the lacquer or at the specimen edge. If initiation starts from within the lacquer tinplate system then the butt-joint test is revealing information about that system but if the fracture originates from elsewhere, then the test becomes less useful as a means of scientific evaluation although the propagating crack presumably moves along the weakest path available so the determination of the fracture propagation path would also reveal useful information about lacquer adhesion and possible weak interfaces or layers.

The principle fracture markings observed fall into two categories: a) river markings around the edges of major features on the fracture surfaces and b) more widely-spaced networks of linear marks, spread over the flat surfaces of the thin lacquer layers. The linear marks are typical of stick-slip and do not seem to be Wallner markings (Smelt 1979) produced by the interaction of reflected shock waves. These markings have some interactive element and in places become inextricably tangled. The river marks may be interpreted as the

Figure 18. Scanning electron micrographs of the $FeSn_2$ defects found at the centre of lacquer-free zones.


070080 10KV X2.00K 15.0um

a

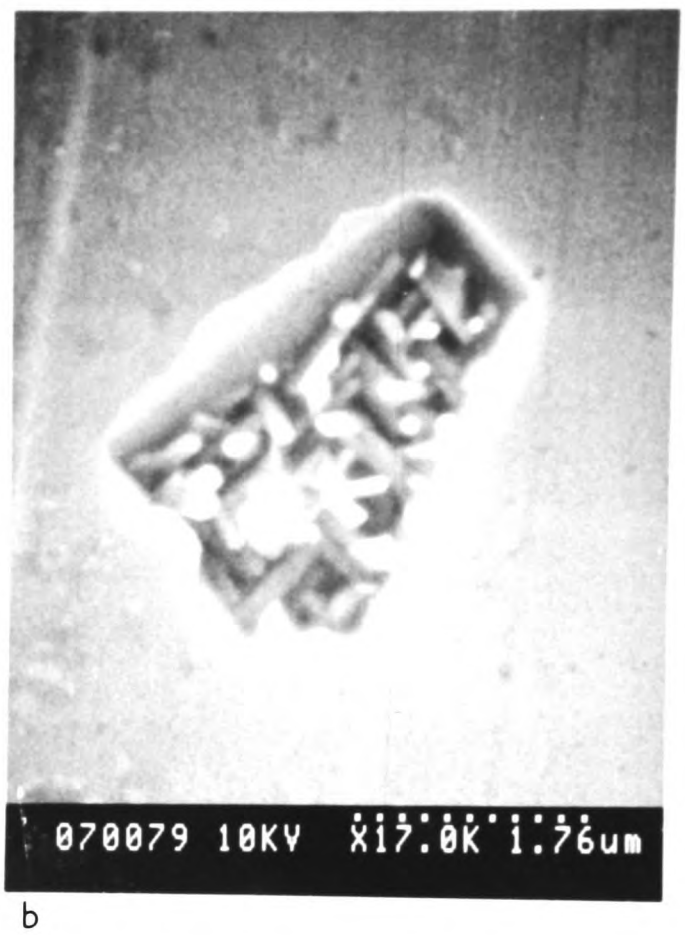
070079 10KV X17.0K 1.76um

b

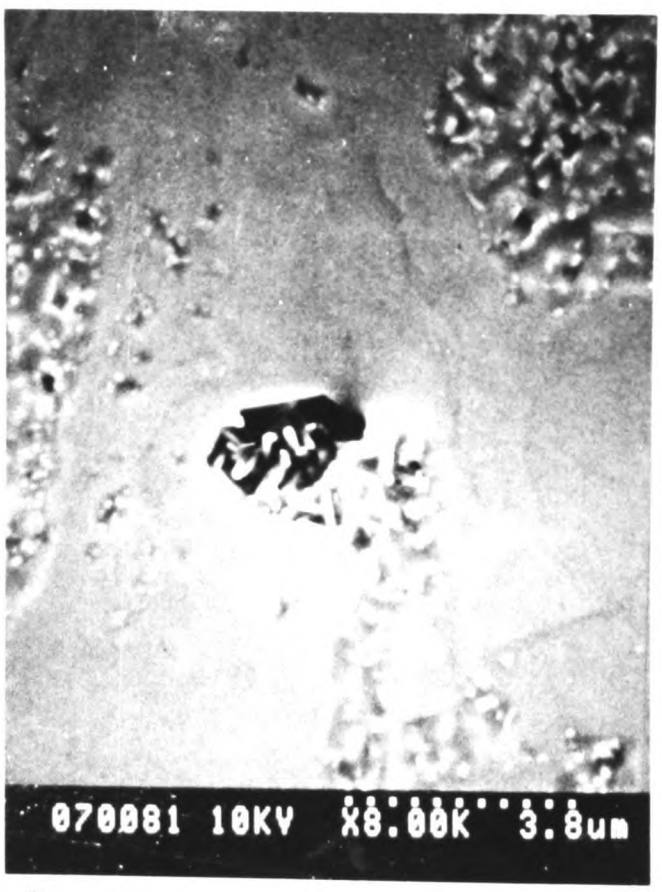
070081 10KV X8.00K 3.8um

c

domination of one running fracture line over another so that the marks coalesce; the direction of propagation is therefore along the direction of coalescence. Stick-slip bands also indicate the direction of crack movement which is perpendicular to the main banding and in the direction of the "feathering" which emanates from one side.

Figure 17 shows optical micrographs of the fracture markings in the lacquer around the lacquer-free zones and around the lacquer islands. On the surface of some of the islands is a layer of the adhesive used to bond the specimen to the test stubs. The fracture path is extremely complicated, often running from one interface, through a bulk or weak boundary layer, to another interface. Scanning electron micrographs in Figure 19 show one of the circular lacquer-free zones (a) and the edges of the fractured lacquer. Examination of the river markings on the edges of lacquer around the circumference of the fractured surface reveal that the fracture has run from the tinplate upwards towards the stub in all the specimens examined and that fracture had therefore initiated within the specimen and below the lacquer. Further evidence for the fracture running up the lacquer edges, away from the tin surface, is shown in Figure 19b where plastically deformed spikes are visible on the lacquer edges. These spikes have been drawn out in the direction of crack propagation; a schematic drawing of the features in Figure 19b is shown in Figure 19d.

The fracture markings left on the thin lacquer layer on the BS samples allow the propagation direction of the crack front across the fracture surface to be determined. Stick-slip marks are found on the thin layers and river marks on the thicker regions. When two or more lacquer-free zones are found in close proximity there is sometimes a thick lacquer ridge lying between them with river markings which indicate fracture running up to the top of the ridge. This is shown

Figure 19. a/ lacquer-free zone on BS 311 fracture surface
b/ plastically-deformed spikes on lacquer edge
d/ lacquer edge c/ schematic of b/.

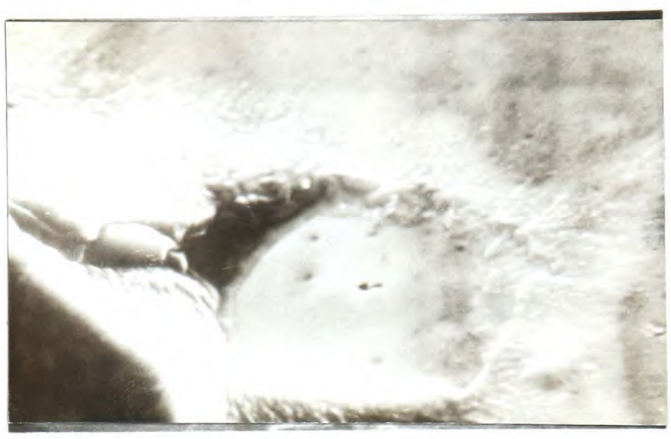

a

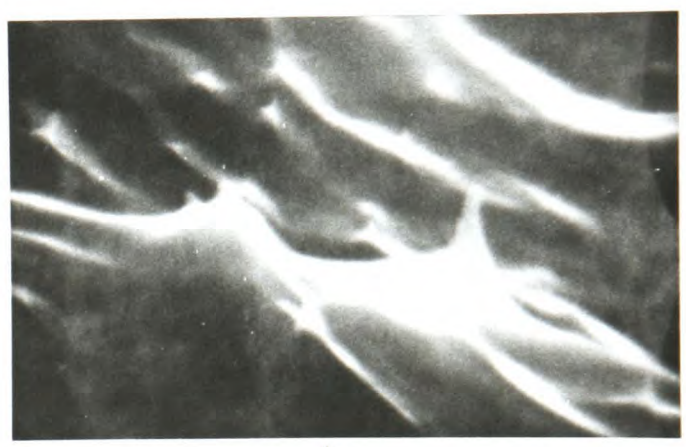

b

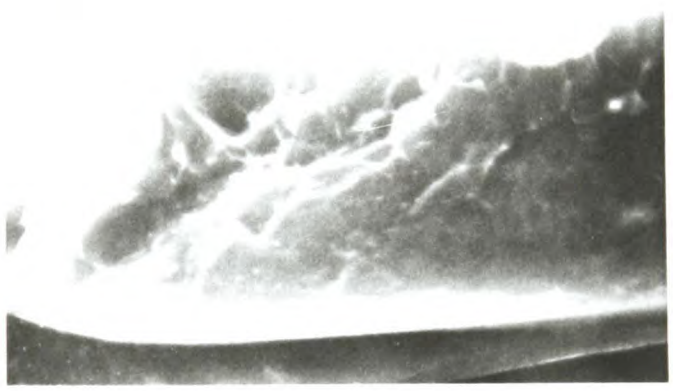

d

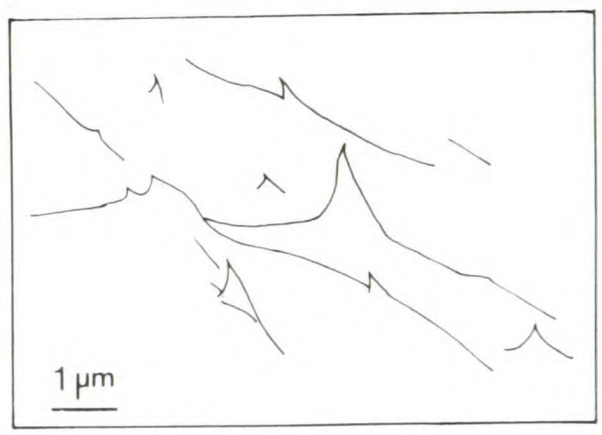

c

schematically in Figure 20. Thus, there is strong evidence for fracture initiation from within these lacquer-free zones, possibly from the central defect. The evidence of the stick-slip marks, however, shows that there is also an approximately linear crack front running across parts of the lacquer surface. If this linear crack had caused secondary initiation at the tinplate surface defects as it moved through the sample there would be a marked interaction (Andrews 1968) causing the stick-slip bands to curve around the secondary fracture and since this is seen in some but not all cases (see Figure 17) it must be assumed that for the BS samples at least, there is a complex fracture mechanism where there is secondary and possibly primary initiation at the lacquer-free zones. Such zones may have been debonded before testing (perhaps by corrosion products if the central defect is a corrosion pit) or may debond during the test. .

At some point during the test the crack propagates from one or more of these zones, producing the river markings on the steep faces and stick-slip bands on level surfaces. This propagating crack encounters more zones which may not have totally debonded or reached critical size for initiation and causes secondary initiations at these sites. The interaction of the propagating crack with the incipient lacquer-free zones will probably depend on the level of adhesion of the lacquer within the zones, leaving strongly bonded lacquer on the tinplate surface. Multiple initiation in fracture has been reported in tensile tests of Lucite (Kies et al 1950) but it is most unlikely that every lacquer-free zone seen on a butt-joint fracture surface represents a separate simultaneous initiation event since the size of the zones and the defects within them vary by at least 50% and would therefore have quite different stress intensity factors.

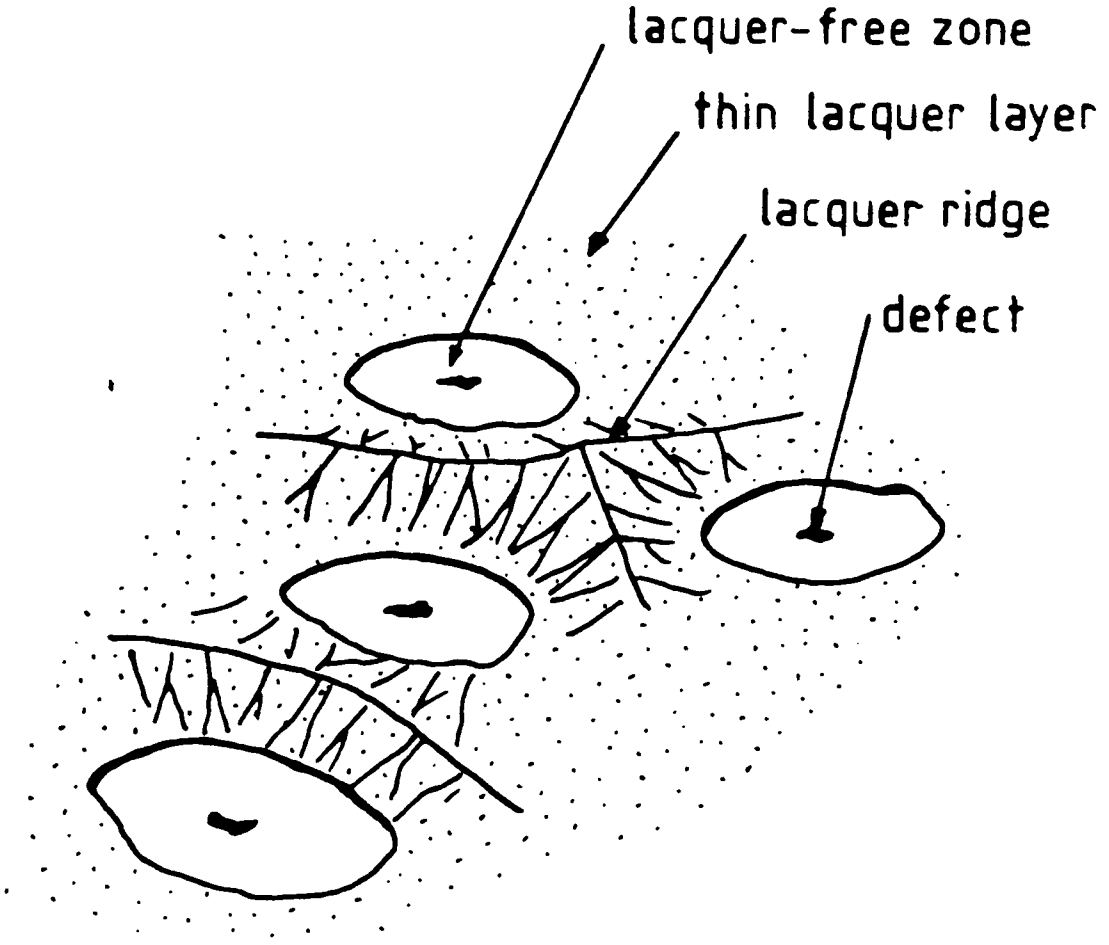

Figure 20. Schematic drawing of ridges visible between lacquer-free zones and fracture markings showing crack propagation outward from the zones.

The exact origins of fractures in the NS 311 and BS 311 samples cannot be determined due to the absence of fracture markings on their "clean" tinplate surfaces. The fractured lacquer edges of these samples also show the crack to have run in the same direction as in BS 311 samples (i.e. away from the tinplate) so implying initiation near the tin surface within the specimen. There are areas in the fracture surfaces from all sample types where no lacquer is visible on the tinplate surface. The location of the fracture path in these areas will be determined by XPS which will identify the passivation layer to find whether it has been removed by the lacquer.

The butt-joint test has revealed a wide variability in results of both failure load and lacquer removal for single sample types. There seems little doubt that this variability is a property of the lacquered tinplate system under test and not a variation of the test method (in view of the rigorous control conditions applied to the test). Brittle fracture is normally initiated at particular defects and unless the samples all contain identical reproducible flaws a wide variation in strength must result.

The statistical analysis method of Weibull (1939, 1951) was developed to describe the type of failure seen in, for example, brittle samples where there is a wide variation in failure load due to intrinsic defects in the material. It has been shown above that there is a specific population of defects in lacquered tinplate samples which may initiate failure and be responsible for the variations in failure load for a given sample set. Indeed, a generally reduced failure-stress found in the butt-joint tests with type 1 stubs (larger bond area) also points to the fractures being defect controlled (Kurzmann and Klemme 1975) although this may be due to initiation at the tinplate edges which were located very close to the stressed zone on some samples.

A Weibull statistical analysis will be able to separate sample sets with different defect populations or initiation mechanisms and is presented below so that the defect populations in each sample set may be characterised. Although BS, NS and KS tinplates all exhibit a wide variation in butt-joint test results the distribution of the data points and hence the defect population can be measured. This distribution is a better description of the population than simple measures of mean values since a lacquered tinplate system with a variability in failure load or lacquer removal may still be acceptable if most of the sample population exists in a regime of good adhesion (ideally defined as high failure load and especially low lacquer removal).

A probability plot for sets of adhesion test results has been used by Bascom et al (1978) who have identified separate failure characteristics and populations, despite large variations in failure load and similar ranges of failure load in all their sample types. Failure in a brittle adhesive system is likely to be defect-controlled and also depends on interfacial bonding. Measured strength then depends on the severity of the defects and intrinsic adhesion between phases. If the severity (size, location and orientation) of defects varies within a sample population, the joint strength will also vary and a population which contains some very severe defects will yield some very weak specimens. The Weibull analysis of a sample set will reveal the distribution of such defects and allow an estimate to be made of the likelihood of such defects in the population.

3.3 Weibull Statistical Analysis

When the strength of brittle materials is measured, the statistics of fracture relate to the defect distributions and in particular the distribution of the largest flaws (Evans and Langdon 1976). The

approach developed by Weibull (1951) to measure, inter alia, the strength of brittle solids considers a body with a distribution of non-interacting defects of which one of a certain critical severity is needed to cause failure. If a measured variable X (e.g. failure load) is obtained from a set of tests from a sample population then the distribution function of X, denoted as F(X) can be defined as the number of all the individuals having a value $X \leq x$ divided by the total number of individuals. The function F(X) also gives the probability, P, of choosing at random an individual having a value of $X \leq x$. Thus:

$$P(X \leq x) = F(X) \tag{1}$$

Weibull arrives at an expression of the form:

$$P_n = 1 - e^{-n\phi(x)} \tag{2}$$

where P_n is the probability of failure of a sample with n defects which is an expression for the principle of weakest link failure if the function $n\phi(x)$ is positive, does not decrease as x increases and vanishes at some value of x, say γ. The most simple function which satisfies these conditions is:

$$n(x) = \frac{(x - \gamma)^{\beta}}{\alpha} \tag{3}$$

where α, β and γ are constants for a given population.

Hence,

$$F(x) = 1 - e^{-(\frac{x - \gamma}{\alpha})^{\beta}} \tag{4}$$

which is the Weibull distribution function or, according to Weibull, "a statistical distribution function of wide applicability".

Whilst this function has no theoretical basis it has been used to describe many different data sets, often with great success (Weibull 1951, Moyer et al 1962, Steiger 1971). In this work the values of x are taken as failure load and the function is linearized by plotting as:

$$\text{loglog}\ \frac{1}{1 - F(x)} = -\log\alpha + \beta \log(x - \gamma) \qquad (5)$$

Weibull plots of the data are presented in Figures 21-30 with default values of γ=0, β=1, α=1. If the curve follows a straight line then γ is zero; a downward curving plot requires a positive γ factor to bring it to linearity and an approximate value for γ may be found by using the value of x which is approached by the curve (Moyer et al 1962). The physical significance of γ may be taken as a minimum level of x present in the population, here characterised by the largest defect. The slope is equated to the β parameter which is a measure of the spread of the distribution - a high value of β indicates low variability in x. The α parameter indicates the position of the line and is a normalising factor.

The term on the left hand side of equation (5) may be converted directly to a probability level. When less than 20 data points are available in each sample set it is recommended that median rank estimates of the probability (percentage failed) are used; these have been published in tabular form by Johnson (1951) and Moyer (1962).

Weibull plots of failure load for BS, NS and KS 311 type tinplates, stoved in air with epoxy-phenolic and other lacquers are shown in Figures 21 to 25. Plots for BS 300 and non-passivated (NP) tinplates are given in Figure 26. Straight-line approximations to the data are given for most samples although some data sets suggest multiple slopes which could be interpreted as two or more different defect distributions. Measurements from the plots are listed in Table 5, giving the Weibull slope, β, characteristic load, median load and sample preparation conditions.

Weibull plots of percent lacquer removed are shown in Figures 27 to 30 with the measured data in Table 6.

TABLE 5

DATA FROM WEIBULL PLOTS OF FAILURE LOAD IN BUTT-JOINT TEST

Tinplate type	TSL	Sample No.	β(±%) error	Characteristic failure load(kN)	Median (50% failed) load (kN)
BS311(B)	715	18	4.0 (48)	1.8	1.6
	715	19	4.5 (48)	3.1	2.9
	715	20	4.3 (38)	2.6	2.3
	715	23	4.7 (58)	4.2	3.8
			(+1.7)(68)		
BS311(A)	616	30	1.7 (48)	2.6	2.1
	616	25	2.4 (48)	5.2	4.4
	611	21	2.5 (37)	3.3	2.9
BS311	411	6	5.0 (53)	1.7	1.6
	414	14	0.61(58)	0.6	0.44
	414	15	0.85(68)	0.9	0.33
	413	7		(1.5)	(1.2)
NS311	111	1	2.1 (35)	1.8	1.5
	142	2	2.4 (37)	1.3	1.2
	111	3	7.6 (40)	4.1	4.0
	111	35	2.5 (53)	0.8	0.7
KS311	211	4	5.7 (37)	4.2	4.1
	211	5	3.7 (42)	1.3	1.2
	252	16	2.5 (53)	2.3	2.0
	262	17	2.2 (53)	2.3	2.0
BS300	312	10	1.7 (48)	2.2	1.9
	323	11	3.1 (53)	1.3	1.2
	342	13	1.3 (45)	1.1	0.9

TABLE 6

DATA FROM WEIBULL PLOTS OF PERCENT LACQUER REMOVED

DURING BUTT-JOINT TESTS

Tinplate type	TSL	Sample No.	β(±%) error	Characteristic lacquer removal	Median lacquer removal
BS311	411	6	0.7 (46)	0.72	0.44
	413	7	1.7 (52)	47	38
	414	15	1.8 (68)	92	91
	416	14	1.9 (52)	71	60
BS311(A)	616	30	0.9 (52)	20	13
NS311	111	1	2.6 (35)	81	73
	142	2	5.7 (35)	85	80
	111	35	2.5 (52)	55	48
KS311	211	5	83 (42)	83	80
	252	16	3.5 (52)	69	61
	262	17	2.1 (52)	60	50
BS300	312	10	1.7 (46)	1.9	1.5
	323	11	- -	-	2
	342	13	30 (42)	100	95
NP	512	8	1.4 (52)	58	38

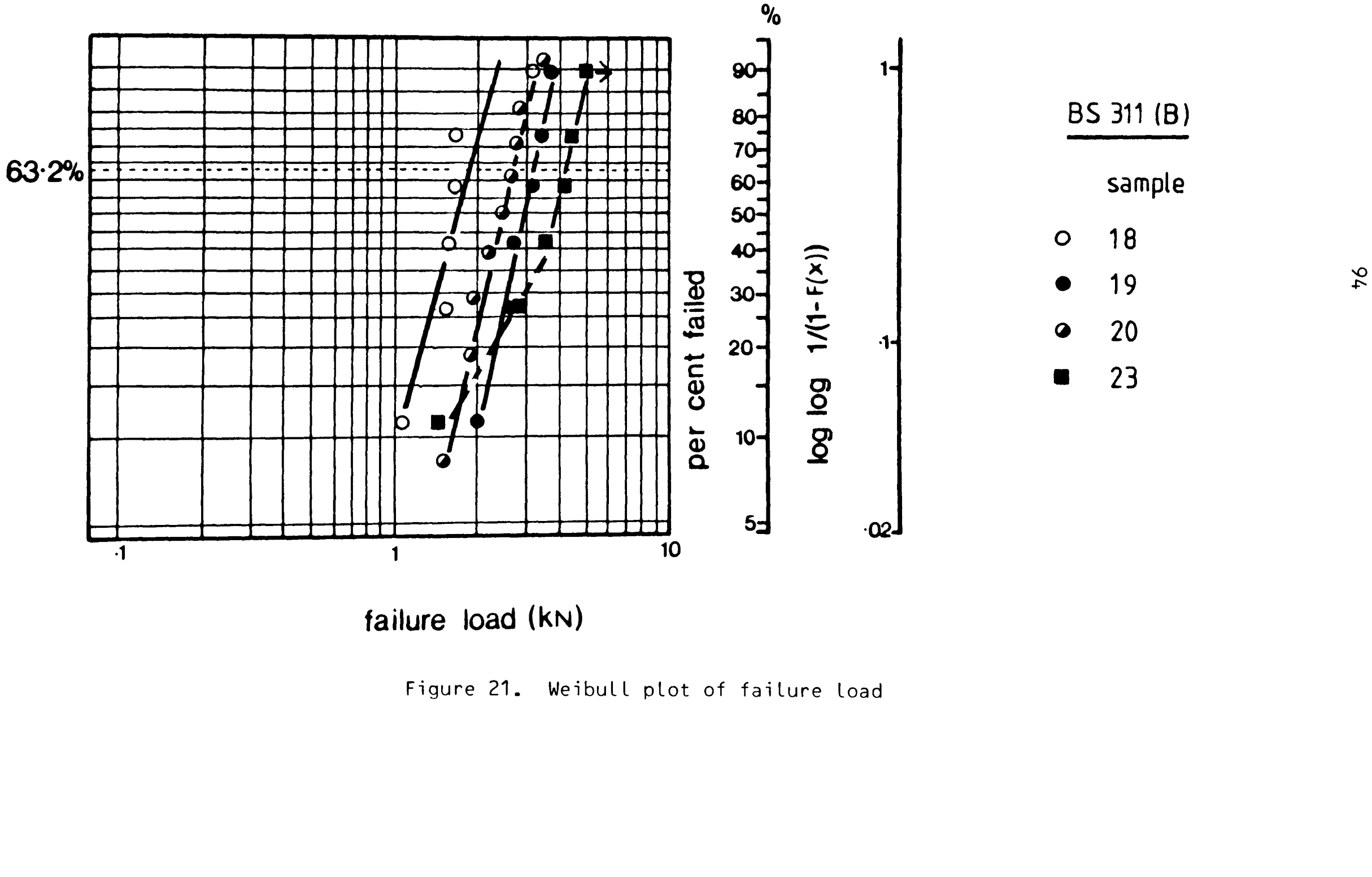

Figure 21. Weibull plot of failure load

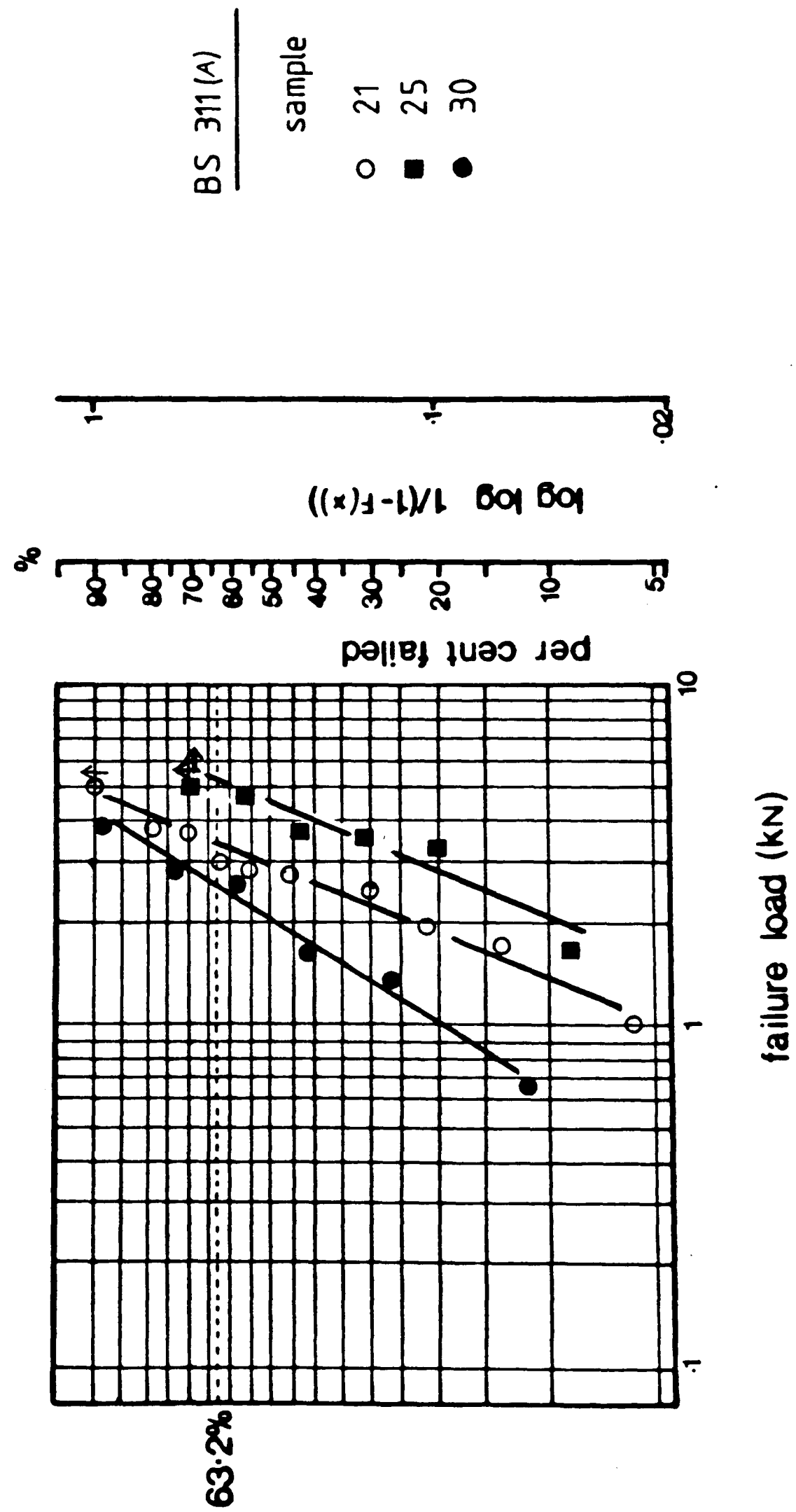

Figure 22. Weibull plot of failure load

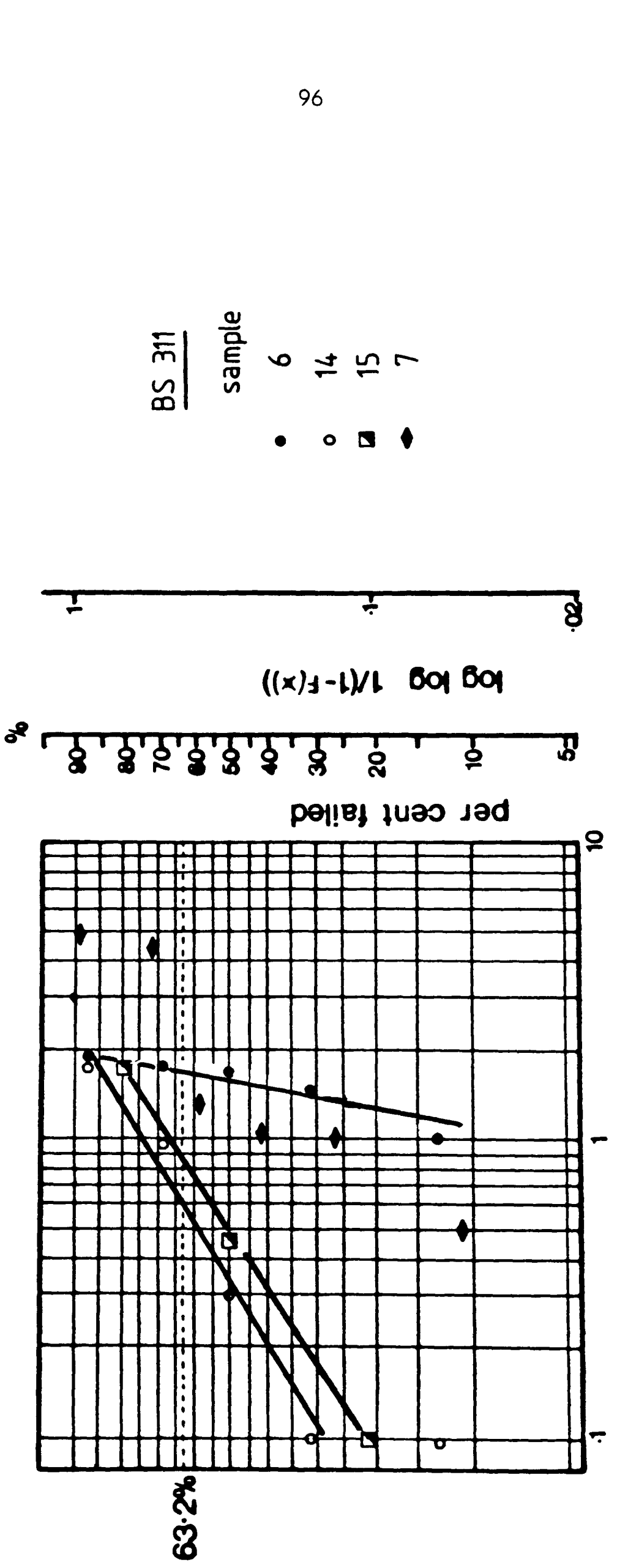

Figure 23. Weibull plot of failure load

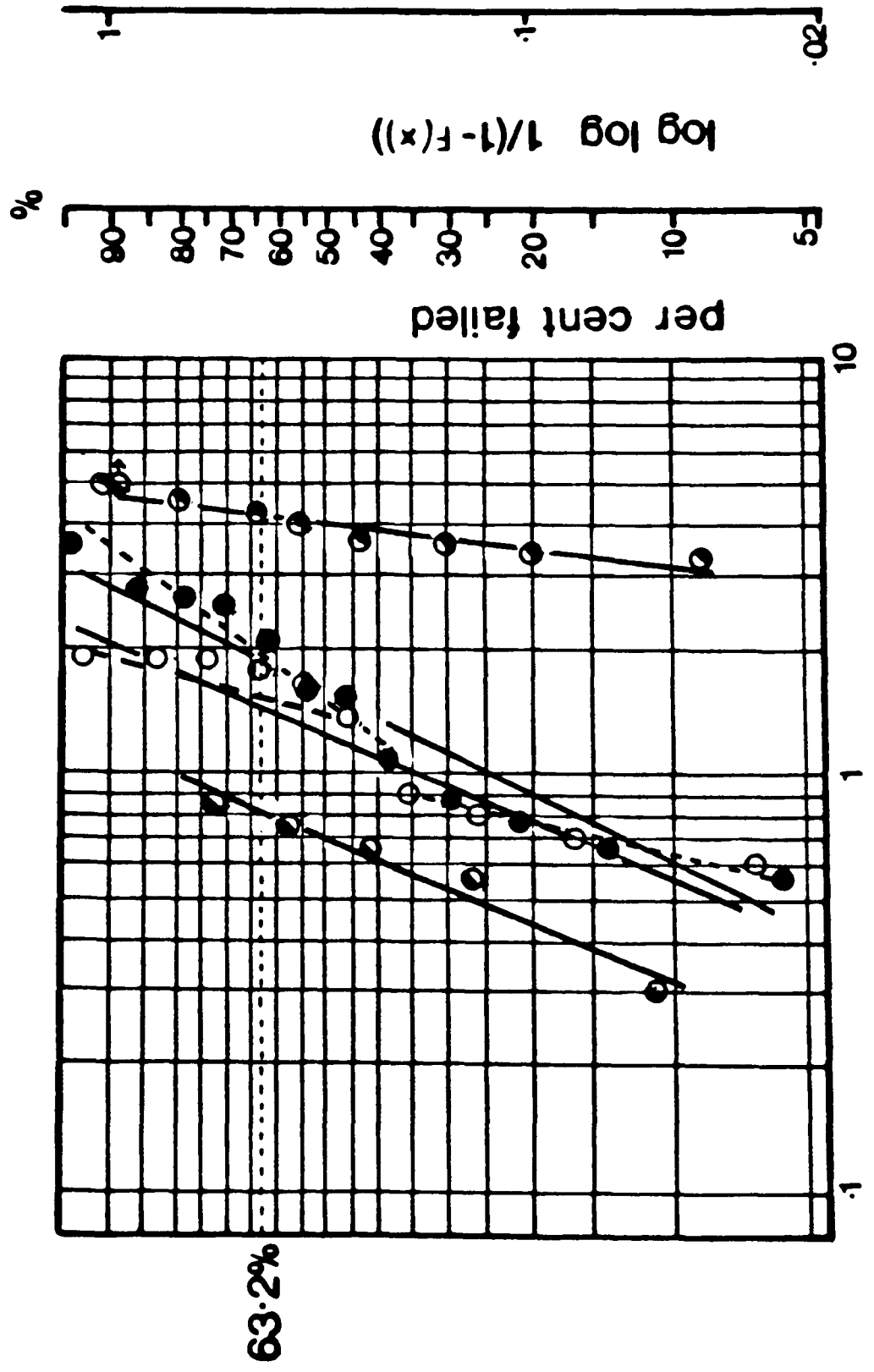

Figure 24. Weibull plot of failure load

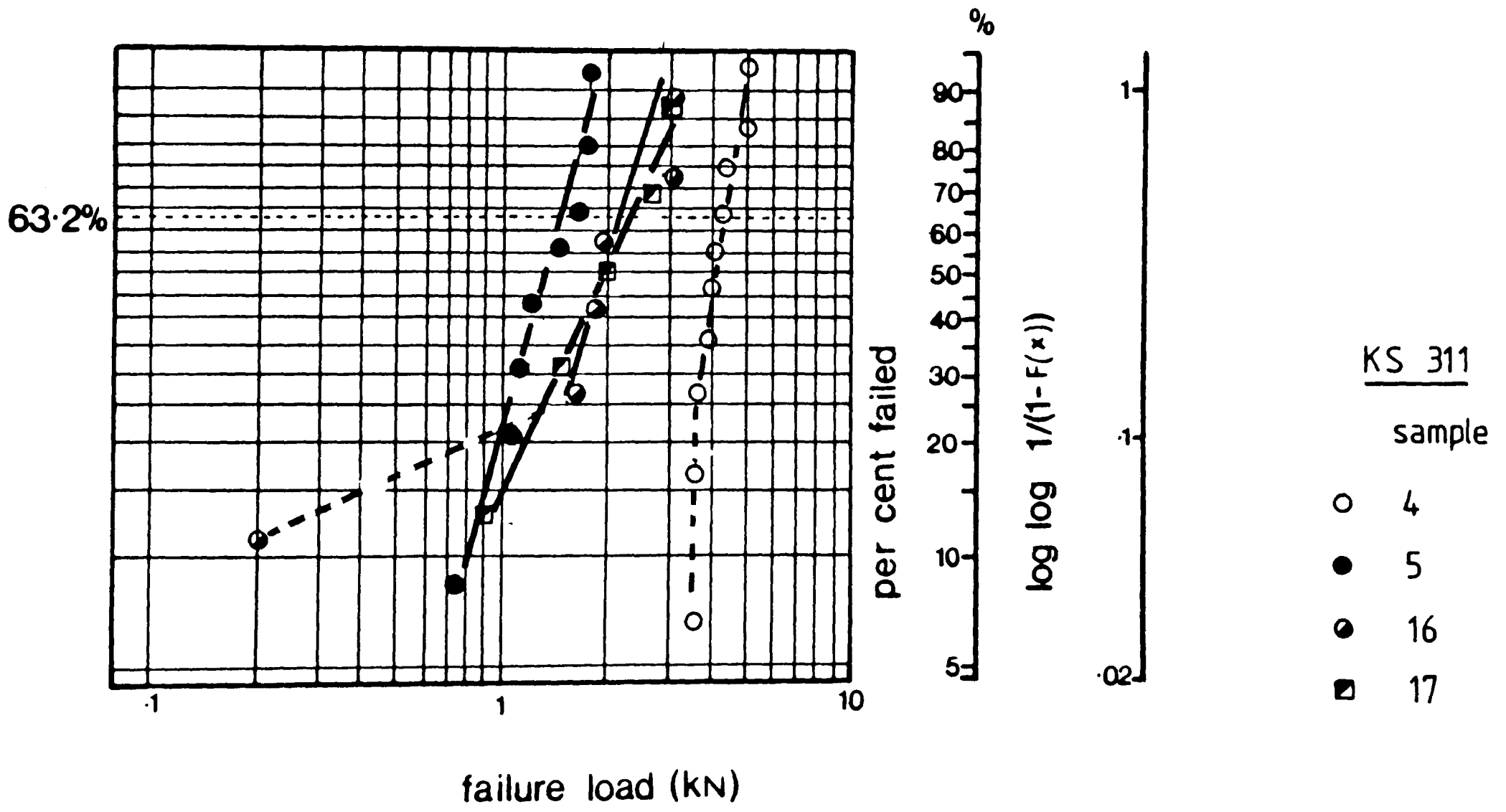

Figure 25. Weibull plot of failure load

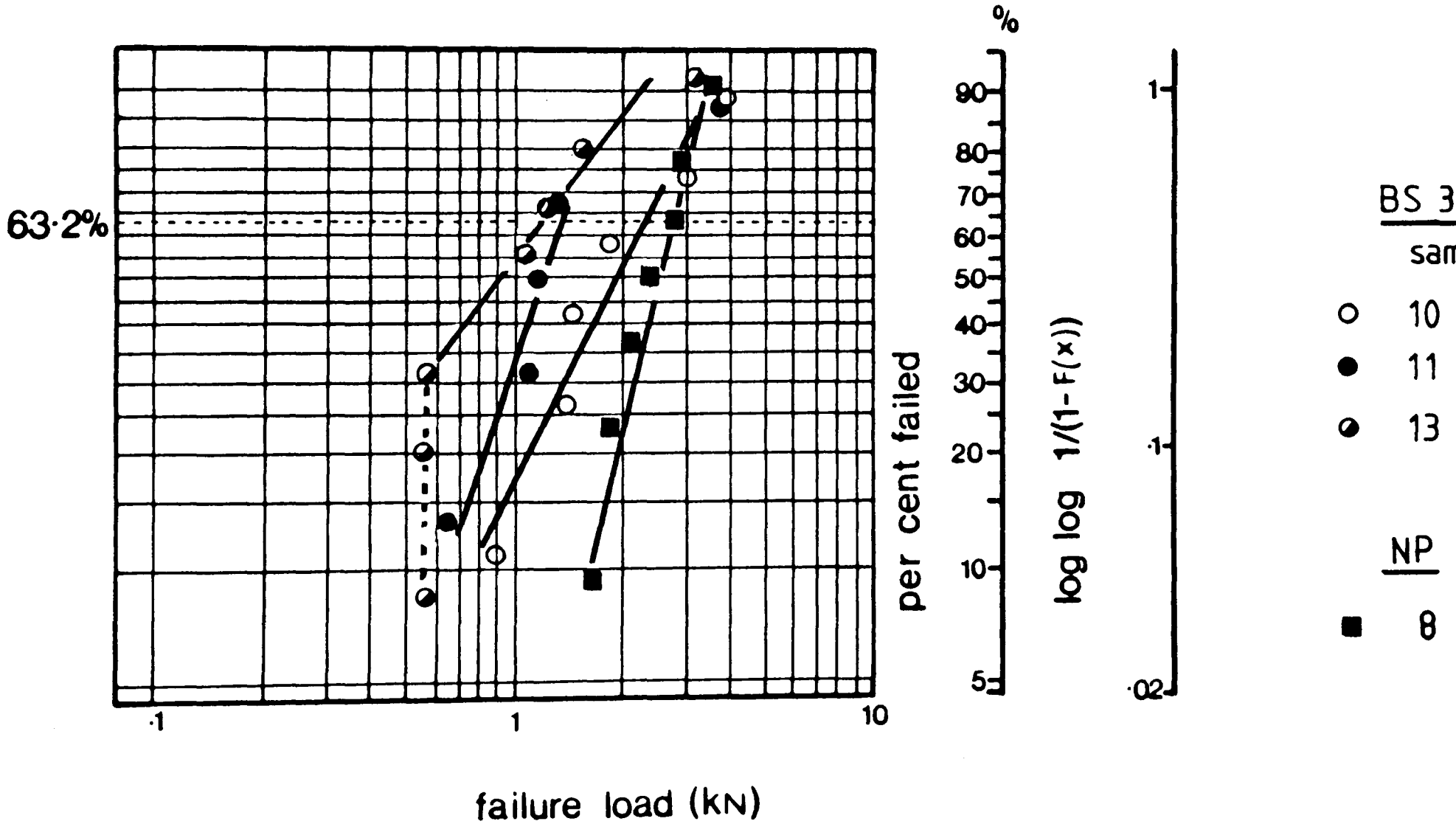

Figure 26. Weibull plot of failure load

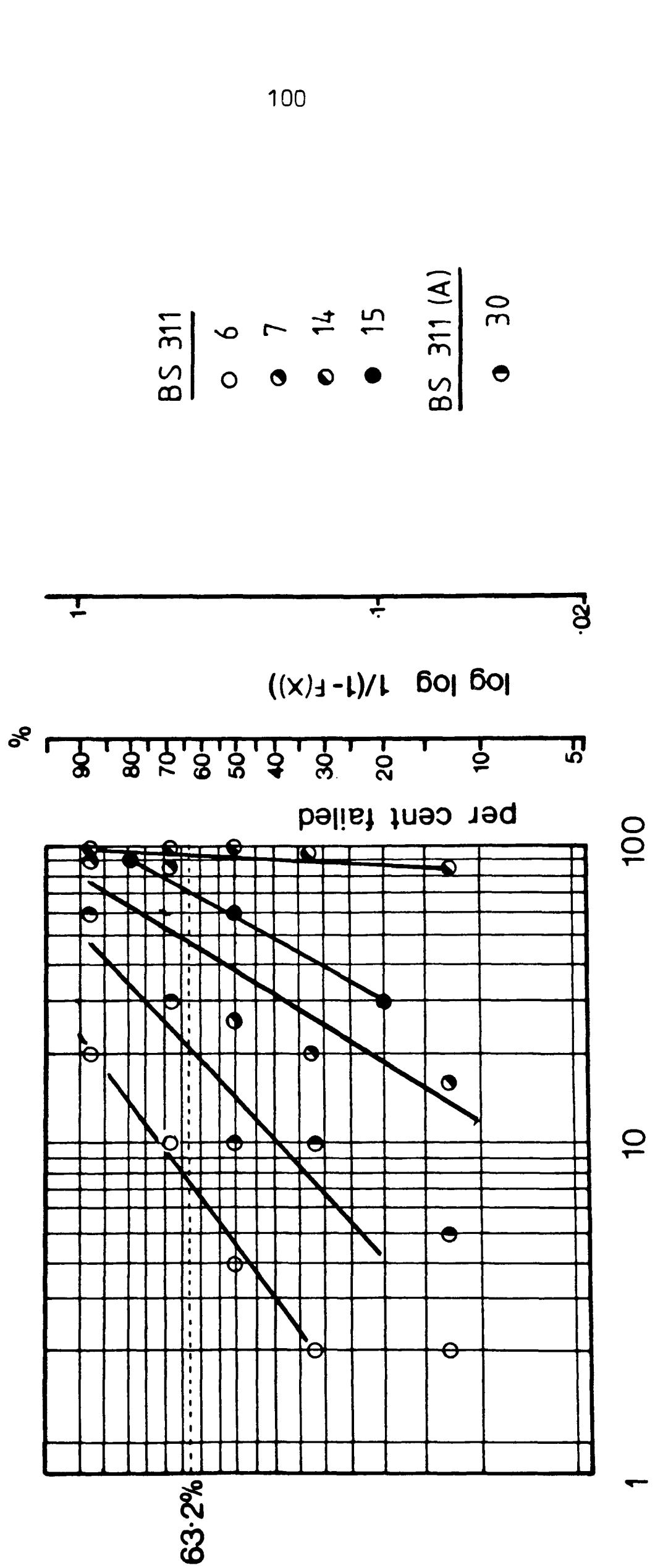

Figure 27. Weibull plot of percent area lacquer removed

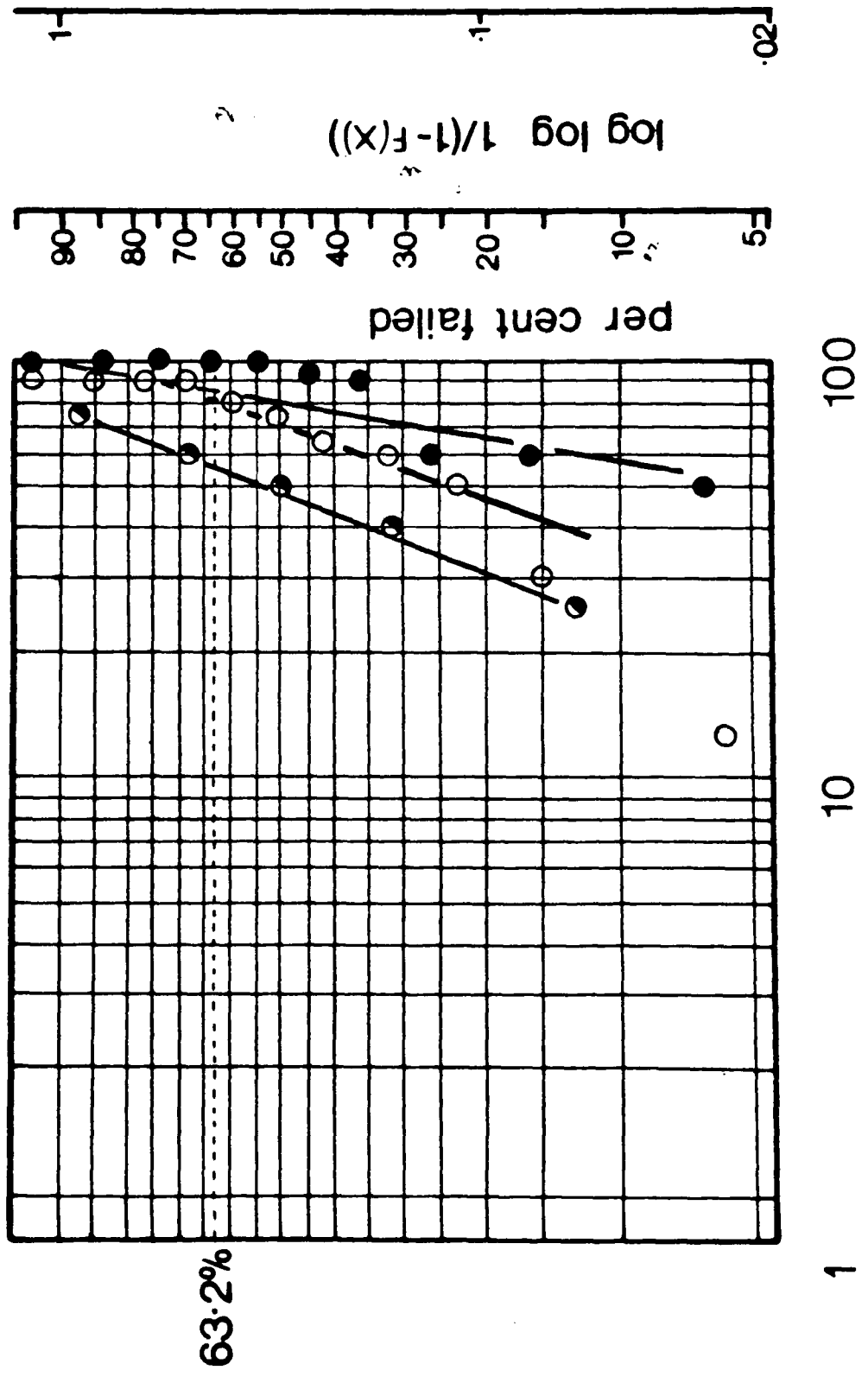

Figure 28. Weibull plot of percent area lacquer removed

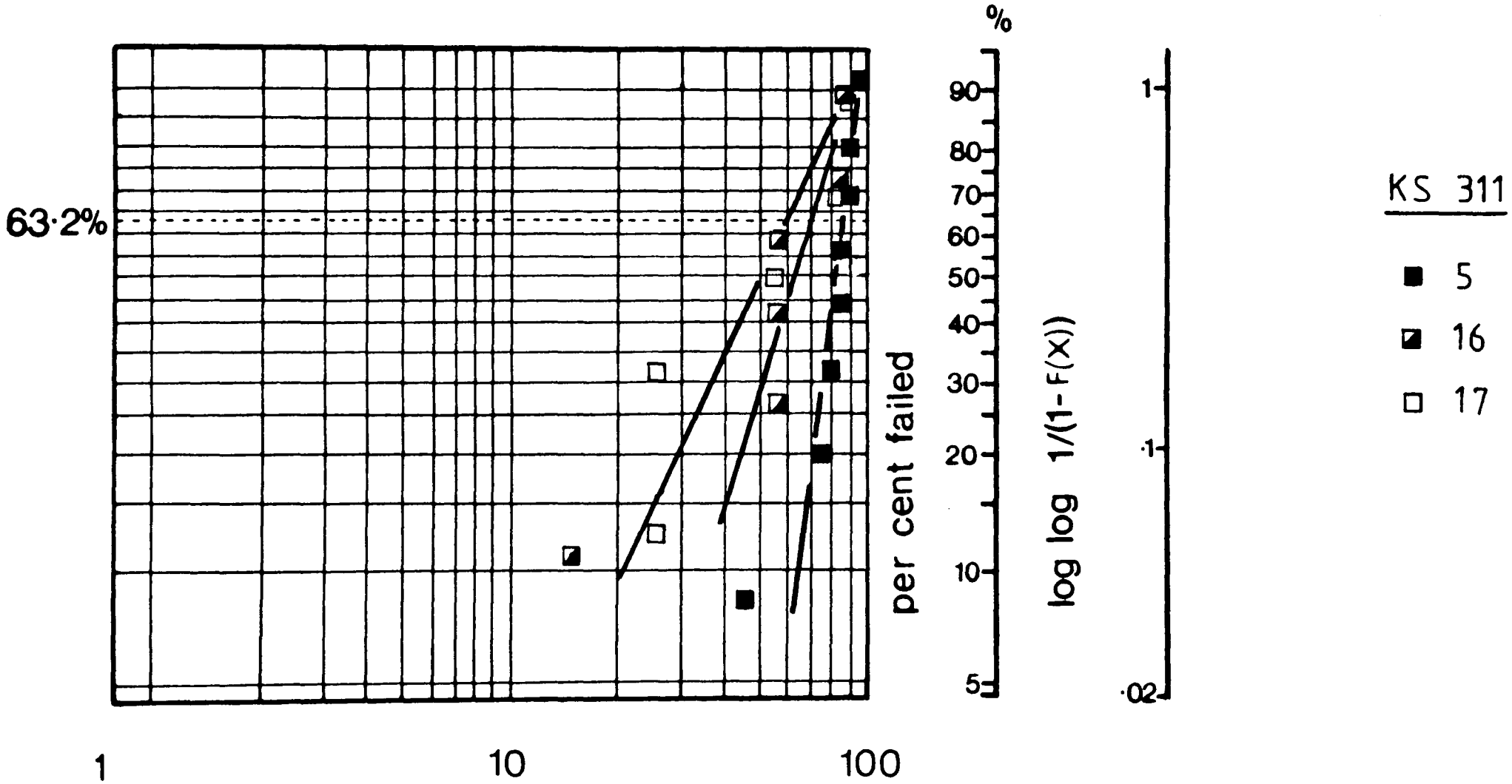

Figure 29. Weibull plot of percent area lacquer removed

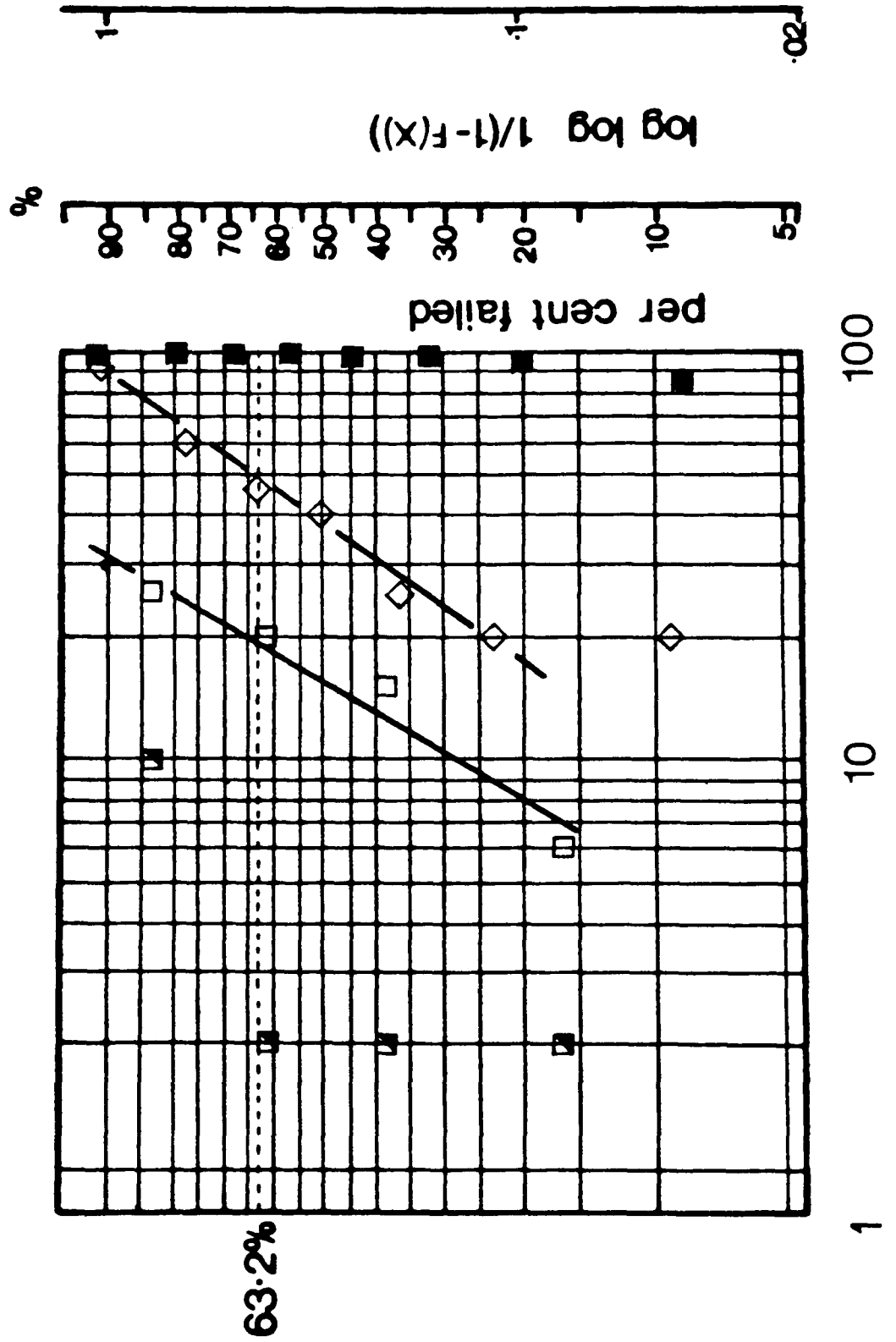

Figure 30. Weibull plot of percent area lacquer removed

Figure 21 shows four BS 311 samples from the same tinplate batch with identical lacquers and stoving treatments. All have similar Weibull slopes and characteristic loads ranging from 1.5 kN to 4.2 kN. A double slope has been attributed to sample 23 which may indicate that two defect populations are operative in the failure process. Another batch of BS 311 tinplate with identical stoving conditions and two lacquer types is shown in Figure 22. The Weibull slopes are lower than in Figure 21 but characteristic loads are similar.

The BS 311 sample set used generally throughout this work as a comparative set (with NS 311 and KS 311) is shown in Figure 23. The sample (no. 6) with air stoved epoxy-phenolic lacquer has a Weibull slope and characteristic load similar to the other batches of BS 311 tinplate but when coated with a phenolic lacquer both quantities decrease, indicating a wide variability in test results and a lower failure load. Evidently, this type of tinplate is unsuited to phenolic lacquer when applied under the conditions used here but behaves well with epoxy-phenolic lacquers of one type (cf. ADF plots in Figure 9 which also show this lacquer-tinplate combination to be unusual for BS tinplates). Sample 7 in this set has been coated with another type of epoxy-phenolic and exhibits an erratic distribution to which no single straight line has been fitted.

Nippon Steel 311 samples (Figure 24) show a wide variation in characteristic load but generally high values of the Weibull slope. Even with the same lacquer and stovings, different samples (1 cf. 35) show a widely differing characteristic load. Altering stoving conditions and lacquer do not alter the distribution (slope) and the characteristic load falls within the range of variability shown by nominally identical samples. (All combinations of lacquer type

and stoving have not been investigated and it is possible that certain combinations would produce very poor adhesion properties).

The Weibull plot of KS 311 samples(Figure 25) shows one sample set in particular (no. 4) to have a consistently high failure load although a nominally identical set (no. 5) has a much lower value. The Weibull slopes of the rest, with values around 3, are similar to those found on other tinplate types as are the characteristic failure loads. From this plot it would be inferred that the KS 311 is a tinplate with good adhesion properties with at least two lacquer types compared with other tinplates but this does not take into account the amount of lacquer removed in the test, which may be a more important parameter in lacquer adhesion for tinplate than failure load. The Weibull plots of failure load for BS 300 and an unpassivated tinplate sample are given in Figure 26 which show Weibull slopes and characteristic loads typical of the 311 tinplates.

Thus, from the Weibull plots of failure load it is seen that the measured slopes have predominant values between 2 and 5 (a slope of 3.25 would indicate a Gaussian distribution); the errors in measuring these slopes from limited numbers of data points are given in Table 5 (Moyer 1962) and in most cases they are too large to allow significant differences in β between samples being inferred. Two samples (14 and 15) have β values of approximately 0.6 and do show a significant broadening of the distribution which is due to the type of lacquer and stoving conditions. To obtain errors of $\leq \pm$ 10% in β 150 data points would be required for each plot. Hence, straight line approximations have been used in most of the graphs with dotted lines to indicate possible multiple distributions or finite values of failure load. (The latter is indicated when the line slopes downward to the approximate value indicated by the intersection with the 5%

failed level).

If it is assumed that the failure is defect-initiated, as would be suggested by the wide variation in failure loads and the fractographic evidence, then the quantity β is a measure of the distribution of such defects and the existence of a single value of β implies a single type of defect population responsible for fracture initiation in all tinplate types (including the non-passivated tinplate).

It has been suggested (Moyer 1962) that the median (50% failed) values may usefully be compared when using small data sets but, as expected from inspection of the raw data, there is no significant difference between tinplate types.

From the failure load plots it may be concluded that a sample batch of ten or so specimens is not sufficient to include the full range of defect severities which accounts for the variations in characteristic loads with (statistically) indistinguishable Weibull slopes. However, the Weibull plots of failure load can describe and attribute values to features of the specimen population in terms of a characteristic and median failure load, failure-producing defect populations (in some cases with a minimum effective value) and highlight the deleterious effect of certain lacquer-tinplate combinations The method does not show up significant differences between tinplate types. The measure of failure load is a measure of fracture initiation which, from these data, is therefore shown not be a function of the passivation layer, stoving conditions or (with two exceptions), the type of lacquer. Fractographic analysis has suggested this, and indicates that the angular $FeSn_2$ defects in the tin coating or the circular lacquer-free zones seen in the microscope are the cause of fracture initiation in lacquered tinplate.

The load at failure, as measured by the butt-joint test, is a measure of the load to initiate failure (as the process is catastrophic) and does not yield information about the propagating crack front. It is the crack propagation, however, which determines whether the lacquer or passivation layer is removed in large areas and, provided a certain minimum value of strength before failure is achieved, may well determine the properties of lacquered tinplate as required in service since a crack which propagates away from the tinplate and out through the lacquer will remove less lacquer than one which propagates in, say, the passivation layer.

The mode of crack propagation is indicated by examining the fracture surface and measurements of the amount of lacquer removed from the tinplate during a test. Values of percent lacquer removed have been plotted on Weibull paper and are shown for BS 311 (Figure 27), NS 311 (Figure 28), KS 311 (Figure 29), BS 300 and non-passivated tinplate (Figure 30). Weibull slopes, characteristic values and median values are given in Table 6. Certain BS 311 and BS 311(A) tinplate samples show significantly low values of slope (nos. 6 and 30) and one KS 311 sample (no. 5) shows a significantly high value. Argon stoving increases the amount of lacquer removal from 300 plate and possibly from NS 311 (the only two tinplate types tested for the effect).

Whereas Weibull plots of failure load describe the distribution of fracture-initiating defects, the plots of percent lacquer removed may be regarded as showing the distribution of areas of weak lacquer-tinplate bonding. British Steel tinplate (311 and 300) show a wide spread of data points but with lower median values than NS 311 or KS 311 for air-stoved tinplates with epoxy-phenolic lacquer coatings. Although these plots overlap at levels of high (> 60%) lacquer removal where some 70% of samples in a population would have failed, the

distributions as measured by the slopes are different for BS 311 and BS 300 tinplates compared with NS 311 and KS 311 tinplates.

4. ENVIRONMENTAL EFFECTS ON LACQUER ADHESION

An important requirement for lacquered tinplate is the ability to retain adhesion during service which usually means immersion in an aqueous, often acidic, environment. Water has been shown to have a serious deleterious effect on adhesion (Kerr et al 1967) for example, reducing bond strengths of epoxide-aluminium specimens by 30% after 10 days exposure (Orman and Kerr 1971). Bond strength is reduced by water adsorption at the interface, a process which may be reversible. For lacquered tinplate in corrosive media corrosion will also take place (Maercks 1978) and this effect is permanent, ultimately causing total debonding of the lacquer. The tests described below are for relatively short periods of time which will not result in corrosion induced delamination (Albu-Yaron et al 1977) but will serve to show whether short exposures in citric acid result in adhesion loss which might be expected in other coated systems.

Lacquered tinplate samples were immersed in 0.1 M citric acid at room temperature for varying times and then removed for butt-joint testing. During immersion, the cut edges of the samples were sealed so that only the lacquered surfaces were exposed. Butt-joint test results are shown for these samples in Table 7 where it can be seen that for periods up to 30 days for BS 300 and 60 days for BS 311 there was no significant effect on either failure load or percent lacquer removed. Tests at longer exposure times were not performed. ADF values for these samples, where available, are low and typical of good lacquer bonding.

Thus, lacquered passivated tinplates retain their good adhesion properties after moderate exposure to a hostile environment and

TABLE 7

BUTT-JOINT TEST RESULTS FOR

LACQUERED TINPLATE SAMPLES

IMMERSED IN 0.1M CITRIC ACID

BEFORE TESTING

Tinplate Type	Lacquer Type	Exposure (Days)	Failure load(kN)	Percent lacquer removed
BS300	epoxy-phenolic	8	5.1	10
			5.0	25
			3.9	2
			1.9	25
BS300	epoxy-phenolic	30	5-2	all failures in adhesive layer
BS311	epoxy-phenolic	60	2.9	
			3.1	
			1.6	
			3.3	All less than
			2.1	25
			4.0	
			2.0	
			2.5	

although environmental attack is not the main theme of this work, it is informative to see that butt-joint tests can be used for samples subjected to immersion in acqueous media and that the results are comparable with dry adhesion tests.

5. SUMMARY

Given the wide variation in results from the butt-joint test between like samples, no significant differences can be discerned between different sample types on the basis of failure load. Their performances on the basis of percent lacquer removed are slightly different with KS 311 being the worst tinplate type. Since the tests were carried out under rigorous experimental conditions, these results reflect true variations and imply that failure is due to defects within the samples. Normalising percent lacquer removed to failure load (ADF) does distinguish the BS 311 and BS 300 tinplates which were originally classified as having good adhesion properties on the basis of factory performance and the Scotch tape test. The ADF values also illuminate effects due to an incompatible lacquer/stoving condition for BS 311 and also to argon stoving for BS 300.

If data are plotted on Weibull graphs, further information is available: plots of failure load reveal that most samples have the same distribution function which means that whatever defects control fracture initiation, they are found in similar concentrations in all samples. Weibull plots of percent lacquer removed, however, distinguish the BS 311 and BS 300 tinplates which have lower slopes and lower median values.

Fractographic analysis of BS 311 samples, with clear fracture markings, shows small angular holes which reveal the underlying $FeSn_2$ in the tin coating which lie at the centre of lacquer-free zones.

These defects are found on all tinplate types and are prime candidates for the initiators of failure in the butt-joint test. It has not been possible to locate a single point of initiation by examining fracture surfaces; in fact, the fracture path is seen to emanate from several lacquer-free zones which might suggest multiple initiation of failure. Whilst this has been reported in some other types of tensile test sample, it is unlikely to occur in the type of specimen examined here and a more feasible explanation would be that some or all of these lacquer-free zones are secondary initiation sites triggered by an approaching crack front (Smekal 1936, Andrews 1968). Examination of the peripheries of test samples shows that the crack front has moved outwards and other fracture markings show that a crack front has moved through the sample, sometimes interacting with the lacquer-free zones. Thus, the initiation of failure is not at the sample edge and may be from one particular lacquer-free zone. It is not clear whether the lacquer-free zones were present before bonding, perhaps arising from corrosion products, or whether they grew from the $FeSn_2$ defects under loading until one was large enough to cause failure of the specimen. The origin of the $FeSn_2$ defects is also unknown but they are quite different in appearance from areas where the alloy layer has grown through the tin during flow-brightening (also shown in Figure 18). The sides of the defects are sharp and angular and unassociated with scratches on the tin surface; corrosion or grain-boundary failure may be possible explanations. Such defects are commonly seen on tinplate surfaces but no explanation of their origin has been advanced (Moger 1985). The defects have been observed on all the tinplates used in this work but are not evident on non flow-brightened tinplate. Pores in the tin surface are seen in non flow-brightened tinplate and are shown in Figure 31; they are generally larger

Figure 31. Scanning electron micrographs of pores on non flow-brightened tinplate.

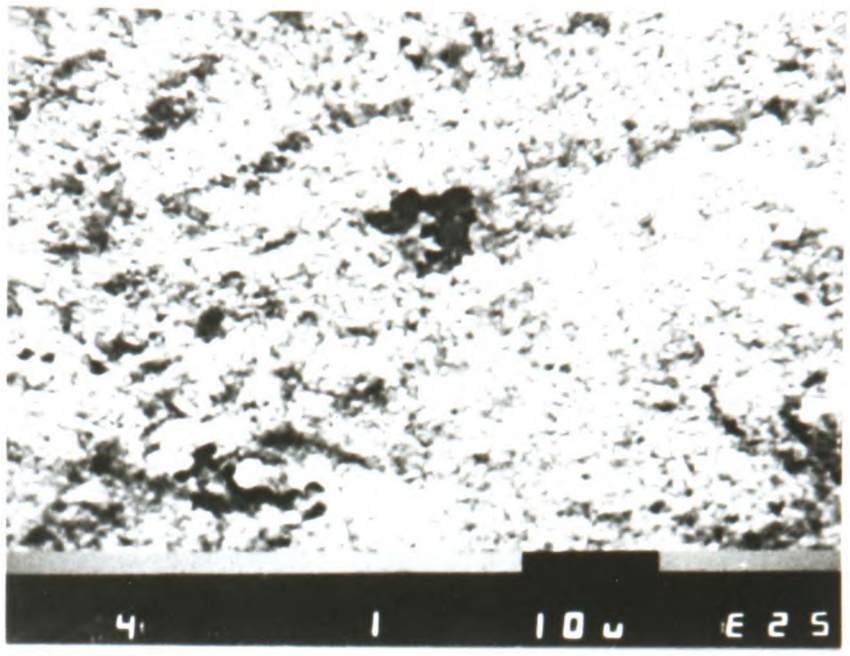
4 1 10u E25

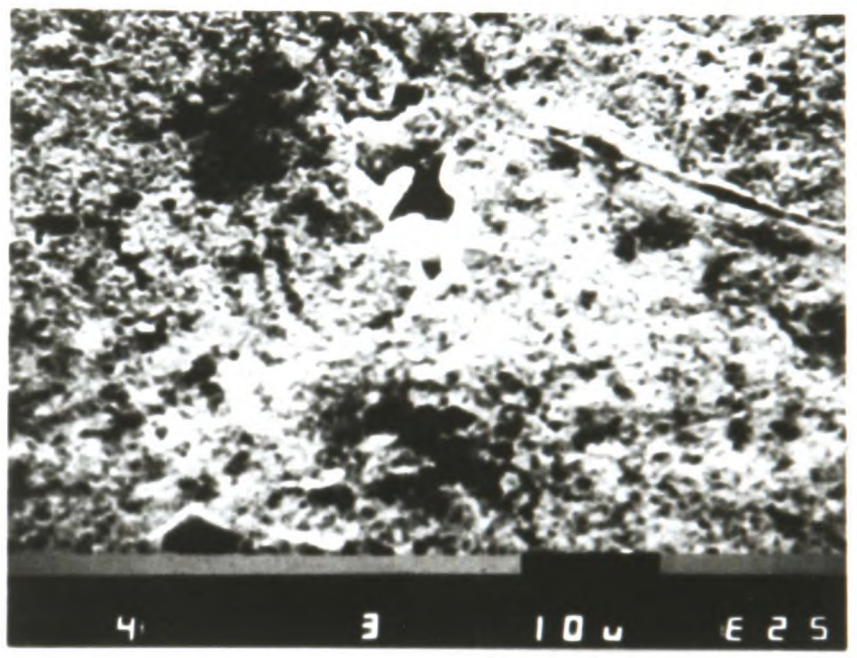
4 3 10u E25

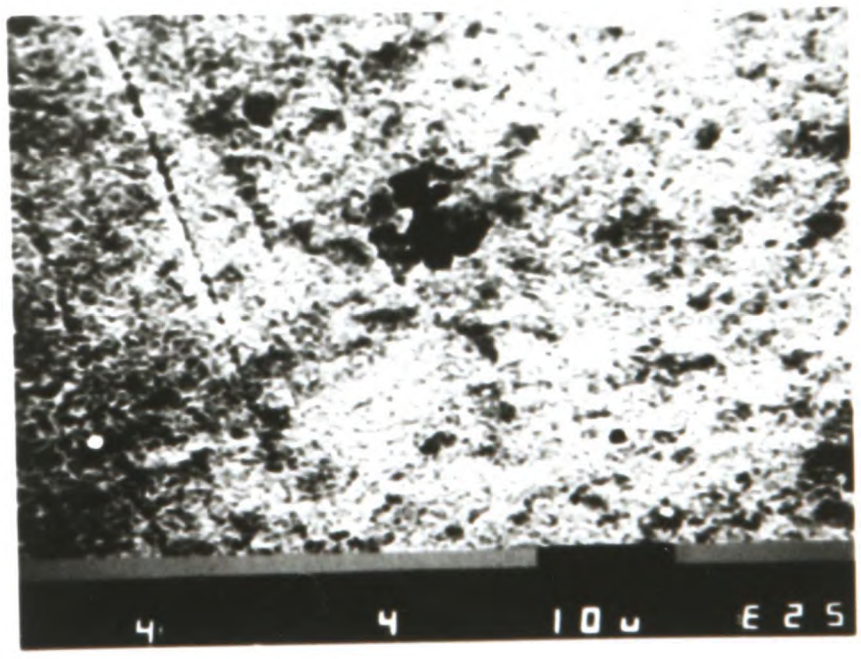
4 4 10u E25

than those angular defects seen in flow-brightened plates and do not possess straight sides. A possible mechanism for the formation of angular pores from those seen in Figure 31 might be the re-flowing of the tin during flow-brightening which would result in pores with straight sides due to crystallographic surface tension effects within tin grains or at grain boundaries. However, $FeSn_2$ formation would not be expected in this case unless the tin was originally covering the steel surface and subsequent de-wetting occurred. Further examination of tin grains in 311 tinplate (after etching in 0.1 M HCl) revealed that the angular $FeSn_2$ defects are present both within individual tin grains and at grain boundaries and also that prolonged etching can form large angular etch pits similar to the $FeSn_2$ defects but often much larger. Further work is required to identify the origins of these defects but both dewetting during flow-brightening and localised corrosion are possible mechanisms.

Fracture initiation may not be the most important aspect of lacquer adhesion to tinplate, however, since some of the tinplate-lacquer combinations have performed well in service and yet show no significant differences in failure load from those samples which are unacceptable. Provided a minimum level of load is achieved, the crack propagation will determine whether the lacquer remains adhering to the tinplate and passivation layer. The Weibull plots of percent lacquer removed yield information about the propagation path and about possible areas of weak bonding in the sample which would allow large areas of lacquer to be removed. The BS 311 and BS 300 samples with air-stoved epoxy-phenolic lacquer have lower median values of percent lacquer removed than KS 311 with similar coatings but also have shallower slopes which take a proportion of the populations into the region of high lacquer removal which signifies poor adhesion properties.

The advantage of plotting data on Weibull graphs is thus demonstrated by clearly showing the distribution of properties (failure load or lacquer removal) and indicating that although a particular sample set may contain individual specimens with both good and bad properties, it is the distribution of those properties which characterises its behaviour. With many data points per sample it would also be possible accurately to predict the fraction of a population which would be expected to achieve a particular minimum value.

The ADF plots distinguish BS 311 and BS 300 tinplates as having low (ADF < 25) values with small standard deviations, showing a positive relationship between failure load and percent lacquer removed. This relationship is not in general found for KS 311 or NS 311 tinplates and suggests a different failure mechanism which is seen in the fractographic analyses where the KS 311 and NS 311 tend to lose lacquer in large areas with sharply defined edges on the remaining lacquer. BS 311 tinplate fracture surfaces, however, are left with thin lacquer layers, many small islands of lacquer and less steeply-sloping edges to the areas of remaining thick lacquer coat. The circular zones with no visible lacquer coat are found in the thin lacquer layer on these samples with central $FeSn_2$ defects. Examination of the fracture markings indicates failure from near the tinplate surface, within the lacquer-free zones. For NS and KS specimens, no fractographic analyses were possible except on the lacquer edges where it was seen that the crack had run upwards from the tinplate through the lacquer. The origins of fracture in NS 311 and KS 311 may well be the same as in BS 311 as suggested by Weibull analysis but there is no fractographic evidence. The $FeSn_2$ defects are also present in NS and KS tinplates and may cause failure initiation but the propagating crack runs between the tinplate and lacquer compared

with the more cohesive failures seen on BS 311 in which fracture markings are visible. XPS will be used to determine the crack propagation paths.

Weibull plots of lacquer removed show that NS 311 and KS 311 have similar distributions and characteristic values, whilst the BS 311 and BS 300 tinplates have significantly lower values for comparable stoving and lacquer conditions, although certain lacquer or stoving combinations are shown to have deleterious effects for lacquer adhesion to BS 311 and BS 300 tinplates. The different modes of crack propagation seen by microscopy are also reflected in the Weibull plots of lacquer removal where the samples with low β (slope) values have lower median values of percent lacquer removal, i.e. a high distribution of weakly-bonded areas leads to crack propagation at the lacquer-tinplate interface.

Distinct differences between tinplate samples have thus been confirmed by mechanical testing and fractographic analysis. The ADF values present a simple method of distinguishing tinplates with good adhesion properties as these will have values of less than 25 with low standard deviations. These values are percent lacquer removal normalised to failure load and for lacquered tinplate samples with good bonding there is a roughly linear relationship between the two parameters; high stresses cause large areas of lacquer removal by increasing interfacial loads and with the high levels of stored energy in the specimen, the crack may be allowed to run along energetically less-favourable interfaces near the tin surface. Alternatively, the high loads achieved before failure in specimens with good bonding create sub-critical cracks, which are seen on the fracture surface as the lacquer-free zones identified as secondary initiation sites. Defect-controlled initiation and strong interfacial bonding are

therefore manifested as positive slopes on a failure load vs. percent lacquer removal plot or as low ADF values with small standard deviations.

In the case of sub-critical crack growth a more complex version of the Weibull statistical treatment would be required to account for defect interactions and sub-critical defect growth (Evans and Langdon 1976) but the method shown above would allow a useful, if not complete, analysis. For samples with strong lacquer bonding, low failure loads produce low areal lacquer removal.

It should be noted that initiation and propagation are separate mechanisms and appear to have different controlling factors; initiation is determined by defects within the sample whilst the crack propagation path depends both on the lacquer-tinplate bond strengths and on failure load for the BS samples. Hence, for the NS 311 and KS 311 samples in which failure load is not a function of percent lacquer removal, large amounts of lacquer may be removed at low loads due to weak bonding but the failure load depends on the distribution of initiating defects. Very weak interfacial bonding could initiate failure in which case a plot of failure load vs. lacquer removal would show a pronounced negative slope where the usual defects which initiate failure are inoperative and weak bonding would be manifested by low failure load and high lacquer removal. This situation is seen in sample 15 (Fig. 7) and possible sample 14 which are BS 311 tinplates coated with phenolic lacquer.

From this rationale it is possible to propose a simple mechanism to describe the initiation and crack propagation in lacquered tinplate. Effects due to stoving conditions, particular lacquers and the passivation layer cannot be included until further information, available from XPS and TEM, is included. Figure 32 shows two possible starting configurations for lacquered, unstressed tinplate. Both include

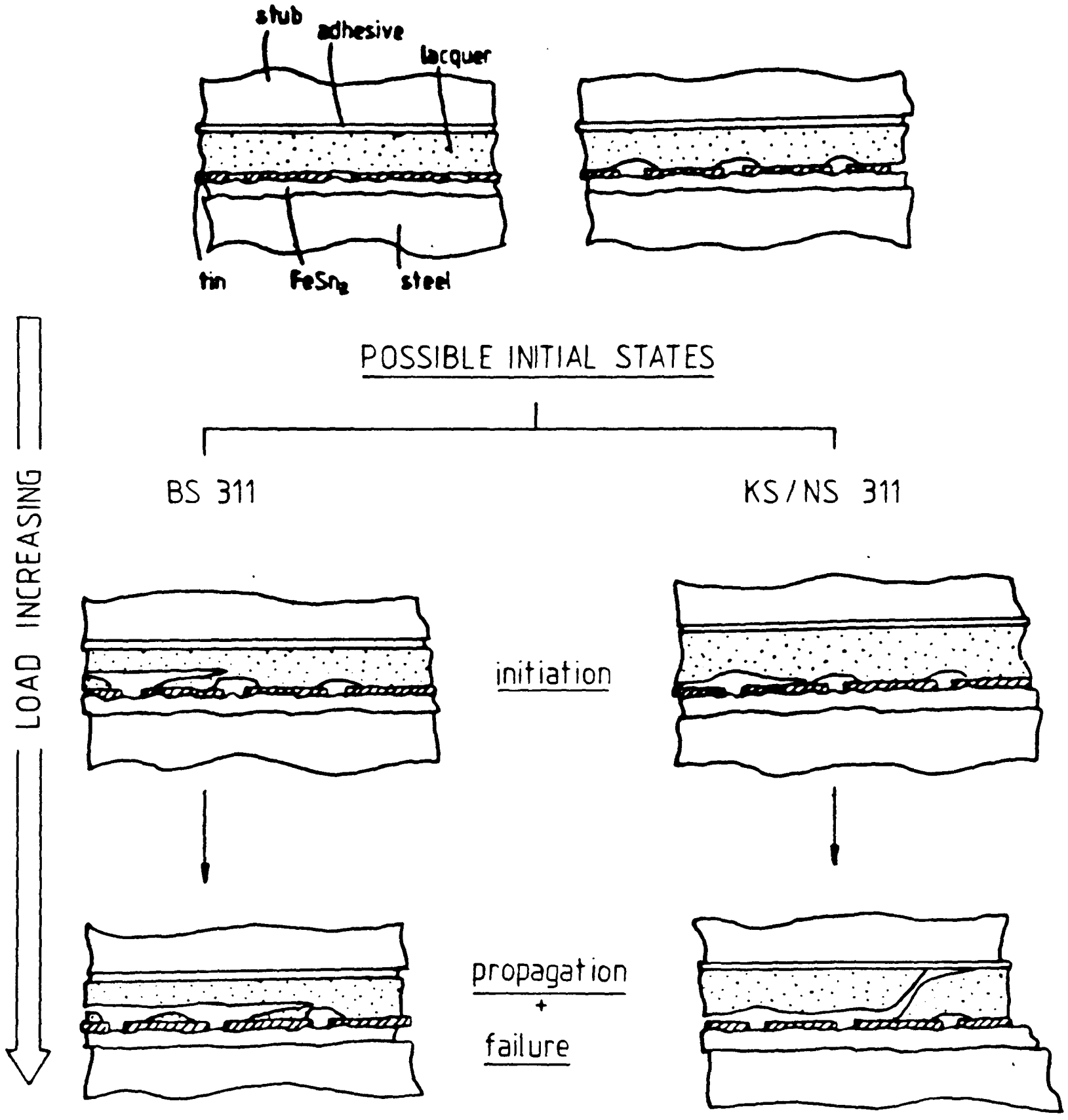

Figure 32. Schematic of failure in the butt-joint test for BS311 and KS311 lacquered tinplate samples

the angular $FeSn_2$ defects as initiation points but the first model assumes no initial lacquer debonding except at the site of the defect itself (possibly due to incomplete wetting by the lacquer) and gradual growth of debonding to form the lacquer-free zones under progressive loading; the second model takes the debonded lacquer-free zones as being present at the start of the test. At catastrophic failure initiation, one of the debonded regions propagates rapidly causing sceondary initiation around the other $FeSn_2$ defects. A distinction is made between the failures seen on BS 311 tinplate where the crack propagates through the lacquer and the KS 311/NS 311 type failures where propagation is beneath the lacquer at the tinplate surface (at least as observed in optical and scanning electron microscopy). In the latter case, crack propagation moves sharply to the lacquer-adhesive or adhesive stub interface and also makes this transition in BS 311 samples, although usually not at so steep an angle.

The fracture surfaces from the mechanical tests will be examined (see XPS chapter) to locate the crack propagation paths. It has been said that adhesive failure in metal-epoxy joints never occurs at the interface and is always cohesive in the polymer (Bascom et al 1975) and even that true interfacial failure never takes place (Bikerman 1947) although this has been strongly disputed (Good 1972). The adhesive-adherend system under study in this work, however, is a complex laminate where the lacquered passivated tinplate may be regarded as a metal-ceramic-polymer joint containing surface defects and inhomogeneities. The mechanism of failure, especially propagation, may well include effects due to all these components and will be treated more fully in the Discussion where results from TEM and XPS are included and a fracture mechanics treatment is made.

The butt-joint test has recorded a wide variability in results

which can be manipulated using ADF and Weibull analysis to show that BS 311 and BS 300 tinplates have better lacquer adhesion properties than NS 311 or KS 311. The butt-joint is measuring a quantity which comprises the intrinsic adhesion of the system due to surfaces and and chemical bonds and also an effect due to defects within the system. Since these defects are present in the tinplates used commercially, samples of which have been used in this work, the results of the butt-joint test show variations in lacquer adhesion which are likely to be encountered in commercial practice which are of more use in characterising the lacquer adhesion properties than measurements of intrinsic adhesion achieved by more simple laboratory-prepared specimens with carefully controlled interface structures and artificial defects.

The requirements for good adhesion are that minimal or zero amounts of lacquer are removed from the tinplate during testing, provided that a minimum value of failure load is achieved.

NS 311 and KS 311 samples have properties whereby there is no clear relationship between lacquer removal and failure load compared with the BS 311 and BS 300 tinplates.

Bibliography

Albu-Yaron A., Semel A. and Berzin A. J. Fd. Techn. 12 (1977) 325.

Albu-Yaron A. and Smith D.A. Br. Corr. J. 14 (1979) 133.

Alwar R.S. and Nagaraja Y.R. J. Adhesion 7 (1976) 279.

Andrews E.H. "Fracture in Polymers" Oliver and Boyd (Edinburgh and London) 1968.

Atsuda M. and Turner D.T. J. Mater. Sci. Let. 1 (1982) 167.

Azzeri N., Splendorini L., Barristoni C. and Paparazzo E. Surf. Techn. 15 (1982) 255.

Baker F.S. J. Adhes. 10 (1979) 107.

Barry B.T.K. and MacKay C.A. Tin and its Uses No. 9 (1972 8.

Bascom W.D., Timmons C.D. and Jones R.L. J. Mater. Sci. 10 (1975) 1037.

Bascom W.D., Becher P.F., Bitner J.L. and Murday J.S. in "Adhesion Measurement of thin films, thick films and bulk coatings" 63 ed. K.L. Mittal (ASTM) 1978.

Bikerman J.J. J. Coll. Sci. 2 (1947) 163.

Calder G.V., Hansen F.C. and Parra A. "Quantifying the Tape Adhesion Test" in "Adhesion Aspects of Polymer Coatings" 569 ed. K.L. Mittal Plenum (New York) 1983).

Chau C.C. and Li J.C.M. J. Mater. Sci. 17 (1982) 652.

Evans A.G. and Langdon T.C. Prog. Mater. Sci. 21 (1976) 320.

Good A.N. J. Polymer Sci. A2 (1974) 283.

ITRI (International Tin Research Institute) (1984)Dr. D. Bearfield (Pers. Comm.

Jennings C.W. J. Adhesion 4 (1972) 25.

Johnson L.G. Industrial Mechanics 2 (1951) 1.

Kerr C., MacDonald N.C. and Orman S. J. Appl. Chem. 17 (1967) 62.

Kies J.A., Sullivan A.M. and Irwin G.R. J. Appl. Phys. 21 (1950) 716

Kinloch A.J. J. Mater. Sci. 17 (1982) 617.

Kinloch A.J. and Young R.J. "Fracture Behaviour of Polymers" Applied Science (London) 1983.

Kuenzi E.W. and Stevens G.H. US Forest Products Laboratory Report FPL-011 (1963).

Kurzmann P. and Klemme D.A. J. Adhesion 7 (1975) 203.

Maercks O. Verpackungs Rundschau 29 No. 4 (1978) 25.

Moger M. Metal Box Research and Development Center (Personal communication) 1985.

Moyer C.A. Mater. Res. Stand. 2 (1962) 405.

Orman S. and Kerr C. "Aspects of Adhesion" 64 ed. D.J. Alner (University of London) 1971.

Packham D.E. in "Adhesion Aspects of Polymer Coatings" ed. K.L. Mittal Plenum (New York) 1983).

Smekal A. Ergeb. Exakt. Naturw. 15 (1936) 106.

Smelt D.H., Smith D.A. and Harpur W.W. J. Mater. Sci. 14 (1979) 2845.

Steiger F.H. Chem. Techn. 225 April 1971.

Takano H. and Watanabe T. Proc. 2nd Int. Tinplate Conference ITRI London (1980).

Weibull W. Ingenioersvetenskapsaked Handl. 151 (1939) 45.

Weibull W. J. Appl. Mech. 293 Sept. 1951.

CHAPTER 4

X-Ray Photoelectron Spectroscopy

THE TECHNIQUE

X-ray photoelectron spectroscopy (XPS), sometimes known as Electron Spectroscopy for Chemical Analysis (ESCA) is a surface analysis technique which has expanded rapidly in the last two decades from initial experiments (Seigbahn et al. 1967) up to the point where it is both a powerful research tool and a standard industrial analytical method (Seah 1980). XPS is extremely surface-sensitive, typically analysing about a ten monolayer thickness on the surface of a specimen. This, along with its ability to provide chemical bonding information, accounts for its widespread use as an analytical technique. The spatial resolution of XPS is not good, however, and normally precludes any imaging methods such as may be found with, for example, scanning Auger spectroscopy (Johannessen et al. 1980). The XPS signal typically emanates from an area of approximately 1 cm^2 in commercially available spectrometers.

XPS, then, yielding elemental and bonding information, well complements TEM examinations which provide structural data and images. In the field of adhesion where very thin interfacial layers can determine the behaviour of a large system, a surface-sensitive analytical technique such as XPS becomes very useful and has been used to study adhesion (Kinloch 1982, Briggs 1982, Hammond et al. 1981, Van Ooij and Kleinhesselink 1980) and the passivation layers on tinplate (Servais et al. 1979, Takano and Watanabe 1980, Coad et al. 1976, Azzeri et al. 1982). The basic principle of X-ray photoelectron spectroscopy is the production of photoelectrons with kinetic energy E_k from a specimen by illuminating it with monochromatic X-rays of energy $h\nu$ according to the equation (Einstein 1905):

$$h\nu = E_k + E_B + \phi \qquad (1)$$

where E_B is the binding energy and ϕ is a small contribution due to the spectrometer work function.

Figure 1 shows an energy level diagram that illustrates the process of electron emission. Auger electron production is included in the diagram because the latter transition will in general also occur. The incident X-ray quanta ionise core electrons which are emitted as photoelectrons, whose energy is dependent upon the X-ray energy (Eq. 1) unlike the Auger electrons.

The kinetic energy E_k of the photoelectrons is measured with a suitable detector and analyser and E_b the binding energy is calculated. Results are presented in the form of a graph of photoelectron emission intensity versus kinetic energy or binding energy.

The components of an XP spectrometer are:

1) X-ray source;

2) Electron analyser and detector;

3) Ultra-high vacuum system and sample manipulation;

4) Ion etching gun.

These are shown schematically in Fig. 2.

i. X-ray Source.

The spectrometer used for this work utilises an X-ray tube with interchangeable Mg or Al anodes offering two sets of X-rays. All the results that follow use Mg K_α radiation of 1253.6 eV energy and a line width of 0.83 eV. Mg and Al are commonly used as X-ray anodes for XPS machines as each yields a very intense K_α X-ray emission. (In fact, the K_α is a doublet of K_1 = 1253.7 eV and K_2 = 1253.4 eV but this is not resolved).

ii. Electron Analyser and Detector.

A 150° hemispherical type analyser is employed on the VG ESCALAB Mk. 1. Its purpose is to measure the photoelectron flux as a function of

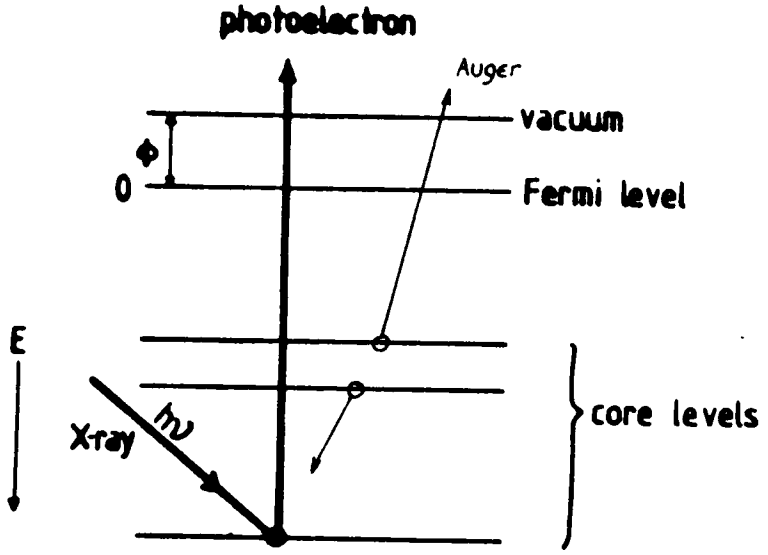

Fig. 1. X-ray Photoelectron spectroscopy (XPS)
The photoemission process produced by absorption of an X-ray photon

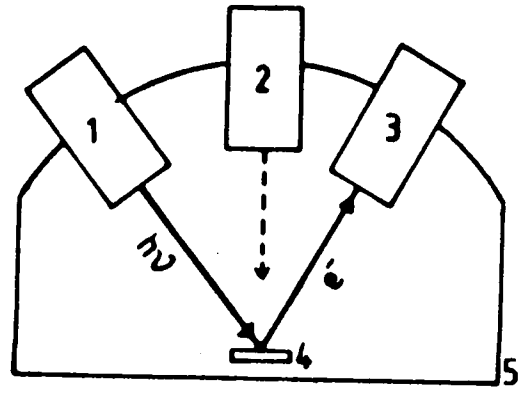

Fig. 2. Schematic layout of an XPS spectrometer
1) X-ray source. 2) Ar ion gun. 3) electron analyser and detector. 4) specimen.
5) UHV containment.

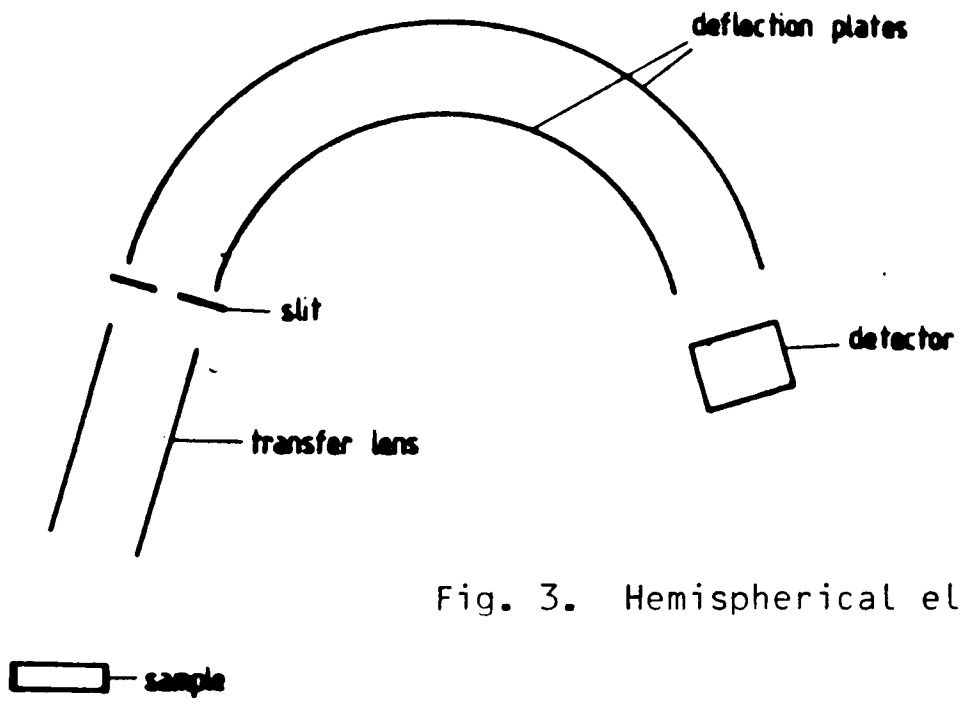

Fig. 3. Hemispherical electron analyser and detector

energy and it consists of concentric plates which are electrostatically charged to deflect the electrons through 150^{o} to a single channel detector. Photoelectrons are collected from the specimen by a transfer lens which focuses them at the analyser entrance slits. In the CAE (constant analyser energy) mode, all the photoelectrons are retarded at this point and are analysed at a constant pass energy. The slit aperture, scan energy width and scan times are all variable but this work has been completed with a constant aperture. The analyser is shown in Fig. 3.

iii. Specimen Manipulation and UHV System.

For very sensitive surface analysis it is critical that there is minimal contamination from the spectrometer. A bakeable ultra high vacuum system is therefore necessary and all the experimental work was carried out at pressures better than 10^{-8} torr, achieved by diffusion pumps and cold traps.

Specimens are transferred to the experimental vessel through a series of airlocks and chambers so that the the experimental vessel itself is always kept at high vacuum. Argon ion etching is carried out in a preparation chamber which may be isolated from the experimental chamber. The specimens themselves are moved either individually or on carousels by means of manipulator arms.

iv. Argon ion Etching for Depth Profiling.

A common means of presenting XPS data is in the form of a 'depth profile' where the concentration of a chemical species is presented as a function of depth through the surface. This information is achieved by removing the specimen surface atoms with an energetic beam of heavy ions, usually argon ions. An analysis is then made and the process repeated. Profiling is typically made up to a depth of < 50 nm. The depth information is provided in units of either depth

or etching time. The latter method is at least unambiguous when multi-component systems are being analysed because the different components are likely to have different sputtering rates (Kim et al 1974, Solomon and Hanlin 1980) leading to enrichment of certain elements as the etching continues. A second artifact due to ion etching is likely to be the reduction of oxides which has been observed to occur especially with chromium oxides (Riviere 1980) which are a major feature of this work. The latter effect is important when etching is done at high energy. It is possible to correct for the effect of different sputtering rates (Seah 1980, Hall and Morabito 1978) as many sputtering rates are known. For example, carbon has a sputtering rate which is an order of magnitude lower than most metals so the C1s peak appears as a persistent feature in many profiles. However, the compensation process is complex for multi-component systems and here data will be presented as a function of sputtering time. Kanaya et al (1973) and Andersen (1979) have calculated sputtering yields using physical models. Both experimental and theoretical rates will be used in summing up to provide approximate values for the passivation layer thickness.

Other potential errors introduced by the etching process are interface broadening by the formation of a rough surface and irregular etching if the ion beam itself is irregular in its spatial intensity. The ion etching was carried out at 7×10^{-7} mbar pressure with 5 kV ion energy.

2. INFORMATION FROM XPS

When a specimen is illuminated by X-rays core electrons are photoemitted from all elements except Hydrogen and Helium (which do not have core levels). The measured binding energies (or kinetic energies) allow discrimination between each element so a first step

in XPS analysis is to scan the spectrum over the total energy range available (1250 eV in the case of Mg K_α radiation) to determine qualitatively which elements are present. A series of 25 eV scans is then made across each peak of interest to yield a detailed plot on which quantitative measurements can be made. There are some instances where a problem arises due to overlapping photoelectron peaks from different elements. For example, O1s/Sb3d, C1s/Ru3d but for the limited range of elements being investigated in this work there were no such difficulties.

At higher binding energies Auger peaks appear in the spectrum which may be used as extra identification. They do not overlap with any XPS peaks of interest and are not normally used for quantitative measurements. If there is confusion in determining whether a particular peak is due to an Auger or XPS process the X-ray source can be changed. When this is done an Auger peak will remain at a fixed energy level but an XPS peak will shift.

There are also small satellite peaks associated with XPS peaks in the spectrum. These are due to the X-ray source being not quite monochromatic. As has been stated, a major advantage of XPS is its ability to provide information on the bonding state of the elements. The binding energy of a particular core level is dependent on its bonding state and the variation can be measured. For instance, the binding energy of metallic tin (Sn^O) is 484.5 eV as compared with 486.1 eV for tin in an oxidised form, often written as (SnO_x) when the exact oxidation state is unknown. It has been possible to determine the binding energies of several tin and chromium oxides, often from the use of standards but experimental resolution in practice is not always possible as the difference between two oxides may be less than linewidth of the analysing radiation. A list of experimentally

determined binding energies for oxides of tin and chromium is shown in Table 1. With sufficient information, it is possible to calculate binding energy shifts (Jolly 1972, Schwartz et al 1972, Seigbahn et al 1969).

An example of a wide scan (1250 eV) spectrum is shown in Fig. 4 with the photoelectron peaks of carbon, tin, chromium and oxygen marked. Having found the prominent peaks from such a spectrum, measurements are then made from a more sensitive scan of 25 eV range. Figs. 5 and 6 show 25 eV spectra for Sn, O, Cr and C in the constant analyser energy (CAE) mode. These clearly indicate the difficulty in extracting precise chemical state information even when the analyser energy is reduced to increase resolution. The resolving power of an electron analyser is proportional to the kinetic energy of the electrons and inversely proportional to the retardation energy. For example, the full-width half maximum (FWHM) line width of silver at a 50 eV pass energy is 2.00 eV compared with 0.95 eV at a pass energy of 10 eV.

Measurements for a particular specimen are always done under the same analyser conditions and the high-resolution mode is used only for clarification.

The intensity of a signal has been measured in this work by graphically integrating each peak over a background noise level. In some spectrometers there is provision for automatic measurement of peak intensities and the subsequent calculations for quantification of results. However, in this work, measurements were made from hard-copy graphical output using either a digitising tablet and microcomputer or a planimeter. The method for obtaining quantitative data will be discussed below.

Some chemical shifts may not be resolvable to the extent that separate peaks are produced even with a reduced analyser energy. Under

TABLE 1. BINDING ENERGIES FOR OXIDES OF TIN AND CHROMIUM

Element	BE (eV)	KE (eV)	References
Sn3d5/2			
Sn^{o}	484.5	769.1	Lin et al (1977)
	485.0	768.6	Leroy et al (1976)
SnO	486.5	767.1	Leroy et al (1976)
	487.1	766.5	Willemen et al (1979)*
	485.9	767.7	Morgan et Van Wazer (1973)*
	487.4	766.2	Grutsch et al (1973)*
SnO_2	486.2	767.4	Lin et al (1977)
	486.9	766.7	Willemen et al (1979)*
	486.6	767.0	Morgan et Van Wazer (1973)*
	486.0	767.6	Grutsch et al (1973)*
$Cr\ 2p_{3/2}$			
Cr^{o}	574.4	679.2	Lin et al (1977)
Cr_2O_3	567.7	676.9	Ikemoto et al (1976)
$Cr(OH)_3.nH_2O$	577.8	675.8	Olefjord et al (1975)
CrO_3	579.4	674.2	Morris and Westwood (1974)
CrO_4^{2-}	580.2	673.4	Azzeri et al (1982)
$Cr_2O_7^{2-}$	579.8	673.8	Ikemoto et al (1976)
O1s			
Cr_2O_3	530.4	723.2	Barristoni et al (1981)
-OH	531.6	722.0	Maeda et al (1980)
SnO	530.8	722.8	Maeda et al (1980)
SnO_2	530.1	723.5	Lin et al (1977)

* Not shown on Figs. 4 and 5.

Fig. 4. A wide scan (1250 eV) XPS spectrum for a 311 tinplate surface. This type of spectrum shows major peaks and is not used for quantitative analysis.

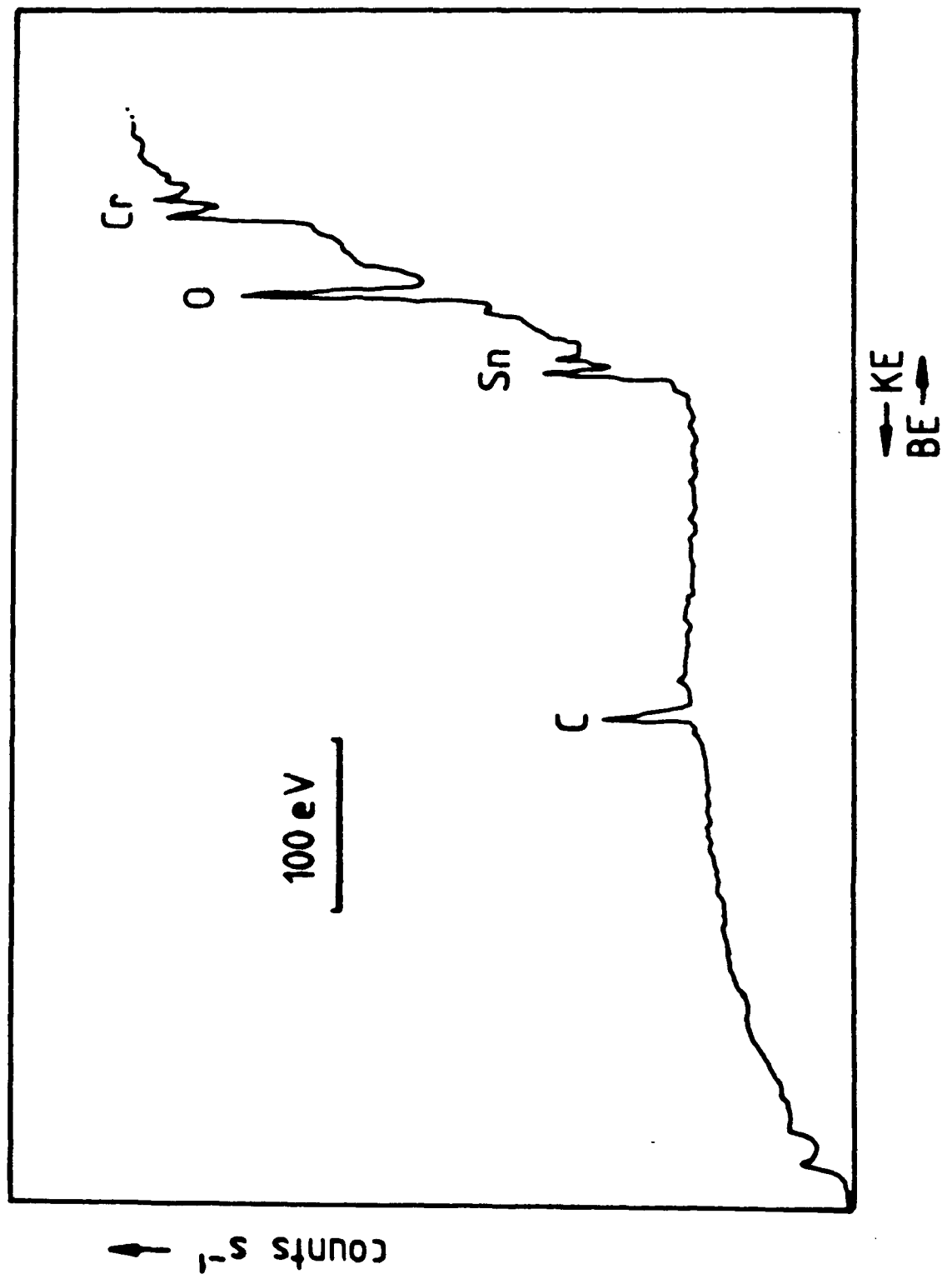

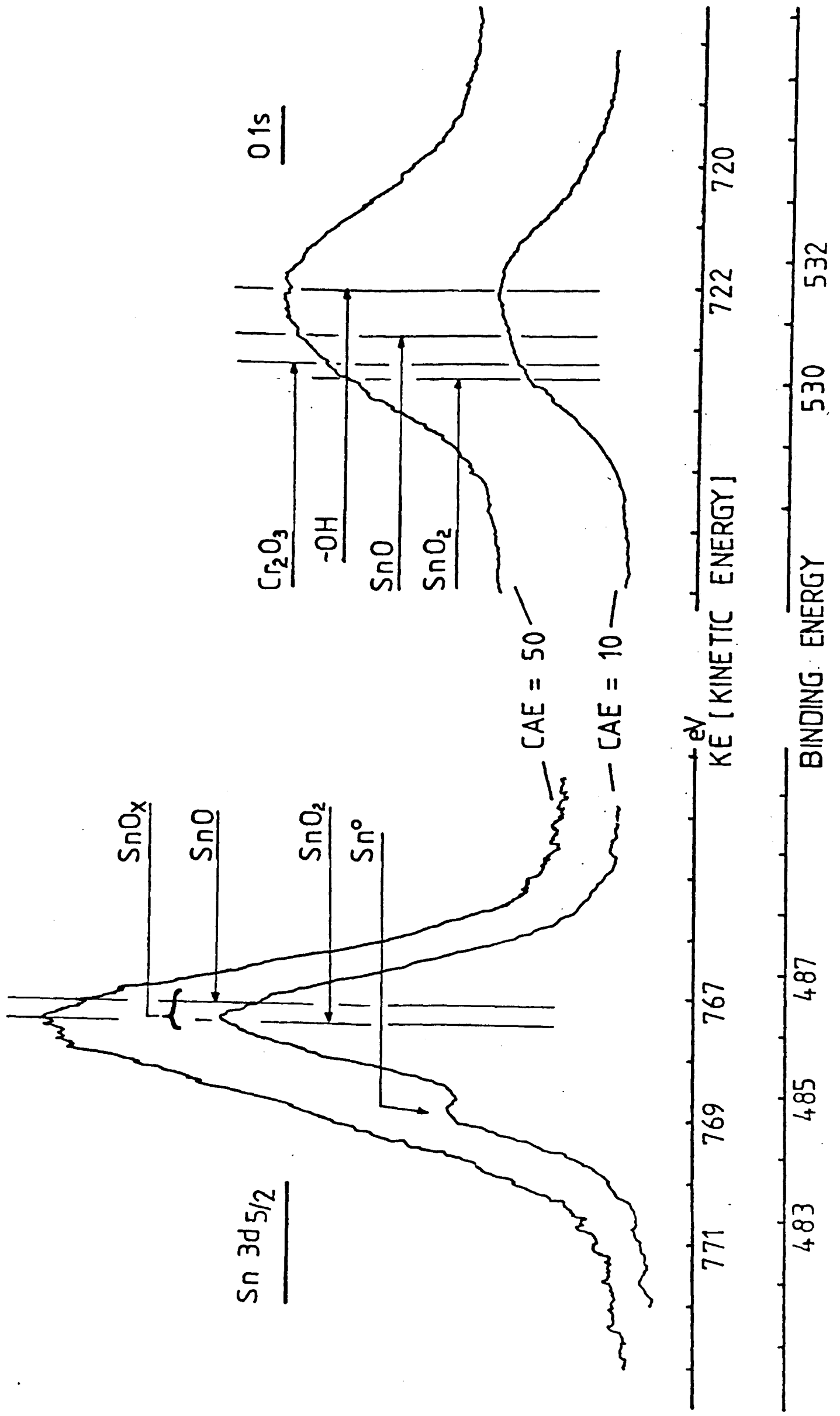

Fig. 5. 25 eV XPS spectra of the Sn 3d 5/2 peak and the O1s peak. Measurements are taken from these spectra for quantitative calculations. The positions of peak centroids for common tin and oxygen compounds are marked.

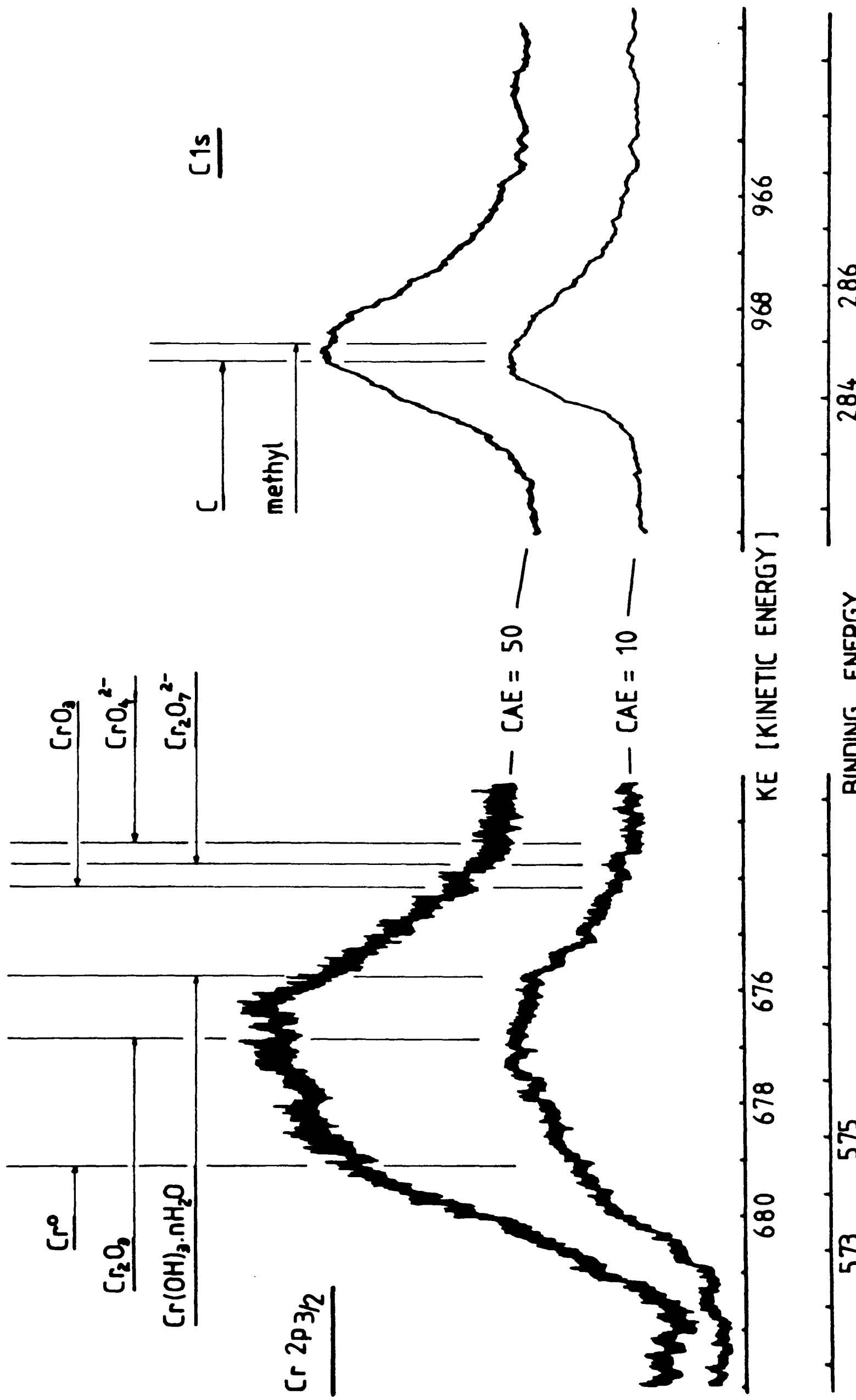

Fig. 6. 25 eV XPS scans of the Cr 2p 3/2 and C1s peaks. C hromium oxide energies are marked.

such conditions it is necessary to deconvolute the peaks, often using a computer program. To do this one has to make certain assumptions about the peak shapes. Firstly, each signal is superimposed on noise caused by secondary electrons from higher kinetic energy peaks. This effect is seen in the 'jumps' in background associated with large XP peaks (as seen in Fig. 4). This background is taken as linear over the energy range of the peak being examined although it is equally acceptable to use a stepped background to account for the noise 'jump'. Peaks usually exhibit a Lorentzian shape (McGuire 1972) with a tail-off at low kinetic energies. For deconvolution by hand these are approximated by Gaussian curves with a linear tail-off. The actual shape of an XP peak is the result of a number of factors. The X-ray source should ideally have a delta function emission but in reality exhibits a finite linewidth. This, combined with the natural linewidth of the emission process and a particular analyser function causes the resultant peak to be a certain shape. This may be represented as:

$$E_m^2 = E_p^2 + E_a^2 + E_n^2 \qquad (2)$$

where:

E_m is the FWHM of the peak (Full Width Half Maximum)

E_p is the X-ray photon source line-width

E_a is the analyser function

E_n is the linewidth of the emission process

Another mecahnism which shifts XP peaks is electrical charging of the specimen. This phenomenon, found with insulating samples, causes shifts of a few eV or less but in a relatively simple system such as is being investigated here the effect may be partially compensated for by using a common peak of known energy as a reference level. The C1s peak is often chosen for this. The charging effect

may not be uniform across the whole XP spectrum (Fadley 1978) and in general it can present serious problems in the investigation of complex polymeric systems (Evans 1977). The C1s peak, found on most samples from contamination, can be used to provide a calibration point for assessment of the energy shifts caused by charging. Another method is to use a deposited layer of gold on the sample to provide a reference (Uwamino et al 1981).

There are other effects found in XP spectra: shake-up satellites are found on the high BE side of XP peaks and arise from valence-level transitions which may accompany core-level photoemission (Dilks 1977). Multiplet splitting is found in 3s and 4s peaks and is due to the formation of multiplet final states from unpaired electrons found in 3d and 4f orbitals (Viinika and Laarson 1975) and consequently does not feature in this work where the main peaks of interest are Sn 3d5/2, Cr 2p3/2, O 1s and C 1s. Valence level peaks are usually very small owing to low photoemission cross-sections. They have been used for identification purposes in samples where core-level emission is much reduced.

3. QUANTITATIVE ANALYSIS

It is valuable to be able to use XPS data in a quantitative manner. The technique has a sensitivity of 0.1% but the simple routines that can be used to achieve quantitative data bring in errors which can leave the final results with a 10% to 20% inaccuracy.

There are three general methods of quantitative analysis in use. These are:

i/ Physical modelling;

ii/ Elemental sensitivity method;

iii/ Comparison with standards.

These are briefly discussed below.

i/ Physical Modelling

Physical models have been developed which describe the intensity of photoelectron emission due to X-ray photon absorption (Powell 1982, Azzeri et al 1982). This method relies heavily on a good understanding of the physical processes which take place during photoemission and the possession of reliable data. In order to calculate the photoelectron flux from the specimen surface the factors which need to be taken into account are incident X-ray flux, spectrometer sensitivity, the number of atoms taking part in the photoemission process and their atomic cross-sections for ionisation, the electron mean free path in the sample and the transmission factor for electrons through the sample surface.

Although highly complex,physical models are becoming more widely used as more data are collected and confidence grows in the accuracy and validity of the method.

ii/ Elemental Sensitivity

The most common route to quantitative results and the method used in this work involves measurement of the peak intensity and the division of these values by appropriate sensitivity factors to yield the number of emitting atoms present in the sample. In this case the assumptions are that the sample is flat and homogeneous and that the XPS line intensities are independent of molecular binding effects (Carter et al 1975).

The program used for calculations is one used at Metal Box Research Centre and is based on the following equation for compound AB:

$$\frac{N_A}{N_B} = \frac{I_A}{I_B} \quad \frac{\sigma_B}{\sigma_A}\sqrt{\frac{E_A}{E_B}}$$

where:

N_A is the number of atoms of element A

N_B is the number of atoms of element B

I_A is the photoelectron intensity for A

I_B is the photoelectron intensity for B

σ_A is the atomic cross-section for A

σ_B is the atomic cross-section for B

E_A is the kinetic energy of the A peak

E_B is the kinetic energy of the B peak

The square root terms are present because the electron mean free path is proportional to the root of kinetic energy.

To obtain the values of N_A and N_B then, the photoelectron intensity from each peak must be measured. The kinetic energy of each peak is easily found from the spectrometer graphical output or obtained from published tables (Seigbahn et al 1969). The atomic cross-sections for photoemission are available from calculated values in the literature (Schofield 1976, Manson and Dill 1978). Accurate determination of the photoelectron intensity is therefore critical in achieving optimum quantitative results and this is obtained from measurement of the area beneath the emission peak. Appropriate care must be taken to fix the level of background and this is most easily done using a straight line approximation linking the start of the peak to the point on the graph where the peak subsides into the background. Although the elemental sensitivity factor is widely used there has been some doubt cast on its suitability for use with multi-phase systems (Wagner 1977) due to variations in the electron mean free paths and surface contamination. Errors also arise in transition metal studies from many-electron processes and therefore the total error in quantitative analyses of this type is estimated to be ± 20%. Such errors, however, tend to

TABLE 2. OPERATING CONDITIONS FOR X-RAY PHOTOELECTRON SPECTROSCOPY

Spectrometer:	Vacuum Generators ESCALAB I
Analysing Radiation:	Mg K_α 1253.6 eV
Analyser Aperture:	C1
Anode Kilovoltage:	9 or 15 (normal; 15 (high resolution)
Current:	10 mA (insulators); 5 mA (conductors)
Analyser pass energy	50 eV (normal)
Constant analyser energy mode, CAE:	10 eV (high resolution)
Spectrum Range:	1250 eV (wide scan; 25 eV (analysis)

CONDITIONS FOR Ar ION ETCHING

Ar pressure:	7×10^{-7} torr
Voltage:	5 kV
Focus:	3.5 kV
Current:	20 μA

be consistent for similar systems under analysis as tests in this work on repeat analyses have shown.

iii/ Comparison with standards

This is probably the simplest method whereby a standard sample of known composition and structure is made up and compared with the test specimen (Leroy et al 1976). The great disadvantage of this procedure is that a wide range of carefully produced standards is needed unless the analysis is limited to a small number of sample types.

4. EXPERIMENTAL WORK

Figs. 4, 5 and 6 illustrate the type of spectrum available and the method for quantitative analysis has been described above. This section of work attempts to characterise the as-received and stoved surfaces of a number of tinplates with widely different lacquer adhesion properties (as defined by factory performance, the "Scotch Tape Test" and other sections of this work). The tinplates investigated are listed in Table 3 by manufacturer, type and adhesion properties.

The process of tinplate manufacture from steel strip to passivation treatments is described in Chapter 1 but to recap, the 311 type has been passivated with a cathodic coating treatment in a dichromate bath to produce a chromium-rich layer on the surface; 300 plate is given a chromium-rich passivation layer by simple dipping in a similar solution. In each case, the object is to give the tinplate surface a protective coating which will inhibit tin oxide growth, considered inimical to lacquer adhesion. It is the structure and properties of these passivation layers which have attracted a considerable body of work which attempts to correlate the properties of the tin oxide and

TABLE 3. TINPLATE TYPES USED

Manufacturer	Type	Lacquer Adhesion property measured by Scotch Tape test	
British Steel	311	good	*
Nippon Steel	311	intermediate	*
Kawasaki Steel	311	poor	*
British Steel (G)	311	good	
British Steel (P)	311	poor	
British Steel	300	good	

* Main set used for comparison

chromium-rich layers with performance in terms of corrosion resistance and lacquer adhesion. There is as yet no satisfactory thesis to describe the latter and a summary of the many investigations using XPS, electrochemistry, electron microscopy and other techniques is given in Chapter 2 .

Several types of lacquer were used in the research programme for mechanical testing and XPS investigations. These were phenolic, epoxy-phenolic and oleoresinous. Some of the lacquer coating was done under normal commerical conditions and some in the laboratory where stoving was carried out in air or in an inert atmosphere of argon or nitrogen. It should be noted that the adhesion ranking of the various tinplates listed in Table 3 were reproduced with several different lacquer types and for lacquering carried out under different conditions at different sites, thus suggesting that the lacquer and stoving conditions were not the sole causes of the varying adhesion properties and that an investigation of the tinplates themselves would reveal differences which affect the adhesion properties.

Samples were prepared for XPS examination by cutting sheet into 1 cm squares for mounting on specimen holders for the spectrometer. In order to prevent damage to the surface before analysis the samples were either washed briefly in methanol or examined as-received. The surface of large sheets of tinplate is given a light coating of oil after manufacture to assist handling in the later stages of can production. on UK can production lines this oil is sometimes removed prior to lacquering by flame treatment but this is not often the case in many other parts of the world (usually dictated by safety considerations) and so this oil layer was accepted in this work as part of the tinplate system to be considered. Fracture surfaces from adhesion tests were examined with no manual surface cleaning and as soon after failure

as possible but the delay between fracture and XPS examination was necessarily hours or days because the two operations were carried out at sites several miles apart and the XPS machine had no fracture stage in the UHV work chamber.

The results of the XPS investigations are presented below in the form of graphical output as received from the spectrometer. This shows photoelectron intensity as a function of kinetic energy (or binding energy: K.E. = 1253.6 - B.E. eV). Values of photoelectron intensity (in counts per second) are not usually given but relative peak magnification factors are given where necessary for the purpose of comparison. Typical counting rates for a strong peak would be $> 10^4$ cps and $< 10^2$ cps for a very weak peak. Depth profiles are shown in Tables of etching time vs. relative atomic concentration.

Table 2 lists the operating conditions used in this work for analysis and Argon ion etching with the Vacuum Generator's ESCLAB I.

Much of this work is based on the comparative study of a batch of tinplates British Steel (BS), Nippon Steel (NS) and Kawasaki Steel (KS) with differing adhesion properties which can be regarded as intrinsic to the tinplates themselves rather than to a particular lacquer or stoving process as has been shown in the chapter on mechanical testing. The large-scale morphologies of these tinplates do not appear to be the cause of the consistent variation in lacquer adhesion between them so the XPS technique has been used to investigate differences in their passivation layers.

At this point it is useful to consider a structural model of the passivation layer derived from other earlier works. From electrochemical studies it has been found (Rauch and Steinbicker 1973) that 311 tinplate possesses a chromium-rich layer of some 60-100 $\mu g\ dm^{-2}$ in weight which is equivalent to a continuous layer of approximately

1 nm in depth. Further studies revealed that the passivation layer was inhomogeneous and a more recent model (Saijo 1976) proposes a population of layered islands on the tin surface surrounded by a "sea" of tin oxides. The Saijo model, shown in Fig. 7, contains chromium in metallic, oxidised and hydrated forms stratified in a particular order but not as precisely segregated as shown in the schematic drawing. This particular model was derived from transmission electron microscopy and XPS and is a convenient model to use for comparison with this work as it combines the many forms of chromium oxides and tin oxides and metallic chromium which have been proposed as constituents of the passivation layer.

The experimental results of the XPS investigation are shown below for the examination of the passivation layer as found on the tinplate surface and on the fracture surfaces of mechanical test specimens.

i) The tinplate surface

The wide scan (1250 eV) spectra of BS 311 unstoved tinplate are shown in Fig. 8 for a series of successive Ar ion surface etches. The etching times are shown next to each spectrum. Whilst the wide scan spectrum is not normally used for quantitative measurements, these plots serve to show the main peaks of interest and the obvious development of the Sn and Cr peaks with the reduction in O and C as etching proceeds. The more detailed 25 eV spectra in Figs. 9 and 10 are used for quantitative analysis and illustrate the changes in peak shape, intensity and chemical shifts along the energy axis. (The chemical shifts of 1 to 2 eV shown for the unetched plate are due to specimen charging and mostly disappear after 30 seconds' etching).

After 30 seconds' etching, the SnO_x peak is almost totally removed, leaving the metallic tin peak. This indicates, using the

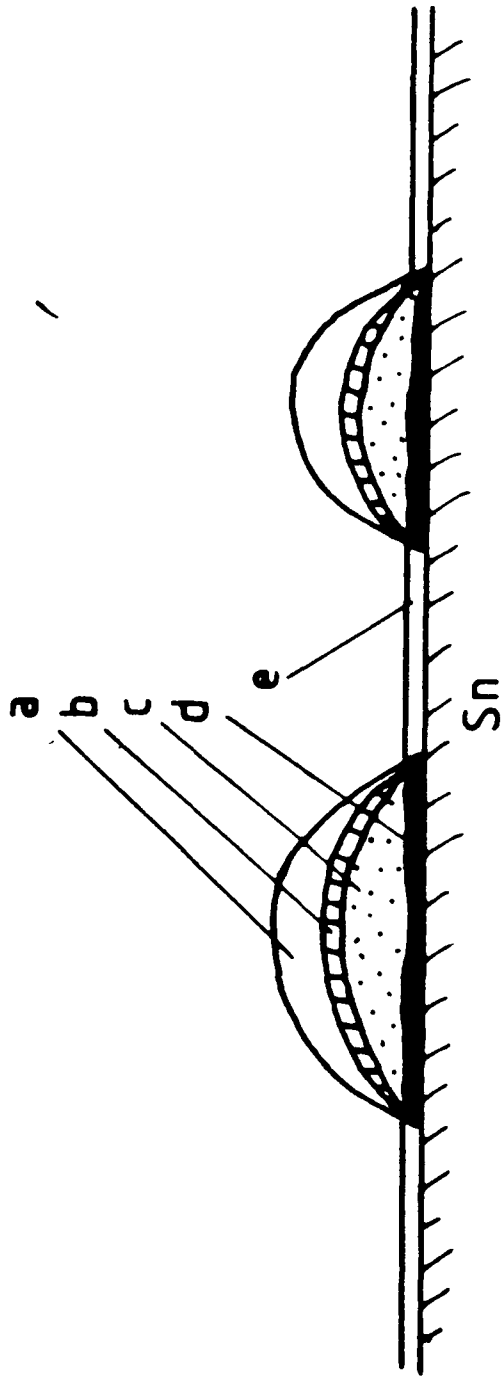

a. $Cr_2O_3.nH_2O$
b. [a+c]
c. Cr_2O_3
d. Cr^o
e. SnO_2, SnO

Saijo et al.

Fig. 7. The model proposed by Saijo for the structure of passivation layers on 311 tinplates.

TABLE 4. QUANTITATIVE RESULTS OF DEPTH PROFILING AND XPS SHOWN AS ETCHING TIME vs. RELATIVE ATOMIC CONCENTRATIONS.

UNSTOVED BRITISH STEEL 311 TINPLATE

Etching Time (minutes)	0	0.5	1	2
Element				
Sn	7	60	72	64
Sn^{O}	3.5	60	72	64
SnO_x	3.5	0	0	0
Cr	15	15	13	17
Cr^{O}	-	3.5	7	8
CrO_x	-	11.5	6	9
O	78	25	15	19

Saijo model, that the tin oxide "sea" has been totally removed and so must be less than 1 nm in thickness. At the same stage in etching the Cr peak has not changed in shape but the O peak has diminished in intensity by 70% as the tin oxide and adsorbed water are removed.

Quantitative results for this sample are given in Table 4 where it is seen that the metallic Cr signal increases up to one minutes' etching and remains constant thereafter. From the work of Riviere (1980) it could be expected that after etching for one minute under these conditions over 6% of the Cr^{3+} would have been reduced to Cr^{0} under the ion beam and after some 2 minutes, some 10%. It is therefore justified to draw conclusions about the trend of Cr^{0} concentrations over short etching times such as used here. It has not been possible to deconvolute the spectra further to yield values for specific chromium oxidation states but, drawing upon the data in Table 4, it is seen that after a 2 minute etch there is a sufficiently large O peak to account for a mixture of chromium oxide such as Cr_2O_3 and CrO_2. In the Saijo model it might be expected that a Cr^{o} signal would not be seen until most of the oxidised chromium had been removed. These results show that metallic chromium is found in equilibrium with the oxidised forms after only a one minute ion etch and therefore that its distribution is not likely to be exactly as shown in Fig. 7. Extended etching is likely to cause reduction of oxidised chromium, and therefore misleading results, so a novel approach to the examination of the deeper layers of the passivation film will be described later in which the entire film is removed from the tinplate and examined from the underside. This method should also reveal whether all the tin oxide has been removed by the 30 second etch or whether there is still some remaining, shielded by the chromium-rich components of the passivation layer.

In commercial practice the application of lacquer to tinplate is followed by a stoving process, typically for about 10 minutes at 200°C, depending on the type of lacquer. It has been suggested (Servais et al 1979) that this stoving can alter the tinplate surface and consequently affect its adhesion properties. Tinplate samples have been lacquered and stoved in the laboratory for experimental examination and several tinplates have also been stoved without a lacquer coating so that the effects on the passivation layer could be observed.

Samples of BS 311 tinplate with good adhesion properties (as shown in Figs. 9 and 10) were stoved in air at 200°C for 30 minutes and in an argon atmosphere at the same temperature and duration. In both cases, the SnO_x is removed by a 30 second Ar etch although the unetched tin spectrum for specimens stoved in both air and argon shows an enhancement of the SnO_x peak. Stoving has evidently further oxidised the tin but not beyond a depth of 1 nm, capable of removal by a 30 second argon etch. The apparent oxidation in the argon environment is unexpected and is possibly due to incomplete purging of the heating box during the stoving process, although this could not be improved in further tests. XPS spectra from the stoved samples are shown in Figs. 11 and 12. The metallic chromium peak is also diminished in the case of the stoved tinplate although the state of hydration or oxidation cannot be exactly determined. The effects of stoving for 30 minutes are therefore a slight increase in the oxidation of tin and chromium as would be expected and for commercially lacquered tinplate such effects are likely to be further reduced as the stoving time is shorter and the tinplate surface is partially protected by the lacquer coat. Growth of SnO_2 after a 5 hour stoving has been detected (Takano and Watanabe 1976) but flame treatment has

no effect on the tin oxide layer (Emerson and Fellows 1981).

Unstoved samples of Kawasaki Steel (KS) tinplate with consistently poor adhesion properties and Nippon Steel (NS) tinplate with 'intermediate' adhesion properties are shown in Figs. 13, 14 and 15,16 respectively. As for BS 311, the tin oxide is quickly removed by Ar ion etching to leave just a metallic tin signal. The results of qualitative analysis are shown in Table 5 from which it is seen that after about one minutes' etching the proportions of Cr^0 to CrO_x are nearly an order of magnitude lower than for BS 311, but that the relative proportions of O and CrO_x are constant. If it is assumed that all the oxygen detected is from chromium compounds and not adsorbed water then these ratios can account for a mixture of chromium oxides and perhaps some hydrated forms. The O1s peaks for BS, KS and NS are identical in shape at this stage and show that similar oxides exist on all three types of tinplates with hydrated chromium in the outer layer. A further difference between the plates can be seen in the relative proportions of Sn^0 and Cr after etching.

The other main type of tinplate used commercially is 300 plate, whose passivation layer is not formed electrolytically but by dipping. No metallic chromium has been found on 300 tinplate (Azzeri et al 1982) but chromium compounds and tin oxides are present. The XPS spectra from a British Steel 300 tinplate are given in Figs. 17 and 18 for successive ion etchings. As expected, no Cr^0 was found but the tin oxide layer is considerably thicker than that found on 311 tinplates. The quantitative results for 300 plate are shown in Table 6. The tin oxide layer is found to be at least twice and possible six times the thickness of the SnO_x on 311 tinplate.

The thicknesses of SnO_x found on NS, KS and BS 311 tinplates are very similar. This may be deduced without incremental Ar ion

etching up to 30 seconds by measuring the relative peak sizes for Sn^0 and SnO_x in the Sn 3d 5/2 photoelectron peaks. The metallic tin signal is assumed to be from underlying metal and is attenuated by the oxide layer (Grundner and Halbritter 1980) so the relative peak intensities are a measure of the oxide thickness.

From the work of other authors (Saijo 1976, Albu-Yaron and Smith 1979) it seems that the passivation layer is deposited as discrete regions on the surface of tinplate rather than a continuous, homogeneous layer. The results of the XPS examination so far may now be compared with the Saijo model (Fig. 7). It should be noted, however, that the models which will ultimately be derived for the passivation layers will not be identical to those given by other workers. There are variations between different types of 311 tinplate cited in the literature, particularly for metallic chromium but also for other constituents, which may be due to the different tinplates or to the experimental methods used. For example, Servais et al (1979) find the metallic chromium content of 311 passivation films to be 17% of the total chromium present compared with 16% (Maeda 1980), 10% (Takano and Watanabe 1980), 3%-10% (Leroy et al 1976), 5% (Saijo 1976) and 54% (Coad et al 1976, Rauch and Steinbicker 1973). Values for the total chromium content, usually measured electrochemically, also vary but most experimenters have measured concentrations of about 0.05 μg cm^{-2} (Servais et al 1979, Takano and Watanabe 1980, Leroy et al 1976).

The removal of tin oxide to reveal metallic tin is accomplished by a 30 second etch for 311 tinplate and by a 3 minute etch for 300 tinplate. If the passivation layer were of constant thickness it would be expected that the chromium component of 311 plate would then be removed by an Ar ion etch of 2.5 minutes duration. (This assumes

that the sputtering yield of the chromium is lower than that of the tin oxide by a factor of 4.4). This is not the case and indicates that the chromium component is located in thicker regions, as suggested by Saijo. When the tin oxide is removed the XPS signal is then produced by Cr and O from these passivation layer "islands" and the bare Sn^0 between them. Quantitative analysis will then yield a value for the relative areas of each which are photoemitting and hence a value for the relative areal coverage of chromium-rich passivation layer on the tinplate surface. These quantities are shown in Table 7 for the unstoved BS, KS, NS and 300 tinplates. It must be pointed out that whilst this approach provides a useful comparison of the areal coverage by chromium, the specimens must each have the same minimal ion beam exposure sufficient to remove the tin oxide. It assumes that the thickness of chromium and chromium compounds remaining is greater than the depth involved in photoemission so that the Sn^0 signal emanates only from the bare tin surface.

From Table 7 it is seen that the BS 311 possesses a surface with a similar coverage of chromium and oxygen to the KS or NS tinplates but with a higher Cr^0 content. The tin oxide thicknesses for these 311 tinplates are similar but it is not possible (using XPS) to distinguish between SnO and SnO_2. Indeed, an intermediate tin oxide, "SnO_x" has been proposed (Aubrun 1970) but the use of transmission electron microscopy should determine which are present. In the same way, the particular oxides of chromium present in the passivation layer will be identified. The XPS results cannot positively resolve the major chromium oxide peak which is due to Cr^{3+}, possibly Cr_2O_3, or $Cr(OH)_3n.H_2O$ (or probably both). There is no evidence for chromium oxides with binding energies higher than 578 eV (Cr^{3+}) on any of the tinplates so far examined.

TABLE 5. QUANTITATIVE RESULTS OF DEPTH PROFILING AND XPS SHOWN AS ETCHING TIME vs. RELATIVE ATOMIC CONCENTRATIONS

	UNSTOVED KAWASAKI STEEL 311 TINPLATE		UNSTOVED NIPPON STEEL 311 TINPLATE	
Etching Time (minutes)	0	1	0	0.5
Element				
Sn	34	73	14	74
Sn^{o}	18	73	2	74
SnO_x	16	0	12	0
Cr	16	9	18	8
Cr^{o}	0	1	-	0.5
CrO_x	16	8	-	7.5
O	50	18	68	18

TABLE 6. QUANTITATIVE RESULTS OF DEPTH PROFILING AND XPS SHOWN AS ETCHING TIME vs. RELATIVE ATOMIC CONCENTRATIONS

UNSTOVED BRITISH STEEL 300 TINPLATE

Etching Time (minutes)	0	1	3	6
Element				
Sn	25	52	92	96
Sn^{O}	7	11	90	96
SnO_x	18	41	2	0
Cr	3	5	2	1
O	72	42	6	2

TABLE 7. AREAL COVERAGE OF TINPLATES BY CHROMIUM-RICH CONSTITUENTS OF PASSIVATION LAYERS

Tinplate	Coverage (%)
BS 311	18
KS 311	12
NS 311	11
BS 300	2

(Unstoved tinplates)

ii) Fracture surfaces

After the mechanical adhesion testing of lacquered tinplates, the fracture surfaces are available for XPS. With such a sensitive technique the locus of failure may be located to see if one particular constituent of the passivation layer is consistently acting as a "weak link". Butt joint fracture surfaces have been examined by Servais et al (1979) who investigated the adhesion of lacquer to 311 tinplates with good and poor adhesion properties. These workers found that, in both cases, the entire passivation film was removed by the lacquer as fracture occurred at the passivation layer-tin interface. In the case of their samples with poor adhesion a thick layer of tin oxide was found at the tin-passivation layer interface and it was suggested that this had grown during stoving and weakened the system. Such conclusions are not supported by this work as the stoving tests have shown and it is possible that the tin oxide layer found by Servais et al formed after the fracture by exposure to air. The same workers report an inability to produce a butt-joint fracture in lacquered 300 tinplate at an interface which would allow XPS examination of the passivation layer. The work described below has, with some difficulty, produced results which allow the examination of fracture surfaces from all tinplate-lacquer combinations including 300 and 311 tinplates with good properties of adhesion.

As described in the chapter on mechanical testing, the lacquered tinplate sample is bonded between two metal stubs which are then pulled apart in a direction normal to the tinplate surface. The resultant fracture surfaces are then available for examination. In some cases, the lacquer is totally removed by this method but more commonly for specimens with good adhesion there is a mixed fracture mode in which areas of lacquer remain on the tinplate surface.

The XPS spectra of a BS311 sample coated with epoxy-phenolic

lacquer is shown in Figs. 19 and 20 from the tinplate and lacquer sides of the fracture respectively. In general, the Cr peak has been used to identify the passivation layer. (Where there is extensive specimen charging the kinetic energy scale has been omitted as precise evaluation of the peak energies has not been possible). From Figs. 19 and 20 it can be seen that the passivation layer has not been removed from the BS 311 tinplate by the lacquer and no trace of tin (or chromium) is found on the lacquer side of the fracture surface. This effect is also shown by lacquered 311 tinplate stoved in Ar (Fig. 21). Ar stoving has already been shown to have no measurable effect on the passivation layer compared with air stoving. The locus of failure in BS 311 samples was examined using an organosol lacquer which could be detected via the chlorine signal and which was found on exposed tinplate surfaces which appeared completely lacquer-free in the optical and scanning electron microscope. Fracture had therefore occurred within the lacquer very close to the passivation layer and not at the interface. The precise distribution of lacquer areas on the tinplate surface could not be determined using XPS which measures large areas.

The presence of thin lacquer layers on BS 311 tinplates when tested with other lacquer types could not be measured since only the organosols possessed an easily-removed chemical "tag" and carbon and oxygen contamination on all samples prevented positive identification of thin layers from other lacquers. It is however possible that all lacquers fail in this way on BS tinplates.

These results are at odds with those of Servais et al but examination of the KS and NS tinplates after tensile adhesion testing show that the passivation layer is removed by the lacquer for these types. Fig. 22 shows the spectra for SnO and Cr from the tinplate side fracture surface of a lacquered KS specimen. Etching for one minute removes the entire O peak, leaving only metallic tin. Lacquer side fracture surfaces are shown in Figs. 23 and 24 from an NS test specimen; Figs. 25 and 26 show spectra from the tin side surface. In the cases of both KS and NS it is seen that the entire passivation layer is removed by the lacquer.

The fracture behaviour of BS 311 is therefore quite different from that of the KS and NS tinplates. The former, usually having good adhesion properties, retains its passivation layer totally. Further tests on non-passivated tinplate, with good butt-joint adhesion, showed that no tin oxide is removed at fracture.

300 type tinplate with good adhesion also retains its passivation layer which is low in chromium.

Figs. 25 and 26 also show a nitrogen peak; this is found on all fracture surfaces and in the bulk of lacquers where cyanoacrylate adhesives were used to bond the lacquered tinplate specimens to the tensile test stubs. It indicates that the adhesive has diffused throughout the lacquer and prompts fears that the adhesive itself has migrated to the tinplate surface and perhaps formed a weak interlayer. In order to test the effect of adhesives on the butt-joint, three types of epoxy adhesives and one cyanoacrylate adhesive were used in a programme of tests on two lacquer types. No significant variation due to the adhesive type was found and the different behaviours of BS, KS and NS were consistently exhibited with all adhesives used.

An interesting and instructive example of the enigmatic nature of adhesion is exemplified by the case of a particular BS 311 tinplate from a different batch from the type used elsewhere in this work. Two pieces from the same batch were lacquered and stoved simultaneously with phenolic lacquer. One set exhibited good adhesion properties whilst the other had very poor properties. Figs. 27-29 are XPS spectra of the tinplate after a 10 minute stoving and Figs. 30 and 31 show analyses of the tin side fracture surfaces. The labels "good" and "poor" indicate adhesion properties.

Firstly, it should be noted that in both cases the passivation layer is left on the tinplate after fracture. The value of XPS as an analytical technique is demonstrated by its ability to illustrate clearly differences between two nominally identical specimens which have different adhesion characteristics. The results of the quantitative analysis are shown in Table 8. The differences between the samples as found with XPS are:

a) the "poor" tinplate has double the ratio of Sn^0:SnO_x compared with the "good" plate. This probably indicates a thinner

tin oxide layer rather than areas of exposed Sn^0.

b) the "poor" tinplate has three times the chromium content of the "good" tinplate as measured in the unetched state (i.e. as used for lacquering). The Cr peaks cannot be further deconvoluted.

c) the "good" tinplate O1s peak is wider but due to specimen charging, no specific chemical species can be attributed. The oxygen signal is produced partly by contaminants on the tinplate surface which, from the C1s peak information, are in similar concentrations for both samples.

d) the "poor" tinplate Cr1s spectrum shows a peak corresponding to high valency chromium oxides which are not present on the "good" plate.

These differences are preserved on the fracture surfaces (tin - side).

Thus, small but certain differences between these two samples have been demonstrated. A precise correlation between lacquer adhesion and passivation layer structure has not yet been established by any workers but has been widely discussed. The implications of these experimental results and the results of other workers who have related chromium or tin oxide levels to the adhesion of lacquer on tinplate will be covered later.

So far, several important features of the passivation layer structure have been identified, although this information has come from the outer levels of the layers exposed by short etching times. Since the failure of NS and KS tinplate systems with poor adhesion takes place at the tin-passivation layer interface it was decided to examine that portion of the passivation layer which is adjacent to the tin. One approach would be to ion-beam etch the passivation layer from the top (outer) surface as attempted by several workers

TABLE 8. QUANTITATIVE RESULTS OF XPS EXAMINATIONS OF A 311 TINPLATE WITH BOTH GOOD AND POOR ADHESION PROPERTIES.
RELATIVE ATOMIC CONCENTRATIONS FOR THE UPPER SURFACE OF THE TINPLATES AND THE TIN SIDE FRACTURE SURFACES

	'GOOD' TINPLATE		'POOR' TINPLATE	
	tinplate	fracture surface	tinplate	fracture surface
Element				
Sn	13	7	18	17
Sn^{o}	2.5	-	6	-
SnO_x	10.5	-	12	-
Cr	3	1	9	4
O	84	92	73	79

(Leroy et al 1976, Maeda et al 1980, Johannessen et al 1980, Servais et al 1979) but this technique introduces errors and ambiguities through preferential etching, topographical changes and reduction of chemical species by the ion beam (Andersen 1979, Riviere 1980). It was therefore decided to remove the passivation layer intact from the tinplate and observe it from the underside. A chemical etch of iodine in methanol was used which had been developed for the preparation of TEM specimens in this work and by others (Albu-Yaron and Smith 1979). This brought about the added bonus that identical specimens could be used for both TEM and XPS examination. It proved necessary to support the very thin passivation layers with a thicker film of carbon, alloprene (a chlorinated rubber) or lacquer, laid down on the tinplate surface before removing the tin. With a lacquer coating as support, it was also possible to examine stoved passivation films.

iii) Isolated passivation layers

XPS spectra from a BS 311 tinplate passivation layer are shown in Figs. 32-34. The passivation layer is supported by a phenolic lacquer and has consequently been stoved for ten minutes. Spectra for Sn and Cr only are shown as the O signal from the passivation layer was swamped by the component from the lacquer. The lacquer was examined separately but it did not prove possible manually to subtract that signal from the specimen 01s peak to yield an oxygen peak for the passivation layer alone. Figs. 35-37 show XPS spectra from a KS 311 passivation layer with a carbon and alloprene backing.

The first point to note in the spectra from all the isolated passivation layers is the existence of a metallic tin peak. This is almost certainly due to incomplete chemical etching and the increase in this peak through the depth of the passivation layer is probably due to an air-formed oxide, grown after film stripping and

sputtered away by the Ar ion beam. Incomplete etching of the tin may be a result of the rough surface of the tinplate, whose topography follows that of the rolled steel substrate or, on a smaller scale, it may be due to the roughening of the metallic tin surface by oxide growth. This latter mechanism is proposed by Boggs et al (1961) in a study of the oxidation of tin where SnO growth results in closed cavities within the oxide layer which block oxidation of the tin beneath and form raised islands of tin on the micron scale as oxidation proceeds. Microtopographical features are revealed by TEM.

The quantitative results of XPS on the isolated passivation films from BS and KS tinplates are given in Table 9. The BS plate possesses over double the chromium content of the KS plate, shown best after a 1 minute Ar ion etch. In both samples the Cr^{0} peak is more prominent than from the outer surface spectra and this allows the metal peak to be used as a reference level for further deconvolution of the chromium peak. Both BS and KS tinplates show Cr^{0}, CrO_3 (Cr^{3+}) and $Cr(OH)_3.nH_2O$ with Cr^{6+} (higher valency) present only on the KS. Approximate relative atomic concentrations for chromium species are shown in Table 10. Whilst having a lower total chromium content, the KS has a higher Cr^{0}:CrO_x ratio of 0.75:1 compared with 0.35:1 for the BS tinplate. This is not the case when considering the results from the upper layer of the passivation film. A further point which must be emphasised is the existence of hydrated chromium oxide on the underside of the passivation layer. Earlier workers have found hydrated compounds to be restricted to the outer surface but these results have almost certainly suffered from the chemical reduction and de-hydration caused by ion beam bombardment.

Table 11 shows the tin, chromium and oxygen ratios in various combinations for the tinplates investigated from which it is possible

TABLE 9. QUANTITATIVE RESULTS OF DEPTH PROFILING AND XPS SHOWN AS ETCHING TIME vs. RELATIVE ATOMIC CONCENTRATIONS

ISOLATED PASSIVATION LAYERS EXAMINED FROM TIN SIDE

British Steel 311

Etching Time (minutes)	0	1
Element		
Sn	16	37
Sn^{o}	1	12
SnO_x	17	24
Cr	14	62

Kawasaki Steel 311

Etching Time (minutes)	0	1	2
Element			
Sn	16	4.5	5
Sn^{o}	6	2	0.5
SnO_x	10	2.5	4.5
Cr	1	1	1

TABLE 10. APPROXIMATE RELATIVE ATOMIC CONCENTRATIONS FOR CHROMIUM SPECIES AS FOUND ON THE TIN SIDE SURFACE OF PASSIVATION LAYERS

Tinplate	Cr^{o}	Cr_2O_3	$Cr(OH)_3 \cdot nH_2O$	CrO_3(?)
BS	20	40	20	0
KS	9	6	5	1

After 1 minute Ar ion etch

TABLE 11. ATOMIC CONCENTRATION RATIOS FOR TINPLATE PASSIVATION LAYERS MEASURED FROM TINPLATE SURFACES (AFTER ONE MINUTE ION ETCHING) AND FROM THE TIN SIDE OF ISOLATED PASSIVATION FILMS

	Sn^{o}:Cr	Cr^{o}:CrO_x	Sn^{o}:Cr+O	Sn^{o}:Cr^{o}
British Steel 311				
Tinplate	5:1	1:1	2.7:1	10:1
Passivation layer	-	0.35:1		
Kawasaki Steel 311				
Tinplate	8:1	0.1:1	2.7:1	73:1
Passivation layer	-	0.75:1		
Nippon Steel 311				
Tinplate	9:1	0.07:1	2.8:1	~140:1
British Steel 300				
Tinplate	45:1	-	-	

to derive values for areal coverage by the different chemical species.

5. SUMMARY OF XPS RESULTS

The characterisation of the various passivation layers by XPS has revealed small but certain differences in the constituents of the layers found on BS, KS and NS 311 tinplates. All have thin tin oxide coats 1 nm or less in thickness lying over metallic tin. The 300 type tinplate possesses a tin oxide layer some 2 to 5 nm in thickness. It is not possible to distinguish SnO from SnO_2 using XPS as the energies for these two oxides are separated by less than 0.5 eV.

Details in the spectra are reproducible but the quantitative results may have up to 20% error owing to the method of quantitative calculation.

Much attention has been given in the literature to the chromium present in passivation layers. The existence of Cr^0 in the 311 passivation layer was originally doubted (Britton 1965) but the presence of Cr° is now accepted (Leroy et al 1976a, Albu-Yaron and Smith 1979), although widely differing concentrations have been reported. The results of this work suggest that the chromium-rich component of the tinplate passivation layer is present as discrete 'islands', surrounded by tin oxide. From Ar ion etching, the depth of such islands is much greater than the thickness of tin oxide, extending to over 15 nm for 311 (Coad et al 1976) for some 311 tinplates and to similar depths for 300 tinplate, although the chromium on 300 contains only oxidised forms, mostly Cr^{3+} and probably hydrated forms.

The Saijo model for 311 tinplate is consistent with these results

(see Fig. 7) but that particular model proposes a layered passivation film with metallic chromium adjacent to the tin surface and progressing through a mixture of oxide types to a hydrated oxide located on the outer surface.

As has been mentioned earlier, Ar ion etching introduces artifacts by reducing chromium oxides to metal. Examination of the lower sections of the passivation layer by removing it intact overcomes this and, using this method, hydrated chromium oxide $Cr(OH)_3.nH_2O$ has been found very close to the tin surface. Analysis of the passivation layer undersides from BS and KS tinplates reveals metallic chromium, Cr^0, oxidised chromium and hydrated oxide in the approximate concentrations shown in Table 10 after one minute's Ar ion etch. Higher valency chromium (Cr^{6+}) was found on the KS 311 tinplate passivation layer at this stage. It may be suggested that these oxidised forms grew on the metallic chromium after etching but these were thick enough to persist after 3 minutes Ar ion etch. A control experiment was performed in which a 311 tinplate was etched for 6 minutes and then let up to air for 24 hours, a period of time comparable with the duration between passivation layer stripping and XPS examination. XPS revealed that some growth of oxidised and hydrated chromium had occurred during exposure to air but that this amount was small compared with the quantity seen on the stripped layer.

The amount of chromium on the unstoved tinplate surfaces varied between the comparative set of BS, KS and NS plates, being highest for British Steel tinplate which had 50% more total chromium than KS or NS as measured after a one minute Ar ion etch. The BS tinplate possessed over 100% more chromium than the KS plate measured at the base of the passivation layer. These values are perhaps surprising in the light of other work (Takano and Watanabe 1980) which correlates high chromium content with poor peel adhesion performance. By

assuming that after a one minute Ar ion etch of the tinplate surface all SnO_x has been removed, a value for the areal coverage of chromium and its oxides may be derived. This value shows BS to have the highest coverage with 18% of the tinplate covered in chromium-rich passivation layer, compared with 12% for KS, 11% for NS and 2% for 300 (see Table 7). 50% of the chromium on the BS tinplate is in the form of Cr^0 compared with only 10% for KS and 7% for NS. When the tin side of the passivation layer is considered, the KS steel is found to have the highest proportion of metallic Cr^0 to CrO_x (40%) compared with 25% for BS, although the total chromium metal value is still greater for the BS tinplate.

It is now possible to discuss a model for the passivation layer of BS 311 with good adhesion properties and KS 311 with poor properties as deduced from the above results. Hydrated chromium oxide is possible throughout the depth of the passivation layer with Cr^{3+} (Cr_2O_3?) and varying amounts of Cr^0. Other oxides (e.g. CrO_2, Cr_5O_{12} but probably not CrO_3 which is soluble in water) are found only on the underside of the KS passivation layer. The model will be refined later with the addition of data from TEM which will provide imaging information.

When failure occurs in the butt-joint adhesion test the passivation layer is left adhering to the BS tinplate whereas it is totally removed from KS and NS tinplates (this result has been confirmed with several test pieces). Chromium oxide other than Cr_2O_3 (Cr^{3+}) has been detected on the underside of passivation films from tinplates with poor adhesion and also on the fracture surfaces. The peaks correspond to CrO_3 (which is unlikely) and may be due to chromium oxides whose binding energy is not listed in Table 1. It has not

been found on BS 311 tinplates with good adhesion and is found only at the tin-passivation layer interface where failure, if it occurs at all, takes place. As fracture in lacquered tinplate with poor adhesion generally seems to occur at this interface (Servais et al 1979) the presence of higher binding energy Cr^{6+} found only in weak systems in this location strongly suggests that it may have a weakening effect, even in low concentrations.

The BS 311 showed a decreasing concentration of Cr^{0} through the passivation layer (from top to bottom) compared with an increasing Cr^{0} content in the KS 311, although the total chromium content and areal coverage is higher for the BS. The implications of these results will be discussed in Chapter 6

THE RESULTS

Figures following are marked where appropriate with Ar ion etching times.

Peak magnification factors are also given.

Fig. 8. A 1250 eV spectrum for unstoved BS 311 tinplate. Ar ion etching times are shown.
Note the development of the Sn and Cr peak and the reduction of the C1s contamination peak.

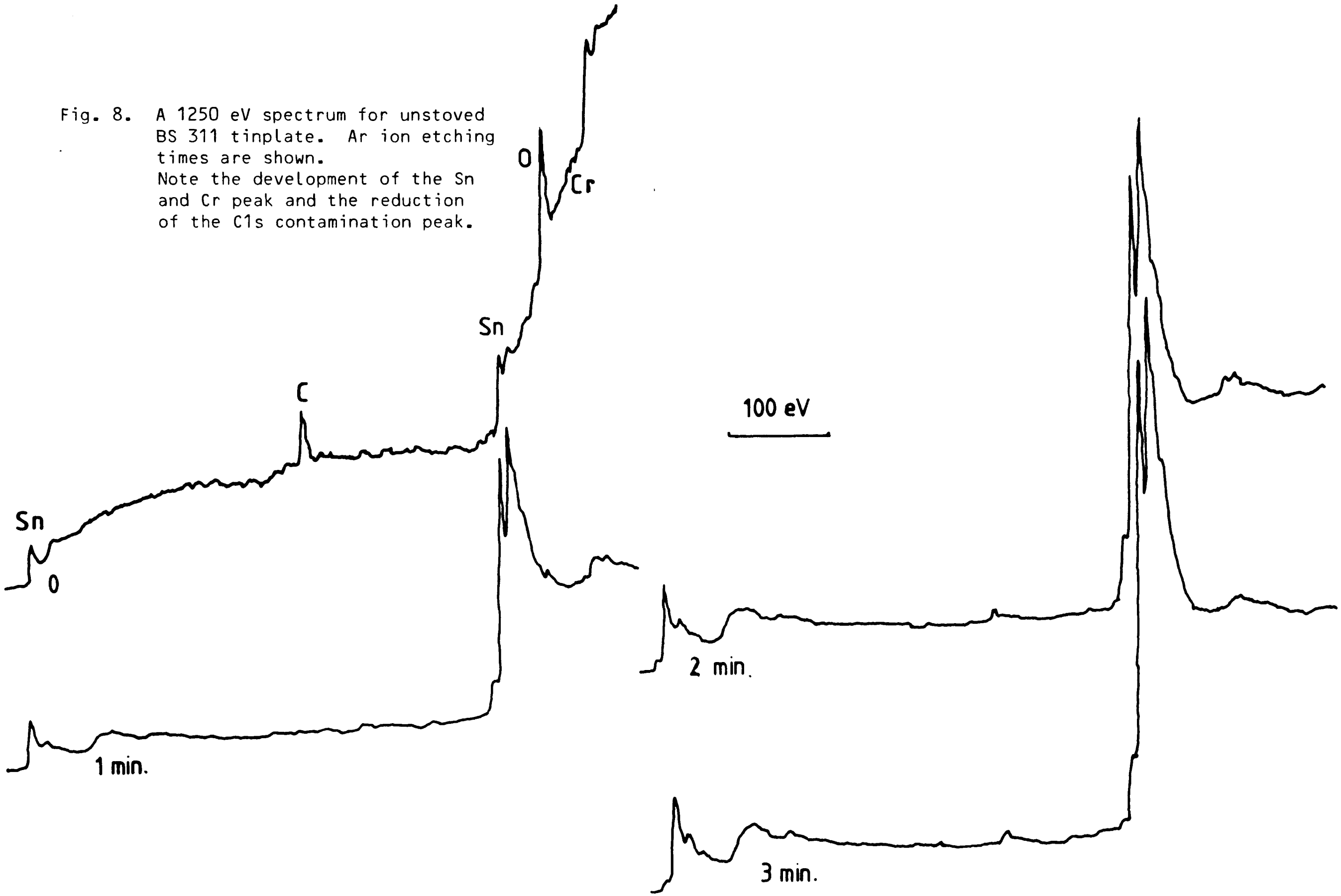

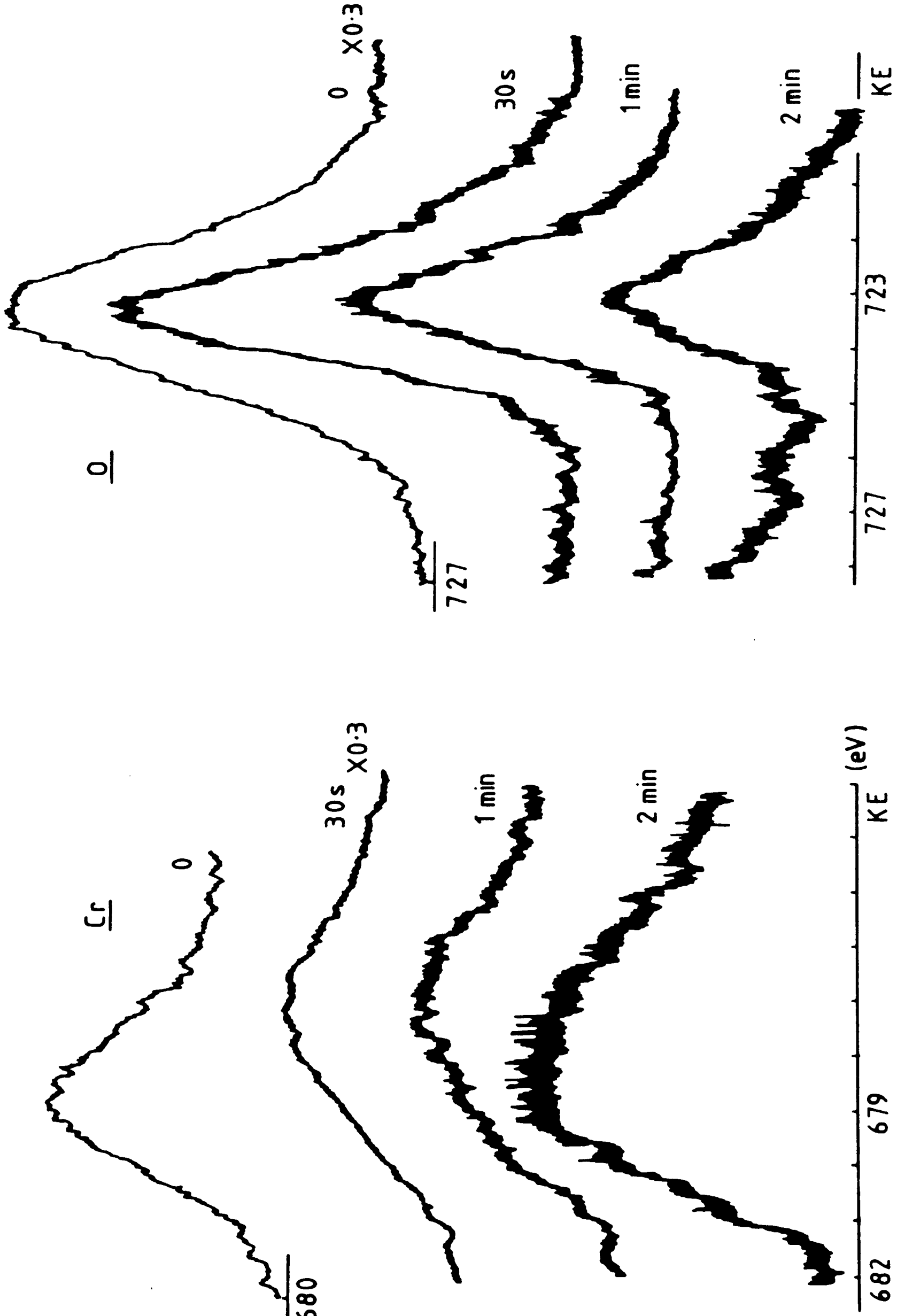

Fig. 9. 25 eV XPS spectra for unstoved BS 31

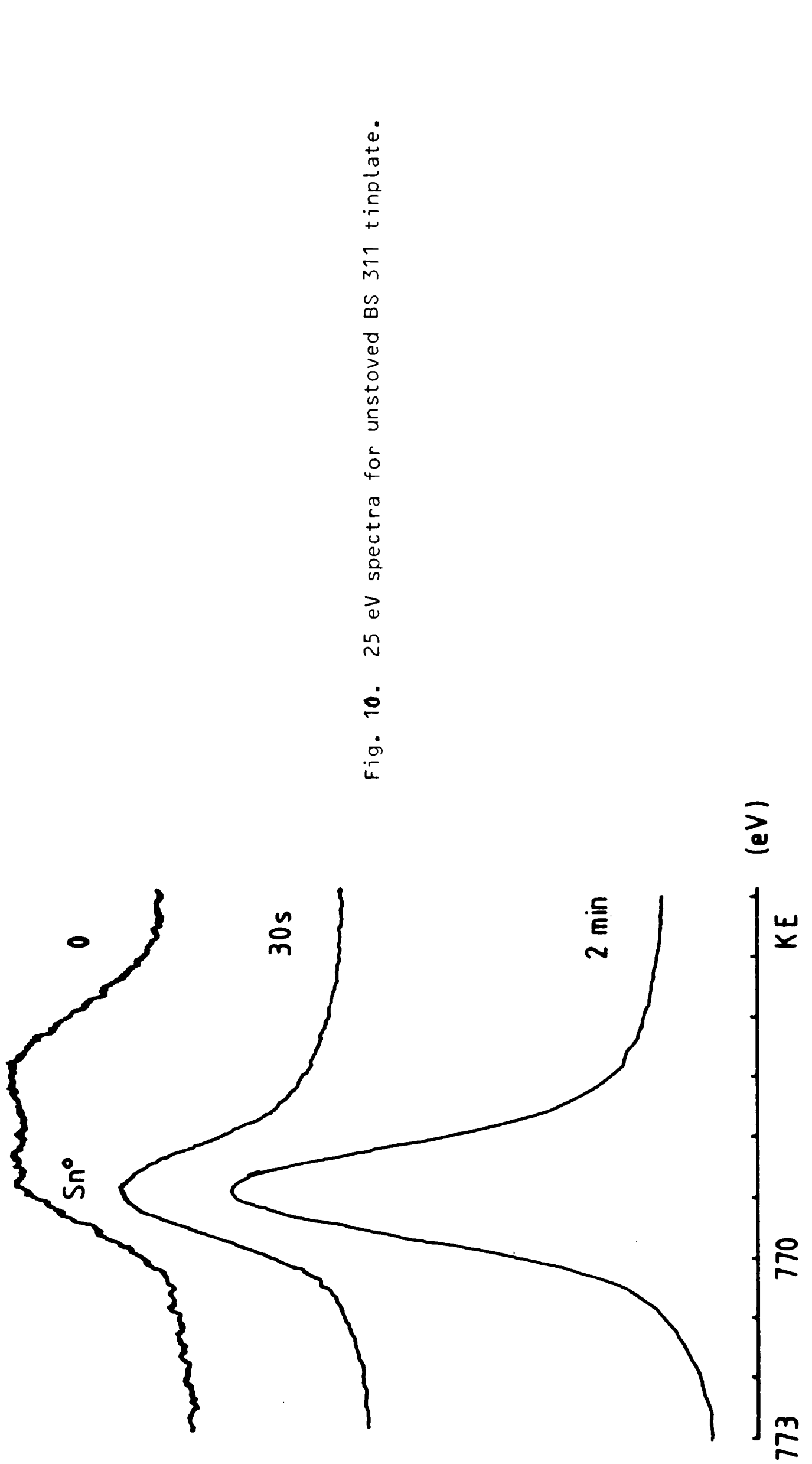

Fig. 10. 25 eV spectra for unstoved BS 311 tinplate.

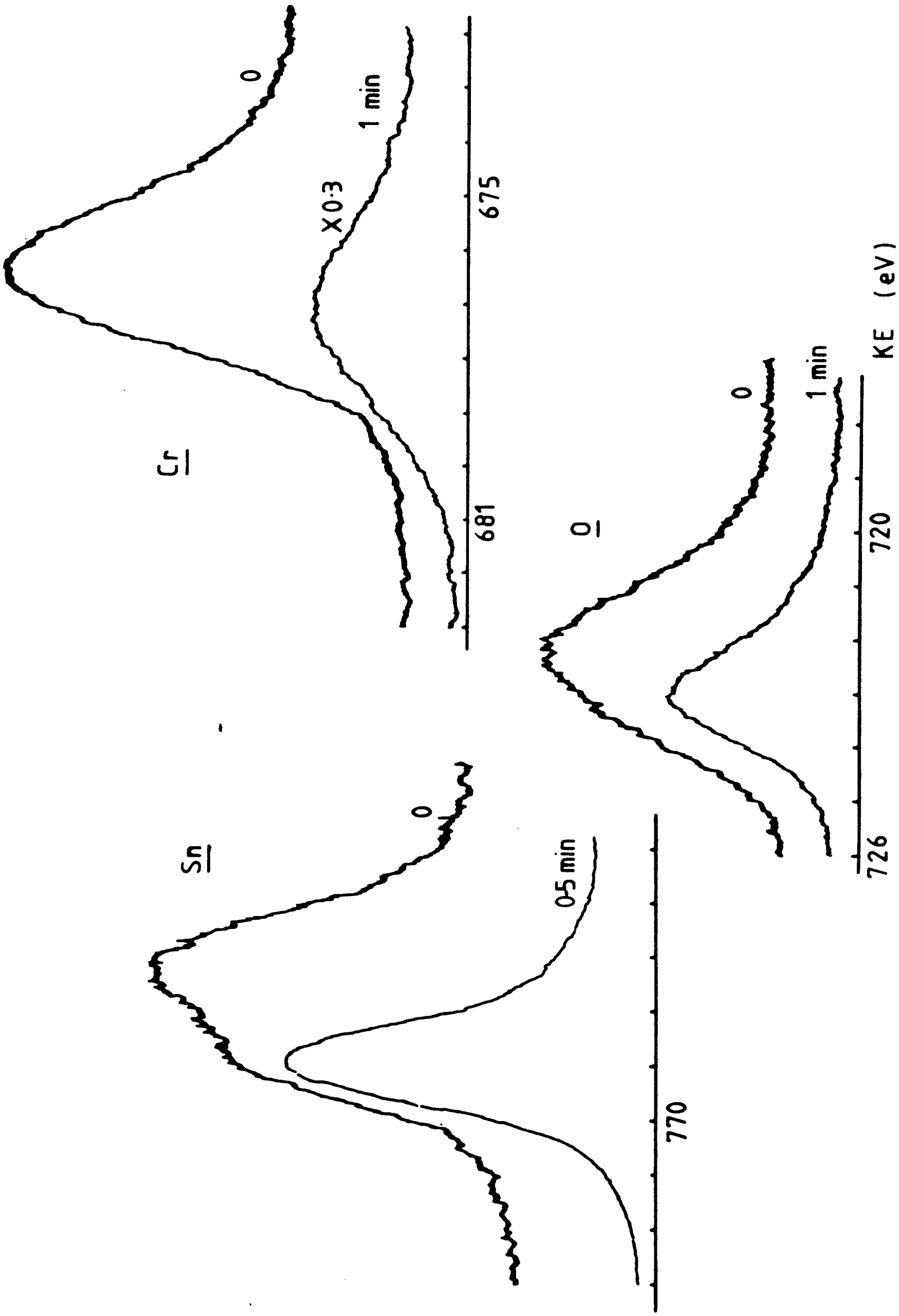

Fig. 11. 25 eV spectra for BS 311 tinplate, stoved 10 minutes at 200°C in air

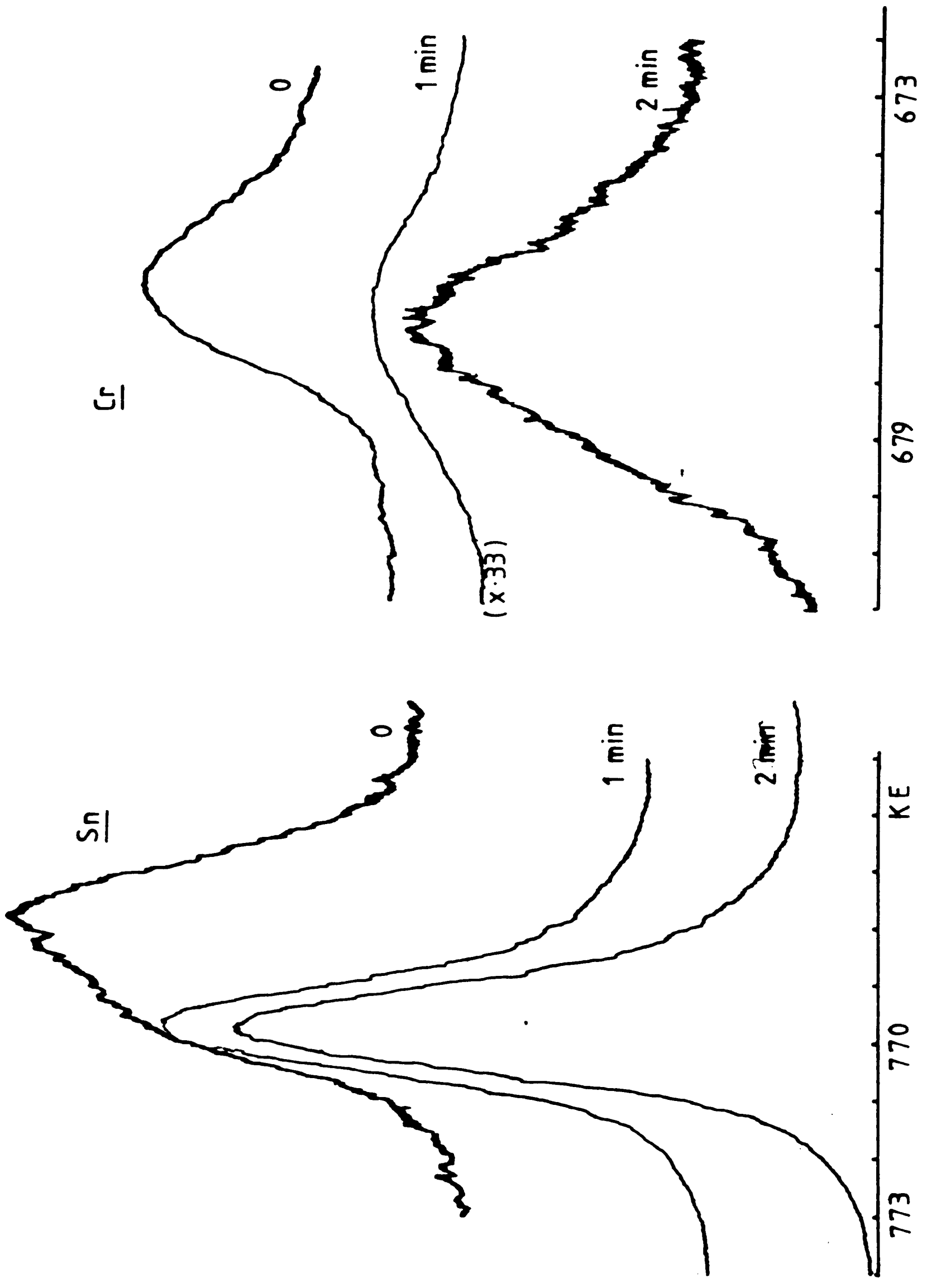

Fig. 12. 25 eV spectra of BS 311 tinplate stoved 10 minutes at 200°c in argon.

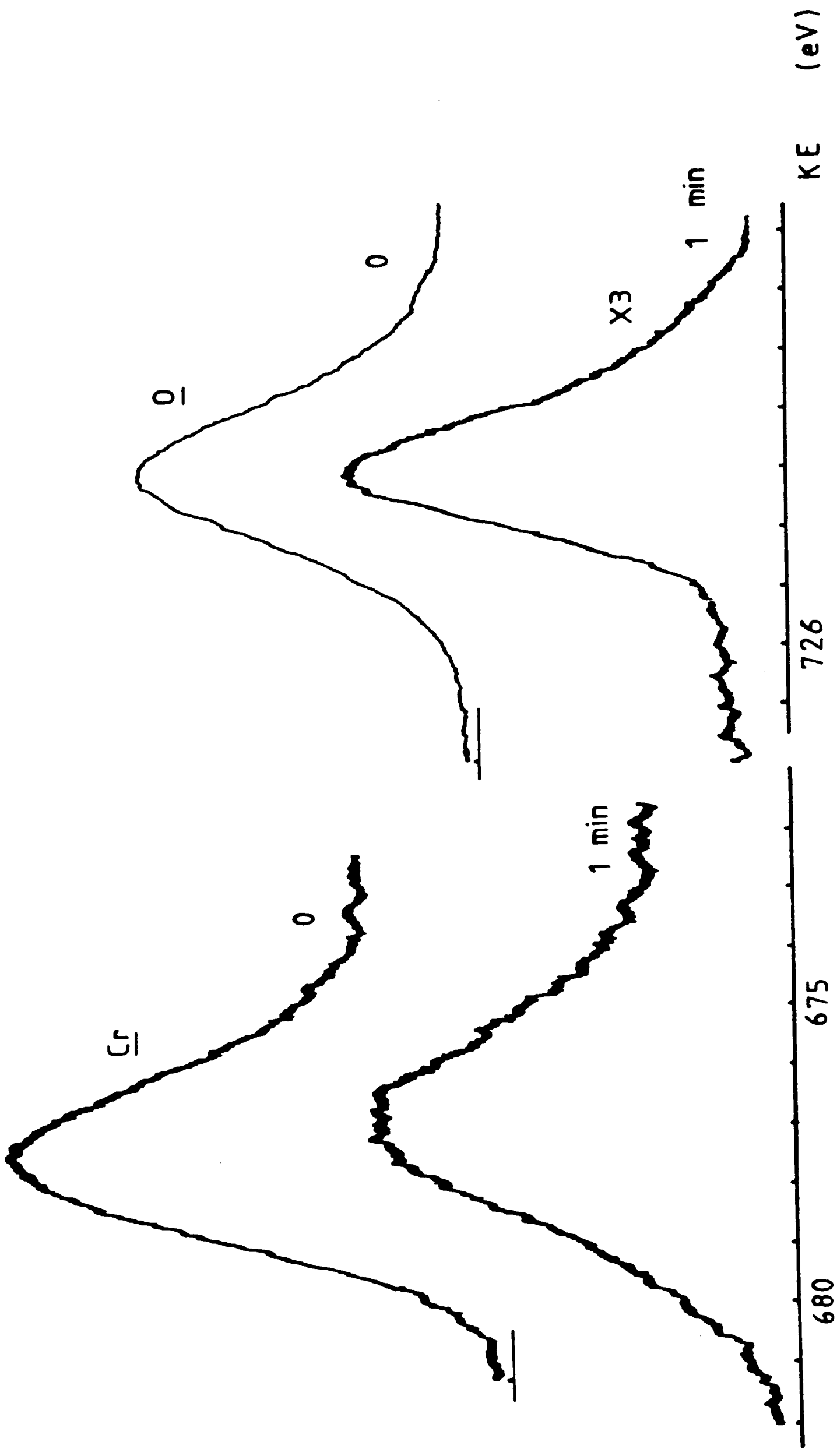

Fig. 13. 25 eV spectra of unstoved KS 311 tinplate.

Fig. 14. 25 eV spectra of unstoved KS 311 tinplate.

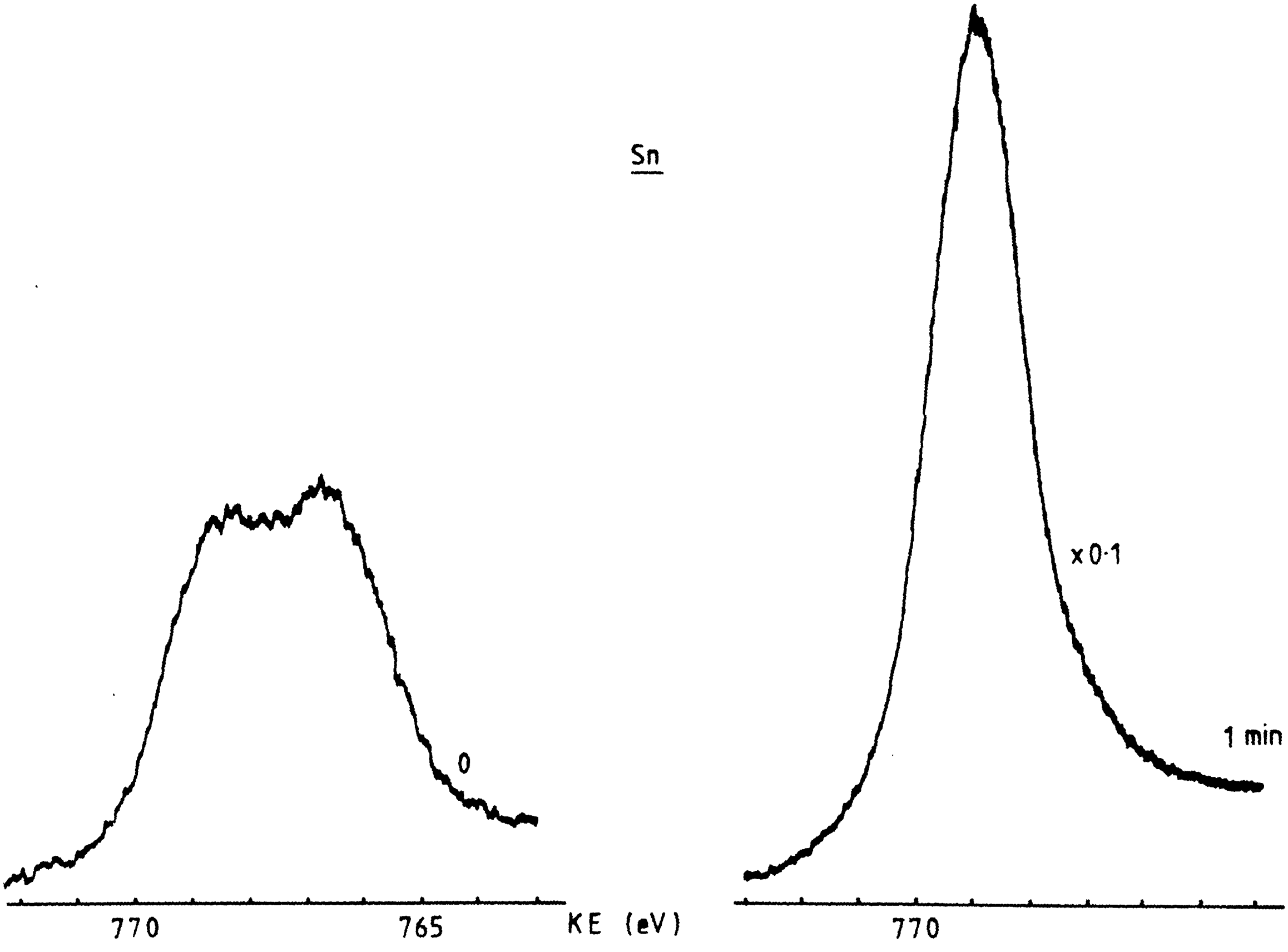

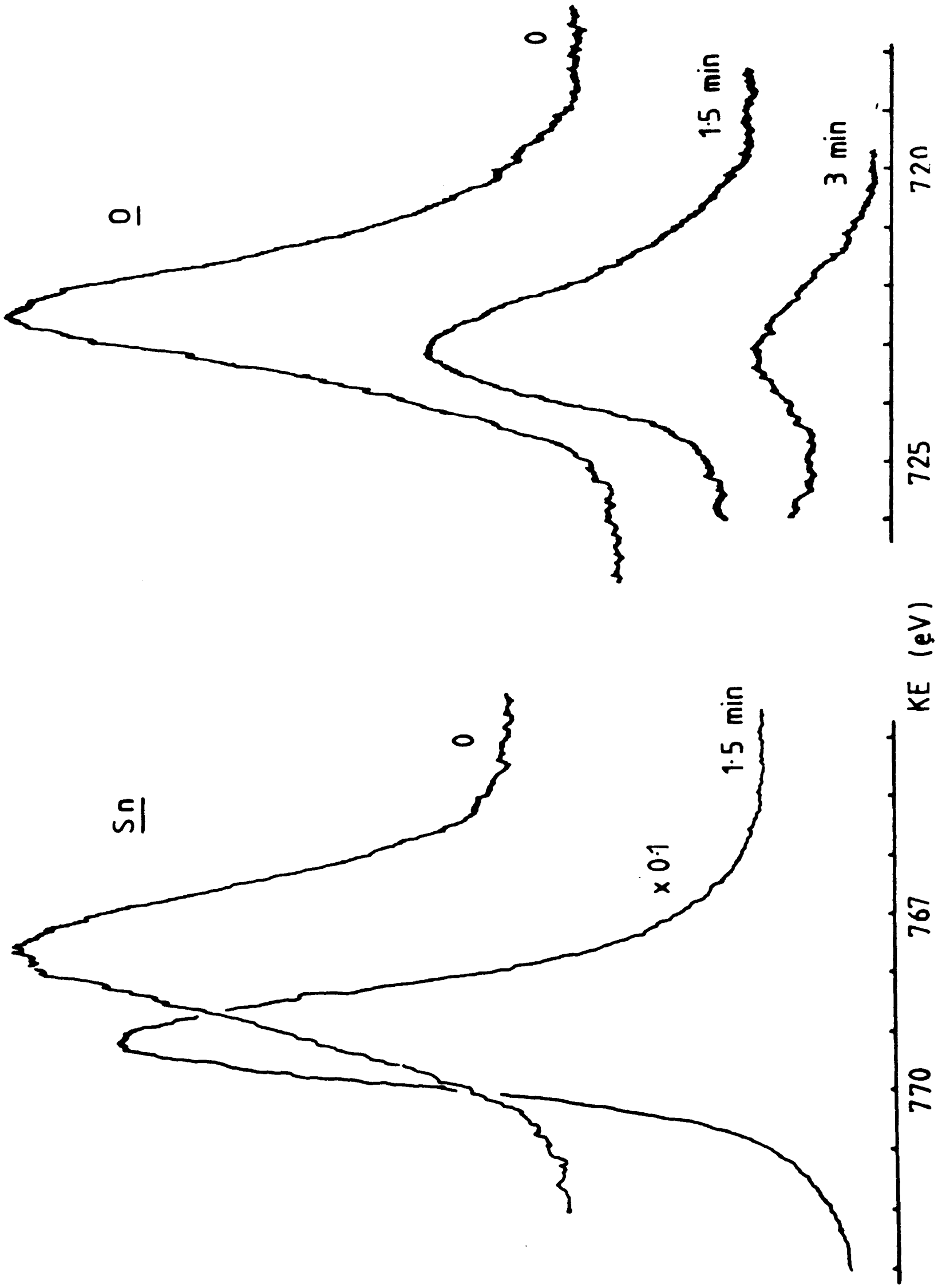

Fig. 15. 25 eV spectra of unstoved NS 311 tinplate.

25 eV spectra of unstoved NS 311 tinplate.

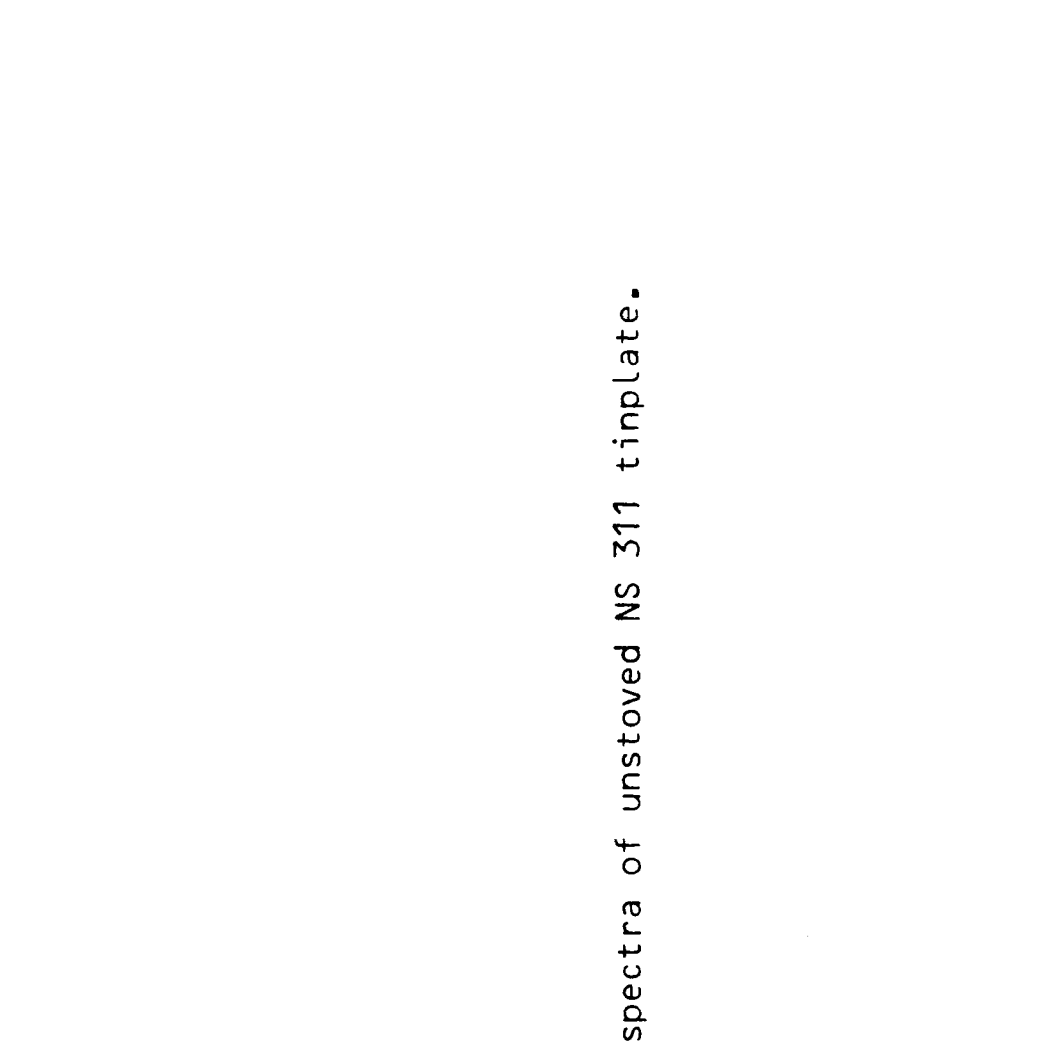

Fig. 16.

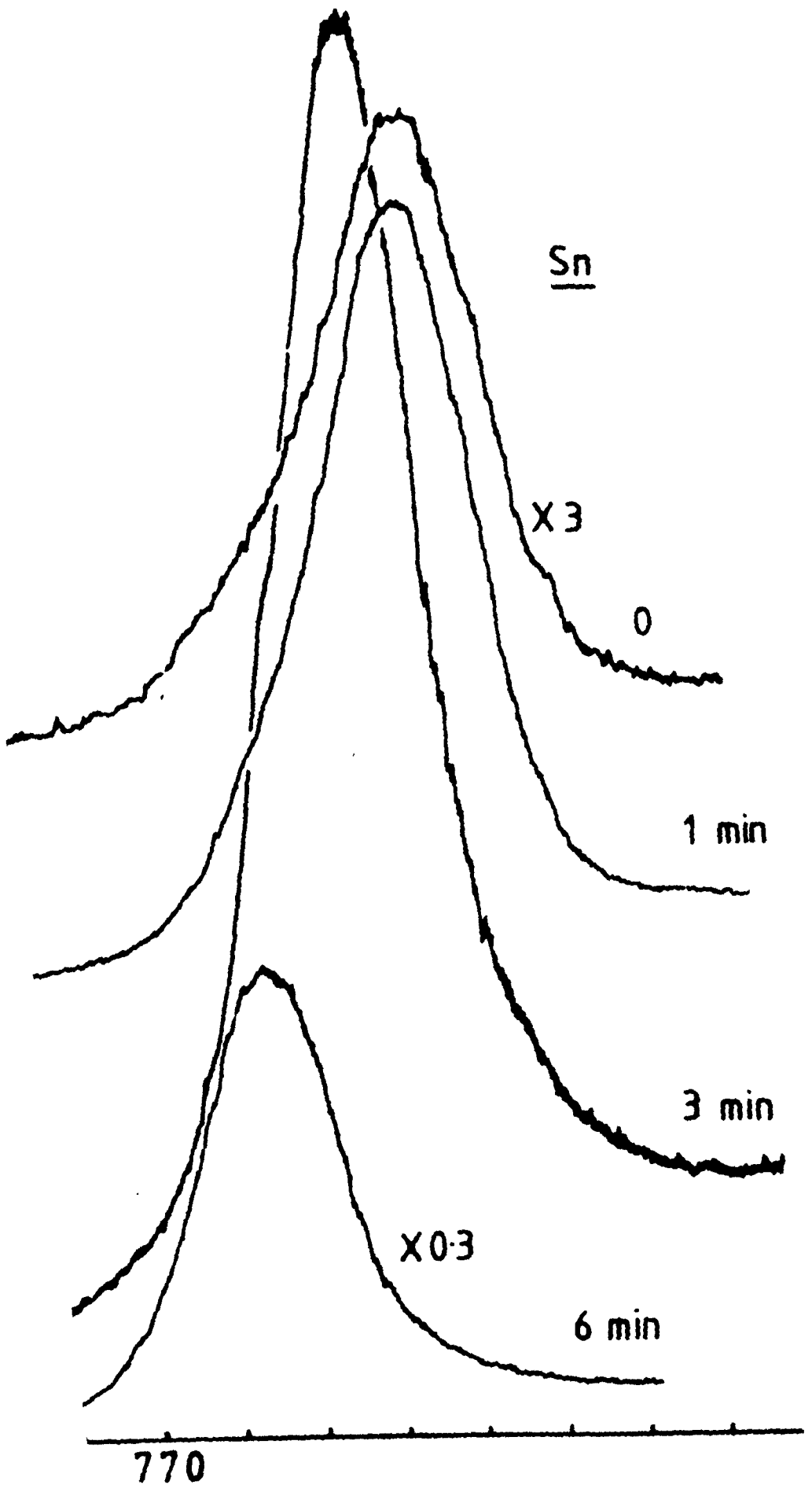

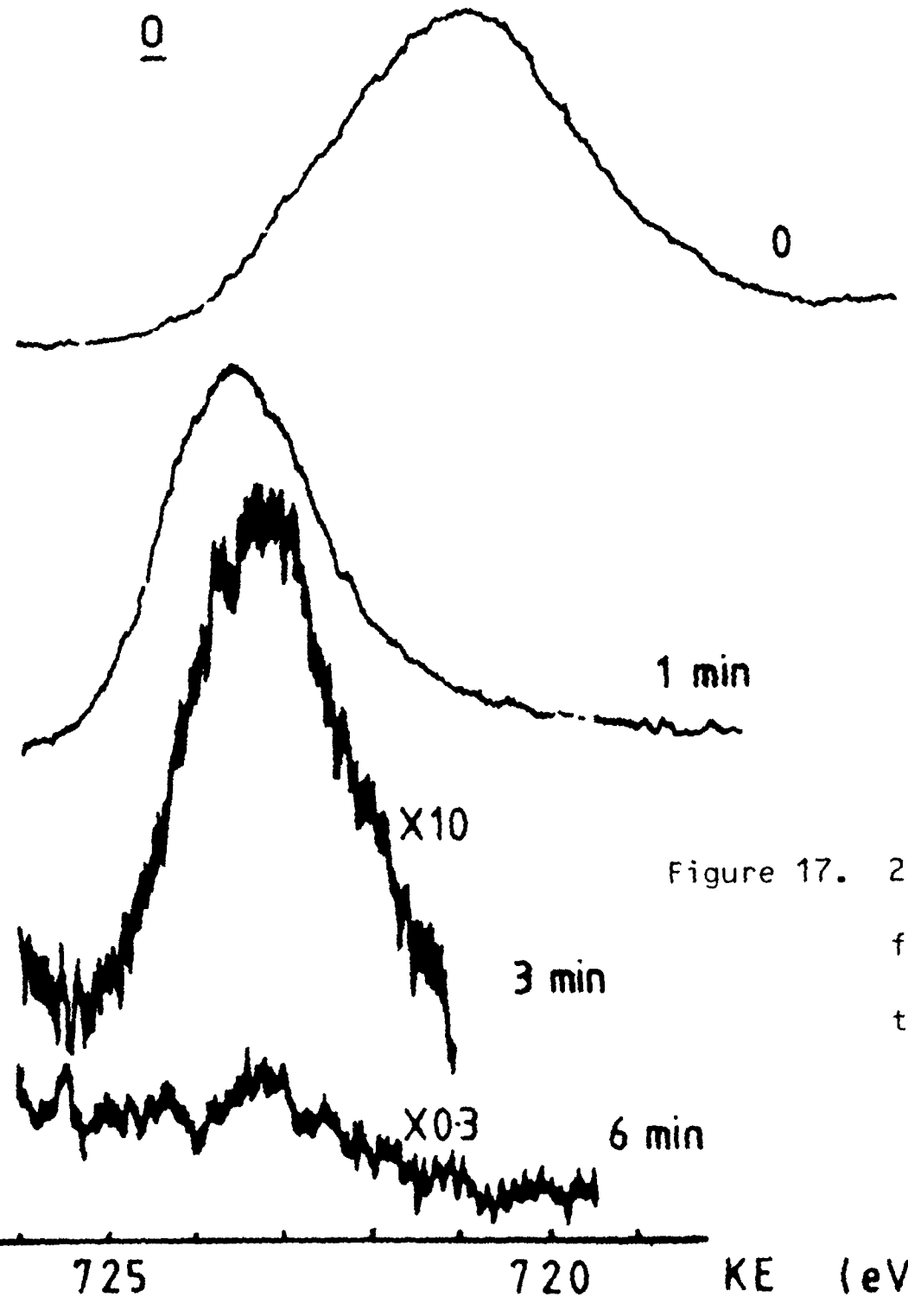

Figure 17. 25 Ev XPS spectra for unstoved 300 tinplate.

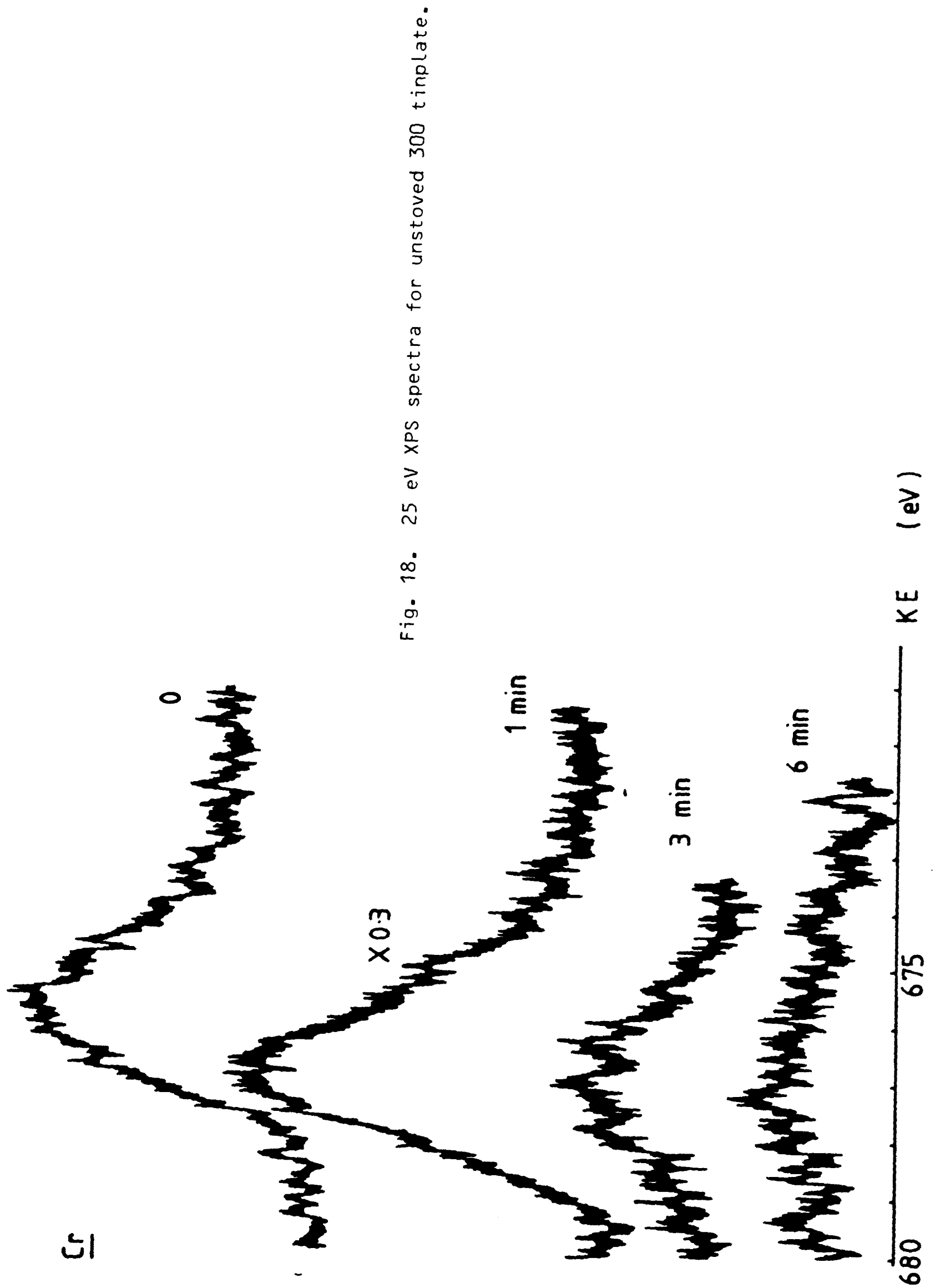

Fig. 18. 25 eV XPS spectra for unstoved 300 tinplate.

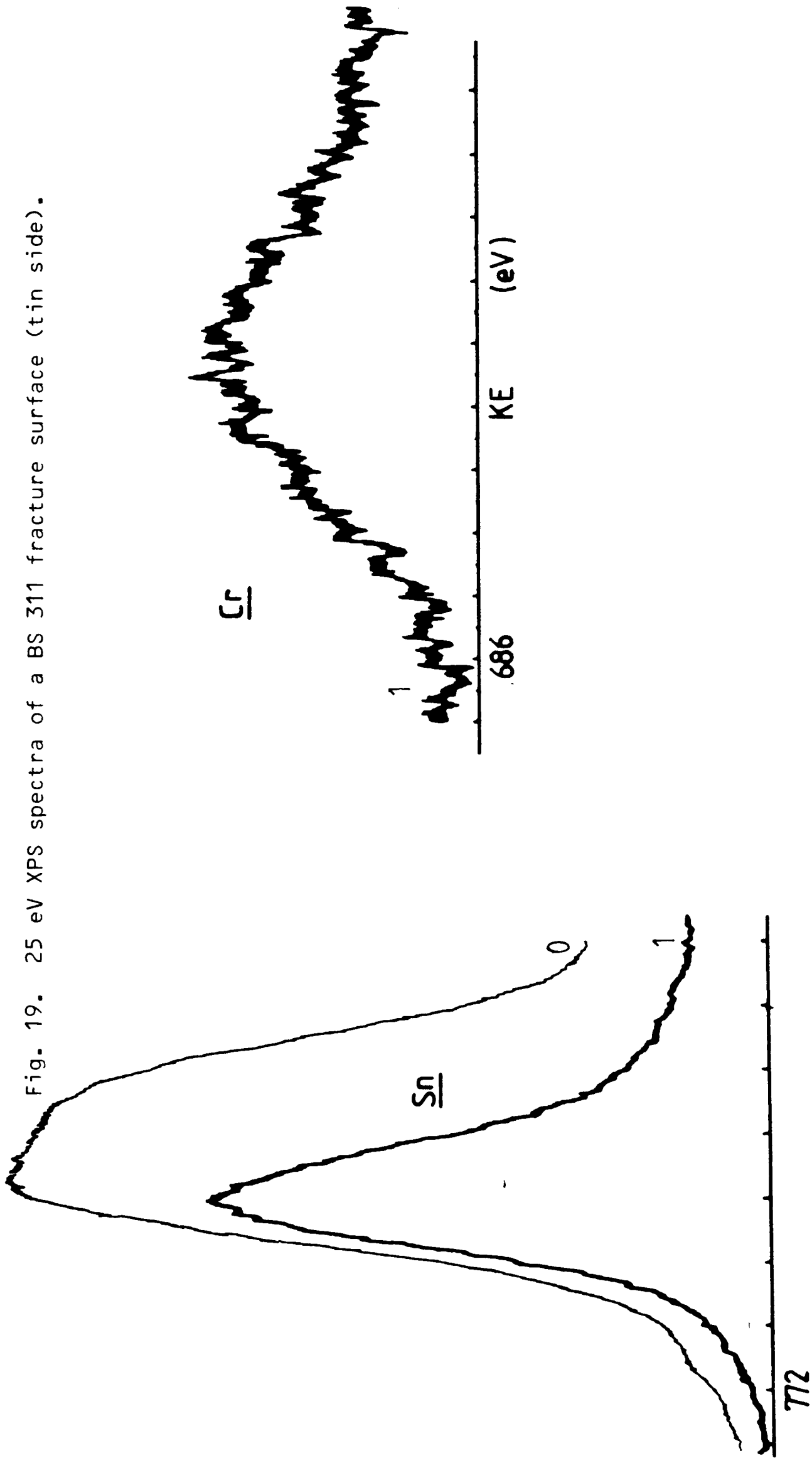

Fig. 19. 25 eV XPS spectra of a BS 311 fracture surface (tin side).

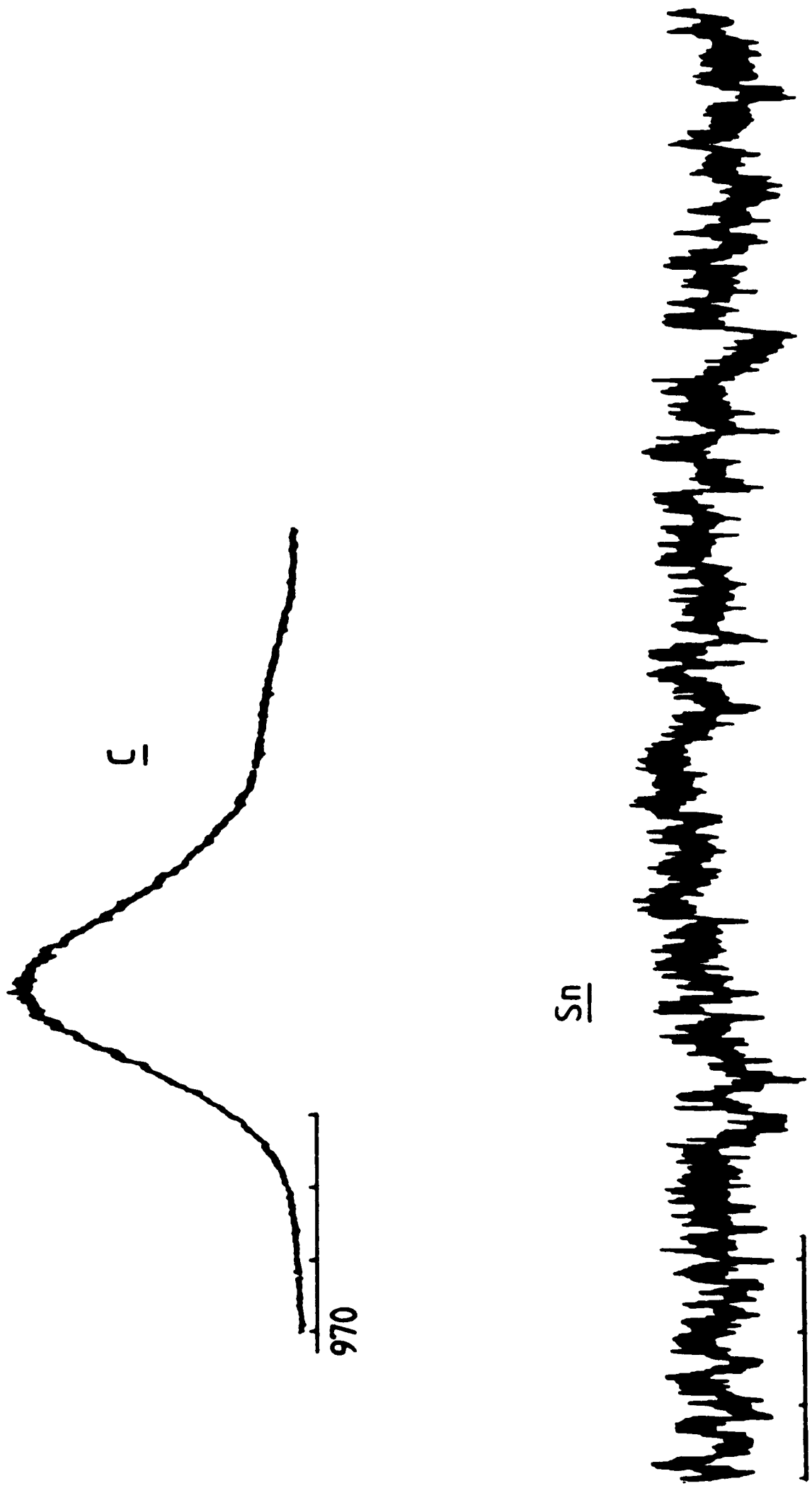

Fig. 20. 25 eV spectra from a BS 311 fracture surface (lacquer side)

Fig. 21. 25 eV XPS spectra from a BS 311 lacquered tinplate.

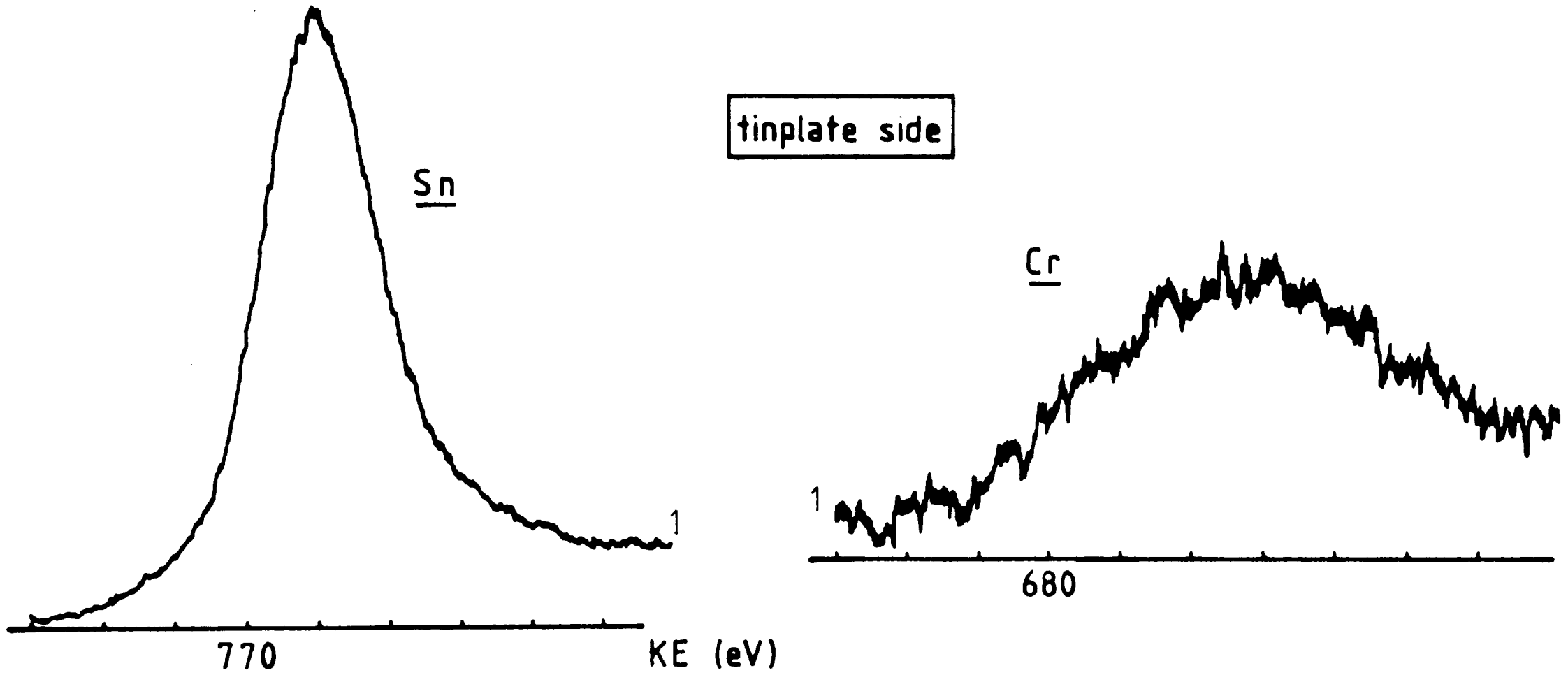

Fig. 22. 25 eV XPS spectra from a KS 311 tinplate (tin side).

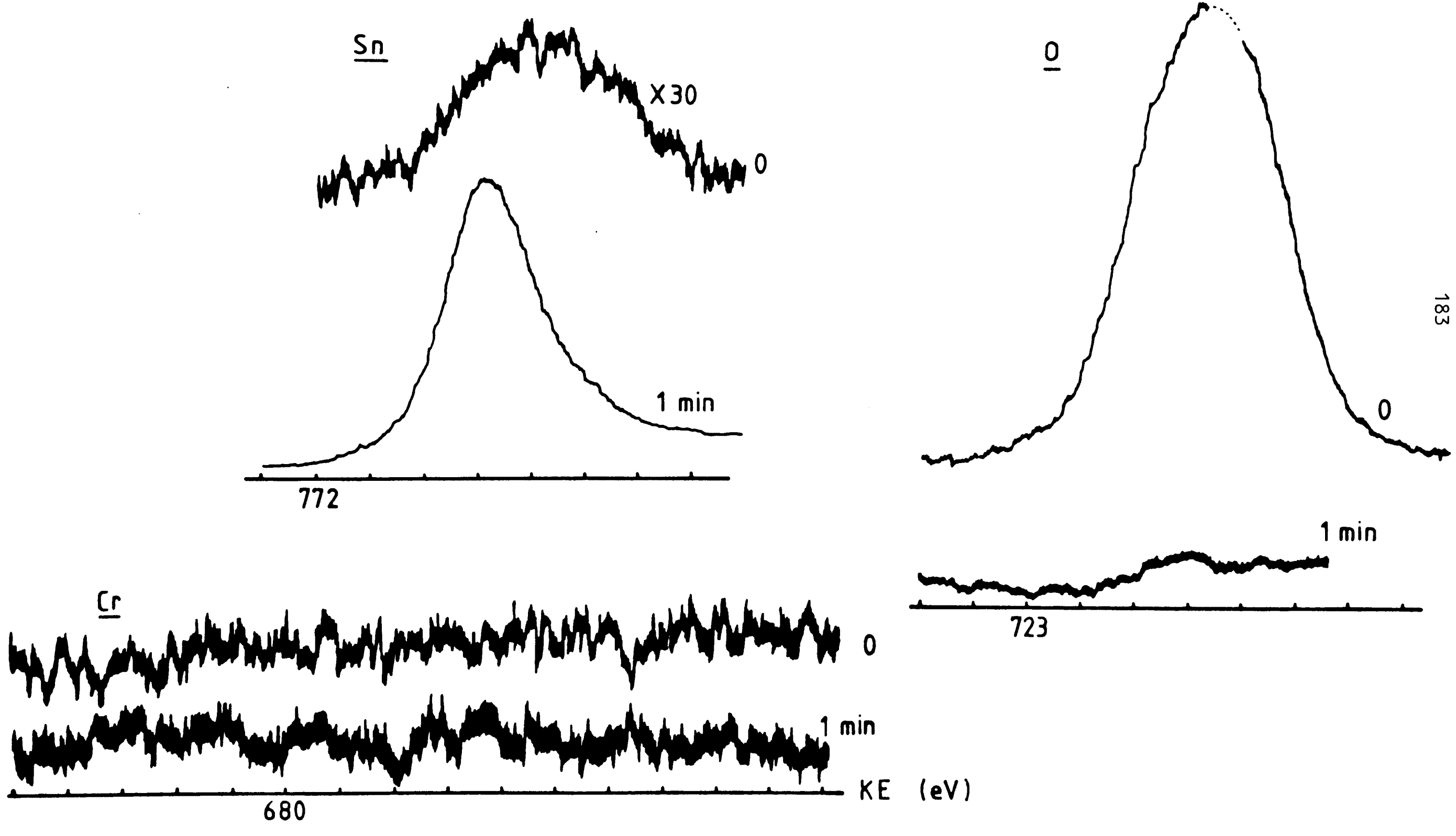

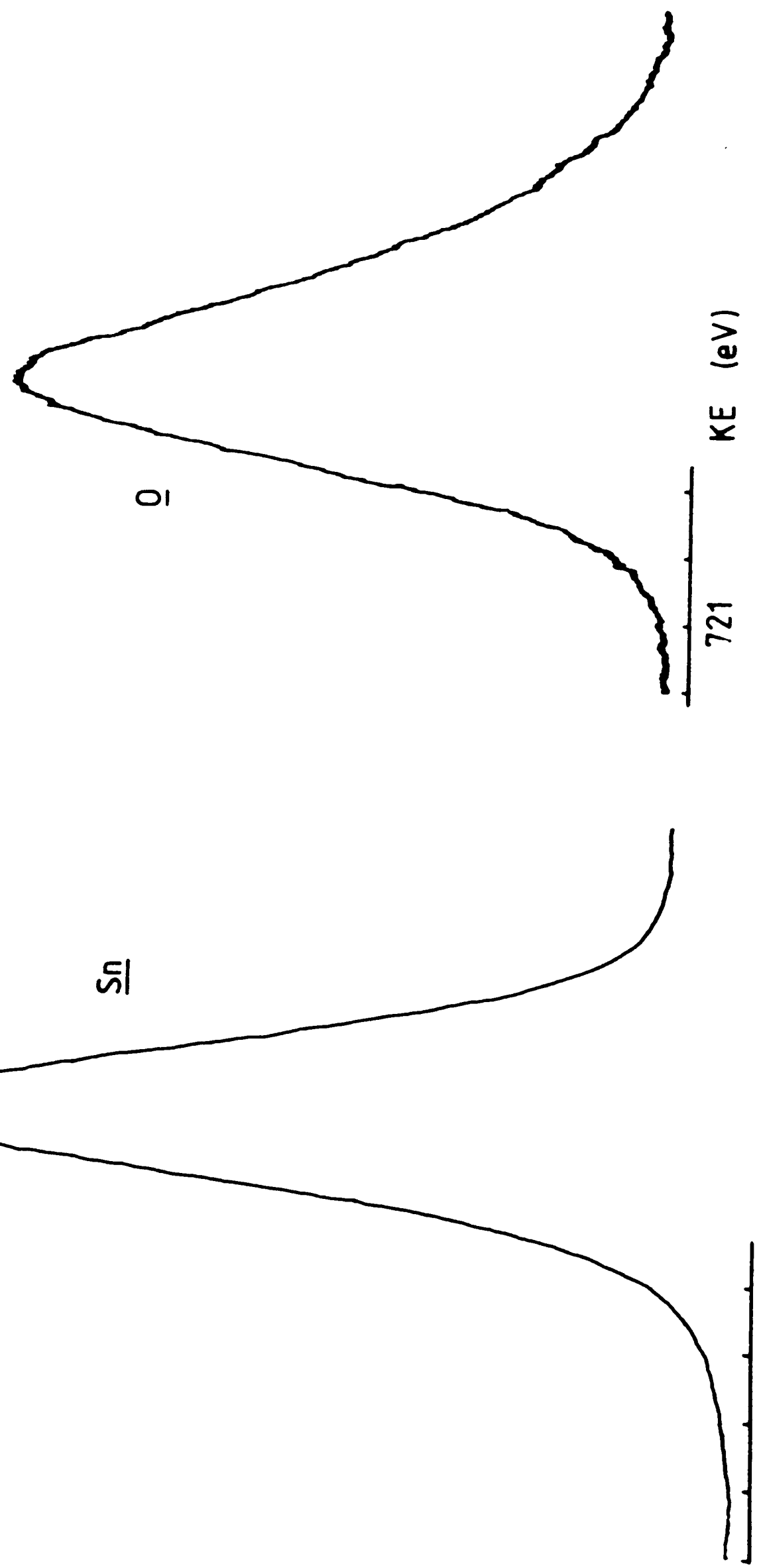

Fig. 23. 25 eV XPS spectra from a NS 311 tinplate fracture surface (lacquer side).

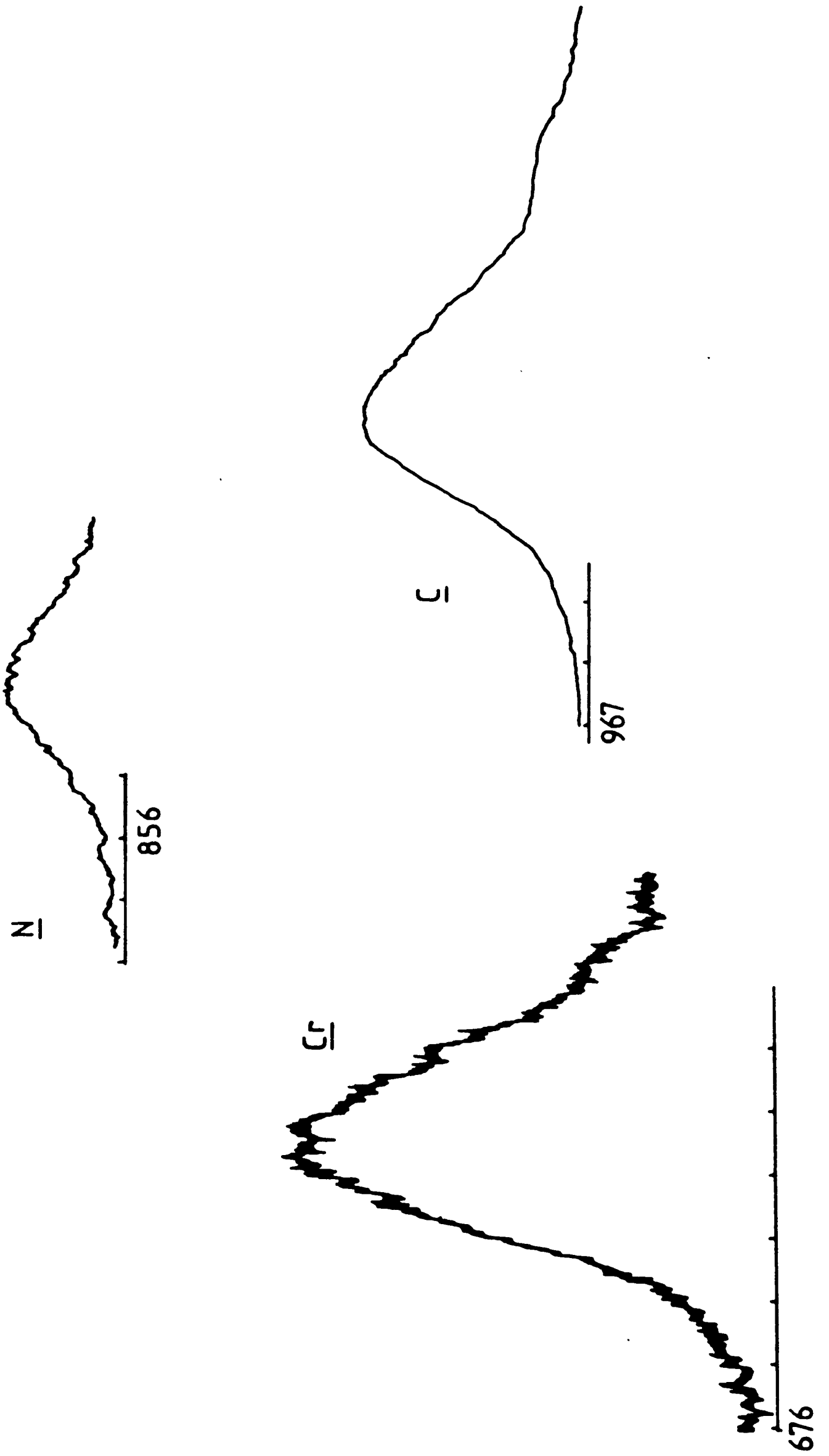

Fig. 24. 25 eV XPS spectra from a NS 311 tinplate fracture surface (lacquer side).

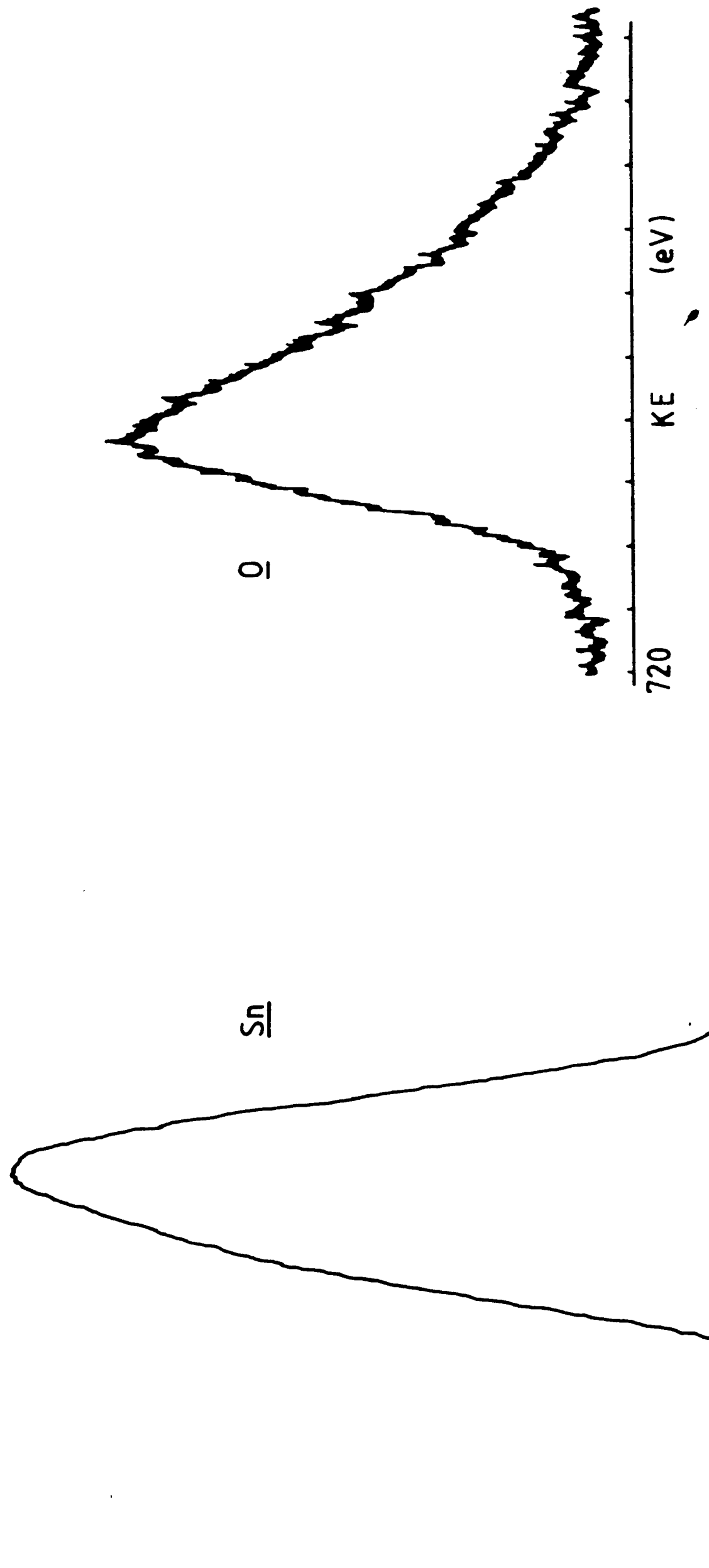

Fig. 25. 25 eV spectra from NS311 tinplate fracture surface (tin side).

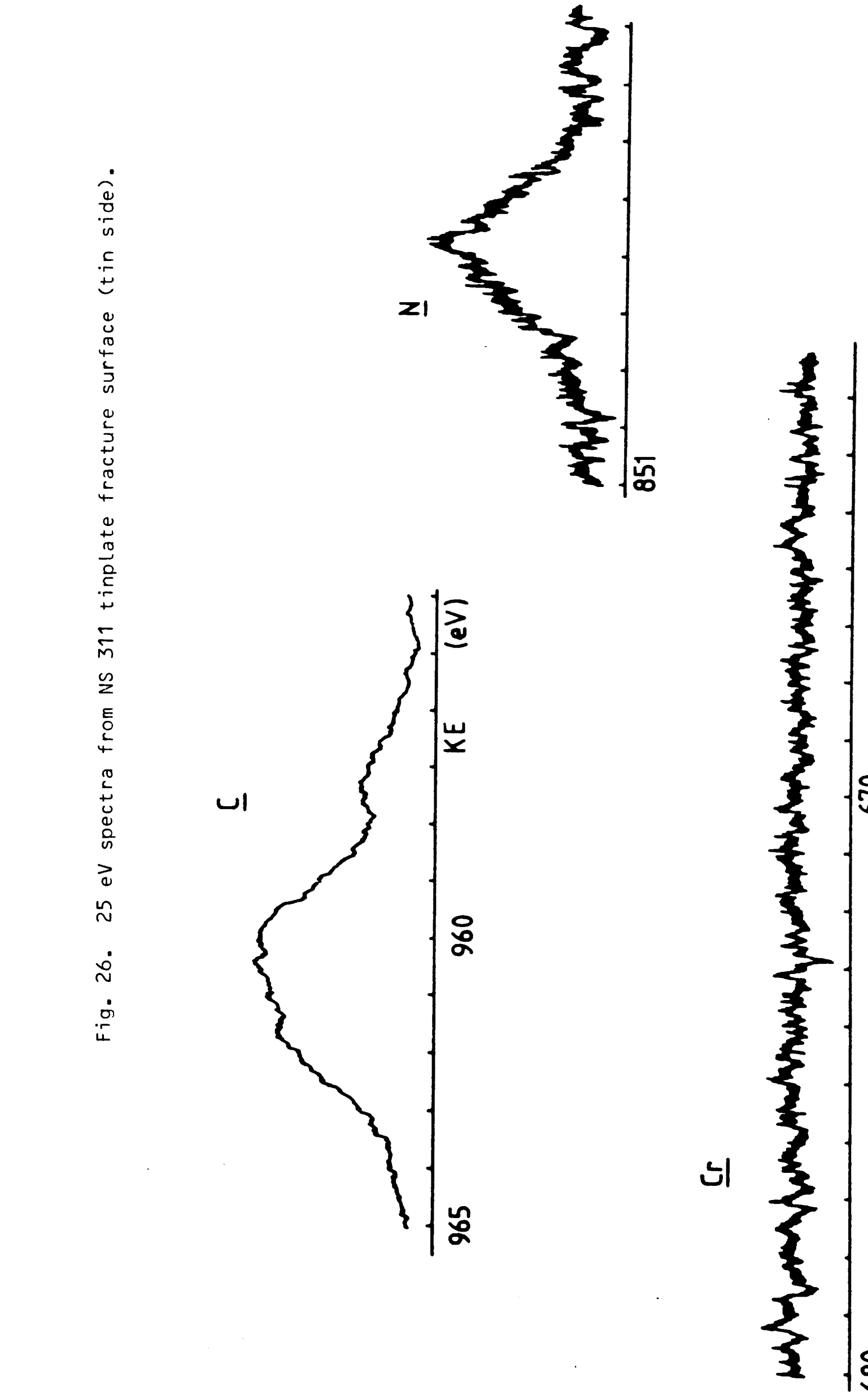

Fig. 26. 25 eV spectra from NS 311 tinplate fracture surface (tin side).

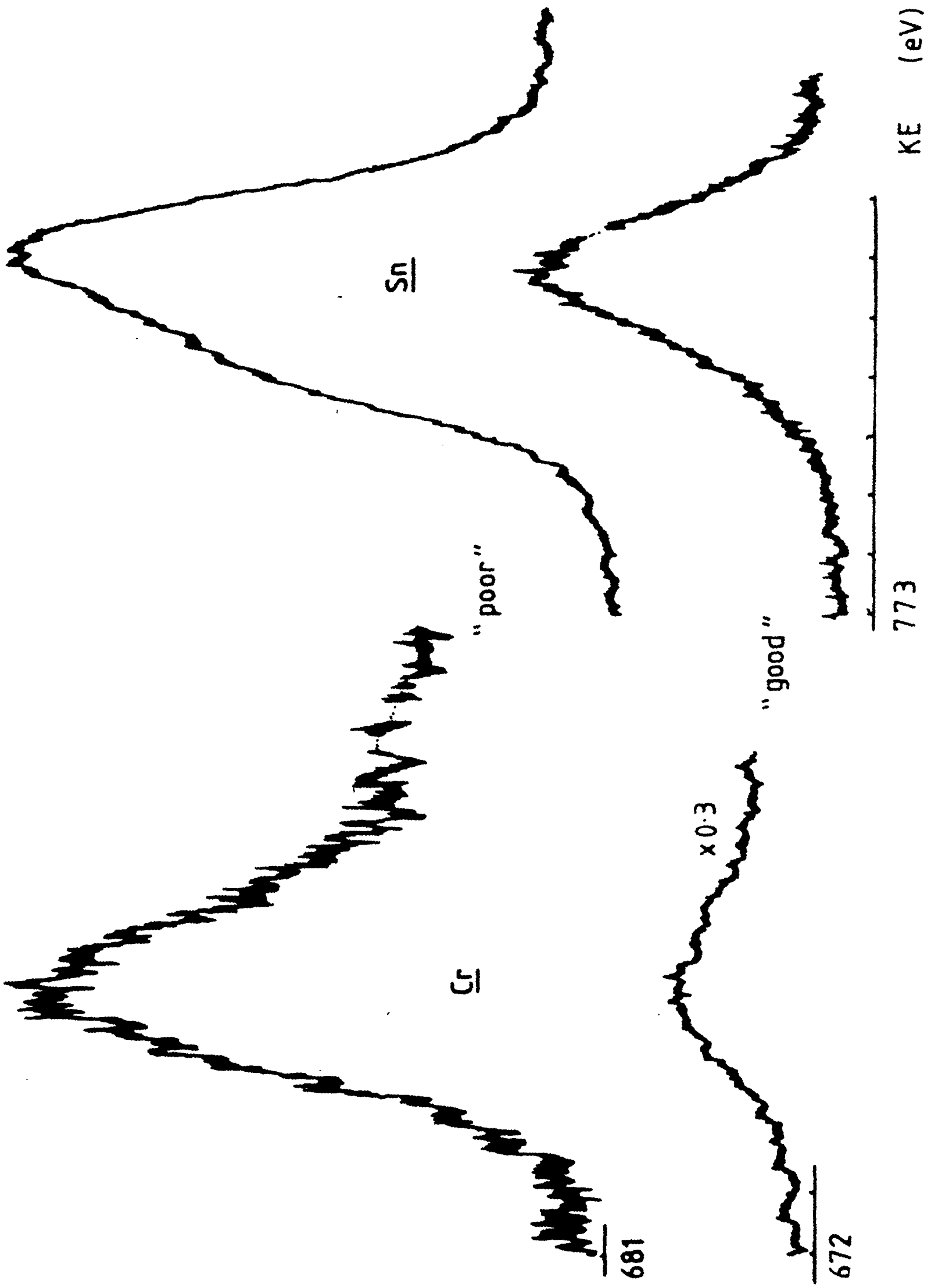

Fig. 27. 25 eV spectra of two nominally identical 311 tinplate surfaces. One has good adhesion properties; the other poor.

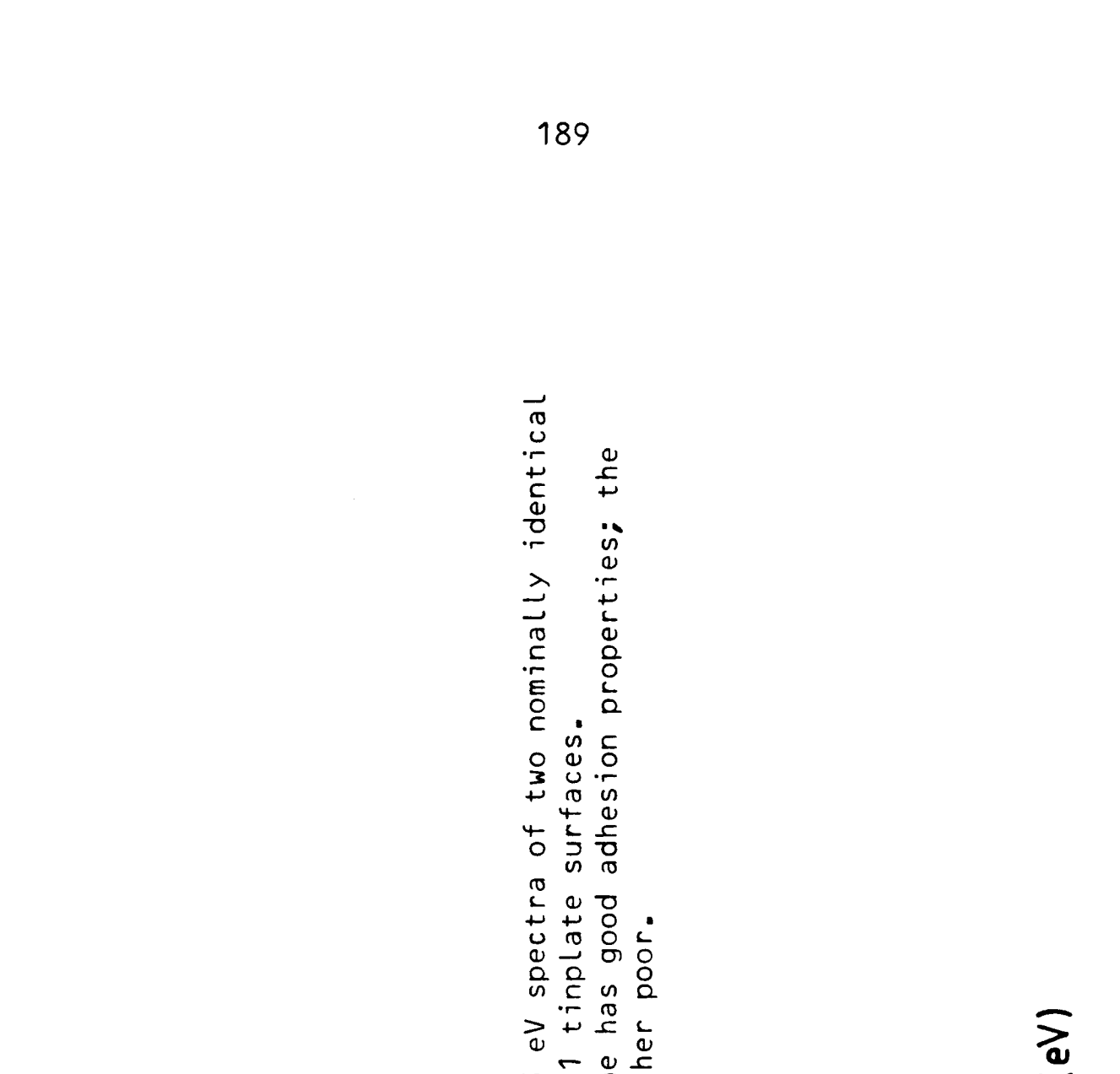

Fig. 28. 25 eV spectra of two nominally identical 311 tinplate surfaces. One has good adhesion properties; the other poor.

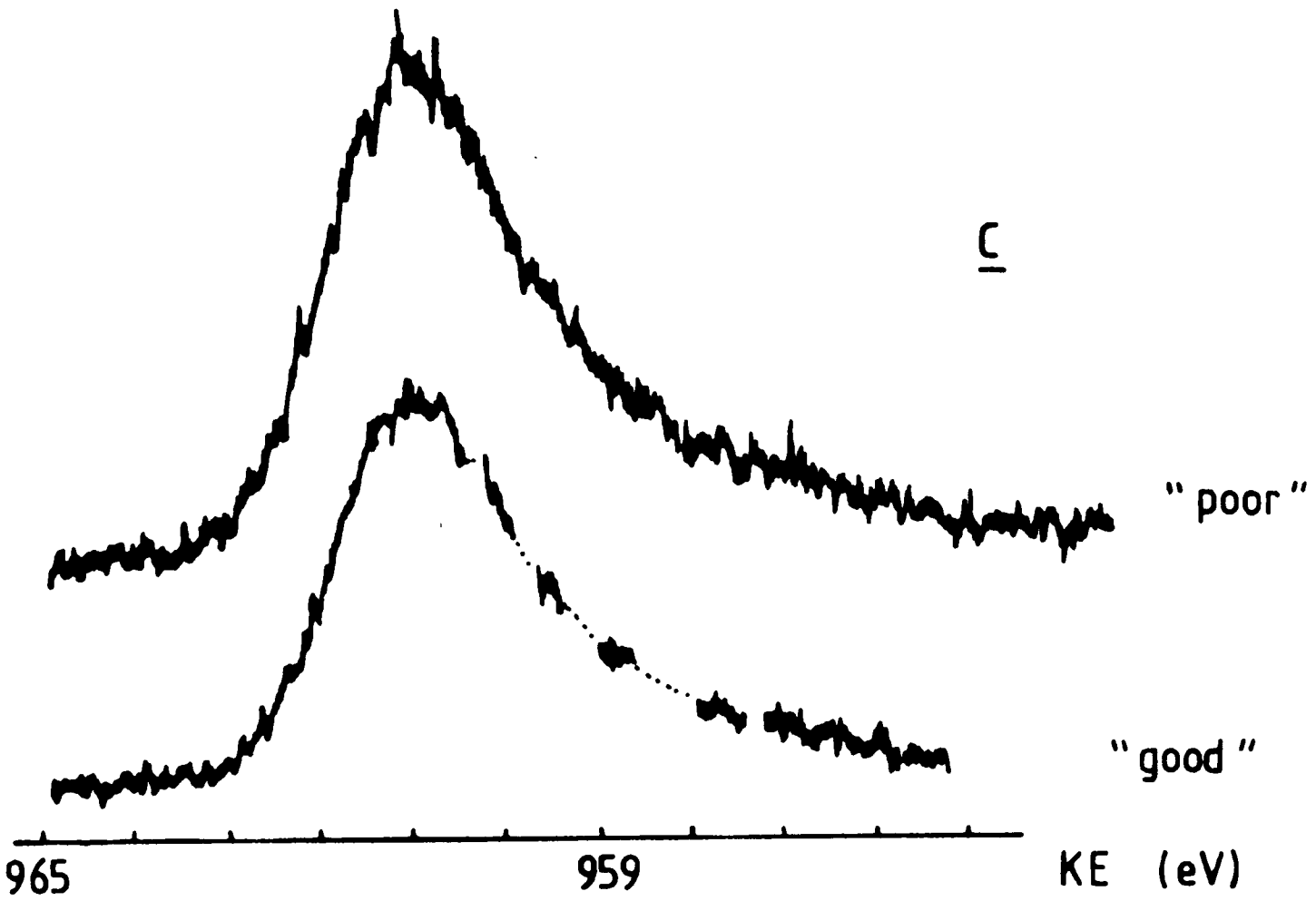

Fig. 29. 25 eV spectra of two nominally identical 311 tinplate surfaces.
One has good adhesion properties; the other poor.

Fig. 30. 25 eV spectra of fracture surfaces from the 'good' and 'poor' tinplates shown in Figs. 27-30.

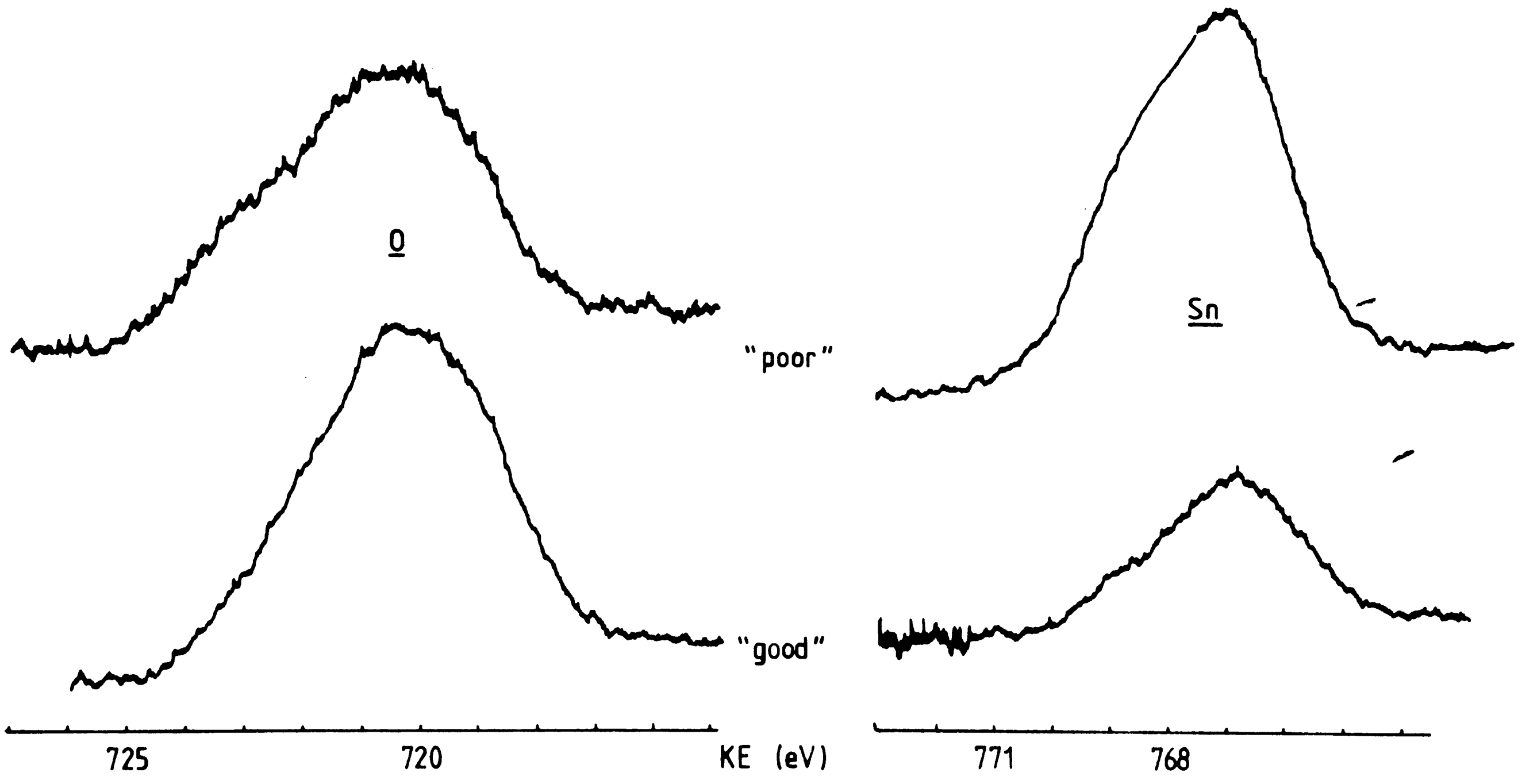

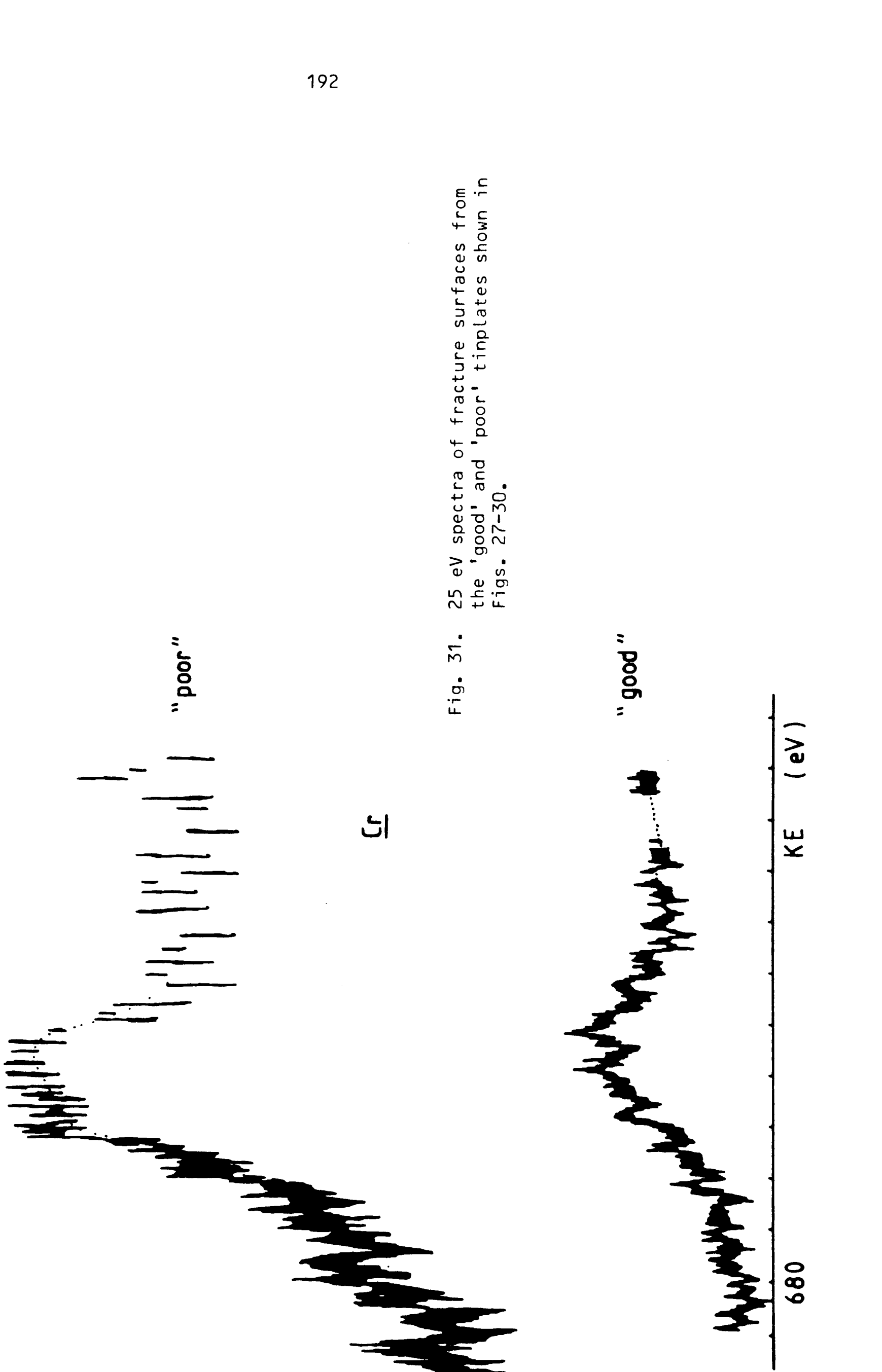

Fig. 31. 25 eV spectra of fracture surfaces from the 'good' and 'poor' tinplates shown in Figs. 27-30.

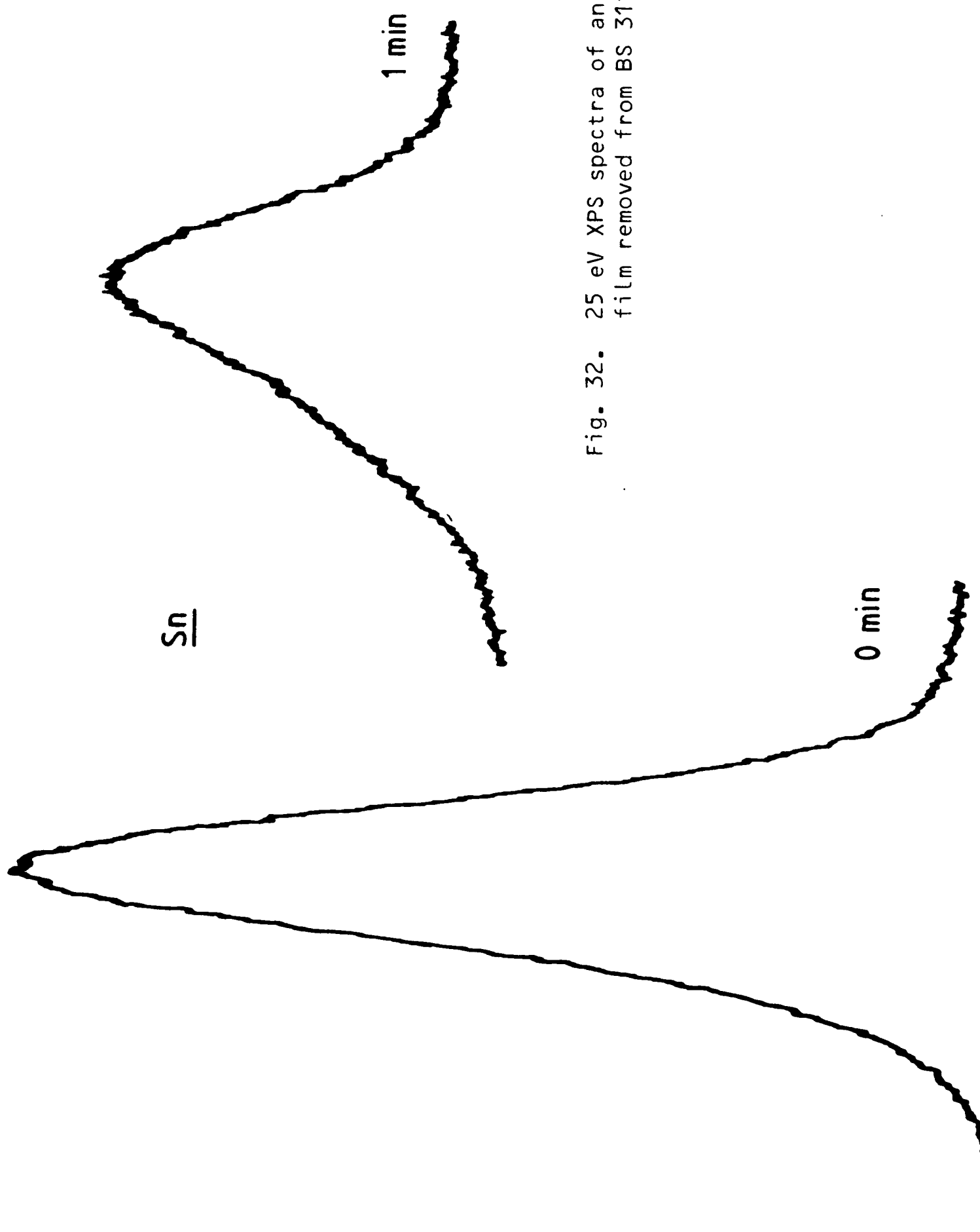

Fig. 32. 25 eV XPS spectra of an isolated passivation film removed from BS 311 tinplate (tin side).

Fig. 33. 25 ev XPS spectra of an isolated passivation firm removed from BS 311 tinplate (tin side)

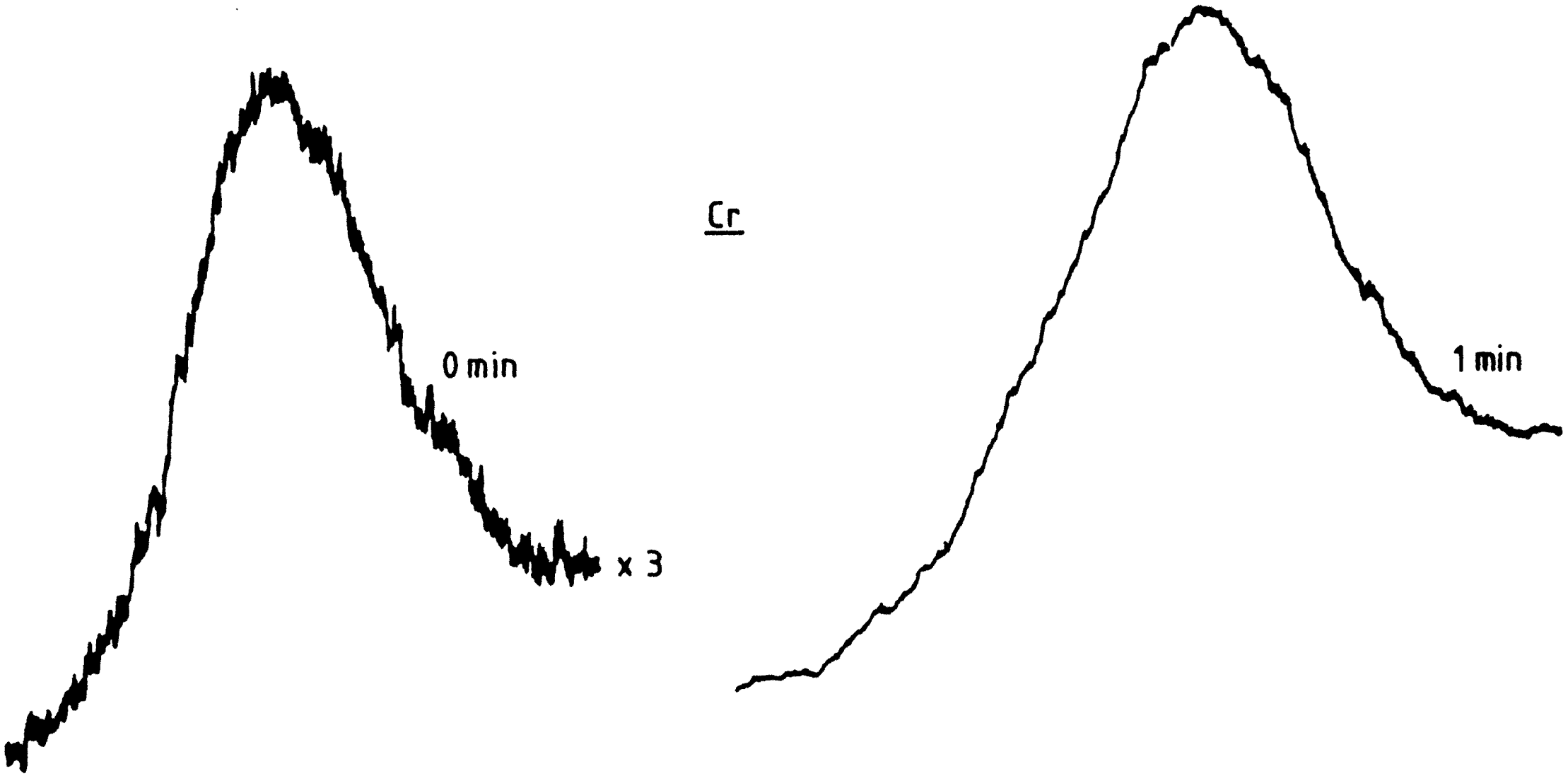

Fig. 34. 25 eV XPS spectra of an isolated passivation film removed from BS 311 tinplate (tin side).

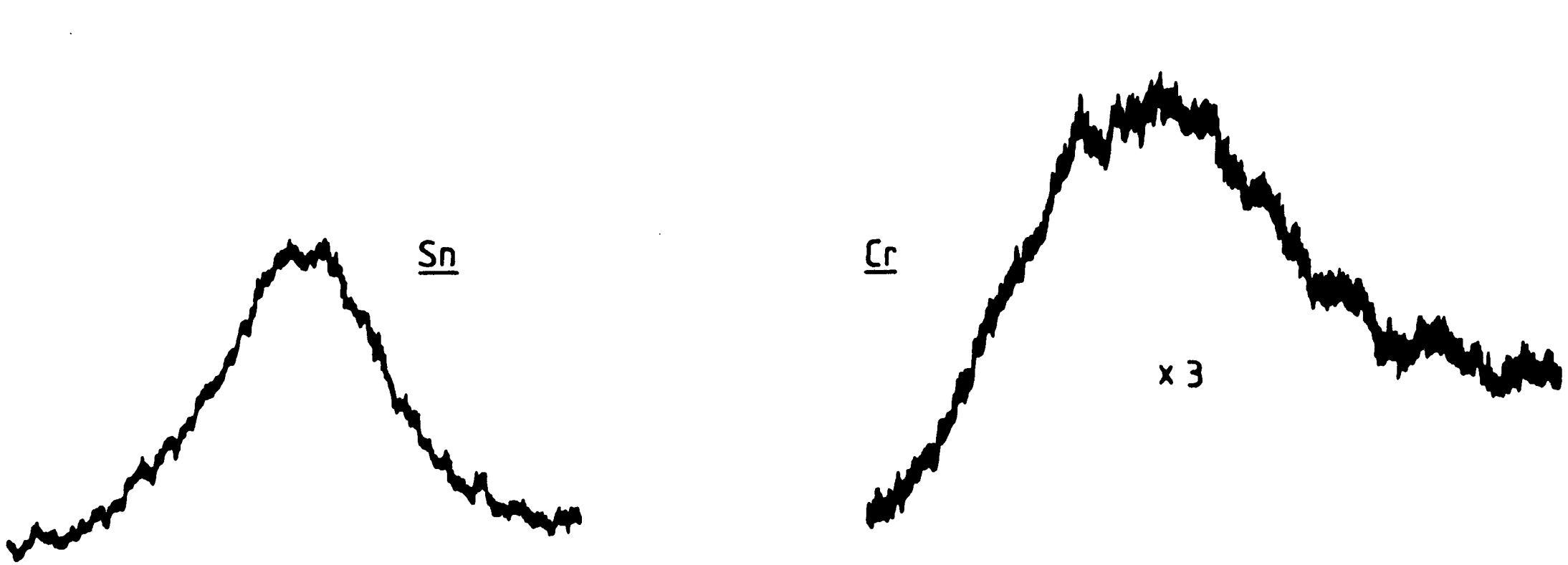

Fig. 35. 25 eV XPS spectra from an isolated KS 311 tinplate passivation layer (tin side).

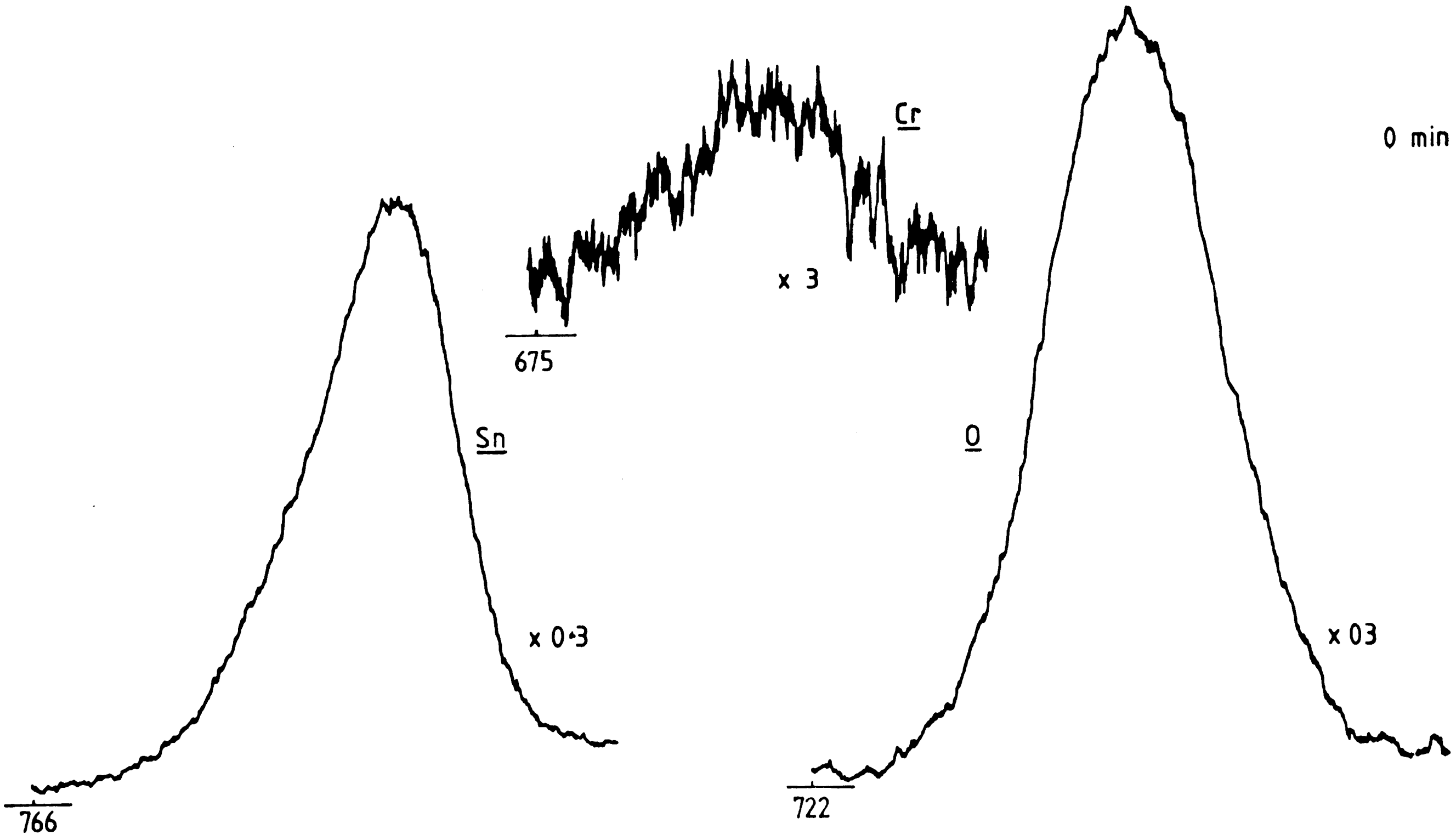

Fig. 36. 25 eV XPS spectra from an isolated KS 311 tinplate passivation layer (tin side).

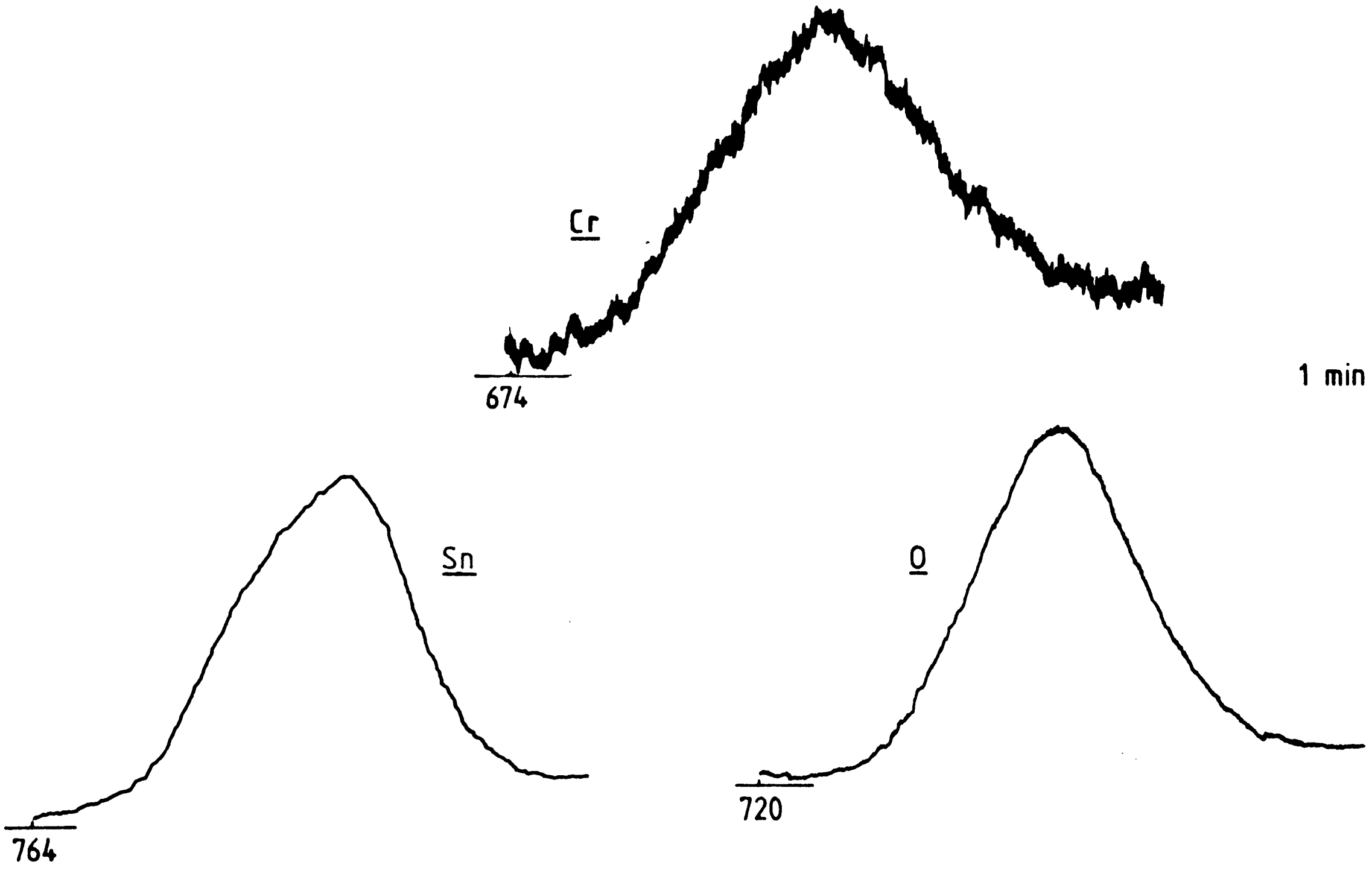

Fig. 37. 25 eV XPS spectra from an isolated KS 311 tinplate passivation layer (tin side).

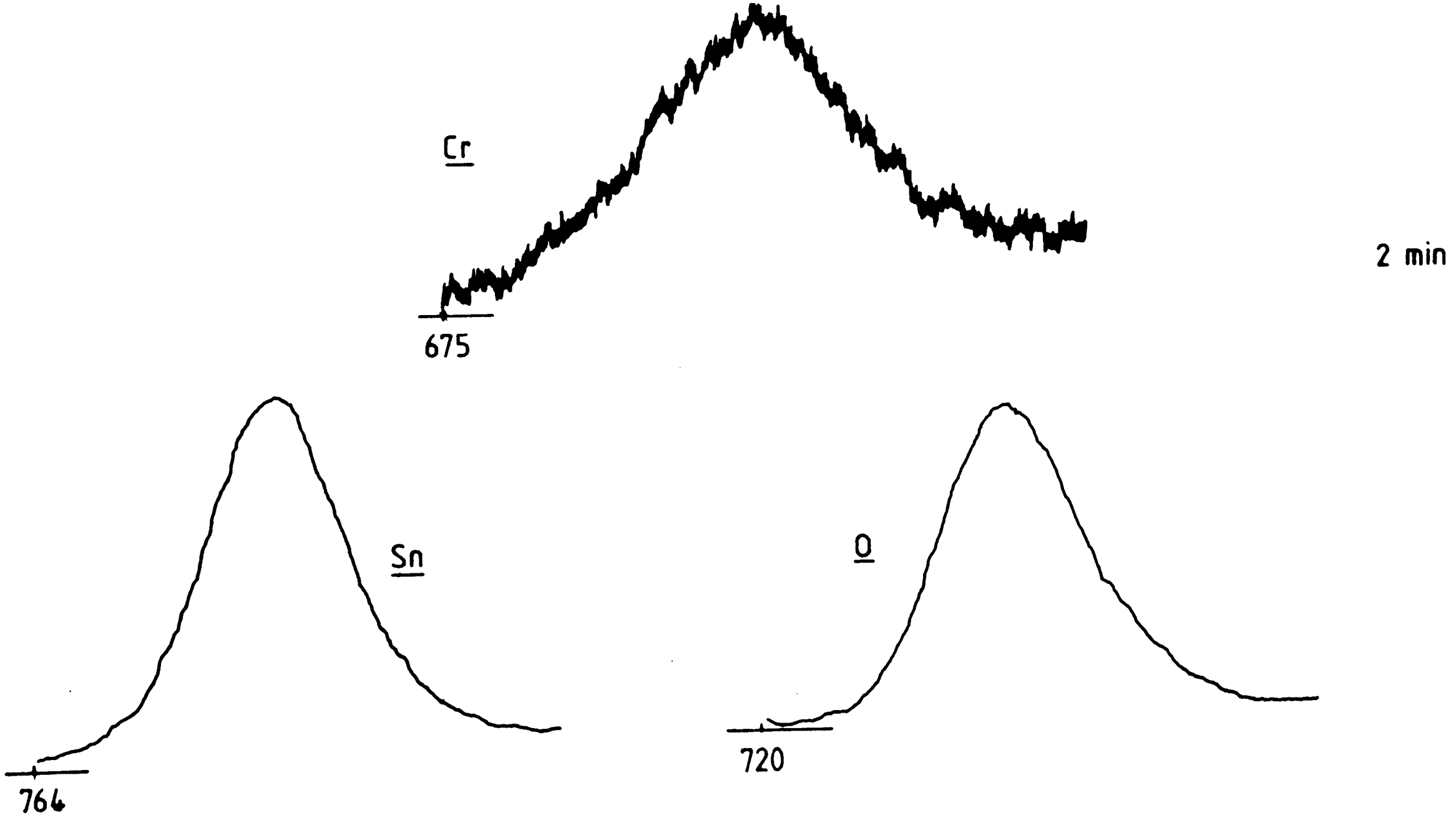

Bibliography

Albu-Yaron, A. and Smith D.A. Br. Corr. J. 14 No. 3 (1979) 133.

Andersen H.H. Appl. Phys. 18 (1979) 131.

Aubrun P. Bull. INACOL 21, 239 (1970).

Abrun P. and Rocquet P. J. Electrochem. Soc. 122 No. 7 (1975) 861.

Azzeri N. , Splendorini L., Battistoni C. and Papparazzo E. Surf. Tech. 15 No. 3 (1982) 255.

Battistoni C., Dormann J.L., Fiorani D., Papparazo E. and Viticoli S. Sol. Stat. Comm. 39 (1981) 581.

Boggs W.E., Kachik R.H. and Pellisier G.E. J. Electrochem. Soc. 108 No. 1 (1981) 6.

Briggs D. Appl. Sufr. Sci 6 (1980) 188.

Briggs D. J. Adhesion 13 (1982) 287.

Britton S.C. Br. Corr. J. 1 91 (1965).

Carter W.J., Schweitzer G.K. and Carlson T.A. J. Elec. Spec. 5 (1975) 827.

Coad J.P., Mott B.W., Harden G.W. and Walpole J.F. Br. Corr. J. 11 No. 4 (1976) 219.

Dilks A. "Handbook of X-ray and Ultraviolet Photoelectron Spectroscopy" Vol. 4 Ch. 5 Ed. D. Briggs, Heyden and Sons, London (1977).

Einstein A. Ann. Phys. 17 (1905) 132.

Emerson J.B. and Fellows L.J. Metal Box Research Centre. Internal Memorandum IDN TR 10010025 April 1981.

Evans S. "Handbook of X-ray and Ultraviolet Photoelectron Spectroscopy" ed. D. Briggs Ch. 3, Heyden and Sons, London (1977).

Fadley C.S. "Progress in Solid State Chemistry" eds. G. Somorjai and J. McCaldin, Pergamon Press, Oxford (1976 265.

Fadley C.S. "Electron Spectroscopy. Theory, Techniques and Application". eds. C.R. Brundle and A.D. Baker, Vol. 2.1 Academic Press, London (1978).

Grundner M. and Halbritter J. J. Appl. Phys. 51 No. 1 (1980) 397.

Grutsch P.A., Zeller M.V. and Fehlne T.P. Inorg. Chem. 12 (1973) 1431.

Hall P.M. and Morabito J.M. CRC Critical Reviews in Solid State and Materials Sciences. December 1978. 53.

Hammond J.S.S., Holubka J.K., DeVries J.E. and Dickie R.A. Corr. Sci 21 No. 3 (1981) 239.

Ikemoto I., Ishii K., Kinoshit S., Hukoda H., Franco M.A.A. and Thomas J.M. J. Sol. Stat. Chem 17 (1976) 425.

Johannessen J.S., Grande A.P. and Notevarp T. Proc. 2nd Internat. Tinplate Conf. paper no. 24, London (1980).

Jolly W.L. "Electron Spectroscopy" ed. D.A. Shirley p. 269. North Holland, Amsterdam (1972).

Kanaya K., Hojou K., Koga K. and Toki K. Japan. J. Appl. Phys. 12 No. 9 (1973) 1297.

Kim K.S., Baitinger W.E., Amy J.W. and Winograd N. J. Electron. Spectroscopy and Rel. Phenom. 5 (1974) 351.

Kinlock A.J., Bishop H.E. and Smart N.R. J. Adhes. 14 (1982) 105.

Leroy V., Habraken J.P., Renard L. and Lempereur S. Proc. 1st Int. Tinplate Conf. London (1979) 399.

Leroy V., Servais J.P., Habraken L., Belgium C.R.M., Renard L., Lempereur J., Cockerill S.A. Proc. Ist Int. Tinplate Conf. London (1976) 34.

Lin A.W.C., Armstrong N.R. and Kawana T. Anal. Chem. 49 (1977) 122.

Maeda S., Asai T. and Sawairi T. Proc. 2nd Int. Tinplate Conf. London (1980) 286.

Mnason S.T. and Dill D. "Electron Spectroscopy. Theory, Techniques and Application" vol. 2, p. 157 eds. C.R. Brundle and A.D. Baker Academic Press London (1978).

McGuire G.E. "Applied Electron Spectroscopy for Chemical Analysis" Ch. 1 eds. H. Windawi and F.F.L. Ho, Wiley New York (1982).

Morgan W.E. and Van Wazer J.R. J. Phys. Chem. 77 (1973) 964.

Morris A. and Westwood N.P.C. Inorg. Nucl. Chem. Lett. 10 (1974) 1009.

Van Ooij W.L. and Kleinhesselink A. Appl. Surf . Sci. 4 (1980) 324.

Olefjord I. and Fischmeister H. Corr. Sci. 15 (1975) 697.

Powell C.J. "Applied Electron Spcetroscopy for Chemical Analysis" Ch. 2 eds. H. Windawi and F.F.L. Ho Wiley New York (1982).

Rauch S.E. Jnr. and Steinbicker R.N. J. Electrochem. Soc. 120 No. 6 (1973) 735.

Saijo K., Yoshioka O. and Oyama T. Tech. Rep. Tokyo Kohan Co. Ltd. 23 (1976).

Schofield J.H. J. Electron. Spect. and Rel. Phenom. 8 (1976) 129.

Schwartz M.E., Switalski J.D. and Stronski R.E. "Electron Spectroscopy" p. 605 ed. D.A. Shirley, North Holland, Amsterdam (1972).

Seah M.P. Surf. and Interf. Anal. 2 No. 6 (1980).

Seigbahn K., Nordling C., Fahlman A., Nordberg R., Hamerin K., Hedman J., Johannson G., Bergmark T., Karlsson S.E., Lindgren I. and Lindberg B. Nova Acta Regiae Sci. Ups. Ser. IV 20 (1967).

Seigbahn K., Nordling C., Johannson G., Hedman J., Heded P.F., Hamrink K. Gelius U., Bergmark T., Werne L.O., Manne R. and Baer Y. "ESCA Applied to Free Molecules" North Holland, Amsterdam (1969).

Servais J.P., Lempereur J., Renard L. and Leroy V. Br. Corr. J. 14 No. 3 (1979) 126.

Solomon J.S. and Hanlin D. "Adhesion and Adsorption of Polymers" part A. ed. L.H. Lee, Plenum Press, New York (1980).

Takuno H. and Watanabe T. Proc. 2nd Int. Tinplate Conf. p. 1 London (1980).

Uwamino Y., Ishizuka T. and Yamatera H. J. Electron. Spect. and Rel. Phenom. 23 (1981) 55.

Viinika and Laarson J. Elect. Spect. 7 (1975) 163.

Wagner C.D. Anal. Chem. 49 No. 9 (1977) 1282.

Willemen H., Van de Vondel D.F. and Van der Kelen G.P. Inorg. Chim. Acta. 34 (1979) 175.

CHAPTER 5

TRANSMISSION ELECTRON MICROSCOPY

1. INTRODUCTION

Experimental work has shown that tinplates with good adhesion properties are characterized by a low area debonding factor and fail in the butt-joint test near the lacquer-passivation layer interface. KS 311 and NS 311 tinplates with poorer adhesion than BS 311 and 300 types fail at an interface below the passivation layer. Optical microscopy of fracture surfaces reveals defects in the tin coating which are likely failure initiation sites in BS 311 and possibly other types while X-ray photoelectron spectroscopy of the passivated tinplates has shown compositional differences in the passivation layers with respect to chromium metal and chromium oxide content which, along with the results of other workers, suggest that the structure and composition of the passivation film have a major influence on lacquer adhesion.

Transmission electron microscopy will be able to image the components of the passivation layer with a resolution better than 2 nm and will distinguish by diffraction the types of chromium oxides and tin oxides present. The design and operation of the microscope, theoretical treatments of the technique and procedures for analysing diffraction patterns are described extensively in the literature (Hirsch et al 1965, Hall 1966, Glauert 1972, Andrews 1971, Edington 1974) and in Appendix 2.

Early attempts to relate lacquer adhesion to the structure of passivation layers on tinplates by TEM were unsuccessful (Neish and Donelson 1960, Britton and Bright 1957) and no extensive conclusions

have yet been made despite several investigations in recent years (Saijo et al 1976, Azzeri et al 1982, Coad et al 1975, Servais et al 1979, Albu-Yaron and Smith 1979, Takano and Watanabe 1980) which have investigated the components of the passivation film using this and other techniques.

Values for the area coverage of chromium and chromium oxides have been calculated from XPS and these may be checked using the high spatial resolution of TEM which can also differentiate from their crystal structures the different tin and chromium oxides which could not be positively identified by the former technique. The oxidation of tin has been studied by other workers: Britton and Sherlock (1974) report that pure tin sheet, when heated above $75^{0}C$, oxidised to form only SnO, supporting the conclusions of an earlier work (Boggs et al 1961). When tinplate is heated to temperatures above $100^{o}C$ however there is TEM evidence that SnO_2 forms (Oyama et al 1966) and that growth of SnO_2 will occur during storage in a humid environment (Oyama 1959). Servais et al (1979) suggest that a tin oxide layer forms beneath the passivation layer during the stoving of lacquered tinplate and that this may be responsible for reducing lacquer adhesion. These workers used XPS and consequently could not distinguish between different tin oxides. However, it is clear that tin oxide is not necessarily inimical to adhesion; the 300 tinplate which has a much thicker oxide covering than 311 has very good lacquer adhesion properties. Specific tin oxides have been associated with lacquer adhesion in one work (Takano and Watanabe 1980) which correlates poor adhesion with tinplates on which αSnO and SnO_2 grow and good adhesion with orthorhombic SnO. The α (tetragonal) SnO was observed in the form of petals or needles up to 1 μm in length and grouped in large areas, the αSnO_2 as a fine

sub-micron granular coverage and the orthohombic SnO as larger (but still sub-mircon) thinly dispersed angular crystals.

Takano and Watanabe also present results which show lacquer adhesion as a function of chromium content. Very low levels of metallic chromium (as measured electrochemically) reduce peel strength but otherwise have no effect; an increase in total chromium content also has the effect of reducing adhesion. These workers, however, only show electron micrographs of metallic chromium in passivation layers which have been produced by a special process and were unable to obtain diffraction data from tinplates typical of commercial types. Albu-Yaron and Smith (1979, 1980) have published micrographs of metallic chromium and Cr_2O_3, both in the form of hexagonal crystals which have been detected on commercial tinplate and Saijo et al (1976) using XPS and TEM find evidence for Cr^o, $Cr_2O_3.nH_2O$, $Cr(OH)_3$, SnO and SnO_2. They assign their chemical formulae on the basis of XPS data and show micrographs of trivalent chromium compounds which appear as thinly-dispersed sub-micron grains.

From the micrographs of stripped passivation layers published by various workers there are obvious and large differences in the areal coverage, size and dispersion of diffracting species. Variations in the passivation treatment can account for these differences (Saijo et al 1976, Takano and Watanabe 1980) so it would be expected that tinplates from different manufacturers would exhibit variations in passivation layer structure as the passivation treatment of each manufacturer is likely to be slightly different (ITRI 1984). Indeed, a single coil of tinplate from a commercial production line may have variations in the passivation layer considering that it is typically 1 m in width and perhaps 10^3 m in length. Since the TEM specimen is a few mm in diameter and the working field of view only a few μm

in diameter this must be borne in mind.

Some of the tinplates used in the work presented below are from the same batch as that used by Albu-Yaron and Smith. They have identified Cr^{o} large (300 nm) crystals of Cr_2O_3, tetragonal SnO_2 and tentatively identified tetragonal SnO. In addition, they speculate on the existence of tin oxides intermediate between SnO and SnO_2 in structure which would account for the existence of diffuse, unidentifiable diffraction rings found during their investigation.

This section of work will compare the topography of the tinplate surface and the structure of the passivation layer by stripping the layer from the surface in a chemical etch. From the work of other experimenters it is expected that tin and chromium oxides (and possibly metal) will be found. The data from the set of tinplates used in the mechanical tests and in XPS will be compared (BS 311, KS 311, NS 311, 300, NP) to seek for significant differences which would help to explain their variations in lacquer adhesion. The XPS results suggest that there is typically a 10-20% area coverage of chromium or chromium oxide on the tinplate surface, probably in layered "islands" such as proposed by Saijo et al. This degree of coverage should be easily visible if it is manifested as large discrete particles but this would not be an ideal arrangement for the coverage of a protective film as the passivation layer is required to be. Adhesion properties of the passivation layer are certain to be a function of its morphology and chemistry and TEM, combined with optical microscopy and XPS, will allow the passivated tinplate surface to be thoroughly examined and characterised.

2. EXPERIMENTAL

All transmission electron microscopy was performed using a JEOL JEM 100C microscope operating at 100 kV accelerating voltage.

Passivation layers were removed from tinplate samples by chemical etching but owing to their extreme thinness the layers were usually first coated with a vacuum deposited carbon film (Bradley 1954) for mechanical strength. Two methods of specimen preparation were used (Figure 1). In method A a thin carbon support film was deposited on the passivated tinplate surface. The underlying tin was then etched away in a solution of iodine in methanol (5% iodine) as used by Albu-Yaron and Smith (1979). Before etching, the tinplate surface was scored into small squares so that stripped passivation layer specimens between 1 and 10 mm^2 in area were created which could be floated onto 3 mm copper grids for insertion into the micro-scope.

Method B avoided the use of a covering support film so that possible artefacts introduced by the carbon coating could be avoided. A gold grid was evaporated directly onto the sample in two stages by depositing the gold through a lined mask rotated through 90^{o} between evaporations. Iodine etching then produced a gold support grid to which areas of passivation film were attached.

Heavy metal shadowing was not necessary to show up the tinplate microscale topography which was clearly visible in the stripped passivation layers.

3. RESULTS

The transmission electron micrographs reveal the distribution of the passivation layer components and microscale topography. Selected area diffraction patterns (SADP) are shown from typical

Figure 1. Preparation of TEM specimens of tinplate passivation layers.

Method A Carbon coating

Method B Gold grid

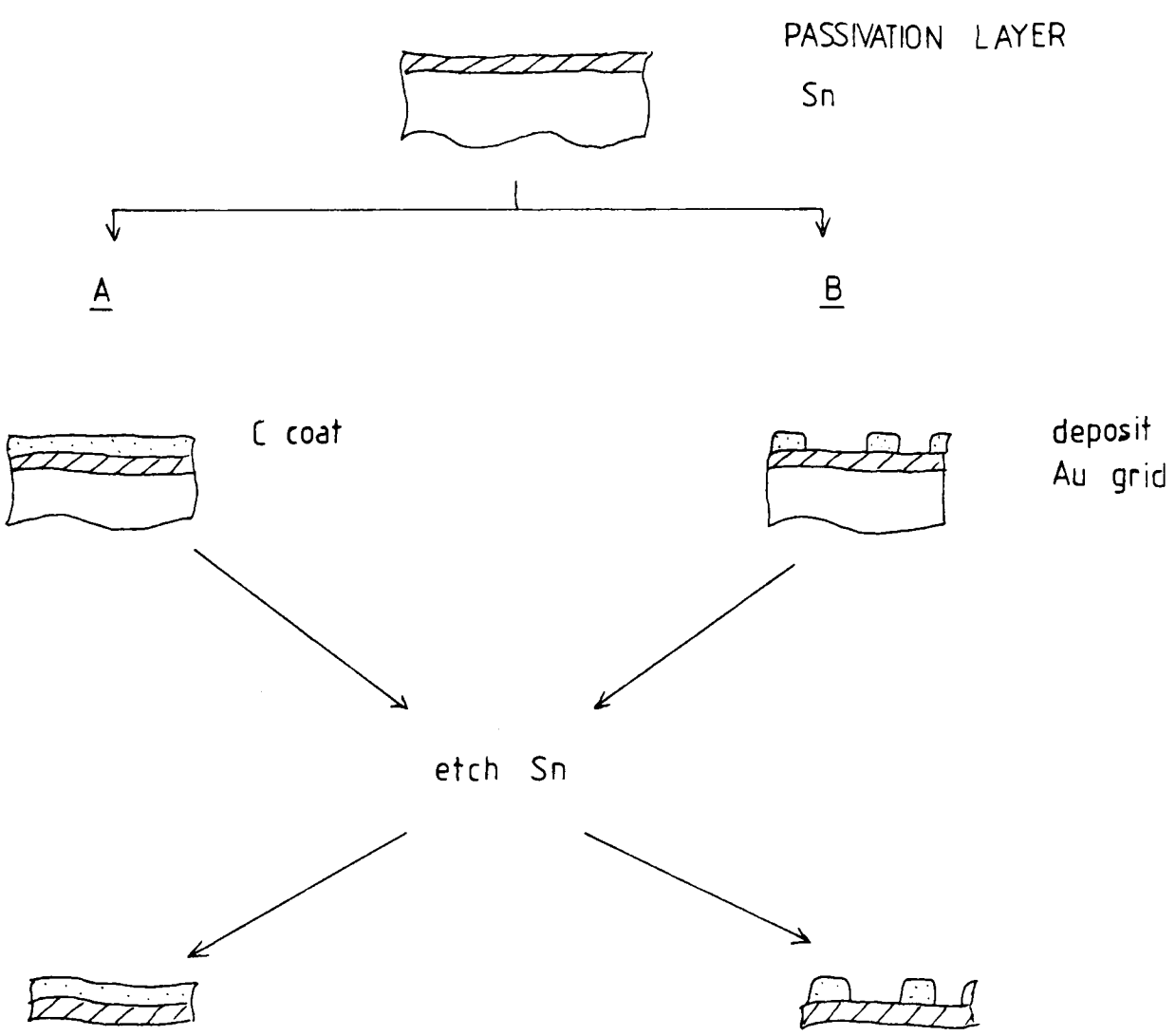

tin and chromium oxides found in the layer and calculated d spacings for identified crystals given in tabular form. Appendix 3 contains the ASTM powder diffraction data cards used to identify the diffracting material.

Since large areas of the passivation layers did not yield identifiable diffraction data because the rings were weak and diffuse, some of the thin specimens were examined with energy dispersive X-ray analysis to give semi-quantitative chemical (elemental) data.

Between 5 and 20 TEM specimens from each type of tinplate examined were observed.

In order to recognise any artefacts arising from the carbon coating an isolated carbon film, prepared under the same conditions as those used to coat the tinplate, was itself examined first. The carbon was evaporated onto a cleaved NaCl crystal surface and removed by dissolving the substrate. As seen in figure 2, the carbon reproduces surface features from the cleaved crystal and exhibits a granularity which is just visible at 50 000x magnification. The thickness of the carbon film was 10 to 20 nm as estimated from the work of Bradley (1954) and in the microscope produced a diffuse-ringed diffraction pattern which would not obscure a superimposed SADP from the passivation film.

Unpassivated tinplate was next examined to study the type and morphology of tin oxides present on tinplate before the passivation treatment and to compare them with the tin oxides found after passivation since the cathodic dichromate (311) treatment not only deposits chromium but also reduces tin oxide. BS 300 tinplate was next investigated, followed by the 311 types: BS 311, KS 311 and NS 311. Stoving effects could also be followed by producing TEM samples from the stoving test specimens used for XPS.

3.1 Selected Area Diffraction analysis and imaging

Specific chemical compounds may be identified from their structures as revealed in the SADP. The procedures are set out in the literature (Hirsch et al. 1965, Andrews et al. 1971) and involve measuring the positions of diffraction spots or rings, calculating d spacings and assigning Miller indices. When a large (> 1 μm) isolated crystal was located a diffraction pattern from it could clearly be assigned but when different crystal types were mixed in the same field of view dark field microscopy (Edington 1974) was used to identify which crystals were producing the measured diffraction pattern.

In all the samples examined in this work various sets of data were obtained which were not inconsistent with the standard patterns of the various oxides of tin and chromium. For the purposes of the further discussion these will be accepted as the identities of the respective phases.

3.1.1 Unpassivated Tinplate (NP)

Four types of tin oxide, tetragonal SnO, orthorhombic SnO, tetragonal SnO_2 and cubic SnO_2 have been found on the unpassivated tinplate. As expected, there is no chromium in either metallic or oxidised form.

Micrographs of the stripped oxide layers with carbon coating are shown in figure 3. The oxide layer is seen to be granular with discrete crystals scattered thinly over the surface. A typical micrograph showing polycrystalline tetragonal SnO is given (figure 3a). This specimen had been stoved in air for 10 minutes at 200°C without lacquer; unstoved tinplate exhibits a coarser structure of SnO (figure 3b). Both stoved and unstoved samples also possessed grains of tetragonal SnO_2 amongst the SnO but these are not always

visible as separate crystals in bright-field micrographs. A polycrystalline growth of tetragonal SnO_2, 0.5 μm in diameter is shown in figure 3c.

Orthorhombic SnO was found as discrete crystals up to 1 μm across. Typically, these crystals are in the form of platelets

(Continued on p. 212)

Key to TEM micrographs and selected area diffraction patterns on the following pages:

Figure 2. Carbon film replica from a cleaved NaCl crystal.

Figure 3. Micrographs of unpassivated tinplate oxide layers.

Figure 4. Typical diffraction pattern.

Figure 5. Micrograph of 300 tinplate passivation layers.

Figure 6. Micrograph of BS 311 (C) tinplate passivation layers

Figure 7. Micrograph of BS 311(6A) tinplate passivation layers

Figure 8. Micrograph of BS 311(5A) tinplate passivation layers.

Figure 9. Micrographs of NS tinplate passivation layers

Figure 10. Micrographs of KS tinplate passivation layers.

Figure 11. Typical diffraction patterns.

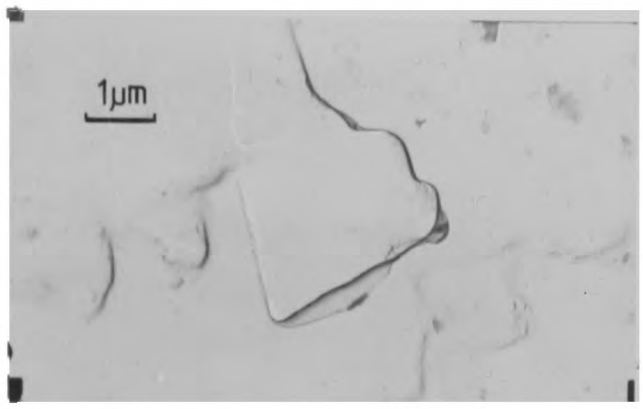

2

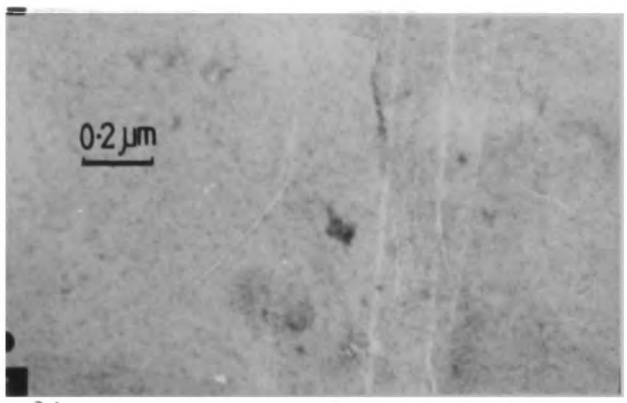

3A

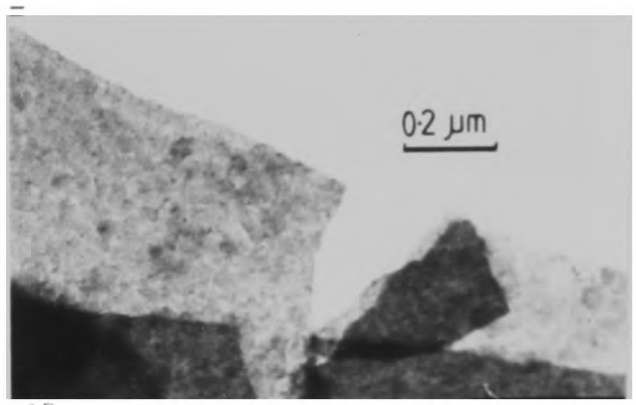

3B

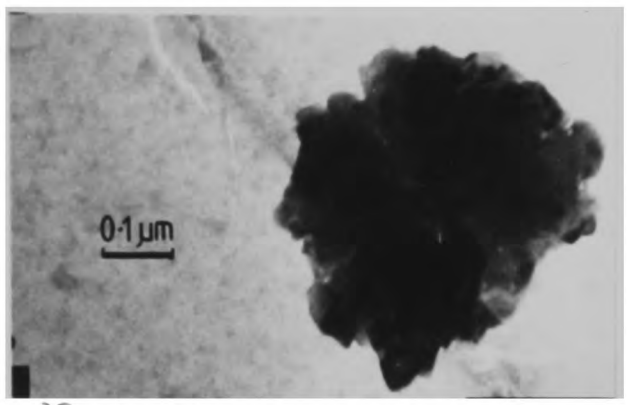

3C

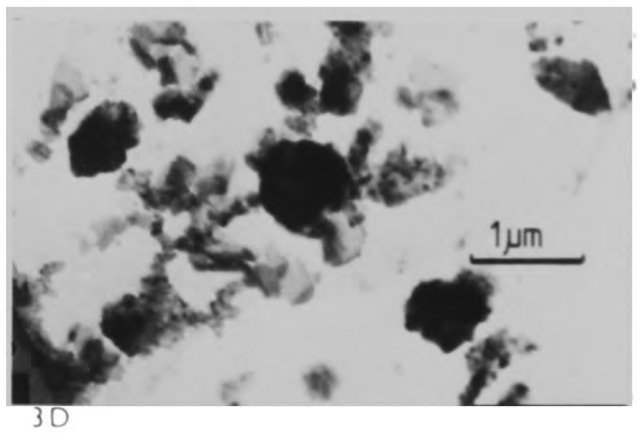

3D

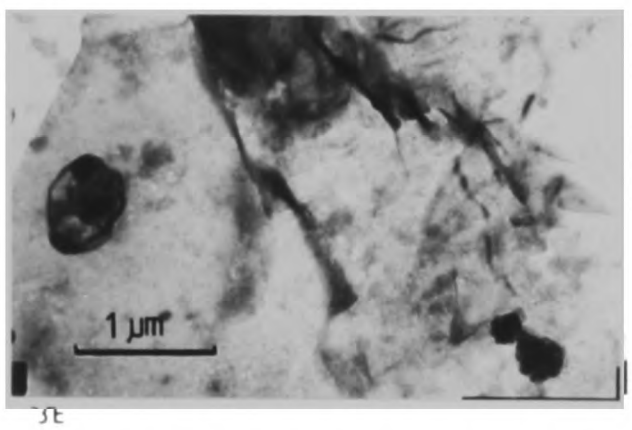

3E

4A SnO_2 c

4B SnO_2 t

4C SnO t

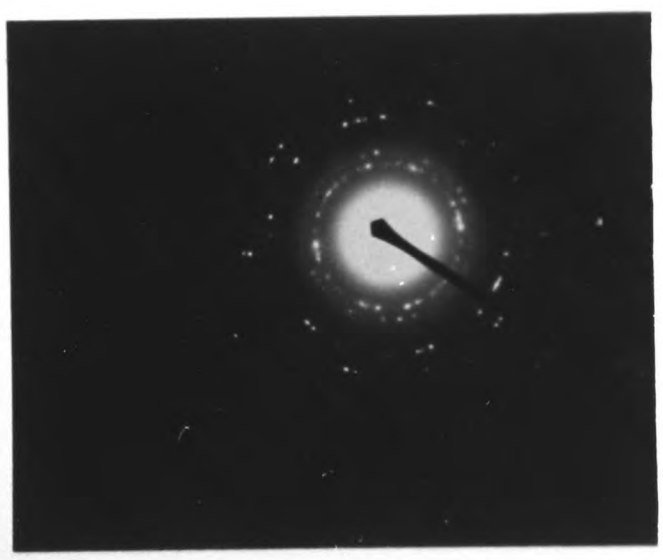

4D SnO o

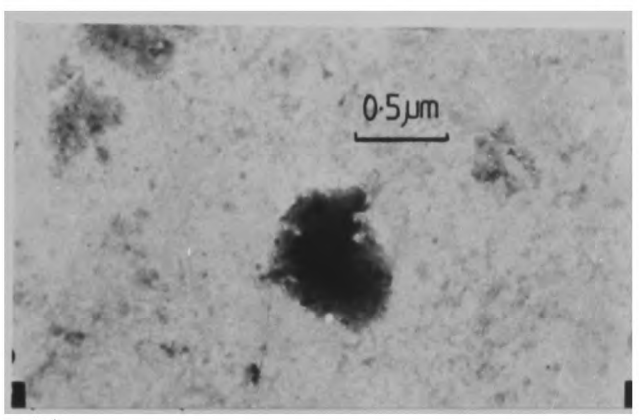

6 A

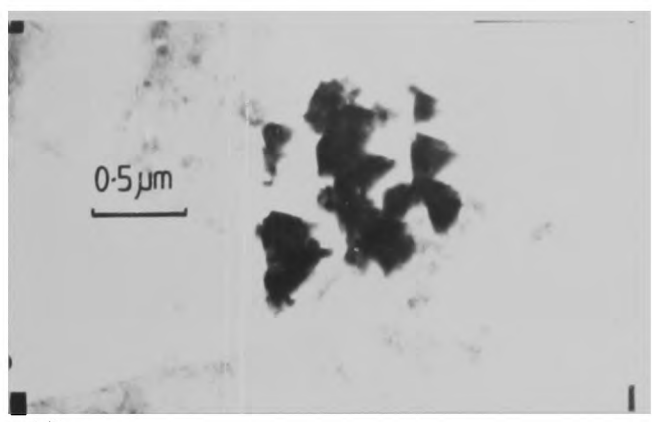

6 B

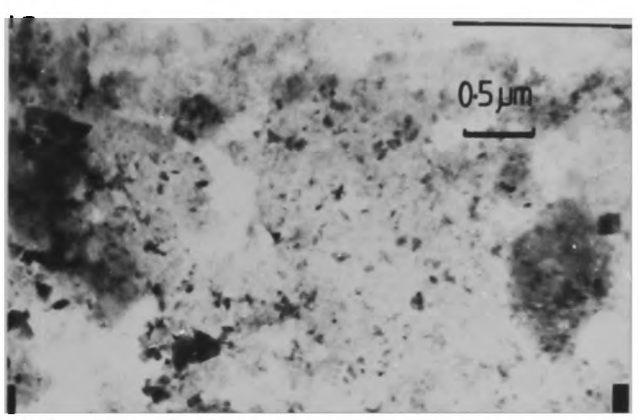

6 C

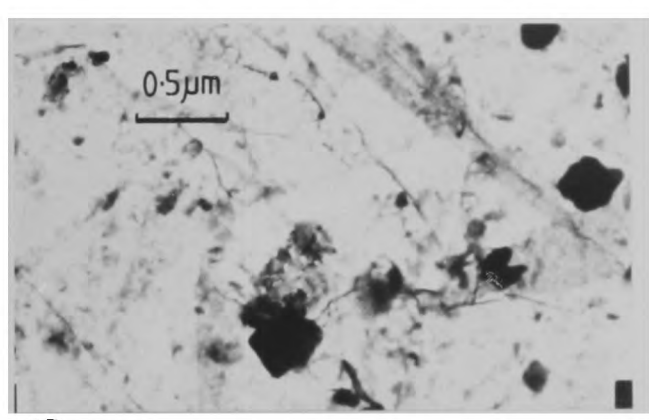

6 D

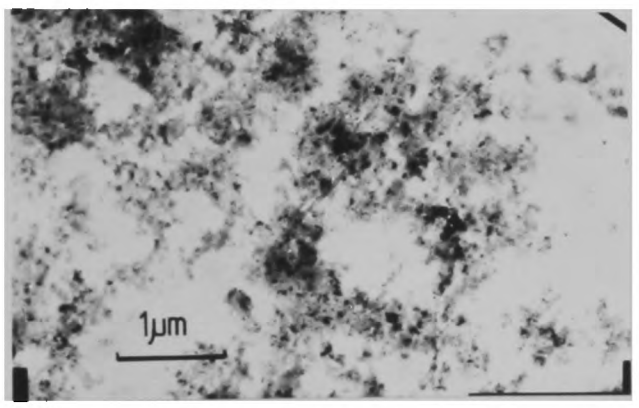

6 E

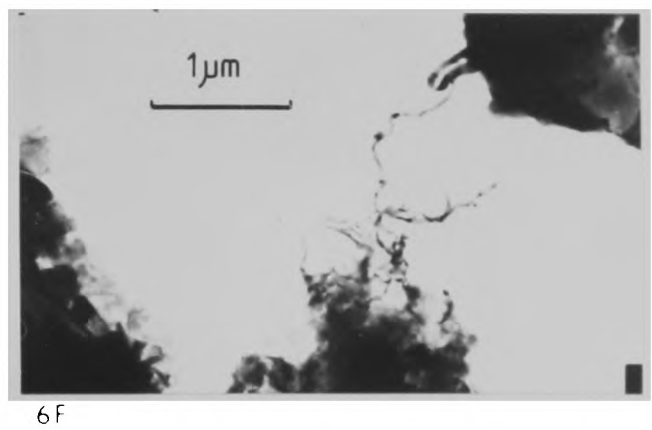

6 F

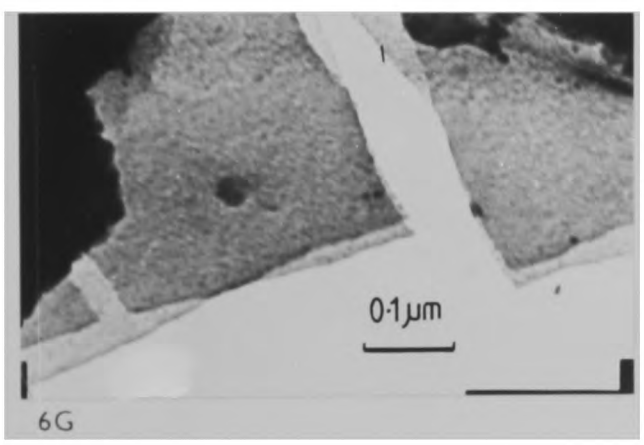

6 G

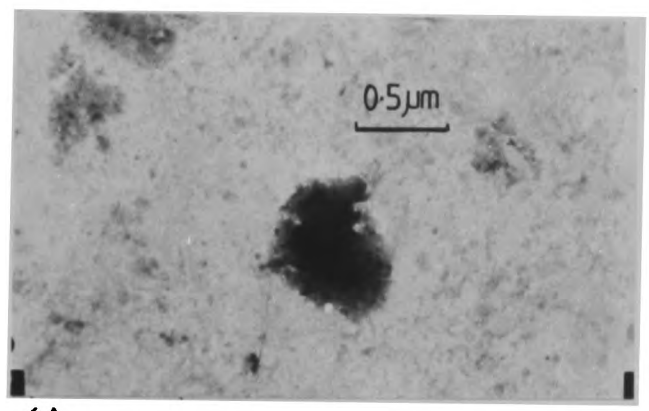

6A

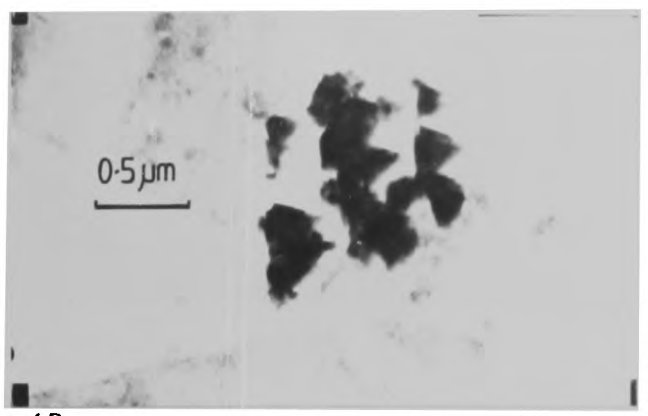

6B

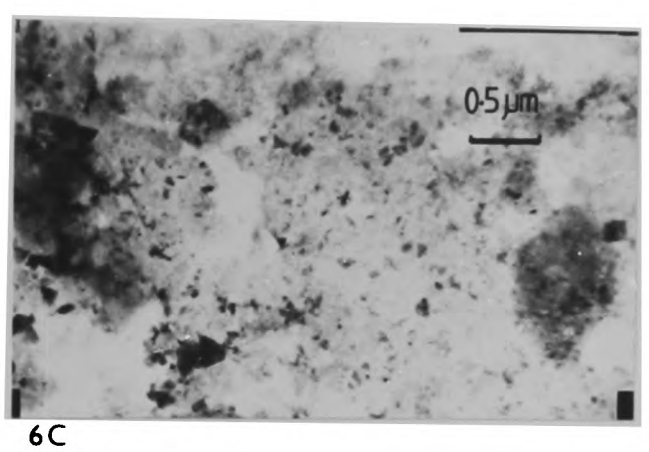

6C

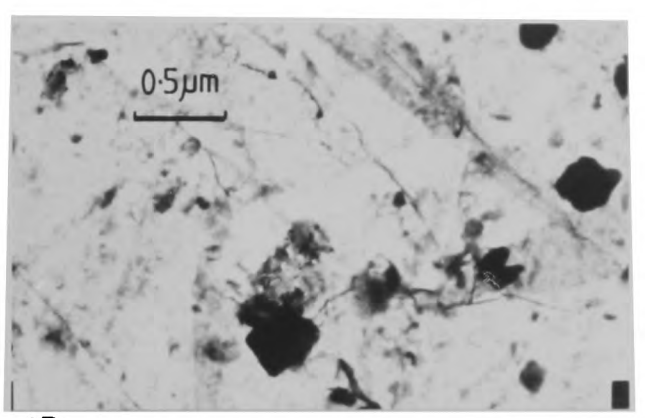

6D

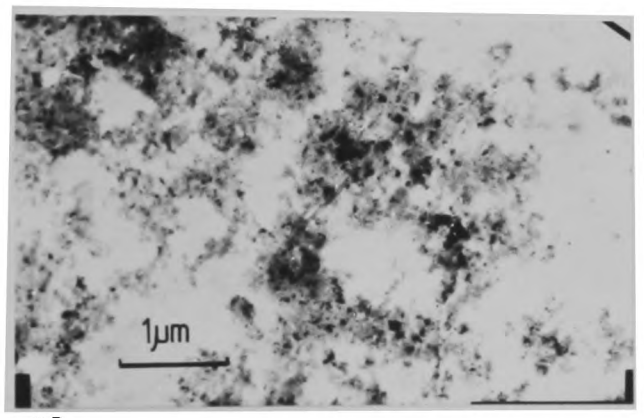

6E

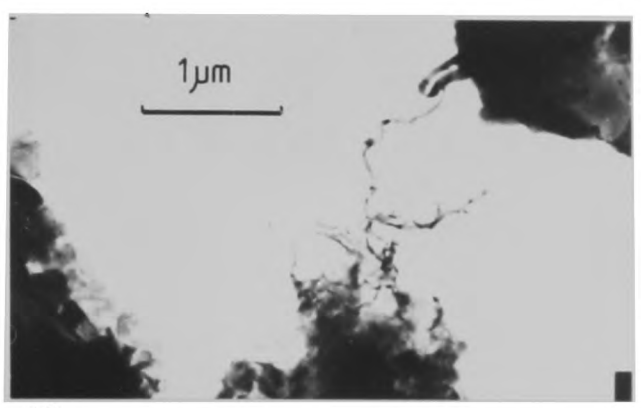

6F

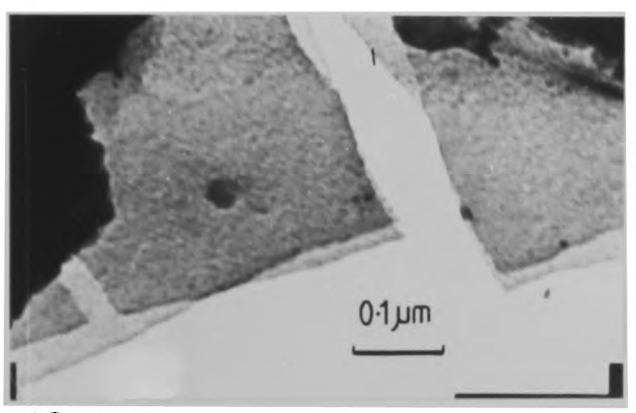

6G

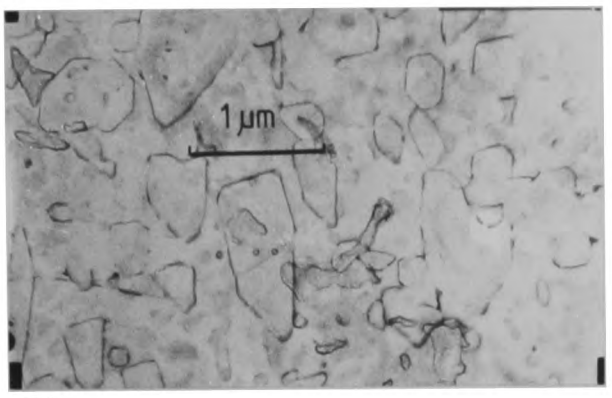

7A

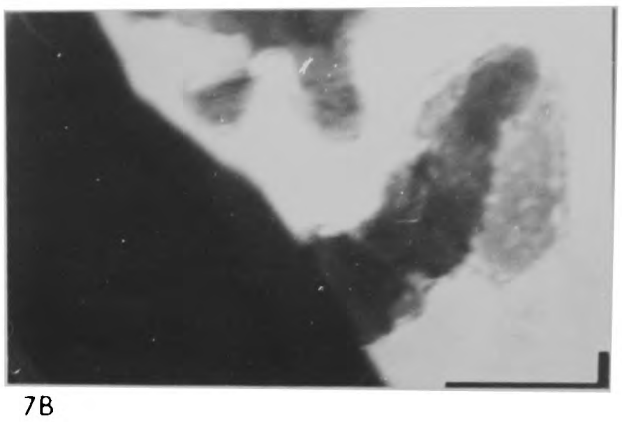

7B

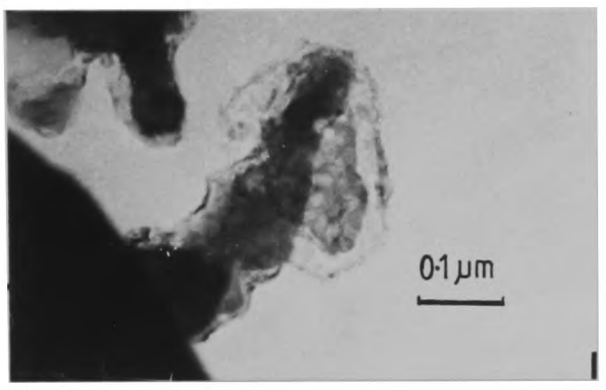

7C

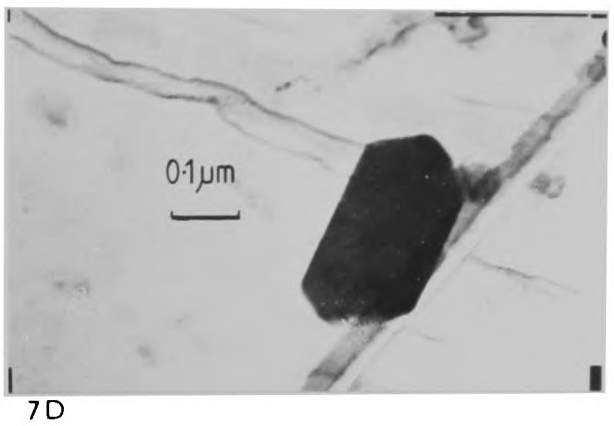

7D

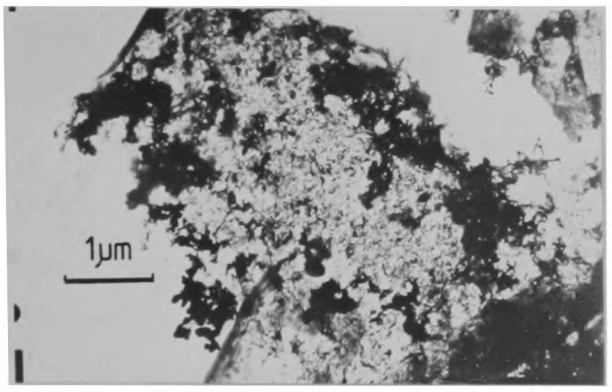

7E

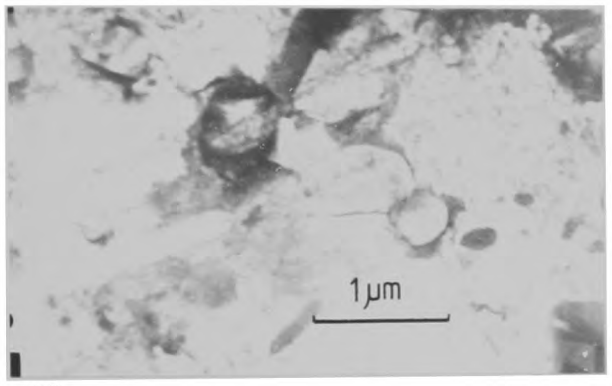

7F

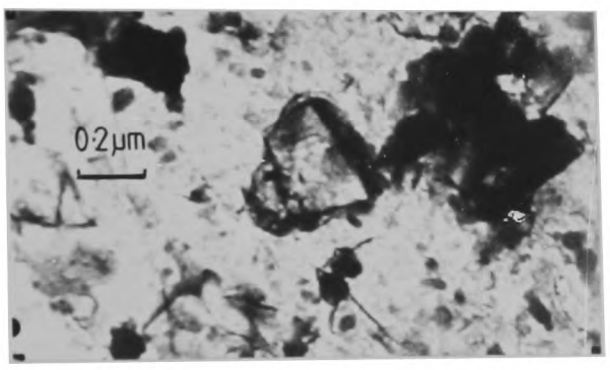

7G

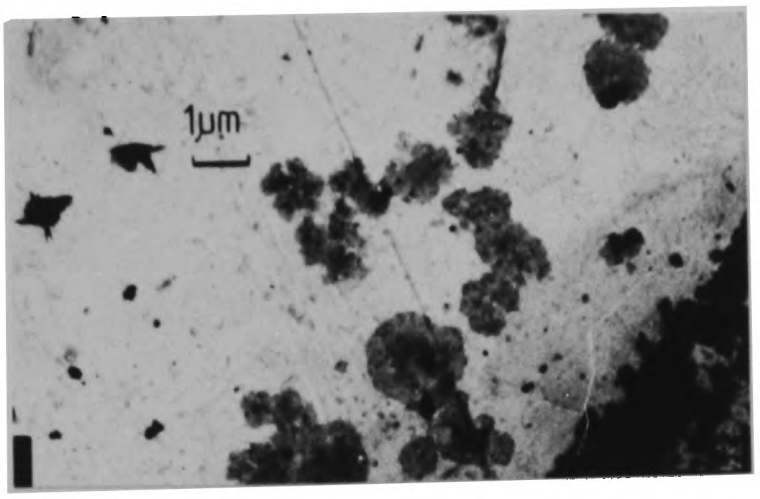

8A

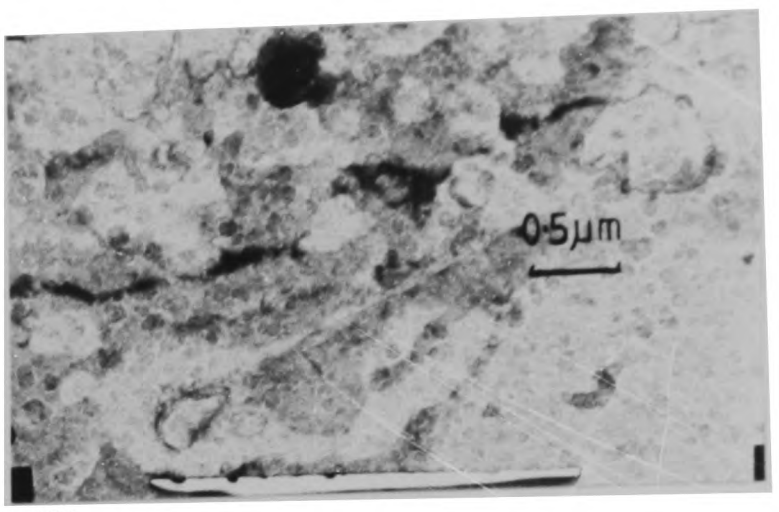

8B

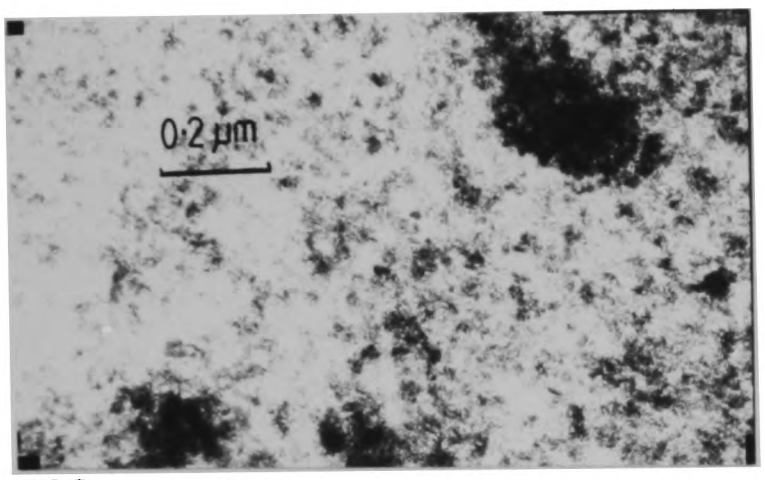

8C

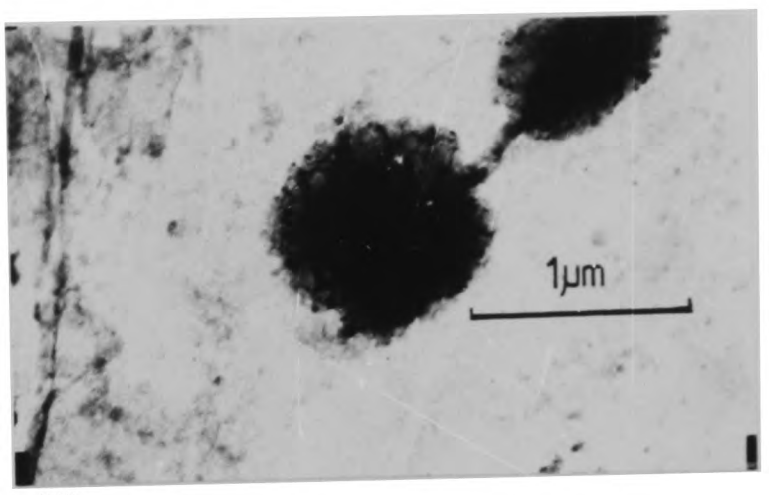

8D

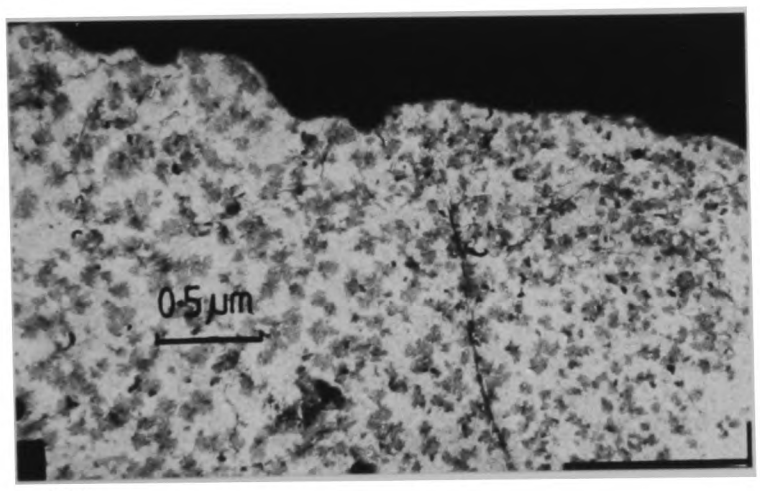

8E

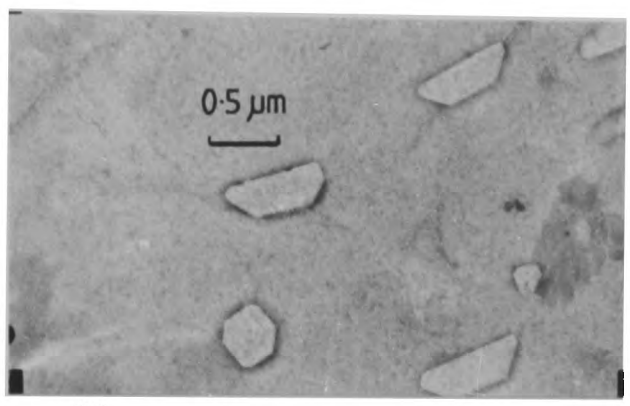

9A

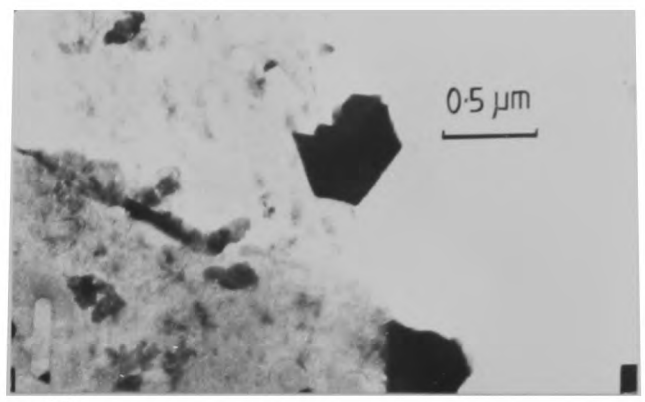

9B

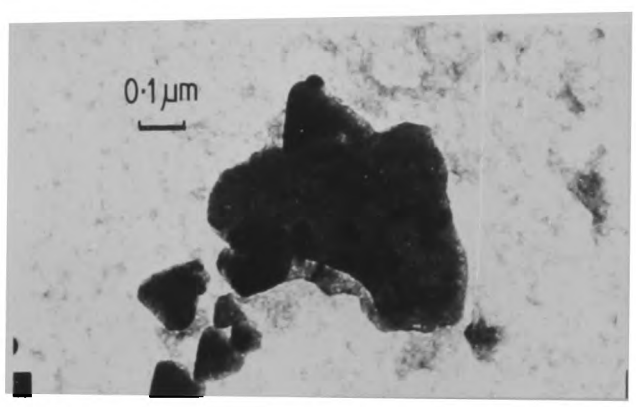

9C

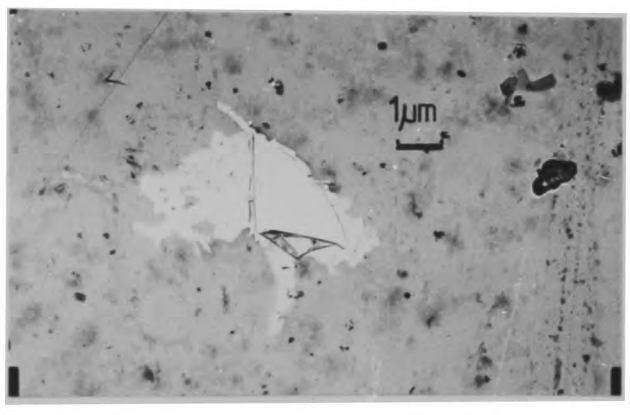

10 A

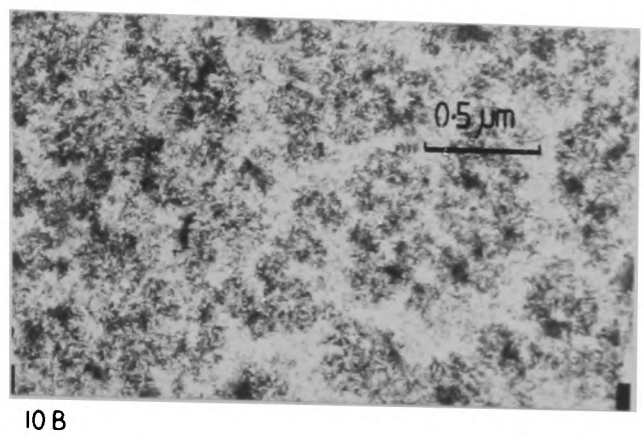

10 B

11A Cr_5O_{12}

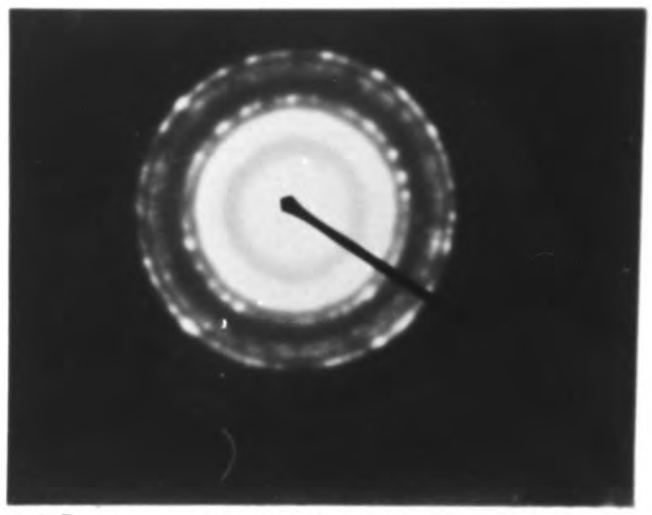

11B $5SnO.2H_2O$

11C Cr_3O_4

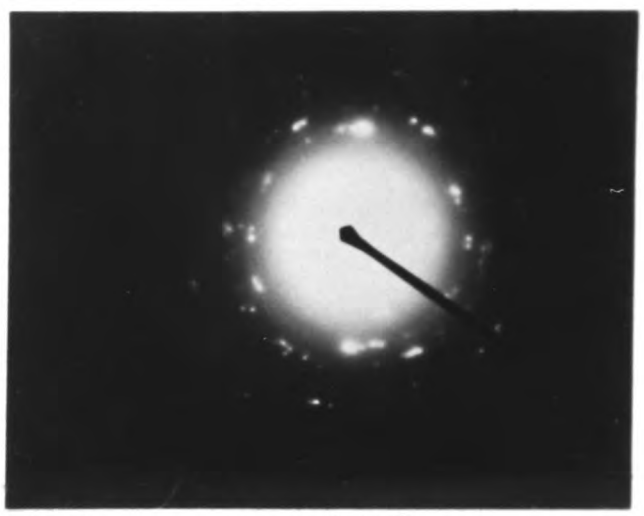

11D $Sn_6O_4(OH)_4$

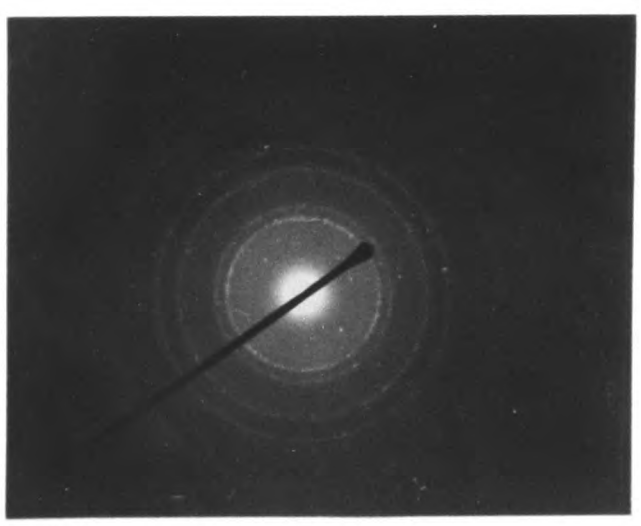

11E CrO_2

11F Cr^{o}

TABLE 1

Selected Area Electron Diffraction

Data from Unpassivated Tinplate

Calculated d spacings (Å)	ASTM X-ray powder diffraction data d(Å)	hkl	Sample
3.17	3.12	112	
2.76	2.78	004	
1.94	1.99	024	SnO
1.65	1.66	116	orthorhombic
1.59	1.61	133	
1.26	1.25	400	
1.07	1.09	-	
2.45	2.47	200	
1.76	1.74	220	SnO_2
1.41	1.42	222	cubic
1.13	1.13	331	
3.02	2.99	101	
2.40	2.42	002	
2.11	2.04	102	SnO
1.62	1.60	211	tetragonal
1.30	1.34		
3.34	3.35	110	
2.36	2.37	200	
2.04	2.12	210	
1.79	1.77	211	SnO_2
1.44	1.44	112	tetragonal
1.34	1.32	202	
1.17	1.12	330	
0.98	0.95	402	
0.90	0.91	332	

with some straight edges but with otherwise undefined shape; they are found in clusters, spreading over some 10^3 μm^2 but with these clusters separated by several hundred μm. They are shown in figure 3d.

Filaments of cubic SnO_2 (figure 3e) were also found to be a constituent of the oxide layer. As with the orthorhombic SnO, they are thinly dispersed and are found on both stoved and unstoved tinplate.

Calculated d spacings and the corresponding ASTM X-ray powder diffraction data are given in table 1 with typical SADP's given in figure 4.

Tetragonal SnO therefore has the highest areal coverage on unpassivated tinplate. In some regions the diffraction pattern is faint and diffuse indicating microcrystalline or amorphous oxides. The other oxides of tin are widely dispersed over the surface and occupy 1-5% of the total surface area. It is not possible to determine whether the large crystals of SnO and SnO_2 are lying on top or within the "background" layer of weakly-diffracting oxide. Since the tetragonal SnO_2 is sometimes found to merge into the background without clearly defined edges to the diffracting regions it is likely that this oxide at least is coplanar with the background oxide layer and is therefore probably in contact with the metallic tin surface in the passivated tinplate.

The topography of the tin surface as replicated by the TEM specimen can be seen to be smooth and flat on a sub-micron scale as expected from a flow-brightened tinplate.

3.1.2 300 tinplate

The type 300 tinplate has been passivated by a dipping process; it has been shown to possess an oxidised chromium component (Leroy et al. 1976, Azzeri et al. 1982) and have a thicker oxide coat than 311 types (this work) but is not expected to contain metallic

TABLE 2

Selected Area Electron Diffraction

Data for 300 Tinplate

calculated d spacings (Å)	ASTM X-ray powder diffraction data d(Å)	hk1	Sample
2.93	2.95	220	
1.71	1.71	422	
1.45	1.48	440	CrO_x
1.10	1.09	731,553	cubic
0.85	0.81	951,773	
3.18	3.12	112	
2.76	2.78	004	
1.94	1.99	024	SnO
1.67	1.68	223	orthorhombic
1.59	1.61	133	
1.26	1.25	400	
2.47	2.47	200	
1.81	1.81	220	SnO_2
1.09	1.10	400	cubic

chromium since the passivation conditions are inappropriate for Cr^{o} deposition (Azzeri et al. 1982).

A typical micrograph of stripped, unstoved passivation layer (with a carbon coating) is shown in figure 5a. It exhibits a similar granularity to the film from unpassivated tinplate but produces only weak and diffuse diffraction rings which could be consistent with several tin oxides. Albu-Yaron and Smith (1979, 1980) interpreted such diffuse rings as intermediate oxides between SnO and SnO_2 but this broadening may be due to microcrystalline oxide. Stoving the tinplate for ten minutes does not alter the appearance of this layer as it does for the unpassivated plate; a micrograph of a stoved passivation layer (10 minutes at $200^{o}C$) is shown in figure 5b where the specimen has broken, revealing the carbon film which is featureless at this magnification and the granular passivation layer. Several small regions within the field of view give strong single crystal diffraction patterns which are identified as orthorhombic SnO. Cubic SnO_2 is also detected (figure 5c) as filamentary growths. Diffracting chromium compounds are widely dispersed over the specimen, covering less than 5% of the surface area. Comparison with the ASTM X-ray data identified the chromium as present in the cubic oxide CrO_x. Further identification was not possible owing to the original ASTM standard being contaminated with CrOOH but the calculated d spacings are also similar to those of Cr_3O_4.

Angular replicated shapes ranging in size from 0.1 μm to 2 μm were frequently observed. They are replicas of features on the tin surface such as protruding $FeSn_2$ crystallites and are not likely to be the replicated shapes of passivation layer constituents (such as chromium oxide crystals) which have been lost in specimen preparation since the passivation layer and carbon layer are unbroken

at these points. Examples of the replicated shapes are given in figure 5e.

Diffraction data for the 300 passivation layer are given in table 2 and the diffraction pattern for CrO_x shown in figure 5f.

3.1.3 British Steel 311 (BS 311)

Type 311 tinplate from three different batches has been examined to investigate the variability in production processes. Each batch possessed good adhesion properties with epoxy-phenolic lacquer as measured by the "Scotch Tape test" and the butt-joint test. The batches investigated were:

a) BS 311 (c) as used for XPS and mechanical testing in the BS/KS/NS comparative set.

b) BS 311 (6A)

c) BS 311 (5A)

3.1.3a BS 311 (c)

The stripped passivation layers from unstoved tinplate possess a uniform find-grained background structure within which are discrete crystals, some of which have regular facetted shapes whilst others are irregular or have unclearly defined edges. The background generally diffracts weakly but in some areas produces a strong single- or polycrystal diffraction pattern from orthorhombic SnO. Figure 6a, a micrograph of tinplate stoved for 10 minutes at 200°C, shows the weakly diffracting background and a strongly-diffracting crystal 0.5 μm in width identified as $Sn_6O_4(OH)_4$. Distinct outcroppings of orthorhombic SnO are shown in figure 6b; these crystals are considerably thicker than the background layer. Tetragonal SnO_2 is found in clusters of small crystals, each some 0.1 μm in diameter (figure 6c). Tetragonal SnO is also present but in much smaller quantities than the other tin oxides and is shown in figure 6d.

TABLE 3

Selected Area Electron Diffraction

Data for BS311(C)tinplate

calculated d spacings (Å)	ASTM X-ray powder diffraction data d(Å)	hkl	Sample
3.25	3.26	211	
2.99	2.96	022	
1.98	1.97	400	$Sn_6O_4(OH)_4$
1.71	1.73	421	tetragonal
1.42	1.41	206	
1.40	1.40	440	
1.16			
3.14	3.11	110	
2.42	2.42	101	
1.49	1.46	002	CrO_2
1.41	1.40	310	tetragonal
1.11	1.10	400	
0.82	0.82	422	
3.31	3.35	110	
	2.64	101	
2.37	2.37	200	
2.02	2.12	210	
1.74	1.77	211	SnO_2
1.41	1.42	112	tetragonal
1.29	1.32	202	
1.15	1.16	222	
1.10	1.12	330	
0.95	0.95	402	
3.58	3.58	111	
3.13	3.12	112	
2.45	2.50	200	
2.22	2.25	023	SnO
1.83	1.86	204	orthorhombic
1.79	1.77	130	
1.27	1.25	400	

No metallic chromium was detected and the only chromium oxide found on BS 311 (c) was tetragonal CrO_2 in the form of crystal groupings covering a few hundred μm^2 with each CrO_2 crystal being approximately 0.1 μm wide. Crystals of tetragonal CrO_2 are shown in figure 6e.

On stoving in air, no change was visible in the morphology or distribution of crystals within the passivation layer with the exception of the filamentary growth of tetragonal SnO_2 which, on stoving for 60 minutes at 200°C, produced long crystalline strands up to 5 μm in length. One such filament is shown in figure 6f.

Using the gold support grid technique, uncoated passivation layers could be examined but due to the weakness of the film only small areas could usually be obtained for inspection. The broken edges of an unstoved passivation layer are shown in figure 6g where, at high magnification, a double layer structure is clearly visible. The diffraction patterns from these layers are too weak and diffuse for analysis but the granularity is clearly visible. Both layers may be tin oxide or a mixture of tin and chromium oxides but the electron transmission values are different for each as seen by the contrast in the micrograph which can be interpreted as either different thicknesses or different chemical compositions with perhaps one layer as tin oxide and the other as a chromium rich layer deposited by the passivation treatment.

Diffraction data for BS 311 (c) samples are given in table 3.

3.1.3b BS 311 (6A)

TEM examination reveals the passivation layer to consist of a uniform, continuous coating which gives a weak diffraction pattern which is probably tin oxide. Granularity is not affected by stoving up to 60 minutes at 200°C. This weakly-diffracting layer is shown

TABLE 4

Selected Area Electron Diffraction

Data for BS311(6A)tinplate

calculated d spacings (Å)	ASTM X-ray powder diffraction data d(Å)	hkl	Sample
3.00	3.11	110	
2.13	2.13	111	
1.94	1.98	210	
1.65	1.63	211	
1.37	1.40	310	CrO_2
1.13	1.13	321	tetragonal
0.88	0.88	402	
0.86	0.87	213	
0.79	0.79	521	
3.12	3.12	112	
3.00	2.86	020	
1.79	1.77	130	SnO
1.13	1.14		orthorhombic
0.83			
2.45	2.47	200	SnO_2
1.74	1.74	220	orthorhombic
2.29	2.30	200	
2.08	2.05	210	
1.55	1.61	220	Cr^o
1.37	1.39	311	cubic
1.22	1.23	321	
1.09	1.02	420	
0.89	0.91	500	

in figure 7a in which can also be seen facetted shapes replicated from the tin surface. Groups of such shapes are present on less than 10% of the specimen and are seen on all type 311 and 300 tinplate samples. One example of a crystal found in the passivation layer, shown in figure 7b, vapourised under the electron beam in a few seconds to leave a facetted replica and residual material (figure 7c) which was identified by its diffraction pattern as metallic chromium, Cr^{o} and probably $Cr(OH)_3$. The unevaporated form degraded too rapidly for diffraction analysis but it seems likely that it was a hydrated form of chromium oxide or chromium hydroxide.

The appearance of the remaining features is unlike the replicated shapes seen in figure 7a which have no internal material and the two are considered to be different phenomena. This identification of Cr^{o} is extremely rare. However, Albu-Yaron and Smith (1979) have identified large hexagonal crystals as metallic chromium and several identical crystals have been located in this work but could not be analysed as they were too thick to form diffraction patterns. One such crystal is shown in figure 7d and despite the lack of diffraction evidence to confirm their composition they must be considered as potential sources of the "missing" Cr^{o} which is detected by XPS but not by electron diffraction in this work.

The only other chromium oxide detected on this type of passivation layer was tetragonal CrO_2, found in clusters of sub-micron grains (figure 7e).

Tin oxides identified by diffraction were filaments of cubic SnO_2 (figure 7f) detected only from tinplate samples which had been stoved for 60 minutes or longer at $200^{o}C$ and orthorhombic SnO found in platelets (shown in figure 7g).

Diffraction data for BS 311 (6A) are given in table 4.

3.1.3c BS 311 (5A)

As with the passivation layers described above, most of the specimen area is weakly diffracting with isolated or grouped crystals of tin oxides and chromium oxides.

Cubic SnO_2 is present on stoved samples but in the form of rosette-shaped growths as well as the filamentary growth seen earlier. The two types are shown in figures 8a and 8b respectively. One hydrated form of tin oxide and one tin oxide hydroxide have also been detected. The hydrated form ($5SnO.2H_2O$) is shown in figure 8c where it is seen to be distributed in a "fluffy" covering over areas of several hundred μm^2; $Sn_4O_6(OH)_4$ is found as isolated crystals (figure 8d).

Tetragonal SnO and orthorhombic SnO are shown in figure 8e where the former is in the form of dark single crystals 0.05 μm or less in size, mixed amongst larger platelets of orthorhombic SnO.

Neither Cr^o nor chromium oxides could be detected by electron diffraction on this type of passivation layer.

Diffraction data are given in table 5.

3.1.4 Nippon Steel 311 (NS 311) tinplate

Passivation layers were removed from NS 311 tinplate which possessed adhesion properties worse than the BS 311 types. The weakly-diffracting coating which covers all the specimen surface is shown in figure 9a. The granularity of this coating is unaffected by stoving at 200°C for periods up to 30 minutes; no examination was made of samples stoved for longer times. Single crystals of tetragonal SnO are visible within the passivation layer (figure 9b) on samples which have been stoved for 10 minutes at 200°C. The only chromium oxide found was tetragonal Cr_3O_4 in the form of poly-

TABLE 5

Selected Area Electron Diffraction

Data for BS311(5A) tinplate

calculated d spacings (Å)	ASTM X-ray powder diffraction data d(Å)	hk1	Sample
2.98	2.99	101	
1.47	1.48	103	SnO tetragonal
1.11	1.10	114	
2.78	2.78	004	
1.90	1.89	220	SnO orthorhombic
1.69	1.68	223	
1.45	1.43	040	
4.57	4.60		
2.87	2.82		
2.44	2.42		
2.03	2.00	not indexed	$5SnO \cdot 2H_2O$
1.68	1.67		
1.57	1.57		
1.44	1.43		
1.24	1.24		
4.53	4.49	002	
2.48	2.48	310	$Sn_6O_4(OH)_4$ tetragonal
2.6	2.26	004	
1.67	1.68	314	
1.09	-	-	
2.78	2.84	111	
2.47	2.47	200	
1.74	1.74	220	SnO_2 cubic
1.48	1.48	311	
1.42	1.42	222	
1.23	1.23	400	
1.12	1.10	420	

TABLE 6

Selected Area Electron Diffraction

Data for Nippon Steel (NS)311 tinplate

calculated d spacings (Å)	ASTM X-ray powder diffraction data d(Å)	hk1	Sample
3.00	2.99	101	
1.80	1.80	122	
1.57	1.60	211	SnO
1.52	1.49	202	tetragonal
1.15	1.13	104	
0.88	0.88	323	
0.85	0.85	314/420	
2.59	2.58	131	
2.28	2.34	113	
1.63	1.66	151	Cr_3O_4
1.58	1.59	333	tetragonal
1.40	1.43	404	
1.33	1.35	602	
1.29	1.29	262	

TABLE 7

Selected Area Electron Diffraction

Data for Kawasaki Steel (KS)311 tinplate

calculated d spacings (Å)	ASTM X-ray powder diffraction data d(Å)	hk1	Sample
3.37	3.35	110	
2.67	2.64	101	
2.13	2.12	210	
1.80	1.76	211	SnO_2
1.24	1.22	321	tetragonal
1.41	1.42	301	
1.24	1.22	321	
1.03	1.04	103	
4.03	4.08	002	
3.12	3.13	221	Cr_5O_{12}
2.10	2.12	223	
1.69	-	-	

crystalline clusters (figure 9c).

Diffraction data are given in table 6.

3.1.5 Kawasaki Steel (KS 311) tinplate

This tinplate has exhibited consistently poor properties of adhesion. Crystals of tetragonal SnO_2 are found scattered widely over the specimen; they are found as sub-micron platelets and are shown in figure 10a. The areas surrounding these platelets give only weak, diffuse diffraction patterns and are considered to be tin oxide. Chromium is detected in the form of orthorhombic Cr_5O_{12}, seen in figure 10b as large areas of granular deposits.

Diffraction data are given in table 10.

Typical diffraction patterns from all the specimen types are shown in figure 11.

4. DISCUSSION

Stripped passivation layers from tinplate samples have been successfully used to identify crystalline deposits found within the passivation layer. Most frequently encountered are oxides and hydrated oxides of tin, and chromium oxides; metallic chromium has been identified once with indirect evidence for further Cr^o crystals, especially in the BS 311 samples. Previously, other workers (Saijo et al 1976, Takano and Watanabe 1980), Albu-Yaron and Smith 1979, 1980) have used TEM to characterise tinplate passivation layers and, in some cases, infer a relationship with lacquer adhesion. It is certainly possible to distinguish different tinplate types by electron diffraction data as summarised in tables 1-7. but the area coverage of chromium species identified in this way (<2%) is much lower than the values obtained from the XPS work (typically > 10%) and by other workers who have used electrochemical techniques

(Servais et al 1979, Coad et al 1976). A further examination of a stripped, uncoated passivation layer as shown in figure 6g was made using energy-dispersive X-ray analysis (EDX). This technique can measure elemental abundances in a sample using the X-ray emission which is a consequence of electron bombardment (see Appendix 2). Only X-rays from elements heavier than Ne can normally be detected so data for oxygen are not available. The EDX spectrum is shown in figure 12 where peaks due to Sn and Cr are visible. (The Fe and Cu peaks are from the microscope and support grid).

For thin film analysis using EDX in a 100 kV microscope the normally complex methods for quantifying results may be bypassed as atomic number effects become of secondary importance and for a binary system AB, the relative atomic concentrations, C, may be directly measured from the peak intensities of A and B (I_A and I_B):

$$\frac{C_A}{C_B} = k.\frac{I_A}{I_B}$$

where k is a constant (Goldstein et al 1981)

Hence, from figure 12, $C_{Sn}:C_{Cr} \leq 2.1$ which is a much better agreement with the XPS results than estimated from TEM. The TEM data are then measuring discrete diffracting crystals in the passivation layer but missing a significant proportion of chromium, either oxidised or metallic, which is present and which does not strongly diffract. Most of the specimen area in the extraction replica yields a weak, diffuse diffraction ring which has been mentioned earlier and is visible on some of the diffraction patterns in figures 4 and 11. An analysis of such rings has been attempted and the data are given in table 8. These data are from rings where an estimate of their radii can be made by measuring the brightest point in the

Figure 12. An energy-dispersive X-ray spectrum from a stripped passivation layer.

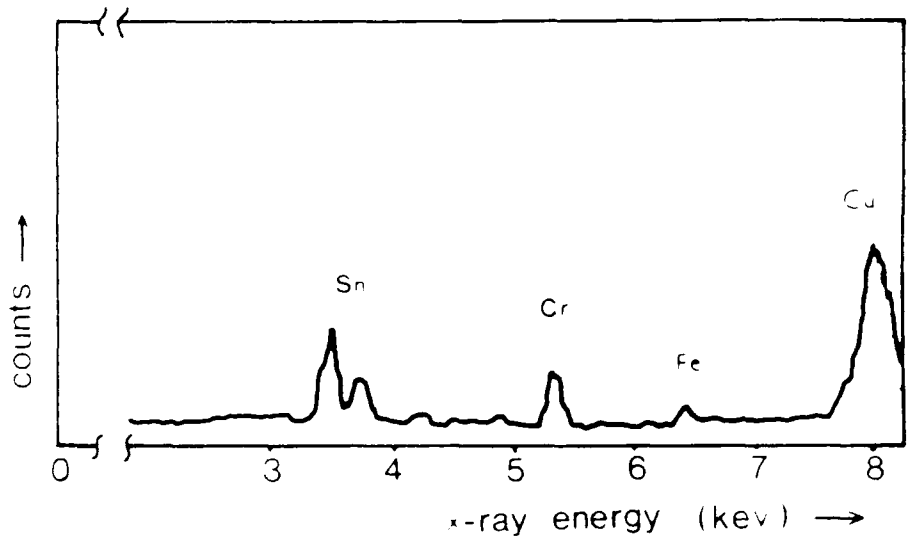

N.B. The Fe and Cu peaks are artifacts due to contributions from the support grid and the microscope.

TABLE 8

Electron Diffraction Data

weakly-diffracting areas (Å)(±0.1Å)

(figures in parentheses are attributed to the carbon film)

Sample	BS311	BS311(6A)	KS311	NS311	300	NP	Carbon film
	(1.96)	(1.92)	2.51	(3.33)	4.54	2.63	3.4
	(1.12)	1.67	2.63	1.96	3.57	2.78	1.93
	(1.11)	2.50	2.08	1.96	(3.45)		1.07
	0.91	0.90	2.17	1.43	1.54		
	(1.11)	3.31	2.22	1.37	2.08		
	(2.02)	(1.90)	(1.18)	(1.92)	1.26		
	(1.07)	(1.07)	1.23	(1.22)	0.83		
	(1.93)	(1.93)	1.12				
	(1.10)	(1.09)	(1.11)				
			2.50				
			(1.96)				
	2.34		(1.10)				
	2.10		3.03				
	(1.15)		2.52				
	2.41		(1.05)				
	(1.1)						

c.f. d spacings of graphite (below) and ASTM X-ray data in Appendix 3

002	3.354	103	1.543
100	2.131	110	1.231
101	2.031	112	1.155
102	1.799	006	1.118
004	1.677		

width of an individual ring. Even more diffuse diffraction rings can be seen but these could not be measured with sufficient accuracy for analysis.

The rings due to carbon can be eliminated by using calculated d values from long-exposure diffraction patterns from isolated carbon films but a definite identification from the remaining data is not possible. However, the remaining diffraction rings can be attributed to the passivation layer and correspond to several tin oxides or chromium in metallic and oxidised forms. It is therefore probable that some of these diffuse rings are produced by micro-crystalline Cr^{o}.

Further evidence for a continuous chromium rich layer is seen when comparing the effects of stoving on passivated and unpassivated tinplates; the latter undergo a coarsening of the passivation film structure on stoving whilst the former are unaffected. Widely-spaced discrete crystals are unlikely to offer this type of protection whilst a continuous passivation layer would shield the tin and tin oxide from further oxidation. Servais et al (1979) suggest that a tin oxide layer forms beneath the passivation layer during lacquer stoving and that this may be responsible for a weakening in the lacquer adhesion. They do not identify the oxide type as their experimental results were obtained using XPS, but Takano and Watanabe (1980), using electrochemical techniques and TEM, do associate poor lacquer adhesion (in the peel test) with tinplates on which tetragonal SnO and SnO_2 crystallize during stoving. Tinplate on which only ortho-rhombic SnO grows was found to have good lacquer adhesion properties. Their results are only for tinplates which have been stoved for longer times than commercial stoving times, since they could not identify any crystalline tin oxide on unstoved passivation tinplate and report

diffuse diffraction patterns as seen in this work. The crystal morphologies of the tin oxides found by Takano and Watanabe are very similar to those reported here but the former show larger crystals which are probably due to the longer stoving times and growth from a microcrystalline tin oxide layer. In a study of the oxidation of pure tin (Boggs et al 1961a, 1961b) demonstrate that oxidation begins at growth centres on the metal surface and spreads out, forming spines and then platelets which eventually coalesce. Their electron microscopy finds no evidence for an amorphous or microcrystalline oxide layer although this has been reported (Hart 1952). The passivation treatment, however, alters the tin oxide layer as well as depositing a chromium rich film and may well favour the formation of a microcrystalline oxide; in the first stages of passivation there is a reduction of some or all of the oxide already present on the tinplate surface (Soepenberg et al 1976, Aubrun and Rocquet 1975) before chromium deposition begins.

On the basis of the diffraction data given in tables 1-7 it is seen that orthorhombic SnO is found only on the tinplates with generally good adhesion properties (i.e. BS 311 (c); BS 311(6A) corresponds to BS 311 (A) in the mechanical adhesion tests, 300, and NP). Tetragonal SnO is found on both categories as are SnO_2 and hydrated tin oxides. The more complex oxides of chromium Cr_3O_4 and Cr_5O_{12} are found on the NS and KS tinplates (with poor adhesion) whilst the only evidence of metallic chromium was found on BS 311(6A). Takano and Watanabe (1980) associate orthorhombic SnO with good adhesion which seems to be borne out by the work presented here.

It has already been stated that the strongly-diffracting crystals of tin oxides and chromium oxides are found on a small percentage of the tinplate surface. Since this and other work can

correlate certain of these oxides with the adhesion properties of the tinplate it must be asked whether these dispersed crystals are themselves responsible or whether they are just large growths from the unidentified oxide coating which covers most of the surface as most of a lacquer coating would be in contact with the background layer which cannot be characterised by TEM and which is probably the main factor in determining lacquer adhesion. If the large identifiable crystals were to control the adhesion then they might be assumed to act as stress-raisers at the lacquer-passivation layer interface but they do not stand proud of the passivation layer or become easily detached (as this would have been observed in the TEM specimens). Such an explanation is therefore unlikely.

Conventional TEM cannot easily distinguish a truly amorphous phase from a microcrystalline one so the larger tin oxide crystals may be exceptional growths of, typically orthorhombic SnO surrounded by the same oxide in microcrystalline form. The fact that these areas give weak diffraction rings would suggest this. Indeed, certain of the diffracting tin oxides (e.g. figure 5d) appear to blend in with the weakly-diffracting background. The measurements made by TEM then become representative of the specimen surface as a whole.

The mechanism of chromium deposition during the passivation treatment has been studied by other workers (Aubrun and Rocquet 1975) and will be reviewed in the Discussion chapter when the passivation layer structure is assessed.

Bibliography

Albu-Yaron, A. and Smith D.A. Br. Corr. J. 14 No. 3 (1979) 133.

Albu-Yaron, A. and Smith, D.A. Proc. 2nd Intl. Tinplate Conf. London (1980) ITRI.

Andrews K.W., Dyson D.J. and Keown, S.R. "Interpretation of Electron Diffraction Patterns" 2nd ed. (1971) Hilger London.

Aubrun Ph. and Rocquet P. J. Electrochem. Soc. 112 No. 7 (1975) 861.

Azzeri N. Splendorini L. Barristoni C. Paparazzo E. Surface Techn. 15 (1982) 255.

Boggs, W.E., Kachik R.H. and Pellissier G.E. J. Electrochem Soc. 13 (Jan. 1961) 6.

Boggs, W.E., Trozzo P.S. and Pellissier G.E. J. Electrochem Soc. 13 (Jan 1961) 20.

Bradley D.E. Br. J. Appl. Phys. 5 (1964) 65.

Britton S.C. and Bright K. Metallurgia 56 (1957) 163.

Coad J., Mott B., Harden G. and Walpole J. Br. Corr. J. 10 (1975) 85.

Edgington J.W. "The Operation and Calibration of the Electron Microscope" (1974) Macmillan, London.

Glauert A.M. "Practical Methods in Electron Microscopy" Vol. 1 (1972), North Holland, London.

Goldstein J.I., Newbury, D.E., Echlin, P.E., Joy, D.C., Fiori C. and Lifshin E. "Scanning Electron Microscopy and X-ray microanalysis" (1981) Plenum, New York.

Hart R.K. Proc. Roy. Soc. 65B (1952) 955.

Hirsch P.B., Howie, A., Nicholson R.B., Pashley D.W. and Whelan M.J. "Electron Microscopy of thin Crystals" (1965) Butterworths, London.

ITRI (International Tin Research Institute) personal communication (1984) Dr. D. Bearfield.

Leroy V., Servais J.P., Habraken L., Renard L. and Lempereur J. Proc. 1st Intl. Tinplate Conf. (1976) 399 ITRI, London.

Nagel Soepenberg E. Vrijburg H.G. and Spruyt A.C. Proc. 1st Intl. Tinplate Conf. (1976) 24 ITRI, London.

Neish R.A. and Donelson J.G. Food Techn. 14 (1960) 37.

Saijo K., Yoshioka O., Oyama T. Tech. Rep. Toyo Kohan Co. Ltd. 23 (1976) 17.

Servais J.P., Lempereur J., Renard L., Leroy V. Br. Corr. J. 14 No. 3 (1979) 126.

Takano H. and Watanabe T. Proc. 2nd Intl. Tinplate Conf. (1980) 1 ITRI, London.

CHAPTER 6

DISCUSSION

The results in Chapters 3-5 have shown that there are distinct differences in the fracture behaviour of lacquered tinplates and complementary differences in the composition of the passivation layers.

Let us first consider the structure of the passivation film:

1 Passivation layer structure and composition

Information about the passivation layer has been derived in this work from transmission electron microscopy and X-ray photoelectron spectroscopy. These experimental results will be considered against other published works.

i/ Chromium in the passivation layer

This work has detected metallic chromium and some oxidised and hydrated oxidised forms by XPS. Earlier works using this technique have reported the oxidised form to be Cr^{3+} as Cr_2O_3 and $Cr(OH)_3.nH_2O$ (Leroy et al 1976, Saijo et al 1976, Coad et al 1976, Servais et al 1979, Maeda et al 1980, Azzeri et al 1982); Leroy et al also detected Cr^{6+}. No mention has been made in the literature of other crystal forms or other possible chromium valencies which is probably due to the many earlier electrochemical experiments in which the trivalent oxidised form is assumed to be stable and to the fact that Cr^0 oxidises only to Cr_2O_3 in air (Gulbransen and Hickman 1947). TEM work (Chapter 5) has shown that other crystal forms (Cr_3O_4, Cr_5O_{12}) are present in some passivation layers as well as, in one tinplate type, CrO_2 (with a valency of 4). The shapes of the chromium oxide crystals were equally varied: angular crystal groupings of Cr_3O_4 on NS 311,

granular areas of Cr_5O_{12} on KS 311 and granular CrO_2 on BS 311. In XPS, Cr^{6+} can be identified with confidence since it has a significantly higher binding energy than Cr^0, Cr^{3+} or Cr^{4+} but the Cr 2p 3/2 peak binding energy due to CrO_2 (measured as 576.1eV (Rao et al 1979) could not possibly be separated from the Cr_2O_3 (Cr^{3+}) peak in a signal from a passivated tinplate by the spectrometer resolution available in this work nor from the resolution available to Azzeri et al (1982) or Leroy et al (1976). (Other workers did not publish the linewidths of their analysing radiation). Further difficulties arise in distinguishing Cr^{3+} (Cr_2O_3) from Cr^{4+} (CrO_2) because measured binding energies can vary from spectrometer to spectrometer (as shown in Table 1, Chapter 4). The other chromium oxides detected using TEM are mixed valency oxides such as Cr_2O_5 which has a mixture of Cr^{3+} and Cr^{6+} in the ratio 2:1. The Cr 2p 3/2 spectrum from Cr_2O_5 (Tsutsumi et al 1981) and CrO_2 are shown in Figure 1 where the peak centroids are superimposed on a typical Cr 2p 3/2 spectrum from a 311 passivation layer; this demonstrates the difficulty of distinguishing Cr^{3+} from Cr^{4+}. Electrochemical evidence for Cr^{3+} is based on the use of Faraday's Law to equate charge passed with chromium valency but 100% current efficiency is never achieved and the estimation of oxide composition in this way is uncertain (Britton 1975b). Thus, the exclusive presence of Cr^{3+} in the form Cr_2O_3 in the passivation layer must be open to doubt since it is not detected in this work by TEM whilst other chromium oxides are. However, Albu-Yaron and Smith (1979) have identified Cr_2O_3 using a very similar method of specimen preparation to that used here but analysing a different tinplate sample. It is clear from this work that different chromium oxides are found on different tinplates and that the oxides formed in air on chromium metal are

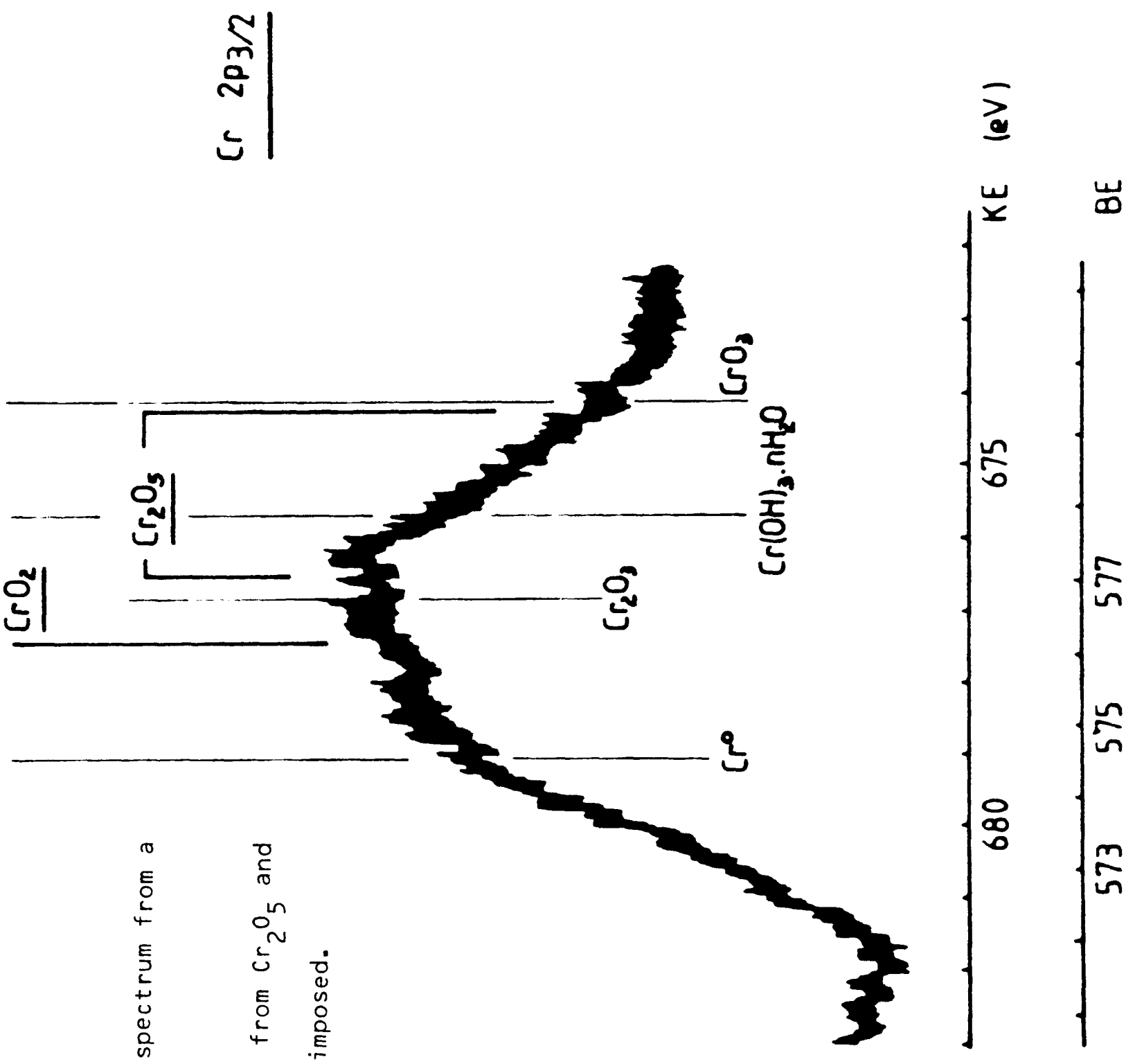

Figure 1. Cr 2p 3/2 XPS spectrum from a 311 tinplate.

Peak centroids from Cr_2O_5 and CrO_2 are superimposed.

likely to be quite different from those found in the passivation treatment of tinplate which takes place in an aqueous environment at a negative applied potential and very rapidly (within one second). TEM identifies only those crystals which formed a strong diffraction pattern which in fact comprised about 2% of the surface area of the specimens; XPS results determine total chromium areal coverages of 18% for BS 311 and about 10% for NS 311 and KS 311 samples. The difference can be readily accounted for by the presence of micro-crystalline or amorphous chromium, either in metallic, oxidised or hydrated oxidised forms, seen in TEM as a weakly diffracting thin layer around the diffracting crystals and which produces a chromium signal when examined with energy-dispersive X-ray analysis. It is mainly this layer which produces the signal for XPS. Information about the lateral distribution of chemical species within this layer is not available since XPS derives its information from an area of several mm^2. No hydrated chromium oxides were found by TEM but were identified by XPS. Since over 100 TEM specimens were observed it is likely that these are present in the weakly-diffracting layer (which is assumed to be amorphous or microcrystalline). The structure of this thin film through its thickness can be inferred from XPS via Ar ion etching. There is hydrated chromium oxide on the outside surface as proposed by several other workers but examination of the layer from the underside suggests that hydrated oxide is in fact present throughout the depth of the film. The apparent depletion of hydrated chromium oxide on the outer surface after short Ar ion etching times may be in part due to reduction or dehydration caused by the ion beam.

The chromium oxides present cannot be positively identified using XPS as explained earlier but TEM has detected different oxides on different tinplates. BS 311 was found to contain CrO_2 and

possibly $Cr(OH)_3$; NS 311 and KS 311 contained Cr_3O_4 and Cr_5O_{12} respectively. The chromium oxide detected on BS 300 could not be assigned a chemical formula because the ASTM sample with which it corresponds had not been positively identified. Metallic chromium was only detected using TEM on BS 311 and then only on one specimen, however, some crystals very similar in appearance to the Cr^0 seen by Albu-Yaron and Smith (1979) were observed on BS 311 but they could not be identified in this work. A model for passivation layer structure has been proposed by Saijo et al (1976) which is shown in Figure 1, Chapter 4. A layered structure of chromium metal and oxides is suggested by them, based on XPS and TEM measurements. In this work diffracting crystals have produced only single crystal or polycrystal patterns from one type of structure per visible crystal and if they comprise a layered structured, one or more must be non-diffracting. It seems likely that the layering suggested by Saijo and supported by the XPS results here is present in the thin layer and not necessarily in the large diffracting crystals. The arrangement of this layering is probably similar to the Saijo et al model. As Ar ion etching progresses, the XPS signal from Cr^0 increases and this is usually taken to indicate an increasing Cr^0 concentration with depth into the passivation layer. The increase in metallic chromium will be in part due to reduction of oxides by the ion beam but examination of the underside of isolated passivation layers in this study does reveal a higher Cr^0 concentration near the tin surface for KS 311 tinplates. Ion etching profiles through BS 311 passivation layers on tinplate produced similar relative distributions of Cr^0 to those seen on KS 311 (although more Cr^0 was always seen in BS 311) but no such concentration gradient was detected from a measurement of a stripped passivation layer from BS 311. However, this observation

was complicated by the presence of metallic tin residues which attenuated the Cr^0 signal. It is not certain in this case whether metallic chromium is concentrated near the tin surface or not but ion etching from the outer surface would suggest that it is.

Cr^{6+} was detected only on KS 311 samples and on one sample of a BS tinplate (311) with poor adhesion as defined by the Scotch Tape test. Since CrO_3 is soluble in water the Cr^{6+} is unlikely to be present in this form and is more probably combined in a mixed-valence oxide such as those seen in TEM.

Diffracting crystals of chromium and chromium oxides are likely to be lying on top of the thin layer in most cases and sometimes appear to be associated with an underlying crack in the film.

No metallic chromium was detected on BS 300 tinplates as expected. From XPS it is seen that a hydrated layer is present on the outer surface which is removed by an Ar ion etch of less than one minute. The valency of the chromium oxide was Cr^{3+} (or Cr^{4+}).

ii/ Tin oxide

XPS was unable to distinguish SnO from SnO_2 but could estimate the thickness. The tin oxides on all 311 tinplates were removed by a one minute Ar ion etch, indicating a thickness of $\leqq$ 1nm; the oxide on BS 300 was found to be some 5 times thicker.

TEM micrographs show that the diffracting crystals are thicker than the surrounding passivation layer; some are discrete crystals which appear to rest on top of the thin passivation layer whilst others have no clearly defined edges and merge into the thin layer and so are likely to have been in intimate contact with the tin.

The tin oxide components of the passivation layer were found to consist of SnO and SnO_2 in several crystal structures. Unpassivated tinplate contained SnO in both orthorhombic and tetragonal forms,

the former usually as a polycrystalline layer and the latter as discrete single crystals, ranging in size up to about 0.5μm. Orthorhombic SnO was detected as crystals, some 1μm in diameter occurring in clusters. Cubic SnO_2 was present as filamentary growths, often several μm in length on both stoved and unstoved samples but over 95% of the stripped oxide film from unpassivated tinplate produced only diffuse diffraction rings which could not be analysed. Diffracting tin oxides found on passivated tinplate samples were widely dispersed; orthorhombic SnO was found only on the BS and unpassivated tinplates. Other work has associated this type of tin oxide with tinplates possessing good adhesion (Takano and Watanabe 1980). Cubic SnO_2 filaments were found to grow on BS 311 tinplates during stoving at 200°C for up to one hour but were not found on either KS 311 or NS 311. Other tin oxides identified on BS 311 were tetragonal SnO_2 and tetragonal SnO, both as small, sub-micron crystals, 5 $SnO.2H_2O$ and $Sn_6O_4(OH)_4$ as "fluffy" outcroppings. Hydrated tin oxides were not found on KS 311 or NS 311 tinplates. The only tin oxide detected on KS 311 was tetragonal SnO_2, seen as widely-dispersed sub-micron platelets; NS 311 contained tetragonal SnO as small single crystals.

Thus, the passivation layer is seen to comprise a series of separate single- or polycrystals set within or on top of a weakly-diffracting microcrystalline layer which probably contains chromium in metallic, oxidised and hydrated oxidised form. The large cyrstals occupy less than 5% of the total surface area of the passivation layer and are detected by TEM. XPS reveals information about the total area of passivation film and a combined approach using these two techniques can reduce the ambiguities of interpretation inherent in each. Deductions may also be made about the structure of the passivation layer from a study of the mechanisms of formation which will

aid interpretation of the experimental results.

iii/ Mechanism of Formation

The mechanism of passivation layer deposition has been studied elsewhere (Carter 1961, Aubrun and Rocquet 1975, Nagel Soepenberg et al 1976) and proposed to be a multi-stage process. The typical conditions for tinplate passivation as used commercially are shown in Table 1. In the cathodic dichromate (311) treatment of tinplate, Aubrun and Rocquet propose the following successive reactions:

i. formation of a chromium oxide primary film

ii. reduction of tin oxides and strengthening of the primary film

iii. formation of a secondary chromium oxide film

iv. alteration of films and hydrogen evolution

v. hydrogen evolution, deposition of chromium in metallic and oxidised forms.

When first reported (Rocquet and Aubrun 1968) the existence of Cr^0 in the passivation layer was doubted (Becker 1970) since the conditions for chromium plating require a catalyst for the metal to be deposited and this is absent in tinplate passivation but its deposition has been explained by the high hydrogen over voltage on tin (Aubrun and Rocquet 1975). Nagel Soepenberg et al report a three stage process:

1/ incubation phase in which tin oxides are reduced

2/ exponential increase in surface chromium (possibly Cr^0 according to them) comparable with chemisorption rates ($\sim$ 5 monolayer thickness)

3/ further increase in chromium deposition consistent with diffusion through a porous layer.

It is seen that the passivation treatment affects the tin oxide layer which is formed during and after flow-brightening. The cathodic conditions will reduce tin oxide (Pourbaix 1966) but some authors

TABLE 1

TYPICAL TINPLATE PASSIVATION CONDITIONS

temperature	$55^{o}C$
pH	4.5
electrolyte	$Na_2 Cr_2O_7.2H_2O$ ($25 g dm^{-3}$)
311 only:	
current density	$400 A m^{-2}$
duration	1 second
300:	
no current	

claim that not all the tin oxide is removed in this way (Nagel Soepenberg et al 1976).

A detailed study of the oxidation of tin (Boggs et al 1961a,b) has revealed that pure tin forms only tetragonal SnO in oxygen and that this oxide is detectable and measurable using TEM. However, other studies have found that SnO_2 is formed at temperatures below 100°C and during storage (Britton and Sherlock 1974). Recently, a TEM investigation of the oxidation of passivation layers and pure tin (Albu-Yaron and Grovenor 1984) reports an initial microcrystalline mixed oxide structure on tinplate in which both tetragonal and orthorhombic SnO grow during stoving in oxygen. It is to be expected, therefore, that a mixture of tin oxides is present on the tinplate surface before passivation and that some of these original oxides may remain after the passivation treatment. The oxides formed on the tin have also been investigated by Finch (1952) who found a variation in oxide type around an area of tin foil which had been heated to melting point. SnO_2 and SnO were located at the molten border; SnO_2 in an adjacent zone and amorphous (possibly microcrystalline) tin oxide in more distant regions.

The secondary chromium oxide film proposed by Aubrun and Rocquet has been defined as comprising trivalent chromium, deposited before the metallic form, the amount of chromium metal being directly dependent on the amount of chromium oxide present in the secondary film. Cr^0 deposition is halted when the electrode (tinplate surface) is completely covered by the metal.

The results of Nagel Soepenberg et al (1976) provide a slightly different interpretation of the mechanics of 311 passivation layer deposition although a double-stage chromium deposition is also proposed. These workers do not positively identify the chromium

valency but state that they are possibly measuring only the metallic form in both layers and that subsequent oxidation to Cr^{3+} occurs. The logarithmic growth of the second film is then due to diffusion of chromate and dichromate ions through the primary film (porous Cr^{3+} oxides) and reduction of these hexavalent ions on the tin surface. Jumps in the growth rate during formation of the second film are attributed to disruption of the primary film caused by poor adhesion and internal stresses at the interface between the primary film and unreduced tin oxides on the tin.

It is instructive to compare the passivation process with the procedure for plating chromium metal which also uses Cr^{6+} ions in solution and electrolytic deposition to form a continuous coating. The electrolyte used for chromium plating is typically 0.5M CrO_3 with an acid (H_2SO_4) catalyst; current density is higher than for tinplate passivation at 20A dm^{-2} (Vagramyan and Usachev 1958, Okada and Yamamoto 1968). Unless the acid catalyst is added only oxide, not metal, is deposited; the catalyst prevents the primary oxide coat from passivating the surface and a two-stage process results in which Cr^{6+} is reduced to a film of Cr^{3+} and subsequent solid state reduction of the latter to Cr^{0} then occurs.

In the models discussed above the deposition of chromium in passivation is proposed to be deposition of chromium oxides followed by chromium metal deposition from solution (Aubrun and Rocquet 1975) or deposition of (probably) metallic chromium via reduction of adsorbed Cr^{6+} (Nagel Soepenberg et al 1976). The former model does not explain the layered structure of the passivation layer where Cr^{0} is seen at its highest concentration next to the tinplate. Hydrated chromium oxides will form during exposure of Cr^{0} to air and in the aqueous environment of the passivation bath and this mechanism accounts for

the hydrated outer layer seen in XPS. Whether Cr^0 deposition occurs directly from Cr^{6+} or via solid state reduction of Cr^{3+} on the tinplate surface it is likely to take place at the tin surface (or possibly on top of existing tin oxide which is a good conductor of electricity). Either process would result in a layered structure of metallic chromium, chromium oxide and hydrated oxide in the outer layer. If oxidation in air of Cr^0 occurred the oxide would be Cr_2O_3 but as the tinplate is exposed to other environments during and immediately after passivation, other oxides may be formed. During the passivation treatment the potential is likely to alter with time. At a pH of 4.5 Cr^0 will be deposited at a potential of $\leq -1.1V$ (Pourbaix 1966) and as the potential goes more positive the oxide will be formed instead. Since metallic chromium is likely to be formed by a solid state reduction on the tinplate surface from oxidised forms a layered structure will also be formed during the growth of the passivation layer. Tin oxide growth will take place when the applied potential is removed. This may occur during the rinsing immediately after passivation when hydrated oxides may form or subsequently in air. Some of the diffracting tin crystals observed in passivation layers by TEM may be residues from the primary oxide coat present before passivation. Although the passivation process reduces tin oxide growth (this is the primary reason for passivation) there will be some growth of tin oxide after treatment (Takano and Watanabe 1980).

The scale of these deposited species is very fine since TEM could not identify specific crystal structures on most of the passivation layer but there are large outcroppings of crystals of both tin oxides and chromium oxides. If the proposal of Nagel Soepenberg et al is correct and the primary chromium film cracks during passivation, areas

of tinplate will be exposed which could allow rapid growth of chromium oxides or, if the potential is no longer being applied, tin oxides. The large diffracting crystals are often seen to lie over a crack in the passivation layer and this mechanism therefore seems possible. Another explanation for the large tin oxide crystals is that they are unreduced portions of the original oxide on the tin surface which was formed during flow-brightening. This is possible since TEM of unpassivated tinplate does reveal a variety of tin oxides including SnO (tetragonal and orthorhombic) and SnO_2. However, other work (Albu-Yaron and Grovenor 1984) found no large crystals of tin oxides on tinplates until they were heated to 170°C for 20 minutes; no such crystals were found on freshly-passivated specimens by Takano and Watanabe (1980).

The tin oxides which are found on passivated and unpassivated tinplates are mostly in microcrystalline form. In the latter, these can have formed during flow-brightening and afterwards by exposure to the air. In passivated tinplates there are three possible mechanisms of formation which can all be expected to occur:

a. some may be part of the original oxide which has not been reduced by cathodic passivation
b. some may be formed in the rinse directly following passivation at areas where the passivation layer is incomplete or thin
c. some will form by ageing on exposure to the air.

In cases a and c above, the same oxide type would probably be expected. In b, the acqueous environment could lead to the formation of the hydrated tin oxides seen on BS 311.

Although TEM can only identify these large crystals if, as is possible, they are large outgrowths from nuclei in the microcrystalline portion of the film then the TEM data may serve to characterize the

entire passivation layer.

The microcrystalline film is also seen for the first time to be a duplex layer when viewed at high magnification. This structure was observed in very few specimens and so it is not known whether the double layer is typical. Differences in electron transmission indicate that the layers are either of different thickness or have different compositions and may be the primary and secondary layers deposited during passivation as measured by Aubrun and Rocquet (1975) and Nagel Soepenberg et al (1976) or one may be a layer of tin oxide which has grown during storage of the tinplate. Since oxidation of this type is usually by cation diffusion the tin oxide growth would be on the outer surface of the passivation layer.

It is now possible to propose a model for the structure of the passivation layers.

iv. Models for passivation layer structure

The general structure and appearance of the passivation layers on all the 311 tinplates examined is very similar but differing in specific oxide composition and metallic chromium content. XPS did not reveal whether the chromium-rich constituents of the passivation layer sit on top of a layer of tin oxide remaining from the original oxide film but we shall suppose that this has been removed.

The layered structure of chromium "islands" proposed by Saijo et al (1976) may be essentially correct but these are too small to be identified by TEM at this degree of resolution. The diffracting crystals are separate entities and must be shown as such. The chromium oxide and metal crystals are situated above the thin passivation layer as are some of the tin oxide crystals.

A schematic diagram is shown in Figures 2 and 3 where the microcrystalline layer is depicted as a series of sub-micron layered

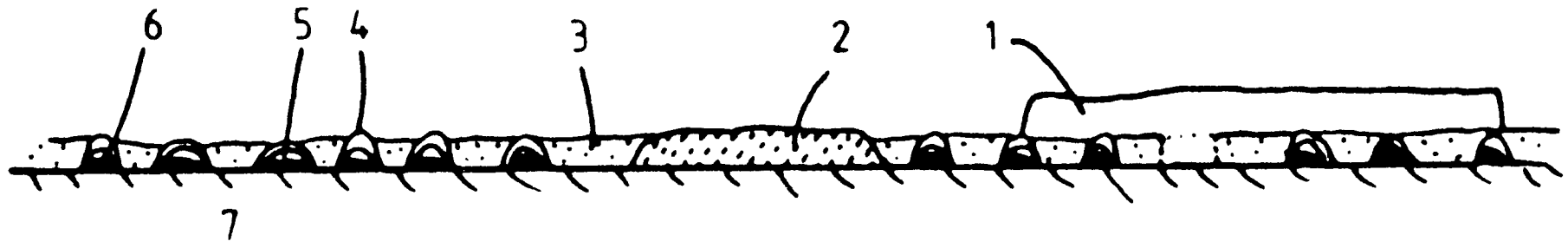

311

Figure 2. Schematic model of passivation layer on 311 tinplate.

	BS	NS	KS
1	Cr° or CrO_2	Cr_2O_3	Cr_5O_{12}
2	SnO_2(c,t), SnO(a,t), $Sn_3O_4(OH)_4$. 5SnO $2H_2O$	SnO(t)	SnO_2(t)
3	SnO_x (≈ 2 ?)		
4	$Cr(OH)_3 . nH_2O$		
5	Cr^{3+} or Cr^{4+}		
6	Cr°		
7	Sn°		

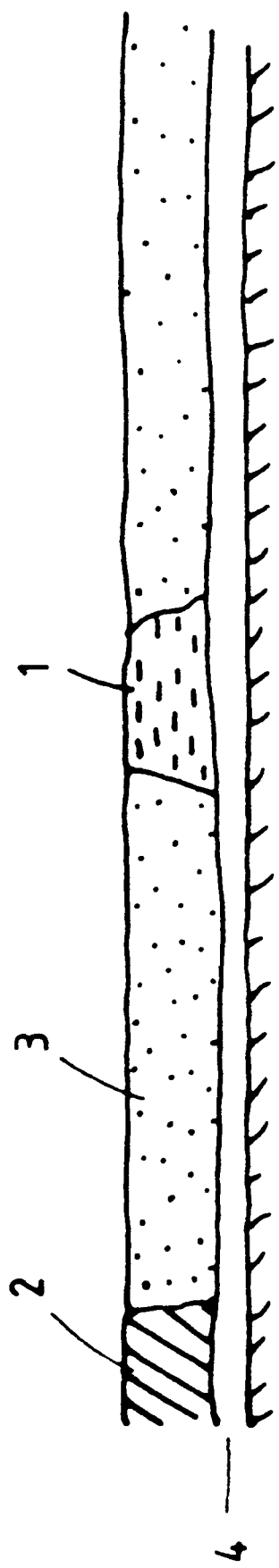

1	$SnO(o)$, $SnO(c)$
2	CrO_x
3	$SnO_x + CrO_x$
4	SnO_x
5	Sn^o

300

Figure 3. Schematic model of passivation layer on 300 tinplate.

islands. Tin oxide, grown after passivation, completes the continuous layer. Hydrated chromium oxide is shown mainly on the outer surface of the film but extends throughout the entire depth in this model, approaching the tin surface between the outcrops of metallic and oxidised chromium. Table 2 shows the differences detected in the composition of the passivation layers from XPS and TEM results.

Measurements of surface coverage by chromium were made by invoking the model of Saijo et al in which thin layers of tin oxide could be removed by Ar ion etching and leave the "islands" of chromium. Relative signal intensities from Sn^0 and Cr will then give a reasonable measure of areal coverage. Since the Saijo model has been shown to be incomplete the rationale for areal coverage must be re-assessed. The thin layer, assumed by Saijo et al to contain only tin oxides, is seen also to contain chromium but since it is very thin (a few nm) the Ar ion etching may selectively remove the tin oxide which has a higher sputtering rate than chromium or its oxide and the measurements of chromium coverage remain as useful and representative values.

2 Butt-joint Test Results

Firstly, in considering the adhesion of lacquer to tinplate, it is necessary to define the optimum properties required of the system. The butt-joint tests have measured adhesion in terms of failure load and percent area lacquer removal and the results subjected to Weibull analysis. An ideal system would combine high failure load and low lacquer removal for all tests within a sample but the sample sets examined in this work exhibit wide variations in both quantities which are characterised in two ways: a) by normalising percent lacquer removal to failure load, and b) by Weibull analysis which

TABLE 2

DIFFERENCES IN TINPLATE PASSIVATION LAYER COMPOSITION

A SUMMARY OF XPS AND TEM RESULTS

Quantity	XPS		TEM
Tin Oxide	same thickness (∿ 1nm)		BS 311: SnO (O)
			SnO_2(C)
			SnO_2(t)
			$Sn_6O_4(OH)_4$
			$5SnO.2H_2O$
			NS 311: SnO (t)
			KS 311: SnO_2(t)
	∿5nm		BS 300 SnO (O)
			SnO_2(C)
			+ weakly-diffracting species
Chromium Oxide	BS 311 / NS 311 / KS 311	Cr^0 / Cr^{3+} or Cr^{4+} / $Cr(OH)_3.nH_2O$	BS 311: CrO_2 (t)
			NS 311: Cr_3O_4(t)
			KS 311: Cr_5O_{12}
			+ weakly-diffracting species
	+KS 311	Cr^{6+}	

		Tinplate	Pass. Layer u.side	
$Cr^0:Cr_{ox}$	BS 311	1:1*	0·35:1	
	NS 311	·07:1 #		-------
	KS 311*	0·1:1	0·75:1	
	BS 311	18%		
$Cr:Sn^0$	NS 311	12%		
(areal coverage)	KS 311	11%		< 5%
	BS 300	2%		

KEY

(O) orthorhombic

(C) cubic

(t) tetragonal

* after 1 minute Ar ion etch

after 1/2 minute Ar ion etch

produces a failure distribution function. Specific tinplates types are distinguished in butt-joint tests by these means.

The variations of failure load and lacquer removal within a particular sample set are very probably due to variations within the sample and are not due to the testing method. Both interfacial bonding and defects play a role in determining these values (for a given system) and these are discussed below.

i/ Interpretation of test data

Catastrophic failure in butt-joint tests produces brittle fracture surfaces with areas of lacquer detachment. Evidence for plastic deformation in the lacquer is seen on some lacquer edges. The accumulated data for tests with different lacquer-tinplate-stoving combinations are given in Chapter 3 where a wide variability in both failure load and percent lacquer removal are evident. The fracture may be regarded as two separate processes, initiation followed by propagation and, in nominally identical brittle samples which show a wide scatter in failure loads, a defect distribution is usually responsible for the former. Weibull plots of failure load have shown that, despite a very wide variability, the sample data for failure load (and hence crack initiation) can be described by a distribution function for the defect population. One distribution function has been shown to be common to all tinplate-lacquer combinations (with a few exceptions which are mentioned below) and leads to the conclusion that this population of defects is not contained within the lacquer or passivation layer but is present in some component of the system which is found in all sample types, including non-passivated tinplate. Microscopy has been used to locate candidates for initiation defects and fracture mechanics will provide an estimate of the size required to induce failure at the measured loads. A

common distribution function indicates a common distribution of defect severities, a term which includes size and orientation for bulk materials. Since the layers within these samples are thin, critical defects are likely to be orientated parallel with the tin-plate and the distribution function then becomes a measure of defect size. The function which describes the flaws responsible for crack initiation is characterised by a slope usually between 2 and 5 on the Weibull plots. In order to confirm that the indivudual slopes for each sample are really a part of the same distribution the data for failure load from many different samples (200 data points) were combined on a single Weibull plot. This is given in Figure 4 although for clarity not all the data points are shown. It is seen that the data fall on a straight line with slope 1.9±17% which, including the errors due to limited data, is within the range of the individual sample slopes. This single plot of failure load data is probably a more accurate description of the defect population which induces failure in the butt-joint test.

As stated above, there are samples which fall outside this range and which have significantly different Weibull slopes for failure load. Samples 14 and 15 are both BS 311 tinplates, air stoved with phenolic (type A) lacquer, the only examples of this particular combination. Both also exhibited higher than normal levels of lacquer removal and this behaviour is possibly linked to the lacquer-ing conditions. Other phenolic lacquers performed well on BS 311 tinplate and the exact cause of the poor performance of samples 14 and 15 is unknown.

In most cases then, the mechanism which initiates failure is independent of tinplate passivation, lacquer type or stoving conditions. When percent lacquer removal is normalised to failure load (the "area

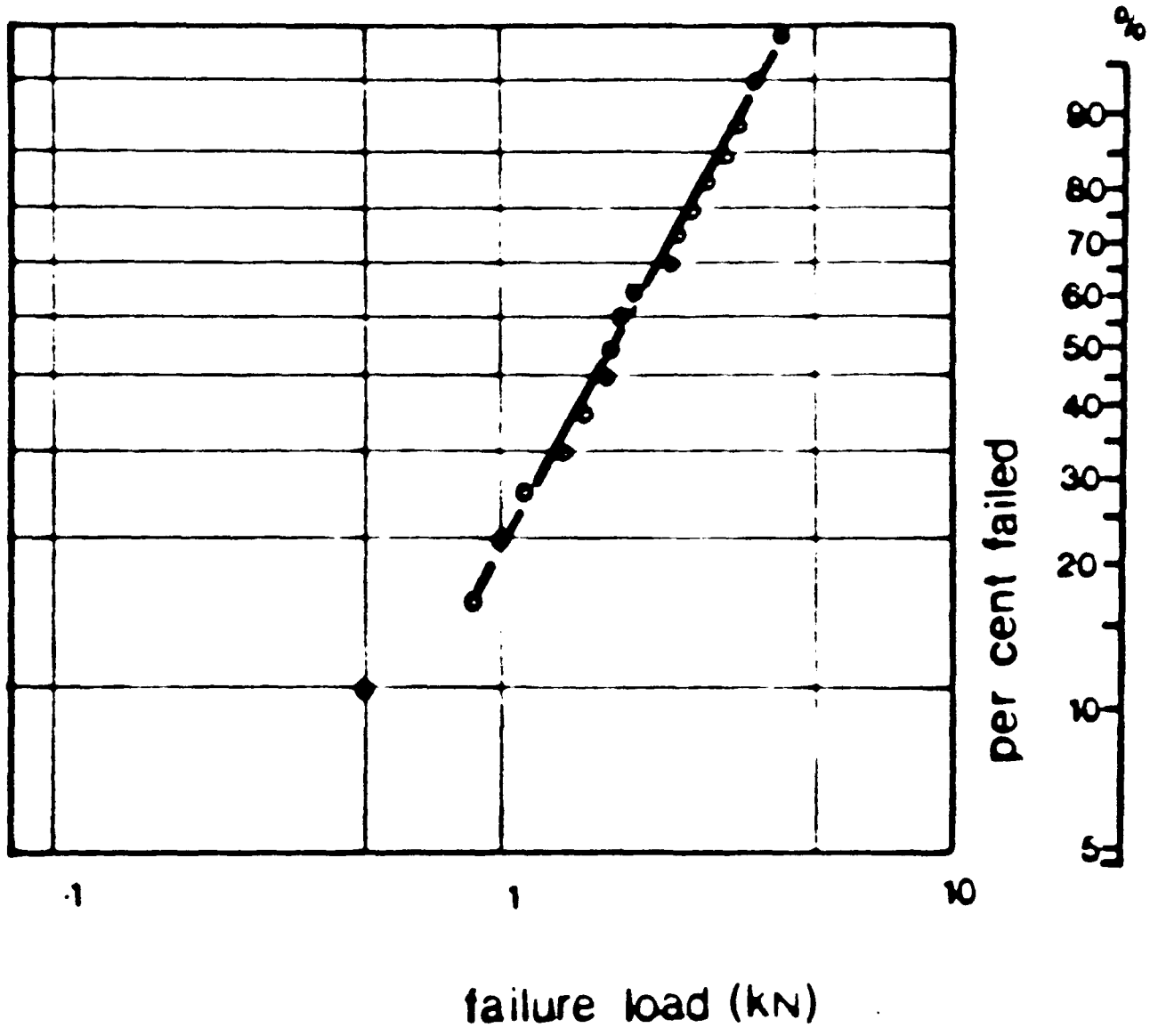

Figure 4. Weibull plot of combined data failure load.

debonding factor", ADF) distinct differences appear between tinplate types, in particular distinguishing BS 311 and BS 300 from NS 311 and KS 311. In the latter pair there is in general no relationship between failure load and lacquer removal producing high values of ADF with wide scatter. BS 311 and BS 300 tinplates with different lacquers and stoving have low ADF values with lower standard deviations indicative of a positive relationship between failure load and lacquer removal. When these two parameters are plotted against each other it is seen for BS samples that either a positive, approximately linear relationship is present or that the data points cluster in a small area of the graph. Thus, the failure load, determined by a defect distribution, also affects the amount of lacquer removed from BS samples but not from NS 311 or KS 311 samples and suggests that different crack propagation mechanisms are operating on these two sample groups. This has been confirmed by fractography and XPS analysis of fracture surfaces and is discussed in detail later. The differences in crack propagation are also revealed when the Weibull plots for percent area lacquer removal are examined. NS 311 and KS 311 samples have steep Weibull slopes showing a high proportion of samples which lose large areas of lacquer compared with the BS 311 and BS 300 samples.

Thus, the behaviour of KS 311 and NS 311 tinplate samples in the butt-joint test is seen to comprise initiation, controlled by defects, and propagation. Initiation in BS 311 is controlled by the same defect distribution but the crack propagation behaviour between these two classes of tinplate is different and is discussed below.

Further information about the fracture mechanism is available from microscopy and spectroscopy of the fracture surfaces which is presented below.

ii/ Fracture surface examinations

Optical and scanning electron microscopy have been used to trace the crack propagation paths on fracture surfaces. The NS 311 and KS 311 fracture surfaces consist of areas of exposed tinplate and sections of remaining lacquer with distinct boundaries. River markings are visible on the edges of the lacquer showing that the crack has run away from the tinplate and had therefore been initiated within the sample between the lacquer and the tinplate and not at the circumference as is the case for a simple adherend-adhesive butt-joint (Gent 1974). Similar markings are visible on the BS 311 and BS 300 specimens with the addition of thin lacquer layers which extend from the sections of remaining lacquer and on which are further fracture marks. The thick lacquer sections left on BS fracture surfaces exhibit different morphologies from those on KS 311 and NS 311; in the latter the lacquer edges are steep but on BS fracture surfaces the edges of thick lacquer areas have a shallower gradient which sometimes progress into the thin lacquer areas. Within the thin lacquer film are approximately circular areas of exposed tinplate referred to earlier as "lacquer-free zones" and at the centre of each of these zones is an angular defect where the $FeSn_2$ layer is exposed through the tin. Interpretation of the fracture markings in the thin lacquer film indicates crack propagation radially outwards from several of the lacquer-free zones, but since simultaneous multiple initiation is extremely unlikely these features are probably secondary initiations triggered by an approaching crack front. Evidence for this is seen in the interaction of fracture marks from the lacquer-free zones with stick-slip marks indicative of an approximately linear crack front having moved through the sample. No single primary initiation point could be located on the fracture

surfaces owing to the complexity of the fracture marks but it is possible that one lacquer-free zone or central defect was responsible, producing a main fracture which then triggered secondary initiation at several points across the sample. As Weibull analysis points to the same initiation mechanism for all samples the angular $FeSn_2$ defects become prime candidates as initiation sites since they are found on all tinplate types including 300 and unpassivated and no other surface feature such as surface roughness or oxide thickness has been found to be common to all samples. The origin of the angular defects is unclear; they are different in appearance to those areas where the tin coating has been consumed during flow-brightening to leave large (e.g. $500\mu m^2$) areas of the alloy layer protruding through the tin. They are not found on non-flow-brightened tinplate and may result from dewetting when the tin coating is molten or from existing gaps in the tin in which case the straight sides of the defect would be low energy crystal faces. Corrosion is also seen to produce angular etch pits in tinplate so further work on the cause of these defects would be very worthwhile.

KS 311 and NS 311 tinplates did not exhibit the thin lacquer layer and lacquer-free zones but on the BS samples where they were observed it could not be definitely determined whether they had been present in the sample before testing or whether they had been produced during the test. Optical microscopy could find no evidence of such small debonded areas before testing or within the remaining tinplate-lacquer interface on the fracture surfaces.

The $FeSn_2$ defects may introduce stress-concentrating cracks by air-entrapment during the lacquering process or may cause debonding of the lacquer (or weaken the interface) during storage by the production of corrosion products. If the latter mechanism occurred

there would be a variation in failure load due to storage time and lacquer-free zones would vary in size with time. The former effect has been observed (Horiguchi et al 1984, Takano and Watanabe 1980) but has been attributed to changes in the passivation layer. The latter effect has not been observed here with BS 311 tinplates where the duration between lacquering and testing has been varied from 5 days to over 1 year. No corrosion products are visible in the lacquer-free zones and the results of this work therefore suggest that corr-osion debonding from the central $FeSn_2$ defects does not significantly affect fracture initiation and that they probably result from debond-ing during the test, possibly by sub-critical crack growth. The direction of crack propagation can be deduced from the fracture mark-ings on the failed surfaces and XPS reveals a major distinction between the fracture of BS 311 tinplates and the NS 311 and KS 311 tinplates. When the exposed tinplate areas on the fracture surfaces are examined it is seen that the passivation layer has been left intact on BS specimens. Tests with an organosol lacquer containing pvc show that XPS could detect the chlorine in the lacquer on visually bare areas of tinplate on fracture surfaces, indicating that the fracture has run through the lacquer but very close to the passivation layer surface. Since XPS derives its information from large (several mm^2) areas it is not possible to say whether this very thin lacquer layer was present over the entire fracture surface.

The passivation layer was totally removed from those areas where tinplate was visible on NS 311 and KS 311 fracture surfaces. The crack propagation path is therefore quite different between BS 311 and the other 311 types and shows that the bonding between the passivation layer and the tinplate is stronger in the former set. Microscopy of fracture surfaces showed that the fracture path is

usually complex, moving from one interface to another within the bonded system and sometimes running cohesively within the lacquer. However, a propagating crack will presumably move along the weakest path available and since initiation is at a point between the lacquer and the tinplate (probably the $FeSn_2$ defects or lacquer-free zones) the initial crack is well placed to allow propagation along the interfaces of interest (i.e. the lacquer-passivation layer interface and tinplate-passivation layer interface) and enable areas of weak bonding within these interfaces to fail. Interfacial failure is observed in the case of the NS 311 and KS 311 samples.

iii/ Correlation of lacquer adhesion performance with sample structure

Defect controlled initiation has been linked with the $FeSn_2$ defects or lacquer-free zones seen on the fracture surfaces from the butt-joint tests. Fracture mechanics provides a means of assessing the effect of flaws on strength and may be applied to this case to compare measured defect dimensions with the actual failure strength of the samples.

The energy-balance approach of Griffith (1920) and Orowan (1948) was developed for a sharp crack of length a in a continuum:

$$\sigma_f = \sqrt{\frac{GE}{a}} \qquad (1)$$

where σ_f is failure stress, G is strain energy release per unit length and E is Young's modulus.

Here, fracture occurs when energy is released (from the applied stress) by crack growth and is sufficient to allow creation of new surfaces. The energy released comes from the stored elastic energy in the stressed specimen. For materials which behave in a perfectly elastic manner up to fracture the energy required to create new surfaces is just the thermodynamic work of adhesion, W_A. In most materials, however, further energy is required since processes such as plastic and visco-

elastic deformations take place. The quantity G combines the thermodynamic work of adhesion and other effects to characterize the total energy required to form two new surfaces. The measurements of G are usually made with specially designed test pieces into which known defects are introduced. The blister test provides one way and this and other methods are discussed by Kinloch (1982).

Considering a lacquered tinplate specimen with strong bonding at all interfaces and with initiating defects in the tin coating, the initial crack induces a stress field in the material ahead of the crack tip. Subsequent propagation will proceed along the path with lowest available fracture energy, G, or the path requiring the lowest force (Gent and Petrich 1969) and since the passivation layer is very thin both of its interfaces may be regarded as experiencing identical stress conditions. Good (1972) has shown that minima in G can occur at interfaces with weak bonding and that minima very near interfaces can result when there is strong bonding between materials with dissimilar values of G and E. Thus, where strong bonding exists there will be preferred regions of low fracture energy which are close to an interface and which may have been mistaken for weak boundary layer failure in earlier works. In this work, the BS samples show that fracture has taken place (for areas where the tinplate is visible on the fracture surfaces) within the lacquer but close to the passivation layer. According to this work of Good, true interfacial failure is only likely when interfacial bonding is weak but may run very close to the interface when there is strong bonding. Thin lacquer layers are found on the BS samples, sometimes only by using XPS due to their thinness and need not indicate weak bonding between the lacquer and the passivation layer. Fracture paths have been identified using XPS to reveal the differences in behaviour between BS and KS 311 and

NS 311 samples. Since the spatial resolution of XPS is poor the exact path taken in fracture cannot be determined and may jump from one interface to another in some areas. However, as both sides of the fractured samples have been examined any such deviations are small since no chromium at all was detected on the KS 311 and NS 311 tinplate surfaces after fracture not on the lacquer-side stub from BS 311 failures.

When fracture mechanics are employed to study adhesive joints (Gent 1974, Kinlock and Shaw 1981, Andrews and Kinloch 1973a,b) the situation is complicated by the laminar structure of the joints; equation 1 was developed for infinite bulk solids and effects of thin layers on G and E must be considered. As shown theoretically by Good (1972) and by experimental work (Andrews and Kinloch 1973a,b) the fracture energy of interfaces cannot always be directly obtained from values of G for the bulk materials. The values of E are also affected since a propagating crack draws energy from a volume of material around the crack tip (Gruntfest 1963) which may be of the order of 1μm (Irwin 1967). The dimensions of this zone in this work are probably greater than the thickness of the passivation layer which can store little elastic energy due to its size. The effective value of E for the passivation layer will therefore be a weighted mean of the moduli of the lacquer and tinplate and the elastic stress field will encompass regions of the tinplate, passivation layer and lacquer.

Table 3 shows calculated fracture stresses, using values of G and E from the literature. Measured failure stresses are in the range 2 to 28MNm^{-2} and it can be seen that in no case will a 1μm defect (typical of the angular $FeSn_2$ defects) produce failure at these stresses. Defects of radius 100μm do however initiate failure at levels approaching the observed range in bulk polymer, bulk glass

TABLE 3

CALCULATED FRACTURE STRESSES FOR

1μm and 100μm RADIUS DEFECTS

Material	$E(Nm^{-2}x)10^9)$	$G(Sm^{-2})$	$\sigma_f(1\mu m).(MNm^{-2}).\sigma_f(100\mu m)$	
Epoxy	3.86	136	720	72
Glass/metal interface	70	2.9	450	45
Al_2O_3	350	20	2600	260
Glass	69	3.7	500	50
Rubber-(rigid polymer) interface	2	2-180	60-600	6-60

References

Wyatt and Dew-Hughes 1974

Becher et al 1977

Bascom et al 1975

Andrews and Kinloch 1973a

(taken as a model for the passivation layer) and at rigid polymer-rubber and glass-metal interfaces. Good (1972) has shown theoretically that G may be reduced near a bonded interface and Andrews and Kinloch (1973a,b), in an experimental study, show that G can be reduced by up to an order of magnitude from values for bulk adhesive to values for failure in joints. Hence, the fracture energies for joints are likely to be reduced from bulk values and subsequently cause a reduction in failure stress. If this is assumed to occur the calculated fracture stresses for 100μm defects are decreased and fall within the range of the experimental values. In all cases it appears that a 100μm defect is more likely to be the cause of fracture initiation and forces the conclusion that the lacquer-free zones seen on BS fracture surfaces are produced by subcritical debonding during the test until one reaches ctitical size. Similar zones may grow on KS 311 and NS 311 specimens but since crack propagation runs beneath the passivation layer they are not present on the fracture surface after testing. Since all the lacquer-free zones are approximately circular, there is further evidence that they are subcritical grows since the stress state within the sample during loading but before failure would encourage radial growth from a defect. Debonding by the central $FeSn_2$ defect in the absence of the lacquer-free zone would be more likely to leave the defect at the edge of a debonded area.

Although no single primary initiation site could be located on the fracture surfaces it is assumed that one of the lacquer-free zones is responsible, producing a propagating crack which then triggers the other zones as secondary initiations. A slightly different explanation may also be proposed whereby the elastic stress wave released by the initiation travels through the sample ahead of the

crack tip and initiates failure in the other partially-debonded zones. The maximum velocity of a crack running through a polymer is approximately one third the speed of sound in the polymer (Gent and Marteny 1982) and as the elastic wave travels at the speed of sound it would reach other incipient cracks before the main crack front.

In the KS 311 and NS 311 samples it is the passivation layer-tinplate interface which is of interest. Some workers have claimed that such failures have occurred in a layer of tin oxide below the passivation layer (Horiguchi et al 1984, Servais et al 1979). In this work, tin oxide was removed by the passivation film from the NS 311 and KS 311 samples and the oxide later detected by XPS on the tinplate can easily be explained by oxidation of the tin in the time between failure and examination as tests have shown. The amount of tin oxide detected on the underside of the passivation layer after fracture is consistent with the amounts measured before failure and no evidence has been found for thick oxide growth during stoving as suggested by Servais et al (1979). Interfacial failure in NS 311 and KS 311 samples at the tinplate-passivation layer interface is therefore considered the most likely mechanism of failure in these samples and the thermodynamic work of adhesion at the interface becomes important in controlling this behaviour. The fracture energy, even in the case of interfacial failure, is usually found to be much larger than W_A because the propagating crack must draw energy from the material around the crack tip and this will probably include the passivation layer, the tin and the lacquer which will be viscoelastically deformed. In the BS tinplates, the failure is probably cohesive within the lacquer and it is the properties of the lacquer which mainly determine the fracture energy, G. The structure and composition of the passivation layer play no direct part in the fracture process and lacquer

adhesion performance here (except to say that the interfacial bonding in these samples is higher than the cohesive strength of the lacquer).

The results of XPS and TEM examinations may now be correlated with lacquer adhesion performance. Surface topography of the passivation film is clearly visible in the TEM specimens; no whiskers or pores are present which would be likely to affect adhesion by producing dewetted areas or interlocking surfaces. Passivation layer topography does not, therefore, play a major role in adhesion in this work.

Since it is the passivation layer-tinplate interface which determines the different adhesion performances of the tinplates the chemical nature of these interfaces must be examined. Differences are noted in the type of tin oxides, chromium oxides and distribution of Cr^0.

Takano and Watanabe (1980) have associated tinplates on which certain tin oxides grow with different lacquer adhesion properties. Namely, growth of orthorhombic SmO indicates tinplates with good lacquer adhesion and growth of tetragonal SnO or SnO_2 indicates poor adhesion properties. These workers did not report where failure occurred in their samples.

In this work, orthorhombic SnO is found only on the BS 311, NP and BS 300 tinplates whereas mixed valence chromium oxides were found on NS and KS 311 samples. Hexavalent chromium was found only on KS 311 and one BS 311 sample which, although possessing poor lacquer adhesion as measured by the Scotch Tape test, did not fail beneath the passivation layer.

Strong interfacial bonding between the tinplate and passivation layer is associated with higher levels of total chromium (18%) on BS 311 compared with 10% on KS 311 and NS 311. BS 311 also possessed higher levels of Cr^0:CrO_x. Low levels of metallic chromium

are associated with poor peel strength by Takano and Watanabe (1980) but total chromium was found by them to be inversely proportional to peel strength. In this work, both high levels of Cr^0 and CrO_x are associated with the BS 311, but the 300 tinplate possesses no Cr^0 and low levels of oxidised chromium and yet still behaves like BS 311. Thus, there is no clear correlation between chromium content and lacquer adhesion which can be used to describe both 300 and 311 tinplates.

It is not possible to attribute causal connections between passivation layer structure and adhesion but correlations may be made. Table 4 lists these correlations for tin oxides, chromium oxides and chromium metal concentrations. It may not be these components, per se, but the factors present before, during or after passivation which influence the adhesion performance. Metallic chromium and tin oxide are almost certainly in contact with the tin surface whilst present in the passivation layer and the other components may also be touching the metal in places. It is unlikely that the different oxides will have greatly different surface energies sufficient to vary W_A and affect the adhesion as observed. It will be valuable for future work to attempt to separate the effects of the different components by a carefully controlled passivating treatment in which specific passivation layer compositions may be formed. The passivation process requires further study to explain the final structure of the surface layer on tinplate; unpassivated tinplate contains an amorphous or microcrystalline coat of tin oxides and diffracting oxides of orthorhombic and tertrgonal SnO and tetragonal and cubic SnO_2. From butt-joint tests, its behaviour is similar to the BS 311 but it contains no chromium at all and the tetragonal SnO_2 otherwise linked with weak bonding. The removal of some or all of these oxides during passivation should be verified.

TABLE 4

CORRELATION OF PASSIVATION LAYER COMPOSITION

WITH PASSIVATION LAYER-TINPLATE INTERFACE STRENGTH

FOR 311 TINPLATES

	Weak	Strong
	(NS311/KS311)	(BS311)
SnO_x	SnO_2 tetragonal	SnO (orthorhombic) $Sn_6O_4(OH)_4$ SnO_2 (cubic) $5SnO.2H_2O$
	(SnO tetragonal)	
CrO_x	Cr_3O_4 Cr_5O_{12} (Cr^{6+})	CrO_2
Cr	10% areal coverage	18% areal coverage

3 Conclusions

Models for the passivation layers on 311 tinplates and 300 tinplates have been derived. The 311 passivation layer consists of a microcrystalline layered structure containing metallic, oxidised and hydrated oxidised chromium with oxides of tin. Larger diffracting crystals are also found. The diffracting tin oxides are likely to have been formed after passivation, probably by exposure to air but the large chromium oxide and chromium metal crystals must have formed during the passivation treatment. The passivation layers on all 311 type tinplates are similar in appearance and differ in the composition of the large (diffracting) crystals of chromium oxides and tin oxides (although these measurements, made by TEM, may also characterise the weakly-diffracting microcrystalline layer). Differences are also seen in the amount of total chromium in the layers.

The 300 tinplates contain no metallic chromium and only 2% oxidised chromium compared with the BS 311, KS 311 and NS 311 tinplates which possess ~18%, 12% and 11% total chromium respectively.

The structural models proposed are similar in some respects to earlier models proposed elsewhere but offer a more complete description than had been available. Saijo et al (1976) also propose a layered model but do not include the large diffracting crystals and do not identify a range of chromium oxide and tin oxide structures. Albu-Yaron and Smith (1979, 1980) have used TEM to observe passivation layers but concentrated on the diffracting components and did not identify the weakly-diffracting chromium constituents.

The use of XPS and TEM has allowed a comprehensive study of tinplate passivation layers on a number of different tinplates. In particular, chromium oxides other than Cr_2O_3 have been found which have not been reported before. Mixed valence oxides such

as Cr_5O_{12} and Cr_3O_4 can account for the Cr^{6+} signal sometimes seen in XPS which had earlier been identified (Leroy et al 1976) as CrO_3, an oxide which is soluble in water and unlikely to persist on tinplate surfaces.

In fracture, distinct differences are seen between two categories of 311 tinplates. The first category (BS 311) fails in the butt-joint test so that the passivation layer is retained totally on the tinplate surface. On the areas of apparently bare tinplate in the fracture surfaces there is a very thin lacquer layer indicating cohesive failure within the lacquer and showing that the interfacial bonding in these samples is greater than the tensile strength of the lacquer. The second category of tinplates, including NS 311 and KS 311, lose their passivation layers when the fracture propagates at the tinplate-passivation layer interface. These modes of crack propagation distinguish tinplate lacquer adhesion properties. Tin-plates which fail below the passivation layer due to weak interfacial bonding are likely to be less suitable for can manufacture than those with strong bonding and which fail cohesively in the lacquer. Fracture initiation is an independent mechanism dependent upon a defect distri-bution within the samples which is common to all tinplate types. Specific flaws have been identified as initiators, namely the angular $FeSn_2$ defects in the tin coating whose origins are unknown. Subcritical debonding from these defects during the test is likely until one reaches a critical size, propagates and then triggers the others as secondary initiation sites.

Since failure in the NS 311 and KS 311 occurs at the tinplate-passivation layer interface the nature of the passivation layer is unlikely to have an effect on the interfacial properties. Certain components of the layer can be correlated with the fracture behaviour

and for good bonding at this interface in 311 tinplate these are orthorhombic SnO, cubic SnO_2, $Sn_6O_4(OH)_4$, $5SnO.2H_2O$, CrO_2 and high (18%) total chromium. For weak bonding, SnO_2 (tetragonal), Cr_3O_4 and Cr_5O_{12} are found with low (10%) total chromium coverage. Type 300 tinplates also appear to behave like BS 311 and contain orthorhombic SnO and cubic SnO_2

In the butt-joint test the tinplates which retain their passivation layers can be distinguished by examining the data. In general, they tend to show lower areas of exposed tinplate on their fracture surfaces but are more easily discerned on a plot of failure load vs. percent lacquer removal (the latter determined by visual inspection). BS 311 and BS 300 tinplates show a strong positive relationship between the two parameters and when plotted on an "area debonding factor", ADF, plot (percent lacquer removal/failure load in kN) show low values (< 25) with small standard deviations. Weibull plots of the butt-joint data enabled the initiating defect population distribution to be described from graphs of failure load. When values of percent lacquer removal are plotted a distribution realting to the interfacial bonding between tinplate and passivation layer can be derived for the NS 311 and KS 311 specimens. The use of Weibull plots allows predictions to be made about the behaviour of sample sets and clearly shows differences in behaviour despite wide variations in both failure load and lacquer removal.

The adhesion of lacquers to tinplate has been shown to be a function of both defects within the sample and the intrinsic adhesion of the interfaces.

FUTURE WORK

In the work presented above several commercial tinplates have been investigated and their passivation layer structure related to lacquer adhesion performance as measured in the butt-joint test. The experimental work was unable to impose conditions on the passivation process or on the production of the tinplate. Further useful studies could be made by following a particular batch of tinplate through its manufacturing stages and analysing samples at each stage so that the origins of the angular defects in the tin coating could be found. This approach would also enable adhesion tests to be made along the way and would measure the change of adhesion associated with natural ageing of the passivation layer.

An extra refinement would be to produce a series of passivated surfaces under controlled laboratory conditions on both tinplate and pure tin sheet, the latter free of surface defects. The effects of surface defects on initiation and the passivation layer on interfacial bonding and crack propagation could then be clearly discriminated. Fracture tests should be performed in ultra-high vacuum conditions and immediately examined by XPS, preferably with a monochromated X-ray source for greater resolution. UHV will prevent oxidation of tin before chemical analysis and will solve the problem of whether tin oxide layers grow beneath the lacquer during stoving or are air-grown after fracture.

Other technical improvements to XPS which would be valuable are the incorporation of a raster-scanning Ar ion gun for uniform etching rates across the specimen surface and a scanning XPS analysis to provide spatial distribution information.

The butt-joint test has proved useful in identifying defect distributions responsible for failure initiation via Weibull analysis

and has allowed loci of failure to be determined. A different type of mechanical test, more closely matching the mode of failure found in can manufacture could next be used and results compared. One such test is the deep-drawing of scored lacquered tinplates.

In summary, then, useful developments and experiments for the continuation of this work would be:

1. Improvements in experimental techniques

   i/ controlled manufacture of passivated tinplate

   ii/ controlled passivation of tin and tinplate surfaces

   iii/ UHV fracture and immediate analysis

   iv/ monochromated X-ray source in XPS

   v/ scanning Ar ion source for etching

   vi/ scanning X-ray source in XPS.

2. Further experiments

   i/ butt-joint tests of passivated smooth tin surfaces (no surface defects)

   ii/ comparison of butt-joint and deep-drawing tests to show applicability of the above results to can-forming applications

   iii/ high-resolution TEM investigation of the microcrystalline portions of passivation films

   iv/ laboratory production of passivated tinplate surfaces for adhesion tests. Variations in passivation time and applied negative potential would alter the amount and type of chromium deposited and the possible effect on adhesion due to chromium could then be separated from effects due to tin oxides.

   v/ investigation of tin oxide growth on tinplates - both in aqueous and atmospheric environments.

Bibliography

Albu-Yaron A. and Smith D.A. Br. Corr. J. 14 (1979) 133.

Albu-Yaron A. and Smith D.A. Proc. 2nd Int. Tinplate Conf. ITRI, London (1980) 256.

Albu-Yaron A. and Grovenor C.R.M. Proc. 3rd Int. Tinplate Conf. ITRI, London (1984) No. 35.

Andrews E.H. and Kinloch A.J. Proc. R. Soc. Lond. A332 (1973) 385 a.

Andrews E.H. and Kinloch A.J. Proc. R. Soc. Lond. A332 (1973) 401 b.

Andrews E.H. J. Mater. Sci. 11 (1976) 2004.

Aubrun Ph.J. and Rocquet P. J. Electrochem. Soc. 122 (1975) 861.

Aubrun Ph. and Pennera G.A. Proc. 1st Int. Tinplate Conf. ITRI, London, (1976) 295.

Azzeri N. and Splendorini L. Imballagio 292 (1980) 65.

Azzeri N. Splendorini L., Barristoni C. and Paparazzo E. Surf. Techn. 15 (1982) 255.

Bascom W.D., Timmons C.O. and Jones R.L. J. Mater. Sci 10 (1975) 1037.

Becher P.F. and Newell W.L. J. Mater. Sci. 12 (1977) 90.

Becker J.J. J. Electeochem Soc. 117 (1970) 1211.

Bikerman J.J. J. Coll. Sci. 2 (1947) 163.

Bikerman J.J. "The Science of Adhesive Joints" 2nd ed., Academic Press, New York (1968).

Boggs, W.E., Kachik R.H. and Pellissier G.E. J. Electrochem. Soc. 108 No. 1 (1961) 6 a.

Boggs W.E., Trozzo P.S. and Pellissier G.E. J. Electrochem. Soc. 108 No. 1 (1961) 13 b.

Britton S.C. and Bright K. Metallurgica 56 (1957) 336.

Britton S.C. Br. Corr. J. 10 (1975) 85 a.

Britton S.C. "Tin versus Corrosion" ITRI (London) publication No. 310 (1975) b.

Carter P.R. J. Electrochem. Soc. 108 (1961) 782.

Cherry B.W. and el Muddarris J. Adhes. 2 (1970) 42.

Coad J., Mott B., Harden G. and Walpole J. Br. Corr. J. 11 (1976) 219.

Corten H.T. in "Fracture - An Advanced Treatise" 7 ed. H. Liebowitz Academic Press, London (1972).

Briggs D. and Seah M.P. "Practical Surface Analysis by Auger and X-ray electron Spectroscopy" Wiley, New York (1983).

Dahlquist C.A. ASTM Spec. Techn. Publ. No. 360 (1964) 46.

Finch G.I. in "Oxidation of Metals and Alloys" ed. O. Kubaschewski and B.E. Hopkins, Butterworths, London, (1953) 55.

Gent A.N. and Petrich R.P. Proc. R. Soc. Lond. A310 (1969) 433.

Gent A.N. and Kinloch A.J. J. Polym. Sci. A2 9 (1971) 659.

Gent A.N. J. Polym. Sci. A2 6 (1974) 283.

Gent A.N. and Marteny P. J. Mater. Sci. 17 (1982) 2955.

Griffith A.A. Phil. Trans. R. Soc. London 221 (1920) 163.

Gruntfest I.J. in "Fracture in Solids" eds. D.C. Crucker and J.J. Gilman, Interscience, New York, (1963).

Good, R.J. J. Adhesion 4 (1972) 133.

Gulbransen E.A. and Hickman J.W. Trans. Amer. Inst. Min. (Metall.) Engrs. 171 (1947) 306.

Horiguchi M., Kurokawa W. and Matsubaguyashi H. Proc. 3rd Int. Tinplate Conf. ITRI, London (1984) No. 29.

Irwin G.R. in "Treatise on Adhesion" ed. R.L. Patrick, Marcel Decker, New York (1967).

Kinloch A.J. J. Adhesion 10 (1979) 193.

Kinloch A.J. J. Mater. Sci. 17 (1982) 617.

Kinloch A.J. and Shaw S.J. in "Developments in Adhesives - 2" ed. A.J. Kinloch, Applied Science, London (1981).

Leroy V., Servais J.P., Habraken L., Belgium C.R.M., Lempereur J. and Cockerill S. Proc. 1st Int. Tinplate Conf. ITRI, London (1976) 399.

Maeda S., Asai T. and Sawairi T. Proc. 2nd Int. Tinplate Conf. ITRI, London (1980) No. 25.

Mecholsky J.J., Freimam S.W. and Rice R.W. J. Mater. Sci. 11 (1976) 1310.

Nagel Soepenberg E., Vriburg H.G. and Spruyt A.C. Proc. 1st Int. Tinplate Conf. ITRI, London (1976) 282.

Okada H. and Yamamoto K. Electrochem. Techn. 6 (1968) 389.

Orowan E. Trans. Inst. Eng. and Shipbuilders, Scotland, 165 (1945).

Pourbaix M. "Atlas of Electrochemical Equilibria in Acqueous Solutions" Pergamon, Oxford (1966).

Rao, C.N.R., Sanna D.D., Vazudevan S. and Hegde M.S. Proc. R. Soc. London A367 (1979) 239.

Rauch S.E. and Steinbicker R.N. J. Electrochem. Soc. 120 (1973) 735.

Rocquet P. and Aubrun Ph. Corrosion-Traitments 16 (1968) 229.

Saijo K., Yoshioka O. and Oyama T. Tech. Rep. Toyo Kahan Co. Ltd. 23 (1976) 17.

Servais J.P., Lempereur J., Renard L. and Leroy V. Br. Corr. J. 14 No. 3 (1979) 126.

Takano H. and Watanabe T. Proc. 2nd Int. Tinplate Conf., ITRI, London (1980) 422.

Tsutsumi T., Ikemoto I., Namikawa T. and Kuroda H. Bull. Chem. Soc. Jpn. 54 (1981) 913.

Vagramyan A.T. and Usachev D.N. Zhur. Fiz. Khim. 32 (1958) 1900.

Wyatt O.H. and Dew-Hughes D. "Metals Ceramics and Polymers" C.U.P., Cambridge (1974).

APPENDIX 1

i. ANALYSIS OF RESULTS FROM BUTT-JOINT TEST

The test results of samples 1-17, comprising 111 ordered pairs of observations, were used in a statistical analysis. This analysis was undertaken by Mr. P.N. Appleby of Metal Box PLC. His report is reproduced below.

Each observation comprised the following values:

i/ the failure load of the bond in kN

ii/ the percentage area of the bond from which lacquer had been removed from the tinplate.

A number of observations were incomplete in that one of the values was either missing or indeterminate.

The number of observations per sample varied between 12 (sample 1) and 2 (sample 12).

It can be seen that the following pairs of samples have identical characteristics: sample 1 and 3, sample 4 and 5, and samples 4 and 15. Hence, in the absence of further information, we might expect values within these pairs to be of similar magnitude. Note that results for an 18th sample were omitted from the analysis since they were atypical of other, unrecorded results for the same sample. Note also that values of (i) recorded as '>2' in sample 12 have been taken as missing, whilst values of (i) recorded as '>5' in samples 3 and 4 (one per sample) have been taken as 5.1 (5kN is in fact the limit of recordable failure load) for the purpose of the analysis.

Statistical analysis

The aim of the analysis was to determine whether the data, and hence the test method itself, show up differences between the samples with respect to either or both of the recorded values, and whether these differences can be 'explained' in terms of the tinplate characteristics detailed above.

A preliminary inspection of the data shows that there are, indeed, marked differences between the samples with respect to both failure load and percentage lacquer removed. Figures 1 and 2 also reveal, however, a considerable variation within many of the samples, expecially regarding failure load, and that this variation is frequently comparable in magnitude to the differences between samples. Further, there is a distinct lack of agreement between samples 1 and 3 and between samples 4 and 5 in terms of observed failure loads, which is unfortunate since these pairs of samples have identical tinplate characterisations (see above). [Note that similar comparisons with regard to percentage lacquer removed are impossible since values of this parameter were not recorded for either of samples 3 and 4]. This may, of course, be due to differences between the samples of which the author is unaware.

Statistical analysis of the data consisted on an attempt to fit, to a suitably transformed version of each recorded variable in turn, a series of linear models 'explaining' the between-sample variation in terms of the three factors described above. An example of such a model would be

$$Y_{ijk} = \mu + t_i + l_j + \varepsilon_{ijk}$$

where Y_{ijk} denoted the (transformed) recorded variable

μ denotes the grand mean

t_i denotes an 'effect' due to the i^{th} tinplate type

l_j denotes an 'effect' due to the j^{th} lacquer, and

ε_{ijk} denotes a random error term

For brevity, such a model will be written y = f(T,L) in an obvious notation. Note that the 'maximal model for either variable (other than fitting the data to itself!) would be y = f(SAM), representing one in which the observed values are estimated by the corresponding sample mean. [Because of the limited number of samples compared with the number of different possible combinations of the three factors (= 5 x 6 x 4 = 120) the addition of terms in T, S and L to the 'null' model should produce a rapid convergence in deviance towards that of the maximal model].

The transformed versions of the recorded variables were $\log_e$ (failure load) and arcsine $\sqrt{\text{(percentage lacquer removed/100)}}$ respectively. The former was chosen in view of the apparent positive skewness of the failure load data (whilst the latter, known as the angular transformation, is often used where the raw data is a proportion, so that the range of values of the parameter changes from [0,1] to $[0,\pi/2]$). Analysis of the data was performed using the GLIM statistics package.

Referring first to models in which y denotes the transformed failure load, the maximal model (y = f(SAM)) explained a mere 51% of the variation about the mean (R^2 = 0.51) as found in the null model (y = f(-)). In other words, roughly half the variability in the transformed failure loads occurs within samples! Between these two extremes the model y = f(L) gave an R^2 value of 0.29 and the model y = f(T) an R^2 of 0.16. Hence although these models point to the existence of systemmatic differences in (transformed) failure loads between different lacquers and different tinplate types respectively they cannot be regarded as having any predictive value.

Values of the transformed failure load, together with the fitted values under models y = f(SAM) (the sample means), y = f(L), and y = f(T), are shown in Figure 1.

Most success in terms of model fitting was achieved using transformed percentage lacquer removed as the y variable. This time the maximal model explained some 72% of the variation about the mean (R^2 = 0.72) as found in the null model, indicating that less than one-third of the variability in the transformed variable occurs within samples. Between these two, the model y = f(S,L) gave an R^2 value of 0.51, and the model y = f(T,S,L), obtained by the addition of a 'T' term, gave an R^2 value of 0.58. These simple 'additive' models point to the presence of systemmatic differences between samples with respect to each of the factors considered, although again one would hesitate to put forward either model for predictive purposes. Values of the transformed percentage lacquer removed, together with the fitted values under modesl y = f(SAM) (the sample means), y = f(S,L), and y = f(T,S,L), are shown in Figure 2.

Finally, it should be noted that the (univariate) analysis of the data described above does not, indeed cannot, take account of the 'bivariate' nature of the observations, and, in particular, of possible correlation between failure load and percentage lacquer removed. The plots of failure load against percentage lacquer removed do not suggest any consistent relationship between the two variables across the different samples. Nevertheless, it remains true that attempts to explain differences between the samples should be made in terms of failute load and percentage lacquer removed <u>jointly</u> instead of separately. In lieu, therefore, of any formal analysis towards this end, Figures 3-5 present plots of transformed

failure load against transformed percentage lacquer removed showing differences between different tinplate types, different stoving conditions, and different lacquers, respectively.

Conclusions

In conclusion, I would say that the bond strength test is capable of showing up differences between different tinplate samples, particularly with respect to percentage lacquer removed, but that the considerable within-sample variability in the data presents a serious practical drawback to its implementation for all but the crudest comparison.

Figure 1

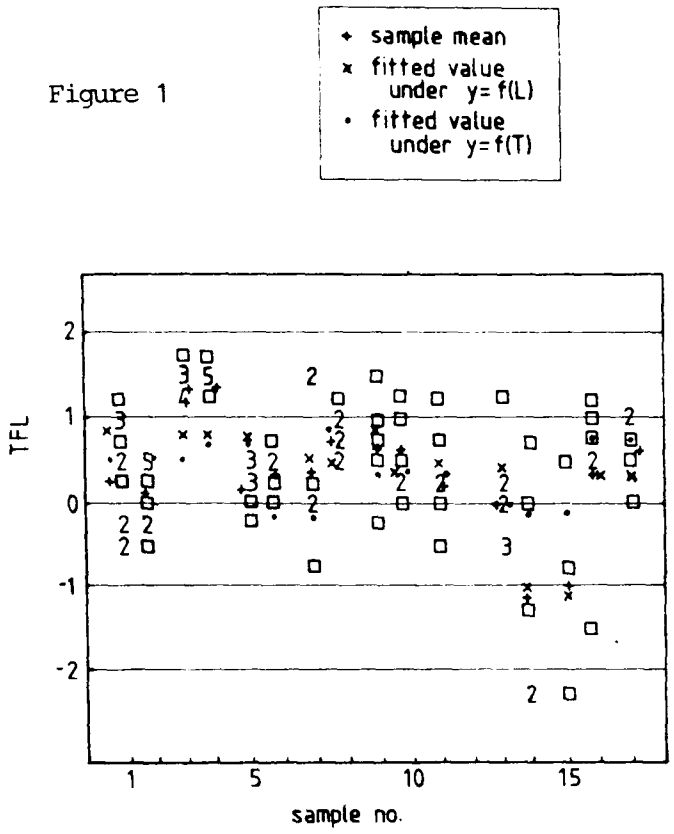

Figure 2

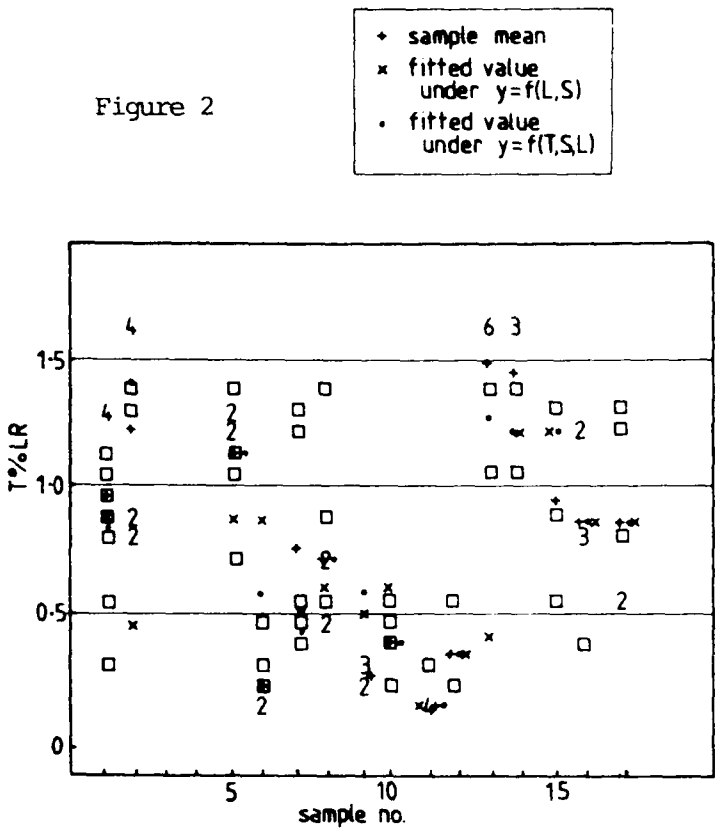

9

0.69

Figure 3

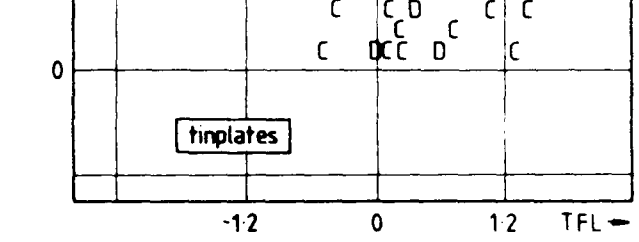

Figure 4

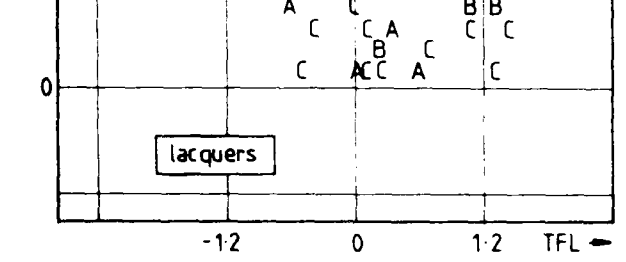

Figure 5

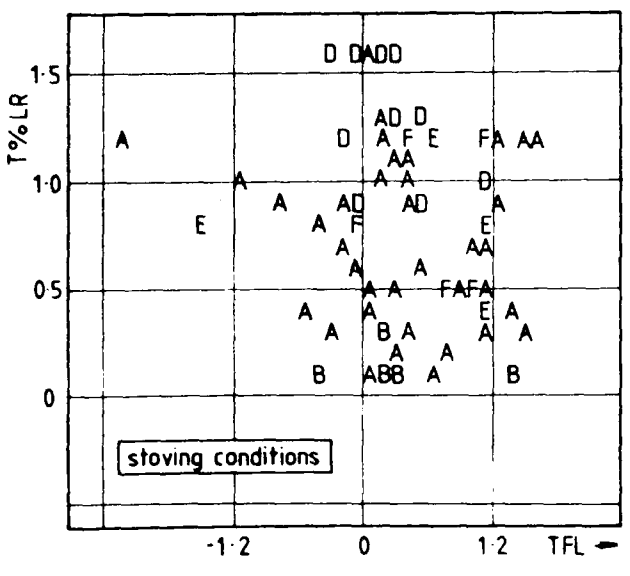

Fitted values corresponding to the models described in the text

I. $y = \log_e$ (failure load)

a) Model y = f(SAM) (sample means)

Sample No.	1	2	3	4	5	6	7	8	9
Fitted value	0.355	0.157	1.349	1.409	0.249	0.371	0.440	0.857	0.69

Sample value	10	11	12	13	14	15	16	17
Fitted value	0.567	0.283	-	-0.004	-1.039	-0.888	0.404	0.613

b) Model y = f(L)

Lacquer 'level'	1	2	3	4
Fitted value	0.767	0.391	0.469	-0.982

c) Model y = f(T)

Tinplate type 'level'	1	2	3	4	5
Fitted value	0.554	0.744	0.343	-0.177	0.857

II. y = arcsine $\sqrt{(\text{percentage lacquer removed}/100)}$

a) Model y = f(SAM) (sample means)

Sample value	1	2	3	4	5	6	7	8	9	10
Fitted value	0.972	1.222	-	-	1.135	0.254	0.762	0.729	0.283	0.408

Sample value	11	12	13	14	15	16	17
Fitted value	0.178	0.375	1.477	1.421	0.905	0.875	0.861

b) Model y = f(S,L)

Fitted value $\hat{y}_{jk}$ given by $\hat{y}_{jk} = \hat{\mu} + \hat{s}_j + \hat{l}_k$ where $\hat{\mu} = 1.476$ and

j,k =	1	2	3	4	5	6
$\hat{s}_j$ =	-0.249	-0.593	-0.397	0.475	0.014	0
$\hat{l}_k$ =	-0.351	-0.615	-0.705	0	-	-

continued....

c) Model $y = f(T,S,L)$

Fitted value $\hat{y}_{ijk}$ given by $\hat{y}_{ijk} = \hat{\mu} + \hat{t}_i + \hat{s}_j + \hat{l}_k$ where $\hat{\mu} = 1.749$ and

i,j,k =	1	2	3	4	5	6
$\hat{t}_i$ =	-0.219	0.087	-0.321	-0.476	0	-
$\hat{l}_k$ =	-0.656	-0.975	-0.783	0	-	-

APPENDIX 2

Electron Microscopy

1/ The Transmission Electron Microscope

The TEM is used in two basic modes for metallurgical examinations. These are:

1. diffraction
2. imaging

although diffracted beams are also used for image contrast as will be shown below.

The basic components of a transmission electron microscope are shown in figure 1. These are:

a) an electron source - usually a heated tungsten filament thermionically emitting electrons. Where extra brightness is required the source may be a LaB_6 filament or a field-emission needle. Emitted electrons are accelerated and focussed down the column.

b) Lenses. Magnetic lenses are widely used and are the most important component of the microscope. The design and operation of electron lenses has been treated in the literature (Hinch et al 1965, Hall 1953, Haine 1961).

The condenser lens focusses the beam onto the specimen. Magnification and focus of the image or diffraction pattern is achieved by the objective, intermediate and projector lenses.

c) viewing screen. This is a phosphor-coated screen which fluoresces under the electron beam and upon which the image or diffraction pattern is examined. It can be tilted to reveal a photographic plate or TV camera for recording.

d) vacuum system.

For crystalline solids an incident beam of electrons will be scattered according to the Bragg Law:

$$n\lambda = 2d\sin\theta$$

where d = interplanar spacing

θ = angle of incidence

Considering a set a crystal planes orientated at the Bragg angle in the microscope (fig. 2), then $R/L = 2\theta \sim \sin\theta$ for small angles and hence

$$Rd = \lambda L$$

where L is known as the camera length. R may be measured from the diffraction pattern and, knowing λ, d may be calculated. It is common to calibrate a microscope in terms of λL, the camera constant, using a crystal with known d spacings.

In imaging, a fundamental advantage over optical microscopy is gained from the much shorter wavelength of electrons compared to light, resulting in a great improvement in resolution.

Electrons accelerated by a potential difference of V volts will have a kinetic energy E where

$$E = \frac{1}{2} mv^2 = Ve$$

where e = electronic charge

m = electron mass

v = velocity

Since

$$mv = \frac{h}{\lambda}$$

where λ = wavelength

h = Plancks constant

then

$$\lambda = \frac{h}{(2meV)^{\frac{1}{2}}} = \frac{12.236}{V^{\frac{1}{2}}} \text{ Å}$$

In fact, for accelerating voltages $> 10^5$ V a relativistic correction is required so that

$$\lambda = \frac{12.236}{V^{\frac{1}{2}}(1 + 0.9788 \times 10^{-6} V)^{\frac{1}{2}}} \text{ Å}$$

The TEM work described in this thesis has been carried out at 100kV which produces an electron beam with a wavelength of 0.037 Å.

Using an optical analogy of a point source subtending half angle θ through a lens and focussed onto a plane, the diffraction limit to resolution indicated by the eiameter of the Airy disc is

$$D_A = \frac{1.22\lambda}{\alpha}$$

where α is the numerical aperture of the lens ($\alpha = \sin\theta$). D_A is referred to as Δr_d, the aperture diffraction aberration. In theory then, the resolution of a system is of the order of the wavelength for small values of θ. However, in practice the spherical aberration, Δr_s, given by

$$\Delta r_s = C_s \alpha^3$$

where C_s, the spherical aberration constant severely limits the resolution obtainable by an electron microscope. Unlike the optical case where large aperture lenses free from spherical aberration can be manufactured, the electron lens must be stopped down. Since the aperture diffraction increases with decreasing α whilst spherical aberration decreases, there is an optimum semi-aperture angle and minimum aberration given by

$$\alpha_{opt} = A\lambda^{\frac{1}{4}} C_s^{-\frac{1}{4}}$$

$$\Delta r_{min} = B\lambda^{\frac{3}{4}} C_s^{\frac{1}{4}}$$

A and B are constants with values of approximately unity; a modern high-resolution TEM can achieve point-to-point resolution of approximately 2 Å with the bonus of a large depth of field and depth of focus owing to the small aperture.

Chromatic aberration due to variations in the wavelength of the electrons are minimal since the stability of power supplies can now be ensured. However, there is an energy spread ΔE introduced by electrons interacting with the specimen which results in a disc of confusion, radius Δr_c, given by

$$\Delta r_c = C_c \alpha \frac{\Delta E}{E}$$

where C_c is the chromatic aberration constant.

i) Image formation

Figure 3 shows the ray paths in a TEM for specimen imaging. An important mechanism which degrades the image is astigmatism which occurs when the lens exhibits different focal lengths. Condenser lens astigmatism reduces the coherence of the beam while objective lens astigmatism causes streaking in the image which can usually be eliminated using electromagnetic stigmators. These produce a small controllable magnetic field which can be adjusted to correct the image. The procedure for alignment of the microscope and astigmatism correction is set out by Edington (1974).

Image contrast can be achieved in several ways. Diffraction contrast is obtained in crystalline specimens by selecting one or more diffracted beams (by use of a moveable aperture) and using this to form the image. Figure 4 shows the formation of a bright field image using the transmitted beam. The diffracted beams from regions in the crystal aligned at the Bragg angle are stopped and such regions will consequently appear darker on the micrograph. Dark field microscopy is used to highlight specifically diffracting areas in the specimen by using only the diffracted rays from those regions to form an image. One way to do this is to move the aperture

to collect the diffracted beam but this will produce an image of poor quality due to large spherical aberration and astigmatism when the electron path is distance from the optical axis. A better method is to tilt the illumination (fig. 5) so that the diffracted beam follows the optical axis. Dark field microscopy is useful in the examination of stripped passivation layers since it allows specific crystals in a crystalline matrix to be correlated with a diffraction pattern. Since the transmission of electrons through matter is a function not only of the electron energy but also the thickness and atomic number of the specimen, these two parameters can also create contrast in electron micrographs. Crystal imperfections such as dislocations or stacking faults produce contrast by the local distortions in the atomic lattice which lead to diffraction effects but these are discussed elsewhere (Hirsch et al 1965) as are the possible artefacts caused by electron-beam specimen interactions.

ii) Diffraction

Figure 6 shows the ray path for diffraction pattern formation. In the imaging mode both diffracted and directly transmitted beams are brought to a focus on the back focal plane of the objective lens. The next lens can then be used to form either an image or diffraction pattern. This is described by Agor (1961) and Philips (1960). It is of prime importance to be able to form a diffraction pattern from a specific area of the sample for which an aperture must be used, coplanar with the image. Diffraction patterns are recorded in the same way as images, usually on photographic plates for subsequent analysis although efforts are being made to automate the indexing and analysis of patterns using a TV camera and on-line microcomputer.

The kinematical theory and dynamical theory of electron diffraction are discussed by Hirsch et al (1965). These describe the

interaction of an electron beam with a period structure. The most convenient method of interpreting electron diffraction patterns is via the reciprocal lattice construction in which the diffraction spot corresponds to a crystal plane in reciprocal space.

For a randomly orientated set of polycrystals the diffraction pattern is seen as a series of concentric circles whereas a single crystal with a limited number of planes satisfying the Bragg condition for one particular exposure orientation produces a diffraction pattern consisting of a geometrical array of spots. The formation of the diffraction pattern and reciprocal lattice construction are thoroughly treated in the literature (Hirsch et al 1965, Nadrews 1967).

iii) The analysis of diffraction patterns

With an accurate knowledge of the camera constant λL, a single diffraction spot displaced R from the centre of the pattern may be related to a set of crystal planes with spacing d by

$$\lambda L = Rd$$

The calculated d spacings may then be compared with the more accurate X-ray diffraction data made available by ASTM. Values of d are not alone sufficient to identify a crystal which must also be indexed by assigning Miller indices (hkl) to the spots (and hence the diffracting crystal planes). There are equations which relate (hkl) to d and the unit cell dimensions; these equations become more complex as the crystal structure becomes complex. If there is a limited choice of possible crystal structures (known by chemical analysis or previous knowledge of the specimen) then the ASTM X-ray data can be scanned to find suitable candidates. The rings or spots can then be indexed using the formulae available (Andrews 1967) to confirm one particular compound. Certain arrangements of rings or

spots in the diffraction pattern are characteristic of certain crystal structures and indexed examples of the most common are available in the literature.

The interpretation of diffraction patterns from multiphase or imperfect specimens can become a formidable task but is not usually required in the examination of stripped passivation layers where discrete single or polycrystal areas are located on a thin, weakly-diffracting background.

2/ The Scanning Electron Microscope

The SEM utilises similar electron sources and lenses to the TEM but images are formed in a different manner. When an electron beam strikes a solid there is an emission of *inter alia* elastically scattered (backscattered) electrons with similar energies to the incident beam and inelastically scattered (secondary) electrons; these emitted electrons may be collected and used to form an image in the SEM.

Since the emitted electrons emanate from the surface of the sample the SEM can be used to image bulk specimens. The introduction of scanning coils into the electron-optical column allows the beam to be scanned in a raster across the specimen surface. The emitted electrons are collected and used to amplitude modulate the brightness on a TV display whose X and Y scans are in synchronisation with the electron beam scan. Thus, regions of high electron emission are seen as bright areas on the TV display.

Figure 7 shows the basic layout of a scanning electron microscope consisting of the following components:

a) electron source - as TEM except that maximum accelerating

voltages are usually 40 kV.

b) lens system - as TEM but fewer lenses are required and the specimen can be examined at a large distance from the objective lens (several cm).

c) electron detectors - the most common detector for secondary electrons is a scintillator disc connected to a photomultiplier via a light pipe. The low energy secondary electrons are attracted to the scintillator by a high voltage bias.

Backscattered electron detectors can also be of the scintillator type or solid-state semiconductor detectors.

d) specimen - the SEM can accommodate large bulk specimens in contrast to the TEM although thin-film specimens and transmitted electron detectors can also be used.

i) Image formation

Current scanning electron microscopes can achieve resolutions of about 2 nm. The resolution depends on lens aberrations as in TEM, and on the properties of the electron probe which is scanned across the surface, and on beam specimen interactions.

The main parameters associated with the probe are diameter of the spot, d, angular divergence, 2α, and and I, the electron current. These are related by the brightness equation:

$$I = B\, d^2\, (2\alpha)^2$$

where B is the source brightness and is typically 10^5 A cm^{-2} sr^{-1} for a W filament at 30 kV.

Typical values for the other parameters are:

d	10 nm to 10 μm
2α	10^{-3} to 10^{-2} rad
I	10^{-12} to 10^{-7} A

Beam spreading in the specimen will also reduce resolution although this can be minimised with thin specimens.

The image is usually formed by collecting the secondary or backscattered electrons in order to amplitude modulate the TV viewing screen. However, other beam-specimen interactions are used for image formation; these included light emission (cathodoluminescence), absorbed electron current and X-ray emission. Secondary electrons typically emanate from the top 10 nm of the specimen surface whereas backscattered electrons come from depths up to 500 nm. The former mode is most common and shows up topography very well whereas backscattered imaging will also reveal variations in atomic number owing to the elastic scattering effect. Using electronic manipulation these signals may be mixed and, more recently, digitised and enhanced.

Chemical Analysis in the SEM

A natural consequence of electron bombardment of solids is X-ray generation. The energies of these X-rays are characteristic of the specimen and may be used for elemental analysis in the energy-dispersive X-ray analyser (EDX) which is commonly fitted to electron microscopes. Another similar technique is wavelength dispersive analysis (WDX) using a crystal spectrometer which is described in the literature (Goldstein et al 1981).

The EDX spectrometer used a solid-state Si-Li detector positioned in the SEM work chamber close to the specimen. X-ray quanta are collected and measured and the data displayed, via a computer, as a graph of intensity vs. atomic number. EDX is a widely used analytical tool since it is rapid and easy to use, does not interfere with SEM operation and is relatively cheap; it is reviewed by Statham (1981).

The limitations of the technique are:

i. energy resolution - certain X-ray peaks may overlap and require deconvolution by hand or computer;

ii. only elemental and not bonding information is available;

iii. low Z materials are difficult to analyse without a special type of detector. Hence, oxygen and carbon are not shown in most EDX spectra.

iv. relatively low spatial resolution. Since the X-ray emission is typically from a volume of 1 μm diameter, signals from thin surface coatings are swamped by X-rays from the bulk specimen. Tilting may improve this but it is usually necessary to either strip the thin film and observe it separately or devise a series of calibrations and analysis routines to calculate coating thickness and composition using computer software.

Bibliography

Agar A.W. Br. J. Appl. Phys. 11 (1973) 185.

Andrews K.W., Dyson, D.J. and K ɔwn S.R. "Interpretation of Electron Diffraction Patterns" (1967) Hilger, London.

Edington J.W. "The operation and calibration of the electron microscope" (1974) MacMillan, London.

Goldstein J.I., Newbury D.E., Echlin P., Joy D.C., Fiori C. and Lifshin, E. "Scanning Electron Microscopy and X-ray Microanalysis" (1981), Plenum, New York.

Hall C.E. "Introduction to Electron Microscopy" (1953) McGraw-Hill, New York.

Haine M.E. "The Electron Microscope" (1961) Spon, London.

Hirsch P.B., Howie A., Nicholson R.B., Paschley D.W. and Whelan M.J. "Electron Microscopy of Thin Crystals" (1965), Butterworth, London.

Philips R. Br. J. Appl. Phys. 11 (1960) 504.

Statham P. J. Microsc. 123 Pt. 1 (1981).

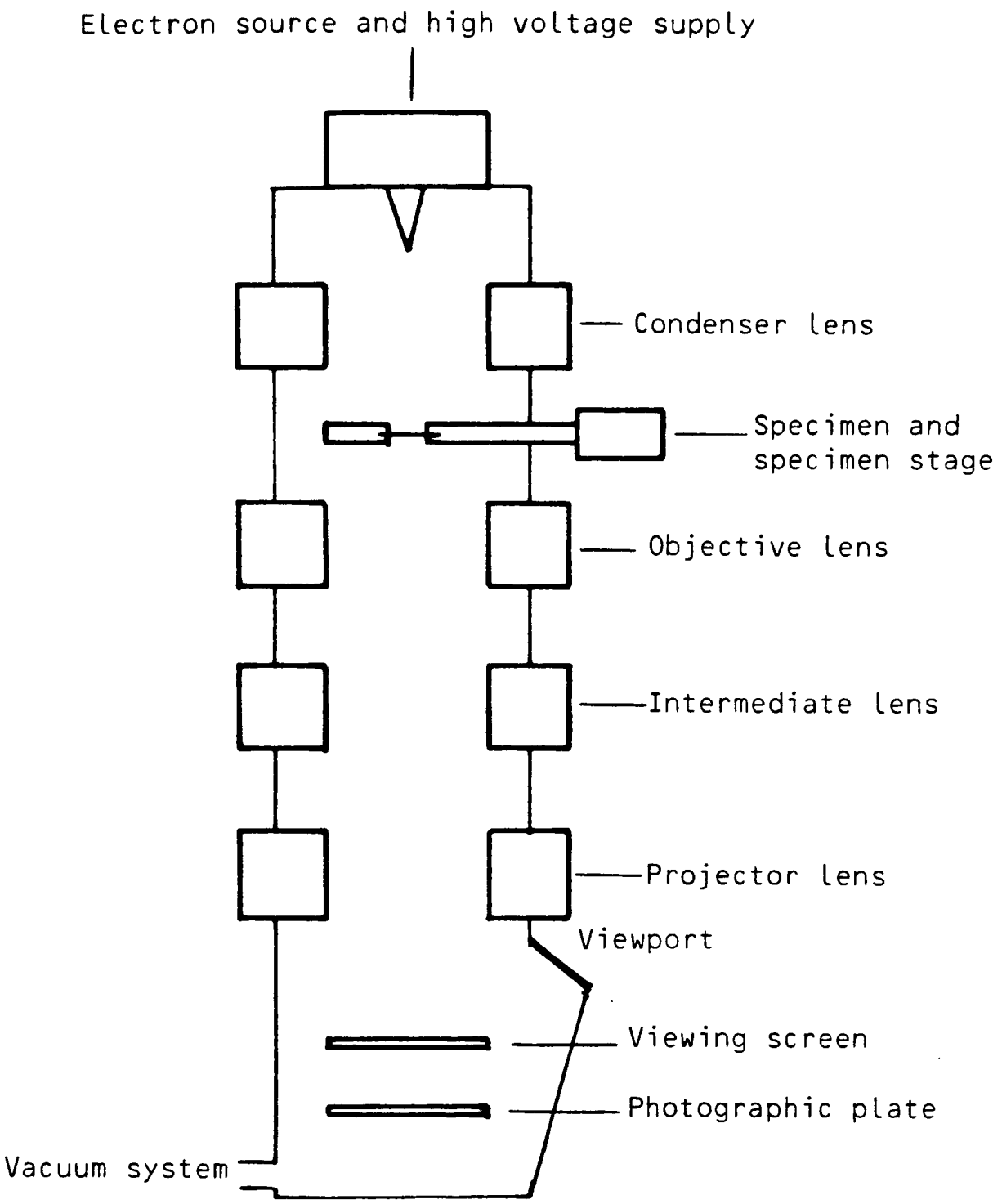

Figure 1. The basic components of a Transmission Electron Microscope

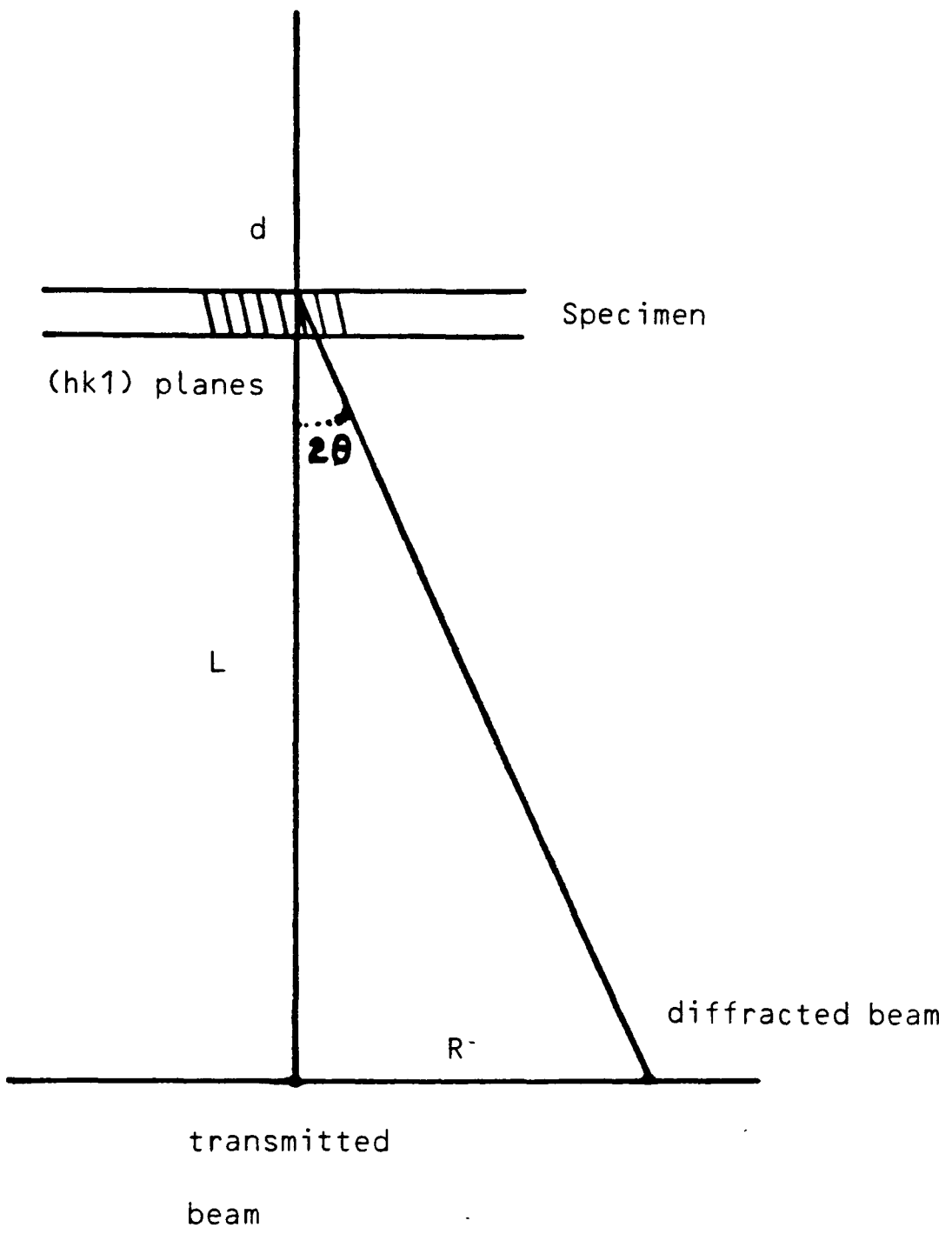

Figure 2. Electron diffraction showing schematically the magnification of the diffraction beam pattern by the microscope lens, where L is the camera length.

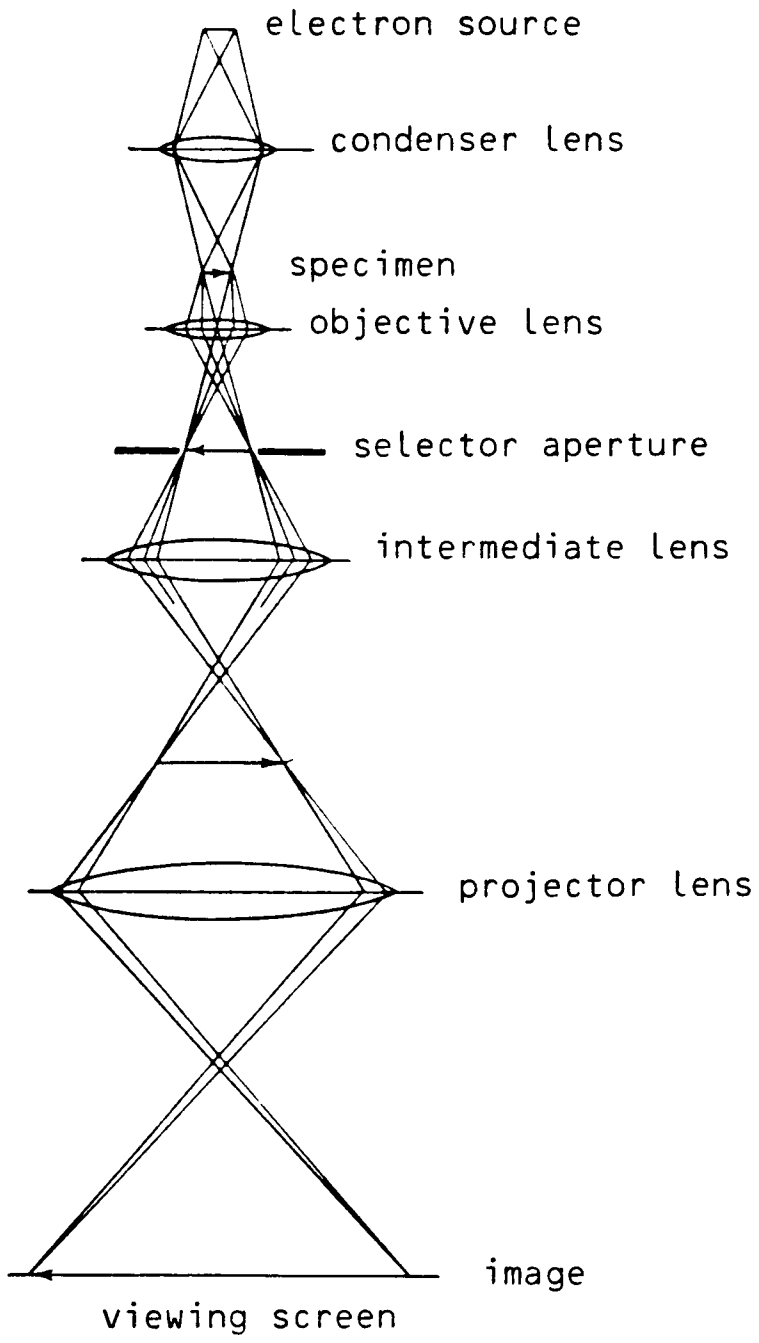

Figure 3. Ray paths for imaging

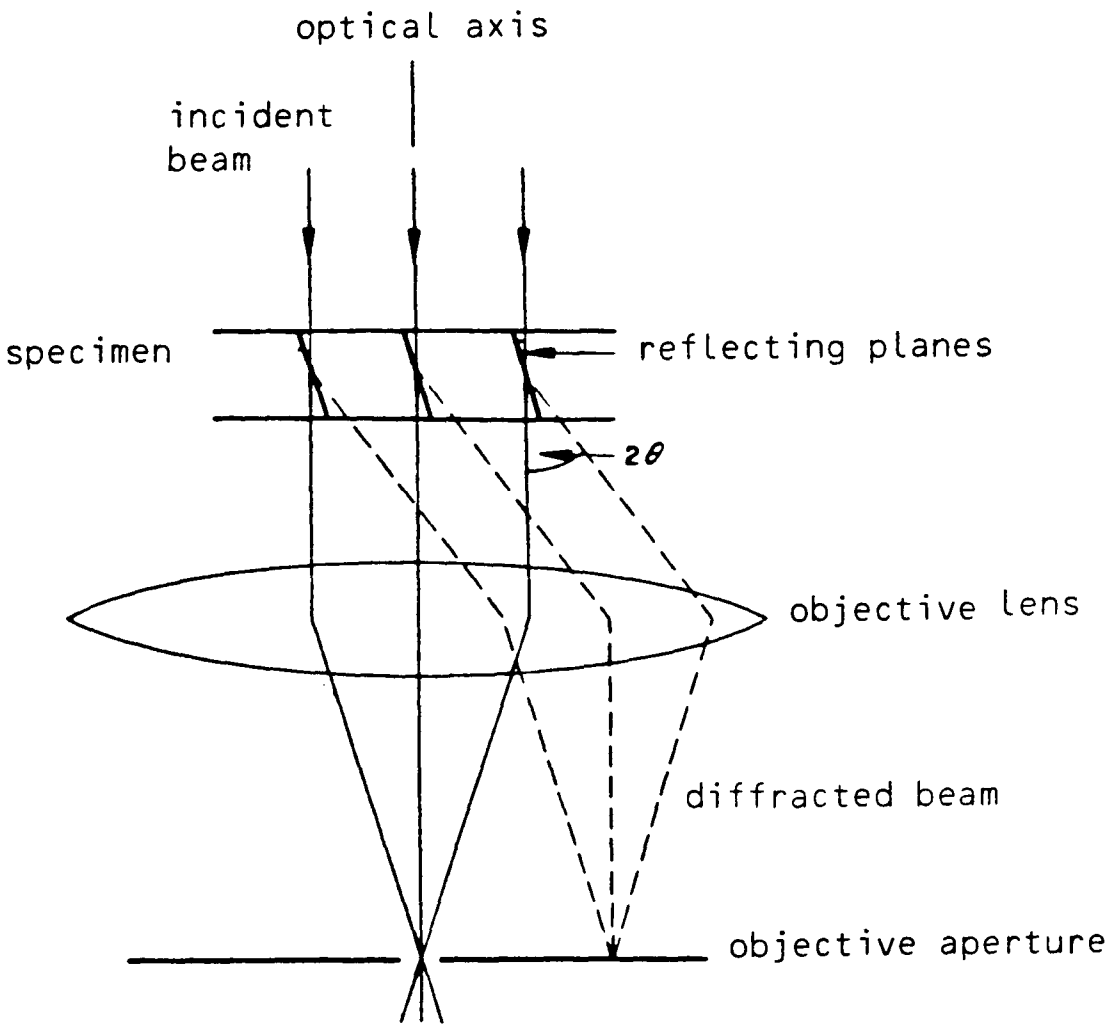

Figure 4. Bright Field Microscopy

The transmitted beam is used to form the image whilst the diffracted beam is stopped.

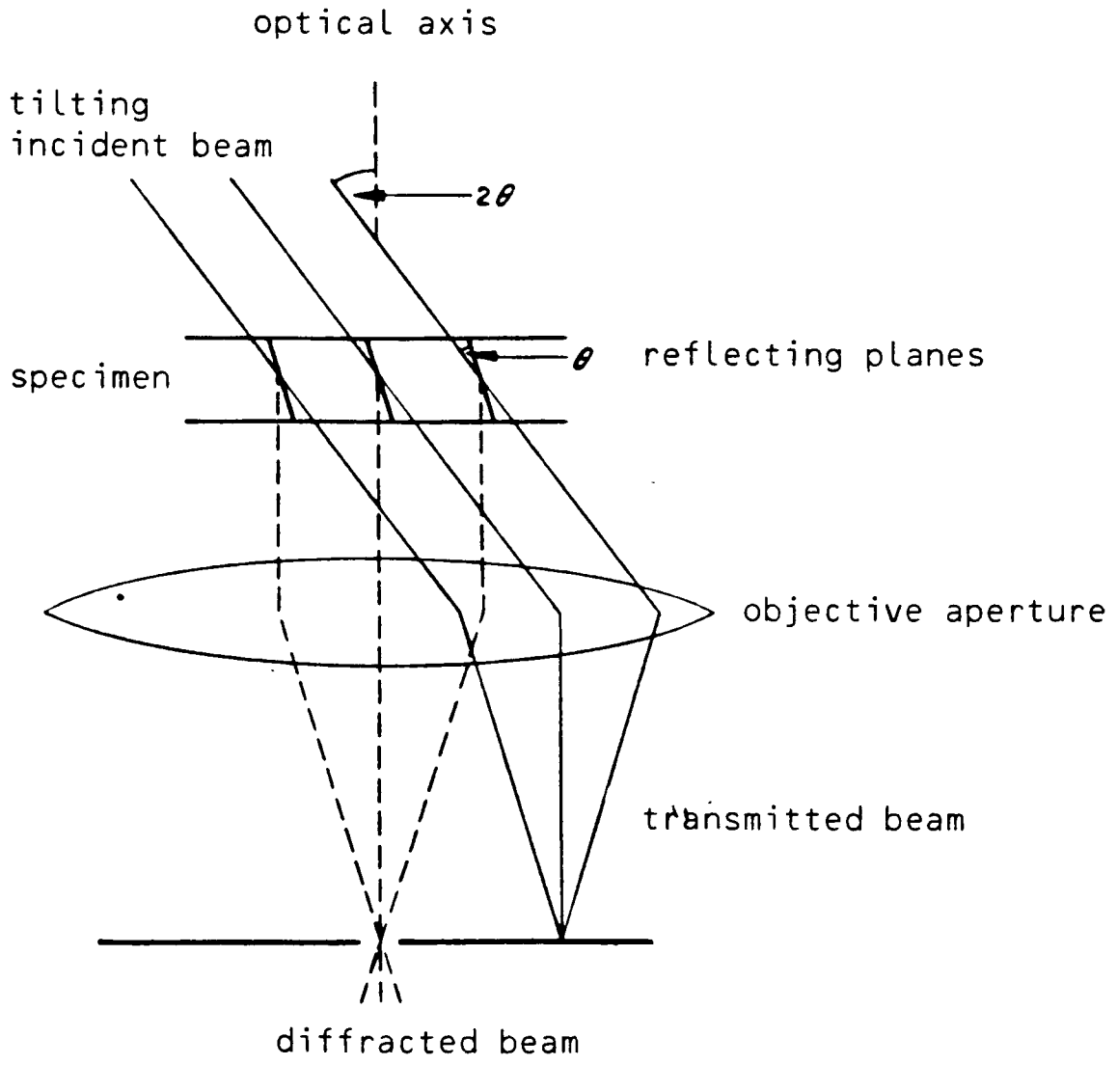

Figure 5. Dark Field Microscopy

The diffracted beam is allowed to pass through the objective aperture by tilting the illumination and is used to form an image. The transmitted beam is stopped.

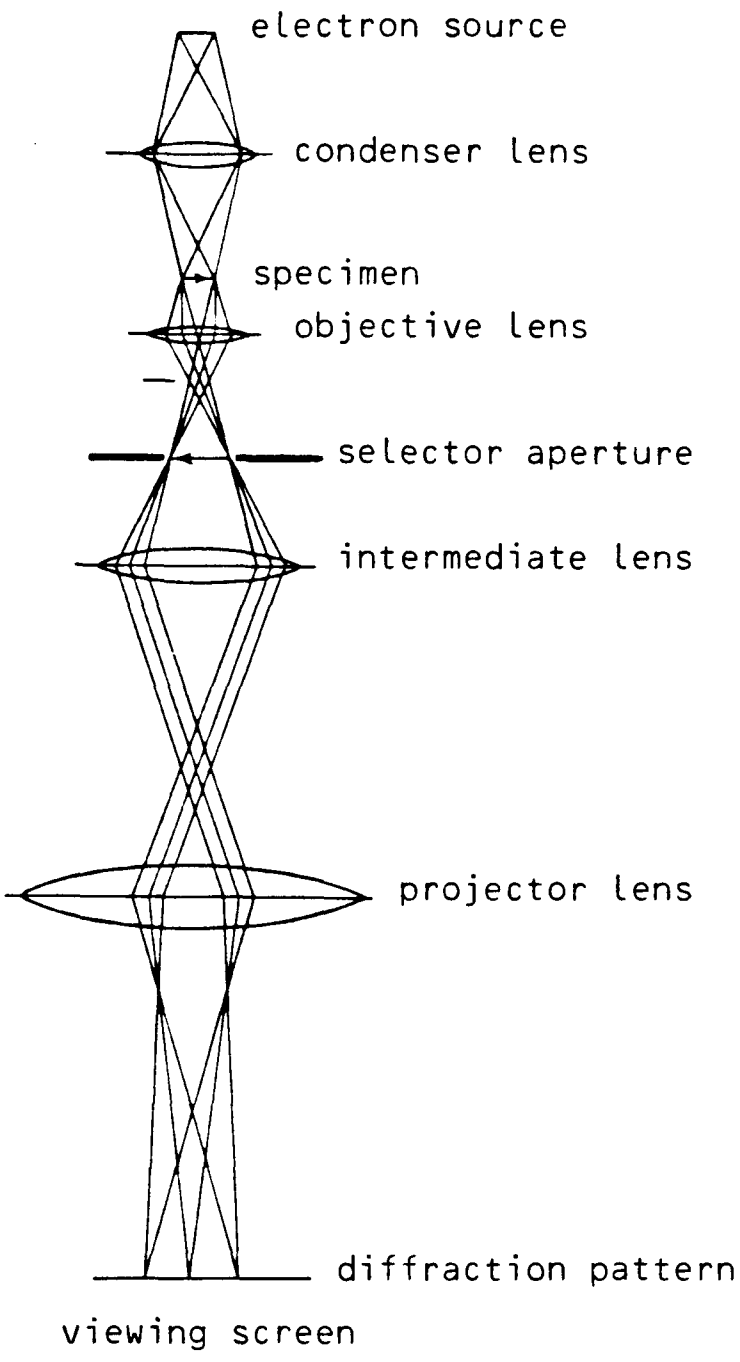

Figure 6. Ray paths for diffraction

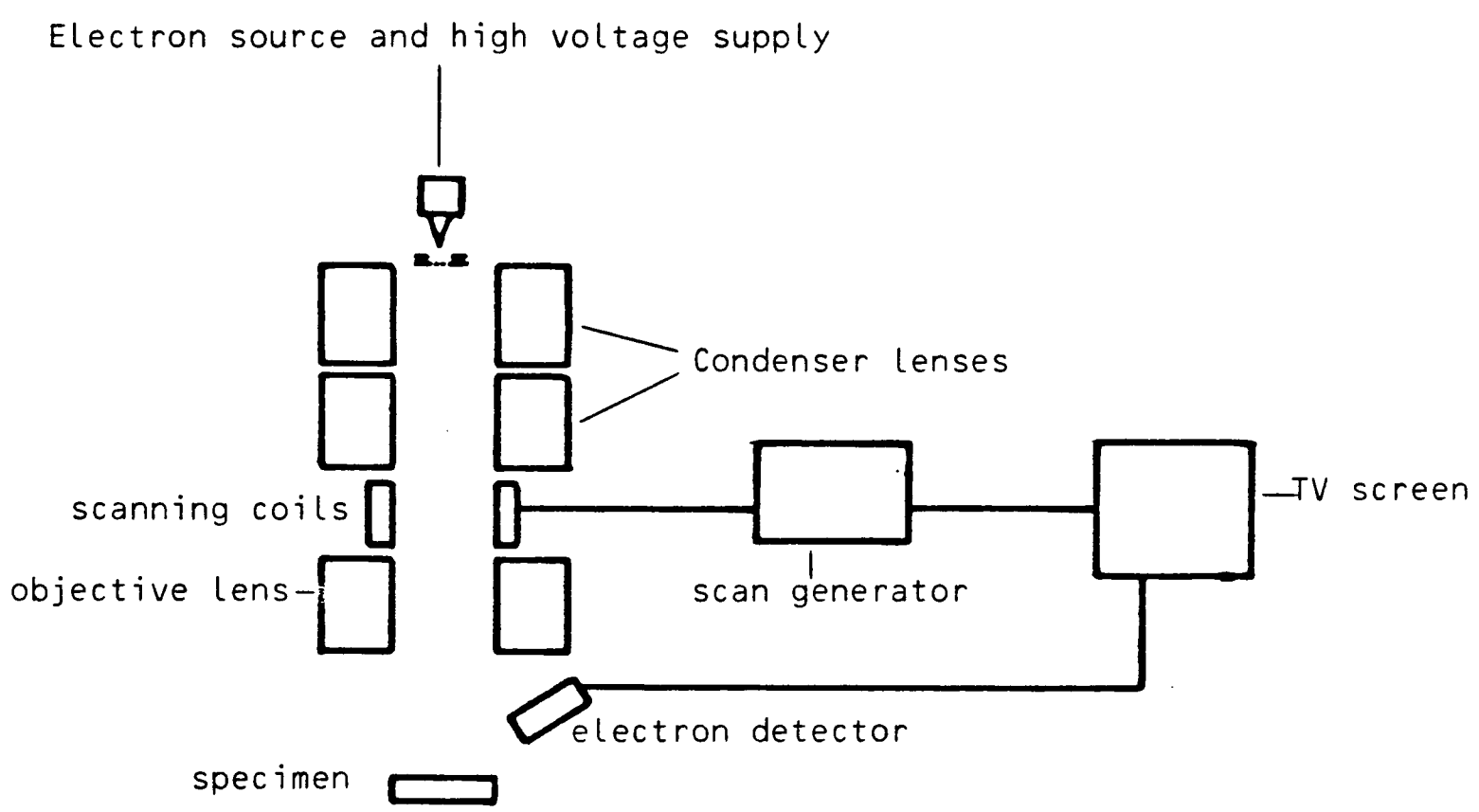

Figure 7. The basic components of a Scanning Electron Miscoscope

APPENDIX 3

ASTM X-ray powder diffraction data

6-0694

d	2.04	1.18	0.91	2.0390	Cr
I/I$_1$	100	39	31	100	Chromium

Rad. Cu λ 1.5405 Filter Dia.
Cut off Coll.
I/I$_1$ d corr. abs.?
Ref. Swanson et al., NBS Circular 539 Vol V (1955)

Sys. Cubic (s.c.) S.G. O_h^9 - Im3m
a_o 2.8839 b_o c_o A C
α β γ Z 2
Ref. Ibid.

εα nωβ εγ Sign
2V Dx 7.900 mp Color
Ref.

Spect. anal. of sample: <0.1% Si; 0.01% Cu, Mn, Sn; <0.001% Ag, Fe.
Hydrogen annealed; cooled in helium.
X-ray pattern at 25°C

Replaces 1-1290, 1-1851, 1-1861

d Å	I/I$_1$	hkl	d Å	I/I$_1$	hkl
2.0390	100	110			
1.4419	16	200			
1.1774	39	211			
1.0195	17	220			
0.9120	31	310			
0.8328	6	222			

19-323

d	2.05	1.87	2.30	2.30	(Cr)8C
I/I$_1$	100	80	60	60	Chromium

Rad. MoKα λ 0.7107 Filter Zr Dia. 57.3mm
Cut off I/I$_1$ Visual
Ref. Kimoto and Nishida, J. Phys. Soc. Japan, 22 744 (1967)

Sys. Cubic S.G. Pm3 (200)
a_o 4.588 b_o c_o A C
α β γ Z 8 Dx
Ref. Ibid.

εα nωβ εγ Sign
2V D mp ° Color
Ref. Ibid.

*Transforms to b.c.c. at 450°C (probably metastable at ~ 20°C).
Produced by evaporation and condensation of Cr in high purity (99.9%) argon at low pressures.

d A	I/I$_1$	hkl	d A	I/I$_1$	hkl
2.300	60	200			
2.049	100	210			
1.873	80	211			
1.611	10	220			
1.441	80	310			
1.387	10	311			
1.327	30	222			
1.274	40	320			
1.226	50	321			
1.145	35	400			
1.022	40	420			
1.002	40	421			
0.9786	20	332			
.9110	40	500			
.8533	40	520			
.8348	30	521			
.8118	30	440			
.7877	10	530			
.7697	40	531			
.7460	30	611			

28-370

28-371

d	3.27	8.42	6.25	8.42	Cr_3O_8
I/I$_1$	100	90	80	90	Chromium Oxide

Rad. CrKα λ 2.2909 Filter Dia.
Cut off I/I$_1$ Visual I/Icor.
Ref. Dismukes et al., Ind. Eng. Chem. Prod. Res. Develop., 10 319-29 (1971)

Sys. S.G.
a_o b_o c_o A C
α β γ Z Dx
Ref.

εα nωβ εγ Sign
2V D mp Color
Ref.

To replace 7-247.

d A	I/I$_1$	d A	I/I$_1$	d A	I/I$_1$
8.42	90	2.800	60		
6.52	10	2.745	60		
6.25	80	2.575	40		
5.93	80	2.455	10		
5.41	5	2.342	10		
4.97	40	2.246	10		
4.68	20	2.174	60		
4.44	10	2.140	60		
4.20	40	2.101	10		
4.10	50	2.087	10		
4.01	5	1.955	10		
3.89	30	1.922	5		
3.55	40	1.898	10		
3.49	60	1.655	10		
3.45	70	1.804	10		
3.27	100	1.674	10		
3.13	60	1.645	10		
3.08	30	1.634	60		
3.02	10	1.626	60		
2.875	5				

3-254

d	2.59	2.04	1.90	2.82	CrO
I/I$_1$	100	30	30	10	Chromium (II) Oxide

Rad. CoKα λ Filter Dia.
Cut off I/I$_1$
Ref. Luz, Z. Anorg. Chemie 257 73-78 (1948)

Sys. S.G.
a_o b_o c_o A C
α β γ Z Dx
Ref.

εα nωβ εγ Sign
2V D mp Color
Ref.

d Å	I/I$_1$	hkl	d Å	I/I$_1$	hkl
2.82	10				
2.59	100				
2.44	10				
2.26	10				
2.04	30				
1.90	30				
1.77	10				

18-390

d	3.51	3.61	2.67	6.01	Cr_2O_{12}
I/I$_1$	100	60	60	20	Chromium Oxide

Rad. CuKα$_1$ λ 1.5405Å Filter Dia. Guinier
Cut off I/I$_1$ Visual
Ref. Wilhelmi, Acta Chem. Scand. 19, 1, 165-76 (1965)

Sys. Orthorhombic S.G. Pbcm (60)
a_o 12.64Å b_o 8.21 c_o 8.18 A C
α β γ Z 4 Dx 3.67
Ref. Ibid.

εα nωβ εγ Sign
2V D 3.68 mp Color
Ref. Ibid.

d A	I/I$_1$	hkl	d A	I/I$_1$	hkl
6.01	20	200	2.348	20	322
5.21	80	111	2.223	20	511
4.10	20	020	2.177	10	331
4.08	20	002	2.122	10	223
3.87	10	102	2.088	10	422
3.67	40	021	2.051	10	040
3.61	60	310	2.046	10	004
3.51	100	121	2.011	20	512
3.50	20	112			
3.38	40	202			
3.29	20	311			
3.13	10	221			
2.861	20	302			
2.814	20	122			
2.670	60	411			
2.535	40	131			
2.528	40	113			
2.422	20	402			
2.382	40	231			
2.374	20	213			

6-0532

d	2.52	1.48	2.95	2.95	*
I/I$_1$	100	60	40	40	Chromium Ic Oxide (cubic)

Rad. MoKα λ Filter
Dia. Cut off Coll.
I/I$_1$ d corr. abs.?
Ref. Laubengayer and McCune, J.Am.Chem.Soc. 74 2362-4 (1953)

Sys. Cubic S.G.
a_o 8.36 b_o c_o A C
α β γ Z
Ref. Ibid.

εα nωβ εγ Sign
2V D mp Color
Ref.

*Formula could not be determined by analysis because specimen contained CrOOH in addition to the cubic oxide.

d Å	I/I$_1$	hkl	d Å	I/I$_1$	hkl
2.95	40	220**			
2.52	100	311			
2.09	40	400			
1.707	80	422			
1.610	40	511,333			
1.478	60	440			
1.277	80	533			
1.088	80	731,553			
0.8075	80	951,773			

**Indexed by editorial staff

12-559

d	2.58	1.66	1.43	4.78	Cr_3O_6
I/I$_1$	100	90	80	40	Chromium Oxide

Rad. ? λ Filter Dia.
Cut off I/I$_1$ Visual
Ref. Hilty, Fongeng and Folkman, Met. Soc. AIME (Trans.) 203 253 (1955)

Sys. Tetragonal* (p.c.) S.G.
a_o 8.72 b_o c_o 7.50 A C 0.86
α β γ Z Dx
Ref. Ibid.

εα nωβ εγ Sign
2V D mp Color
Ref

*Distorted spinel type. A smaller b. c. unit cell can be selected a_o=6.16, c_o=7.50

d Å	I/I$_1$	hkl	d Å	I/I$_1$	hkl
4.78	40	111			
3.05	30	220			
2.86	40	202			
2.58	100	131			
2.39	20	222			
2.34	10	113			
2.16	60	400			
1.90	20	004			
1.725	30	242			
1.655	90	151			
1.590	20	333			
1.528	60	440			
1.432	80	404			
1.348	10	602			
1.287	30	262			
1.280	50	353			
1.217	10	335			

16-817

d	4.58	4.87	3.34	4.87	$Cr(OH)_3$
I/I$_1$	100	55	55	55	Chromium(III) Hydroxide

Rad. CuKα$_1$ λ 1.5405 Filter Dia. 114.6mm Guinier Camera
Cut off 50A I/I$_1$ Photometer
Ref. deWolff, Techn. Phys. Dienst, Delft, Holland

Sys. Hexagonal S.G.
a_o 5.288 b_o c_o 4.871 A C 0.920
α β γ Z 2 Dx 2.897
Ref. Ibid.

εα nωβ εγ Sign
2V D mp Color
Ref

Sample prepared at Chemistry Dept., T.U. Delft.
Baverite-type

d Å	I/I$_1$	hkl	d Å	I/I$_1$	hkl
4.87	55	001			
4.58	100	100			
3.34	55	101			
2.437	4	002			
2.321	18	111			
2.151	12	102			
2.070	10	201			
1.791	16	210			
1.731	6	210			
1.668	12	202			
1.631	6	211			
1.528	4	300			
1.458	2	301			
1.411	2	212			
1.385	4	113			
1.326	4	220,203			

9-332

d	3.11	1.63	2.42	3.11	CrO_2
I/I$_1$	100	75	60	100	Chromium Di Oxide

Rad. CuKα λ 1.5418 Filter Ni Dia. 114.6mm
Cut off I/I$_1$ Densitometer
Ref. Thamer et al., J. Am. Chem. Soc. 79 547-50 (1957)

Sys. Tetragonal S.G. D_{4h}^{14} - $P4_2/mnm$
a_o 4.421 b_o c_o 2.916 A C
α β γ Z D_x
Ref. Ibid.

ε α nωβ εγ Sign
2V D mp Color
Ref.

Replaces 7-246

d Å	I/I$_1$	hkl	d Å	I/I$_1$	hkl
3.114	100	110	0.8718	10	213
2.424	60	101	.8479	5	332
2.207	10	200	.8460	15	431,501
2.126	20	111	.8183	< 5	422
1.976	10	210	.8113	5	303
1.634	75	211	.7901	10	521
1.562	25	220			
1.457	15	002			
1.398	15	310			
1.322	10	112			
1.316	25	301			
1.219	< 5	202			
1.130	10	321			
1.104	5	400			
1.067	10	222			
1.042	5	330			
1.008	20	312			
0.9889	< 5	420			
.9501	< 5	103			
.8812	< 5	402			

6-0504

d	2.67	2.48	1.67	3.633	Cr_2O_3
I/I$_1$	100	96	90	74	Chromium (III) Oxide

Rad. Cu λ 1.5405 Filter
Dia. Cut off Coll.
I/I$_1$ d corr. abs.?
Ref. Swanson et al., NBS Circular 539 Vol. V(1955)

Sys. Hexagonal S.G. D_{3D}^6 - $R\bar{3}c$
a_o 4.954 b_o c_o 13.584 A C
α β γ Z 6
Ref. Ibid.

ε α nωβ εγ Sign
2V D:5.23 mp Color
Ref.

Sample from Johnson, Matthey and Co. Ltd.
Spect. anal.: <0.001 % Ca, Mg <0.0001 % Si, Cu.
X-ray pattern at 26°C. Fe_2O_3 structure type.

Replaces 1-1294, 2-1362, 3-1124, 4-0765

d Å	I/I$_1$	hkl	d Å	I/I$_1$	hkl
3.633	74	012	0.9370	12	410
2.666	100	104	.8957	14	1.3.10
2.480	96	110	.8883	7	3.0.12
2.264	12	006	.8658	23	416
2.176	38	113	.8425	8	4.0.10
2.048	9	202	.8331	11	1.0.16
1.8156	39	024	.8263	9	330
1.672	90	116	.7977	15	3.2.10
1.579	13	122			
1.465	25	214			
1.4314	40	300			
1.2961	20	1.0.10			
1.2398	17	220			
1.2101	7	306			
1.1731	14	128,312			
1.1488	10	0.2.10			
1.1239	10	134			
1.0874	17	226			
1.0422	16	2.1.10			
0.9462	13	324			

XXIX

7-267

d	3.44	3.34	3.08	11.8	Cr_nO_n (55.2 wt. % Cr)
I/I$_1$	100	80	80	70	Chromium Oxide

Rad. Cu λ 1.542 Filter Ni Dia. 114.6mm
Cut off I/I$_1$ Visual estimate
Ref. Schwartz, Fankuchen and Bard, J.Am.Chem.Soc. 74 1676-7 (1952)

Sys. S.G.
a_o b_o c_o A C
α β γ Z D_x
Ref.

ε α nωβ εγ Sign
2V D mp Color Black
Ref

d Å	I/I$_1$	hkl	d Å	I/I$_1$	hkl
11.8	70		1.511	20	
6.19	50		1.351	20	
5.44	50				
4.95	30				
4.49	30				
3.88	100				
3.72	70				
3.34	80				
3.21	50				
3.08	80				
2.95	30				
2.81	20				
2.67	30				
2.60	30				
2.13	20				
2.01	20				
1.939	20				
1.856	20				
1.718	20				
1.659	20				

32-285

32-286

d	3.44	4.19	3.38	4.28	CrO_3
I/I$_1$	100	90	64	19	Chromium Oxide

Rad. CuKα$_1$ λ 1.540598 Filter Mono. Dia.
Cut off I/I$_1$ Diffractometer I/I cor. 1.41 (13)
Ref. Nat. Bur. Stand. (U.S.) Monogr. 25, Sec. 17, 25 (1980)

Sys. Orthorhombic S.G. Ama2 (40)
a_o 5.7494 (15) b_o 8.556(2) c_o 4.7961(11) A 0.67197 C 0.56055
α β γ Z 4 D_x 2.815
Ref. Ibid.

ε α nωβ εγ Sign
2V D mp Color Dark reddish brown
Ref. Ibid.

The sample was from J. T. Baker Chemical Company, Phillipsburg, New Jersey, USA.
Si used as internal standard (a_o = 5.43088Å).
CAS #1333-82-0.
P_{30} = 50.8(0.016,32).
$\sigma(I/I_o)$ = ±5.
To replace 9-47.

d A	I/I$_1$	hkl	d A	I/I$_1$	hkl
4.28	19	020	1.5954	2	042
4.19	90	011	1.5706	3	013
3.435	100	120	1.5512	1	151
3.383	64	111	1.5380	2	142
2.874	44	200	1.5159	4	113
2.454	4	031	1.5097	4	331
2.368	17	002	1.4366	6	400
2.370	18	211	1.4262	3	060
2.255	18	131	1.4124	4	322
2.139	2	040	1.4062	6	251
2.091	2	022	1.3956	3	242
2.006	8	140	1.3795	5	213
1.9658	10	122	1.3555	6	133
1.8657	2	231	1.2773	2	260
1.8424	5	202			
1.7491	10	320			
1.7435	11	311			
1.7167	5	240			
1.6921	3	222			
1.6112	3	051			

FORM M-8

311

7-195

d	3.38	2.89	2.66	3.38	β-SnO
I/I$_1$	100	90	90	100	BETA TIN (II) OXIDE

Rad. A Filter Dia.
Cut off I/I$_1$
Ref. GEISER AND WILLIGAN, J. PHYS. CHEM. 36 3042 (1932)

Sys. S.G.
a$_o$ b$_o$ c$_o$ A C
α β γ Z Dx
Ref.

ε α n_ω β γ Sign
2V D mp Color
Ref.

d Å	I/I$_1$	hkl	d Å	I/I$_1$	hkl
3.38	100				
2.99	50				
2.92	50				
2.88	90				
2.66	90				
2.08	10				
2.02	40				
1.767	80				
1.675	20				
1.595	20				
1.496	20				
1.414	20				
1.294	20				
1.201	20				
1.096	20				

6-0395

d	2.99	2.69	1.80	4.85	SnO
I/I$_1$	100	37	27	10	TIN (II) OXIDE

Rad. Cu λ 1.5405 Filter
Dia. Cut off Coll.
I/I$_1$ d corr. abs.?
Ref. SWANSON ET AL., NBS CIRCULAR 539 VOL IV P 28-9 (1953)

Sys. TETRAGONAL S.G. D_{4h}^7 - P4/nmm
a$_o$ 3.802 b$_o$ c$_o$ 4.836 A C
α β γ Z 2
Ref. IBID.

ε α > 2.0 n_ω β γ Sign
2V Dx 6.398 mp Color
Ref. IBID.

SAMPLE FROM THE BAKER CHEMICAL CO. SPECT. ANAL.: <0.01% CA, CU, FE, MG, SB, SI; <0.001% AL, BA, NI, PB.
X-RAY PATTERN AT 26°C.

REPLACES 1-0902, 1-0991

d Å	I/I$_1$	hkl	d Å	I/I$_1$	hkl
4.85	10	001	1.0766	6	312
2.989	100	101	1.0303	4	321
2.688	37	110	1.0201	3	204
2.418	14	002	0.9965	1	303
2.039	<1	102	.9852	1	214
1.901	13	200	.9674	<1	005
1.797	27	112	.9507	3	400
1.604	25	211	.9371	3	105
1.494	11	202	.9056	4	411
1.484	12	103	.8988	4	224
1.382	3	113	.8824	5	323
1.344	5	220	.8524	4	314
1.225	4	301	.8503	4	420
1.209	3	004	.8405	6	215,332
1.202	4	310	.8062	1	006
1.1747	6	222	.8020	<1	422
1.1697	8	213	.8002	1	413
1.1520	1	104			
1.1026	4	114			

XXX

14-140

d	2.82	3.55	3.00	6.02	5SnO.2H$_2$O
I/I$_1$	100	80	80	20	TIN(II) OXIDE HYDRATE

Rad. CuKα λ 1.5418 Filter Ni Dia. 11.64cm
Cut off I/I$_1$ VISUAL
Ref. DONALDSON AND MOSER, J. CHEM. SOC. (LONDON) 835 (1961)

Sys. S.G.
a$_o$ b$_o$ c$_o$ A C
α β γ Z Dx
Ref.

ε α n_ω β γ Sign
2V D mp Color
Ref.

d Å	I/I$_1$	hkl	d Å	I/I$_1$	hkl
6.02	20		1.568	50	
5.68	20		1.539	50	
5.01	10		1.503	20	
4.60	10		1.476	50	
3.55	80		1.427	10	
3.31	50		1.398	40	
3.00	80		1.341	20	
2.82	100		1.304	20	
2.52	40		1.282	10	
2.42	40		1.244	30	
2.29	30		1.207	10	
2.00	10		1.200	10	
1.94	50		1.188	80	
1.92	50		1.162	10	
1.83	30		1.149	10	
1.78	80		1.123	50	
1.77	30				
1.74	30				
1.67	50				
1.63	50				

160

13-111

d	3.12	1.86	2.78	5.56	(SnO)16O
I/I$_1$	100	60	40	10	TIN(II) OXIDE

Rad. CuKα λ 1.542 Filter Ni Dia. 11.64cm
Cut off I/I$_1$ VISUAL
Ref. DONALDSON, MOSER AND SIMPSON, J. CHEM. SOC. (LONDON) 830 (1961)

Sys. ORTHORHOMBIC S.G. PBCN (60)
a$_o$ 5.00 b$_o$ 5.72 c$_o$ 11.2 A 0.874 C 1.96
α β γ Z 8 Dx 5.63
Ref. IBID.

ε α n_ω β γ Sign
2V D 5.56 mp Color RED
Ref.

SINGLE CRYSTAL DATA TAKEN. STABLE IN AIR UP TO ABOUT 270°C.

d Å	I/I$_1$	hkl	d Å	I/I$_1$	hkl
5.56	10	002	1.239	20	
3.71	10	102	1.213	20	
3.56	30	111	1.183	20	
3.12	100	112	1.141	20	
2.86	20	020	1.095	30	
2.78	40	004	1.028	10	
2.50	30	200			
2.25	20	023			
1.994	10	024			
1.888	20	220			
1.857	60	204			
1.773	40	130			
1.681	30	223			
1.662	20	116			
1.610	20	133			
1.540	30	312			
1.429	40	040			
1.393	20	008,042			
1.342	10	043			
1.251	20	400			

29-1484

d	2.98	3.64	2.61	3.64	SnO_2 II
I/I1	100	30	25	38	Tin Oxide (High pressure modification)

Rad. A Filter Dia.
Cut off I/I1 Visual I/I cor.
Ref. Saito, K. et al., Mater. Res. Bull., 10 677 (1975)

Sys. Orthorhombic S.G.
a_0 4.714 b_0 5.727 c_0 5.214 A 0.823 C 0.910
α β γ Z 4 Dx 7.11
Ref. Ibid. V 140.8Å³

εα nωβ εγ Sign
2V D mp Color
Ref.

Synthesized at 800°C and 150 kbars.
C.D. cell: a_0 = 5.214, b_0 = 5.727, c_0 = 4.714, A = 0.9104, C = 0.8231.

d A	I/I1	hkl	d A	I/I1	hkl
3.64	30	110	1.191	S	241
2.984	100	111	1.141	S	313
2.861	S	020			
2.609	25	002			
2.508	20	021			
2.365	10	200			
2.120	15	112			
1.927	S	022			
1.819	S	220			
1.768	20	130			
1.749	25	202			
1.718	20	221			
1.568	15	113			
1.492	S	222			
1.486	10	023			
1.463	15	132			
1.455	15	311			
1.381	S	041			
1.257	S	223			
1.213	S	330			

29-1483

1662

20-1293

d	2.72	2.68	4.84	8.17	Sn_3O_4
I/I1	100	50	30	15	Tin Oxide

Rad. A Filter Dia.
Cut off I/I1 Visual
Ref. Lawson, Nature, 215 955-56 August 26, 1967

Sys. Triclinic S.G.
a_0 4.86 b_0 5.88 c_0 8.20 A C
α 93.00° β 93°21' γ 91°0' Z Dx
Ref. Ibid.

εα nωβ εγ Sign
2V D mp Color
Ref.

d A	I/I1	hkl	d A	I/I1	hkl
8.17	15	001			
4.84	30	01$\bar{1}$			
4.08	5	002,101			
3.30	25	012			
2.916	35	020			
2.827	15	02$\bar{1}$			
2.793	30	$\bar{1}$12			
2.778	5	1$\bar{1}$2			
2.721	100	003,021			
2.645	50	112			

1XXX

25-1259

d	3.30	2.83	2.72	8.2	Sn_2O_3 $SnO \cdot SnO_2$
I/I1	100	50	30	12	Tin Oxide

Rad CrKα λ 2.2909 Filter V Dia.
Cut off I/I1 Diffractometer I/I cor.
Ref. Marken and Trömel, Z. anorg. allgem. Chem., 397 117-26 (1973)

Sys. Triclinic S.G.
a_0 5.457 b_0 8.179 c_0 3.714 A 0.667 C 0.454
α 93.8° β 92.3° γ ~90° Z 2 Dx 5.73
Ref Ibid.

εα nωβ εγ Sign
2V D 5.90 mp Color
Ref. Ibid.

Formed by decomposition of SnO above 300°C.
To replace 18-1386.

d A	I/I1	hkl	d A	I/I1	hkl
8.2	12	010	1.885	1	221
5.48	<1	100	1.850	2	002
4.08	3	020	1.829	14	01$\bar{2}$
3.71	12	001	1.812	18	300
3.45	6	01$\bar{1}$	1.783	4	012
3.30	100	011	1.773	16	$\bar{3}$10
3.02	<1	101	1.743	25	041
2.829	50	02$\bar{1}$	1.724	6	02$\bar{2}$
2.773	25	111	1.703	3	231
2.715	30	200	1.649	12	022
2.446	20	$\bar{1}$30	1.633	1	050
2.430	20	$\bar{1}$21	1.574	2	03$\bar{2}$
2.255	12	03$\bar{1}$	1.562	1	12$\bar{2}$
2.247	12	20$\bar{1}$	1.553	<1	32$\bar{1}$
2.184	<1	21$\bar{1}$	1.846	4	21$\bar{2}$
2.137	1	031	1.525	1	321
2.067	1	$\bar{1}$31			
2.039	<1	040			
2.006	<1	$\bar{1}$31			
1.929	<1	230			

25-1260

24-1342

d	2.63	2.90	2.78	2.90	SnO (at 90K bars)
I/I1	100	80	80	80	Tin Oxide

Rad. MoKα λ 0.7107 Filter Dia.
Cut off I/I1 Visual
Ref. Serebryanaya et al., Soviet Phy. Dokl., 14 672 (1970)

Sys. Orthorhombic S.G. Pm2n (31)
a_0 3.82 b_0 3.61 c_0 4.30 A C
α β γ Z 2 Dx
Ref. Ibid.

εα nωβ εγ Sign
2V D mp Color
Ref.

d A	I/I1	hkl	d A	I/I1	hkl
2.90	80	101			
2.78	80	011			
2.63	100	110			
2.24	10	111			
2.12	10	002			
1.95	30	200			
1.80	10	020			
1.75	20	201			
1.66	50	021,112			
1.572	50	211			
1.521	50	121			
1.426	10	202			
1.382	20	022			
1.311	50	220			

24-1343

33-1374

d	2.84	2.47	1.74	2.84	SnO_2
I/I_1	100	70	60	100	Tin Oxide

Rad MoKa λ 0.710688 Filter Dia.
Cut off I/I_1 I/I cor.
Ref Liu, L., Science, 199 422 (1978)

Sys Cubic S.G.
a_0 4.925(5)* b_0 c_0 A C
α β γ Z 4 Dx
Ref. Ibid.

εα nωβ εγ Sign
2V D mp Color
Ref.

*Measured at room temperature, ~250 kbar.
X-ray diffraction patterns obtained in situ in a diamond-anvil pressure cell after laser heating and quenching.
On release of pressure, transition to α-PbO_2 form results in 8% volume change.
F_{16} = 11.7(0.0409,21).

d A	I/I_1	hkl	d A	I/I_1	hkl
2.642	100	111			
2.466	70	200			
2.211	10	201			
1.743	60	220			
1.483	60	311			
1.423	15	222			
1.226	5	400			
1.130	20	331			
1.101	20	420			
1.004	10	422			

33-1375

16-737

d	3.29	2.82	2.77	8.17	Sn_3O_4
I/I_1	100	80	50	5	Tin Oxide

Rad. CuKα λ 1.5405 Filter Dia. Monochromator
Cut off I/I_1 Visual
Ref. Gazzi, Ann. Chim. (Rome) 53 1503-6 (1963)

Sys. S.G.
a_0 b_0 c_0 A C
α β γ Z Dx
Ref.

εα nωβ εγ Sign
2V D mp Color
Ref.

d Å	I/I_1	hkl	d Å	I/I_1	hkl
8.17	5		1.519	40	
3.69	30		1.463	30	
3.44	5		1.424	10	
3.29	100		1.407	5	
2.818	80		1.391	10	
2.768	50		1.379	5	
2.711	50		1.357	5	
2.423	40		1.277	5	
2.237	30		1.215	5	
1.845	5		1.210	5	
1.822	40		1.198	5	
1.806	40		1.190	30	
1.767	30				
1.736	30				
1.731	5				
1.719	10				
1.644	40				
1.587	5				
1.570	5				
1.541	10				

175

21-1250

d	3.35	2.64	1.77	3.35	SnO_2
I/I_1	100	80	65	100	Tin Oxide (Cassiterite)

Rad. CuKα₁ λ 1.5405 Filter Ni Dia.
Cut off I/I_1 Diffractometer
Ref. Swanson and Tatge, NBS Circular, 539, 1, 56 (1955)*

Sys. Tetragonal S.G. P4/mnm (136)
a_0 4.738 b_0 c_0 3.188 A C 0.673
α β γ Z 2 Dx 6.995
Ref. Ibid.

εα nωβ εγ Sign
2V D mp Color White
Ref. Ibid.

*See Errata-National Bureau of Standards, Mono. 25, Sec. 5 (1967)
Sample from Johnson, Matthey and Co., Ltd.
Their spec. anal. showed no impurities greater than faint trace.
X-ray pattern taken at 26°C.

d A	I/I_1	hkl	d A	I/I_1	hkl
3.35	100	110	0.9505	8	402
2.644	80	101	.9291	4	510
2.369	25	200	.9143	4	332
2.309	6	111	.9081	8	501
2.120	2	210	.8819	8	422
1.765	65	211	.8814	6	303
1.675	18	220	.8480	6	521
1.593	8	002	.8375	2	440
1.498	14	310	.8261	4	323
1.439	18	112	.8125	2	530
1.415	16	301	.8026	6	512
1.322	8	202			
1.215	12	321			
1.184	4	400			
1.155	8	222			
1.117	4	330			
1.092	8	312			
1.081	8	411			
1.059	4	420			
1.036	4	103			

25-1303

25-1302

d	3.50	2.77	2.96	4.49	$Sn_6O_4(OH)_4$
I/I_1	100	90	80	3	Tin Oxide Hydroxide Hydromarchite

Rad. CuKα λ 1.5418 Filter Ni Dia. 114.6mm
Cut off I/I_1 Visual I/I cor.
Ref. Mandarino, Royal Ontario Museum, Toronto, Ontario, Canada

Sys. Tetragonal S.G. P4/mnc (128)
a_0 7.98 b_0 c_0 9.17 A C 1.1491
α β γ Z Dx
Ref. Howie and Moser, Am. Mineral., 58 552 (1973) (for synthetic material)

εα nωβ εγ Sign
2V D mp Color
Ref.

Sample from tin pannikin found at Boundry Falls, Winnipeg River, Ontario, Canada.
Cell dimensions calculated from X-ray diffraction powder data: a_0=7.89, c_0=9.01.

d A	I/I_1	hkl	d A	I/I_1	hkl
4.49	3	002	1.550	20	510
3.50	100	112	1.526	2	511
3.26	50	211	1.495	1	006+
2.96	80	022	1.467	10	520+
2.77	90	212	1.413	1	206+
2.48	40	310	1.395	8	440+
2.40	20	311	1.356	1	530
2.37	2	222	1.318	2	523+
2.26	20	004	1.239	5	326
2.19	1	320+	1.194	10	406
2.12	1	321			
1.97	1	400+			
1.92	50	313+			
1.90	50	214			
1.87	<1	411			
1.81	2	402			
1.77	40	323+			
1.73	10	421			
1.68	20	314			
1.62	20	413			

ii/ Fracture surface examinations

Optical and scanning electron microscopy have been used to trace the crack propagation paths on fracture surfaces. The NS 311 and KS 311 fracture surfaces consist of areas of exposed tinplate and sections of remaining lacquer with distinct boundaries. River markings are visible on the edges of the lacquer showing that the crack has run away from the tinplate and had therefore been initiated within the sample between the lacquer and the tinplate and not at the circumference as is the case for a simple adherend-adhesive butt-joint (Gent 1974). Similar markings are visible on the BS 311 and BS 300 specimens with the addition of thin lacquer layers which extend from the sections of remaining lacquer and on which are further fracture marks. The thick lacquer sections left on BS fracture surfaces exhibit different morphologies from those on KS 311 and NS 311; in the latter the lacquer edges are steep but on BS fracture surfaces the edges of thick lacquer areas have a shallower gradient which sometimes progress into the thin lacquer areas. Within the thin lacquer film are approximately circular areas of exposed tinplate referred to earlier as "lacquer-free zones" and at the centre of each of these zones is an angular defect where the $FeSn_2$ layer is exposed through the tin. Interpretation of the fracture markings in the thin lacquer film indicates crack propagation radially outwards from several of the lacquer-free zones, but since simultaneous multiple initiation is extremely unlikely these features are probably secondary initiations triggered by an approaching crack front. Evidence for this is seen in the interaction of fracture marks from the lacquer-free zones with stick-slip marks indicative of an approximately linear crack front having moved through the sample. No single primary initiation point could be located on the fracture

surfaces owing to the complexity of the fracture marks but it is possible that one lacquer-free zone or central defect was responsible, producing a main fracture which then triggered secondary initiation at several points across the sample. As Weibull analysis points to the same initiation mechanism for all samples the angular $FeSn_2$ defects become prime candidates as initiation sites since they are found on all tinplate types including 300 and unpassivated and no other surface feature such as surface roughness or oxide thickness has been found to be common to all samples. The origin of the angular defects is unclear; they are different in appearance to those areas where the tin coating has been consumed during flow-brightening to leave large (e.g. $500\mu m^2$) areas of the alloy layer protruding through the tin. They are not found on non-flow-brightened tinplate and may result from dewetting when the tin coating is molten or from existing gaps in the tin in which case the straight sides of the defect would be low energy crystal faces. Corrosion is also seen to produce angular etch pits in tinplate so further work on the cause of these defects would be very worthwhile.

KS 311 and NS 311 tinplates did not exhibit the thin lacquer layer and lacquer-free zones but on the BS samples where they were observed it could not be definitely determined whether they had been present in the sample before testing or whether they had been produced during the test. Optical microscopy could find no evidence of such small debonded areas before testing or within the remaining tinplate-lacquer interface on the fracture surfaces.

The $FeSn_2$ defects may introduce stress-concentrating cracks by air-entrapment during the lacquering process or may cause debonding of the lacquer (or weaken the interface) during storage by the production of corrosion products. If the latter mechanism occurred

there would be a variation in failure load due to storage time and lacquer-free zones would vary in size with time. The former effect has been observed (Horiguchi et al 1984, Takano and Watanabe 1980) but has been attributed to changes in the passivation layer. The latter effect has not been observed here with BS 311 tinplates where the duration between lacquering and testing has been varied from 5 days to over 1 year. No corrosion products are visible in the lacquer-free zones and the results of this work therefore suggest that corrosion debonding from the central $FeSn_2$ defects does not significantly affect fracture initiation and that they probably result from debonding during the test, possibly by sub-critical crack growth. The direction of crack propagation can be deduced from the fracture markings on the failed surfaces and XPS reveals a major distinction between the fracture of BS 311 tinplates and the NS 311 and KS 311 tinplates. When the exposed tinplate areas on the fracture surfaces are examined it is seen that the passivation layer has been left intact on BS specimens. Tests with an organosol lacquer containing pvc show that XPS could detect the chlorine in the lacquer on visually bare areas of tinplate on fracture surfaces, indicating that the fracture has run through the lacquer but very close to the passivation layer surface. Since XPS derives its information from large (several mm^2) areas it is not possible to say whether this very thin lacquer layer was present over the entire fracture surface.

The passivation layer was totally removed from those areas where tinplate was visible on NS 311 and KS 311 fracture surfaces. The crack propagation path is therefore quite different between BS 311 and the other 311 types and shows that the bonding between the passivation layer and the tinplate is stronger in the former set. Microscopy of fracture surfaces showed that the fracture path is

usually complex, moving from one interface to another within the bonded system and sometimes running cohesively within the lacquer. However, a propagating crack will presumably move along the weakest path available and since initiation is at a point between the lacquer and the tinplate (probably the $FeSn_2$ defects or lacquer-free zones) the initial crack is well placed to allow propagation along the interfaces of interest (i.e. the lacquer-passivation layer interface and tinplate-passivation layer interface) and enable areas of weak bonding within these interfaces to fail. Interfacial failure is observed in the case of the NS 311 and KS 311 samples.

iii/ Correlation of lacquer adhesion performance with sample structure

Defect controlled initiation has been linked with the $FeSn_2$ defects or lacquer-free zones seen on the fracture surfaces from the butt-joint tests. Fracture mechanics provides a means of assessing the effect of flaws on strength and may be applied to this case to compare measured defect dimensions with the actual failure strength of the samples.

The energy-balance approach of Griffith (1920) and Orowan (1948) was developed for a sharp crack of length a in a continuum:

$$\sigma_f = \sqrt{\frac{GE}{a}} \qquad (1)$$

where σ_f is failure stress, G is strain energy release per unit length and E is Young's modulus.

Here, fracture occurs when energy is released (from the applied stress) by crack growth and is sufficient to allow creation of new surfaces. The energy released comes from the stored elastic energy in the stressed specimen. For materials which behave in a perfectly elastic manner up to fracture the energy required to create new surfaces is just the thermodynamic work of adhesion, W_A. In most materials, however, further energy is required since processes such as plastic and visco-

elastic deformations take place. The quantity G combines the thermodynamic work of adhesion and other effects to characterize the total energy required to form two new surfaces. The measurements of G are usually made with specially designed test pieces into which known defects are introduced. The blister test provides one way and this and other methods are discussed by Kinloch (1982).

Considering a lacquered tinplate specimen with strong bonding at all interfaces and with initiating defects in the tin coating, the initial crack induces a stress field in the material ahead of the crack tip. Subsequent propagation will proceed along the path with lowest available fracture energy, G, or the path requiring the lowest force (Gent and Petrich 1969) and since the passivation layer is very thin both of its interfaces may be regarded as experiencing identical stress conditions. Good (1972) has shown that minima in G can occur at interfaces with weak bonding and that minima very near interfaces can result when there is strong bonding between materials with dissimilar values of G and E. Thus, where strong bonding exists there will be preferred regions of low fracture energy which are close to an interface and which may have been mistaken for weak boundary layer failure in earlier works. In this work, the BS samples show that fracture has taken place (for areas where the tinplate is visible on the fracture surfaces) within the lacquer but close to the passivation layer. According to this work of Good, true interfacial failure is only likely when interfacial bonding is weak but may run very close to the interface when there is strong bonding. Thin lacquer layers are found on the BS samples, sometimes only by using XPS due to their thinness and need not indicate weak bonding between the lacquer and the passivation layer. Fracture paths have been identified using XPS to reveal the differences in behaviour between BS and KS 311 and

NS 311 samples. Since the spatial resolution of XPS is poor the exact path taken in fracture cannot be determined and may jump from one interface to another in some areas. However, as both sides of the fractured samples have been examined any such deviations are small since no chromium at all was detected on the KS 311 and NS 311 tin-plate surfaces after fracture not on the lacquer-side stub from BS 311 failures.

When fracture mechanics are employed to study adhesive joints (Gent 1974, Kinlock and Shaw 1981, Andrews and Kinloch 1973a,b) the situation is complicated by the laminar structure of the joints; equation 1 was developed for infinite bulk solids and effects of thin layers on G and E must be considered. As shown theoretically by Good (1972) and by experimental work (Andrews and Kinloch 1973a,b) the fracture energy of interfaces cannot always be directly obtained from values of G for the bulk materials. The values of E are also affected since a propagating crack draws energy from a volume of material around the crack tip (Gruntfest 1963) which may be of the order of 1μm (Irwin 1967). The dimensions of this zone in this work are probably greater than the thcikness of the passivation layer which can store little elastic energy due to its size. The effective value of E for the passivation layer will therefore be a weighted mean of the moduli of the lacquer and tinplate and the elastic stress field will encompass regions of the tinplate, passivation layer and lacquer.

Table 3 shows calculated fracture stresses, using values of G and E from the literature. Measured failure stresses are in the range 2 to 28MNm^{-2} and it can be seen that in no case will a 1μm defect (typical of the angular $ReSn_2$ defects) produce failure at these stresses. Defects of radius 100μm do however initiate failure at levels approaching the observed range in bulk polymer, bulk glass

TABLE 3

CALCULATED FRACTURE STRESSES FOR

1μm and 100μm RADIUS DEFECTS

Material	$E(Nm^{-2}x)10^9)$	$G(Sm^{-2})$	$\sigma_f(1\mu m).(MNm^{-2}).\sigma_f(100\mu m)$	
Epoxy	3.86	136	720	72
Glass/metal interface	70	2.9	450	45
Al_2O_3	350	20	2600	260
Glass	69	3.7	500	50
Rubber-(rigid polymer) interface	2	2-180	60-600	6-60

References

Wyatt and Dew-Hughes 1974

Becher et al 1977

Bascom et al 1975

Andrews and Kinloch 1973a

(taken as a model for the passivation layer) and at rigid polymer-rubber and glass-metal interfaces. Good (1972) has shown theoretically that G may be reduced near a bonded interface and Andrews and Kinloch (1973a,b), in an experimental study, show that G can be reduced by up to an order of magnitude from values for bulk adhesive to values for failure in joints. Hence, the fracture energies for joints are likely to be reduced from bulk values and subsequently cause a reduction in failure stress. If this is assumed to occur the calculated fracture stresses for 100μm defects are decreased and fall within the range of the experimental values. In all cases it appears that a 100μm defect is more likely to be the cause of fracture initiation and forces the conclusion that the lacquer-free zones seen on BS fracture surfaces are produced by subcritical debonding during the test until one reaches ctitical size. Similar zones may grow on KS 311 and NS 311 specimens but since crack propagation runs beneath the passivation layer they are not present on the fracture surface after testing. Since all the lacquer-free zones are approximately circular, there is further evidence that they are subcritical grows since the stress state within the sample during loading but before failure would encourage radial growth from a defect. Debonding by the central $FeSn_2$ defect in the absence of the lacquer-free zone would be more likely to leave the defect at the edge of a debonded area.

Although no single primary initiation site could be located on the fracture surfaces it is assumed that one of the lacquer-free zones is responsible, producing a propagating crack which then triggers the other zones as secondary initiations. A slightly different explanation may also be proposed whereby the elastic stress wave released by the initiation travels through the sample ahead of the

crack tip and initiates failure in the other partially-debonded zones. The maximum velocity of a crack running through a polymer is approximately one third the speed of sound in the polymer (Gent and Marteny 1982) and as the elastic wave travels at the speed of sound it would reach other incipient cracks before the main crack front.

In the KS 311 and NS 311 samples it is the passivation layer-tinplate interface which is of interest. Some workers have claimed that such failures have occurred in a layer of tin oxide below the passivation layer (Horiguchi et al 1984, Servais et al 1979). In this work, tin oxide was removed by the passivation film from the NS 311 and KS 311 samples and the oxide later detected by XPS on the tinplate can easily be explained by oxidation of the tin in the time between failure and examination as tests have shown. The amount of tin oxide detected on the underside of the passivation layer after fracture is consistent with the amounts measured before failure and no evidence has been found for thick oxide growth during stoving as suggested by Servais et al (1979). Interfacial failure in NS 311 and KS 311 samples at the tinplate-passivation layer interface is therefore considered the most likely mechanism of failure in these samples and the thermodynamic work of adhesion at the interface becomes important in controlling this behaviour. The fracture energy, even in the case of interfacial failure, is usually found to be much larger than W_A because the propagating crack must draw energy from the material around the crack tip and this will probably include the passivation layer, the tin and the lacquer which will be viscoelastically deformed. In the BS tinplates, the failure is probably cohesive within the lacquer and it is the properties of the lacquer which mainly determine the fracture energy, G. The structure and composition of the passi vation layer play no direct part in the fracture process and lacquer

adhesion performance here (except to say that the interfacial bonding in these samples is higher than the cohesive strength of the lacquer).

The results of XPS and TEM examinations may now be correlated with lacquer adhesion performance. Surface topography of the passivation film is clearly visible in the TEM specimens; no whiskers or pores are present which would be likely to affect adhesion by producing dewetted areas or interlocking surfaces. Passivation layer topography does not, therefore, play a major role in adhesion in this work.

Since it is the passivation layer-tinplate interface which determines the different adhesion performances of the tinplates the chemical nature of these interfaces must be examined. Differences are noted in the type of tin oxides, chromium oxides and distribution of Cr^0.

Takano and Watanabe (1980) have associated tinplates on which certain tin oxides grow with different lacquer adhesion properties. Namely, growth of orthorhombic SmO indicates tinplates with good lacquer adhesion and growth of tetragonal SnO or SnO_2 indicates poor adhesion properties. These workers did not report where failure occurred in their samples.

In this work, tetragonal SnO_2 is found only on the NS 311/KS 311 tinplates whereas mixed valence oxides were found on NS 311 and KS 311 samples. Hexavalent chromium was found only on KS 311 and one BS 311 sample which, although possessing poor lacquer adhesion as measured by the Scotch Tape test, did not fail beneath the passivation layer.

Strong interfacial bonding between the tinplate and passivation layer is associated with higher levels of total chromium (18%) on BS 311 compared with 10% on KS 311 and NS 311. All had similar relative levels of Cr^0:CrO_x (0.4:1). Low levels of metallic chromium

are associated with poor peel strength by Takano and Watanabe (1980) but total chromium was found by them to be inversely proportional to peel strength. In this work, both high levels of Cr^0 and CrO_x are associated with the BS 311, but the 300 tinplate possesses no Cr^0 and low levels of oxidised chromium and yet still behaves like BS 311. Thus, there is no clear correlation between chromium content and lacquer adhesion which can be used to describe both 300 and 311 tinplates.

It is not possible to attribute causal connections between passivation layer structure and adhesion but correlations may be made. Table 4 lists these correlations for tin oxides, chromium oxides and chromium metal concentrations. It may not be these components, per se, but the factors present before, during or after passivation which influence the adhesion performance. Metallic chromium and tin oxide are almost certainly in contact with the tin surface whilst present in the passivation layer and the other components may also be touching the metal in places. It is unlikely that the different oxides will have greatly different surface energies sufficient to vary W_A and affect the adhesion as observed. It will be valuable for future work to attempt to separate the effects of the different components by a carefully controlled passivating treatment in which specific passivation layer compositions may be formed. The passivation process requires further study to explain the final structure of the surface layer on tinplate; unpassivated tinplate contains an amorphous or microcrystalline coat of tin oxides and diffracting oxides of orthorhombic and tertrgonal SnO and tetragonal and cubic SnO_2. From butt-joint tests, its behaviour is similar to the BS 311 but it contains no chromium at all and the tetragonal SnO_2 otherwise linked with weak bonding. The removal of some or all of these oxides during passivation should be verified.

TABLE 4

CORRELATION OF PASSIVATION LAYER COMPOSITION

WITH PASSIVATION LAYER-TINPLATE INTERFACE STRENGTH

FOR BS 311 TINPLATES

	Weak	Strong
	(NS311/KS311)	(BS311)
SnO_x	SnO_2 tetragonal	SnO (orthorhombic) $Sn_6O_4(OH)_4$ SnO_2 (cubic) $5SnO.2H_2O$
	(SnO tetragonal)	
CrO_x	Cr_3O_4 Cr_5O_{12} (Cr^{6+})	CrO_2
Cr^0	10% areal coverage	18% areal coverage

3 Conclusions

i. Passivation Layers

The use of XPS and TEM has allowed a comprehensive study of tinplate passivation layers on a number of different tinplates. Models for the passivation layers on 311 tinplates and 300 tinplates have been derived.

The 311 passivation layer consists of a weakly-diffracting microcrystalline layered structure containing metallic, oxidised and hydrated oxidised chromium with oxides of tin. Larger diffracting crystals are also found. The diffracting tin oxides are likely to have been formed after passivation, probably by exposure to air but the large chromium oxide and chromium metal crystals must have been formed during the passivation treatment. The passivation layers on all 311 type tinplates are similar in appearance but differ in the composition of the large (diffracting) crystals of chromium oxides and tin oxides. Differences are also seen in the total amount of chromium in the layers.

In the 300 tinplates the passivation layers contain no metallic chromium and only 2% oxidised chromium compared with the BS 311, KS 311 and NS 311 tinplates which possess 18%, 12% and 11% total chromium respectively.

The structural models proposed are similar in some respects to earlier models proposed elsewhere but offer a more complete description than had been available. In particular, chromium oxides other than Cr_2O_3 have been found which have not been reported before. Mixed valence oxides such as Cr_5O_{12} and Cr_3O_4 can account for the Cr^{6+} signal sometimes seen in XPS which had earlier been identified as CrO_3, an oxide which is soluble in water and unlikely to persist on tinplate surfaces.

ii. Fracture Behaviour

In fracture, distinct differences are seen between two categories of 311 tinplates. The first category (BS 311) fails so that the passivation layer is retained totally on the tinplate surface. On the areas of apparently bare tinplate in the fracture surfaces there is a very thin lacquer layer indicating cohesive failure within the lacquer and showing that the interfacial bonding in these samples is greater than the tensile strength of the lacquer. The second category of tinplates, including NS 311 and KS 311, lose their passivation layers when the fracture propagates at the tinplate-passivation layer interface.

These modes of crack propagation distinguish tinplate lacquer adhesion properties. Tinplates which fail below the passivation layer due to weak interfacial bonding are likely to be less suitable for can manufacture than those with strong bonding and which fail cohesively in the lacquer.

Fracture initiation is an independent mechanism dependent upon a defect distribution within the samples which is common to all tinplate types. Specific flaws have been identified as initiators, namely the angular $FeSn_2$ defects in the tin coating whose origins are unknown. Subcritical debonding from these defects during the test is likely until one reaches a critical size, propagates and then triggers the others as secondary initiation sites.

Certain components of the passivation layer can be correlated with the fracture behaviour and for good bonding at the interface in BS 311 tinplates these are orthorhombic SnO, cubic SnO_2, $Sn_6O_4(OH)_4$, $5SnO.2H_2O$, CrO_2 and high (18%) total chromium. For weak bonding in NS 311 and KS 311, SnO_2 (tetragonal), $Cr_3O_4$and Cr_5O_{12} are found with low (10%) total chromium coverage. Type 300 tinplates also

appear to behave like BS 311 and contain orthorhombic SnO and cubic SnO_2.

In the butt-joint test the tinplates which retain their passivation layers can be distinguished by examining the data. In general, they tend to show lower areas of exposed tinplate on their fracture surfaces but are more easily discerned on a plot of failure load vs. percent lacquer removal (the latter determined by visual inspection). BS 311 and BS 300 tinplates show a strong positive relationship between the two parameters such that the "area debonding factor" (percent lacquer removal/failure load in kN) is generally low (< 25) with small standard deviations. Weibull plots of the butt-joint data enabled the initiating defect population distribution to be decribed from graphs of failure load. The use of Weibull plots allows predictions to be made about the behaviour of sample sets and clearly shows differences in behaviour despite wide variations in both failure load and lacquer removal.

The adhesion of lacquers to tinplate has been shown to be a functior of both defects within the sample and the intrinsic adhesion of the interfaces.

FUTURE WORK

In the work presented above several commercial tinplates have been investigated and their passivation layer structure related to lacquer adhesion performance as measured in the butt-joint test. The experimental work was unable to impose conditions on the passivation process or on the production of the tinplate. Further useful studies could be made by following a particular batch of tinplate through its manufacturing stages and analysing samples at each stage so that the origins of the angular defects in the tin coating could be found. This approach would also enable adhesion tests to be made along the way and would measure the change of adhesion associated with natural ageing of the passivation layer.

An extra refinement would be to produce a series of passivated surfaces under controlled laboratory conditions on both tinplate and pure tin sheet, the latter free of surface defects. The effects of surface defects on initiation and the passivation layer on interfacial bonding and crack propagation could then be clearly discriminated. Fracture tests should be performed in ultra-high vacuum conditions and immediately examined by XPS, preferably with a monochromated X-ray source for greater resolution. UHV will prevent oxidation of tin before chemical analysis and will solve the problem of whether tin oxide layers grow beneath the lacquer during stoving or are air-grown after fracture.

Other technical improvements to XPS which would be valuable are the incorporation of a raster-scanning Ar ion gun for uniform etching rates across the specimen surface and a scanning XPS analysis to provide spatial distribution information.

The butt-joint test has proved useful in identifying defect distributions responsible for failure initiation via Weibull analysis

and has allowed loci of failure to be determined. A different type of mechanical test, more closely matching the mode of failure found in can manufacture could next be used and results compared. One such test is the deep-drawing of scored lacquered tinplates.

In summary, then, useful developments and experiments for the continuation of this work would be:

1. Improvements in experimental techniques

   i/ controlled manufacture of passivated tinplate

   ii/ controlled passivation of tin and tinplate surfaces

   iii/ UHV fracture and immediate analysis

   iv/ monochromated X-ray source in XPS

   v/ scanning Ar ion source for etching

   vi/ scanning X-ray source in XPS.

2. Further experiments

   i/ butt-joint tests of passivated smooth tin surfaces (no surface defects)

   ii/ comparison of butt-joint and deep-drawing tests to show applicability of the above results to can-forming applications

   iii/ high-resolution TEM investigation of the microcrystalline portions of passivation films

   iv/ laboratory production of passivated tinplate surfaces for adhesion tests. Variations in passivation time and applied negative potential would alter the amount and type of chromium deposited and the possible effect on adhesion due to chromium could then be separated from effects due to tin oxides.

   v/ investigation of tin oxide growth on tinplates - both in acqueous and atmospheric environments.

Bibliography

Albu-Yaron A. and Smith D.A. Br. Corr. J. 14 (1979) 133.

Albu-Yaron A. and Smith D.A. Proc. 2nd Int. Tinplate Conf. ITRI, London (1980) 256.

Albu-Yaron A. and Grovenor C.R.M. Proc. 3rd Int. Tinplate Conf. ITRI, London (1984) No. 35.

Andrews E.H. and Kinloch A.J. Proc. R. Soc. Lond. A332 (1973) 385a.

Andrews E.H. and Kinloch A.J. Proc. R. Soc. Lond. A332 (1973) 401b.

Andrews E.H. J. Mater. Sci. 11 (1976) 2004.

Aubrun Ph.J. and Rocquet P. J. Electrochem. Soc. 122 (1975) 861.

Aubrun Ph. and Pennera G.A. Proc. 1st Int. Tinplate Conf. ITRI, London, (1976) 295.

Azzeri N. and Splendorini L. Imballagio 292 (1980) 65.

Azzeri N. Splendorini L., Barristoni C. and Paparazzo E. Surf. Techn. 15 (1982) 255.

Bascom W.D., Timmons C.O. and Jones R.L. J. Mater. Sci 10 (1975) 1037.

Becher P.F. and Newell W.L. J. Mater. Sci. 12 (1977) 90.

Becker J.J. J. Electeochem Soc. 117 (1970) 1211.

Bikerman J.J. J. Coll. Sci. 2 (1947) 163.

Bikerman J.J. "The Science of Adhesive Joints" 2nd ed., Academic Press, New York (1968).

Boggs, W.E., Kachik R.H. and Pellissier G.E. J. Electrochem. Soc. 108 No. 1 (1961) 6 a.

Boggs W.E., Trozzo P.S. and Pellissier G.E. J. Electrochem. Soc. 108 No. 1 (1961) 13 b.

Britton S.C. and Bright K. Metallurgica 56 (1957) 336.

Britton S.C. Br. Corr. J. 10 (1975) 85 a.

Britton S.C. "Tin versus Corrosion" ITRI (London) publication No. 310 (1975) b.

Carter P.R. J. Electrochem. Soc. 108 (1961) 782.

Cherry B.W. and el Muddarris J. Adhes. 2 (1970) 42.

Coad J., Mott B., Harden G. and Walpole J. Br. Corr. J. 11 (1976) 219.

Corten H.T. in "Fracture - An Advanced Treatise" 7 ed. H. Liebowitz Academic Press, London (1972).

Briggs D. and Seah M.P. "Practical Surface Analysis by Auger and X-ray electron Spectroscopy" Wiley, New York (1983).

Dahlquist C.A. ASTM Spec. Techn. Publ. No. 360 (1964) 46.

Finch G.I. in "Oxidation of Metals and Alloys" ed. O. Kubaschewski and B.E. Hopkins, Butterworths, London, (1953) 55.

Gent A.N. and Petrich R.P. Proc. R. Soc. Lond. A310 (1969) 433.

Gent A.N. and Kinloch A.J. J. Polym. Sci. A2 9 (1971) 659.

Gent A.N. J. Polym. Sci. A2 6 (1974) 283.

Gent A.N. and Marteny P. J. Mater. Sci. 17 (1982) 2955.

Griffith A.A. Phil. Trans. R. Soc. London 221 (1920) 163.

Gruntfest I.J. in "Fracture in Solids" eds. D.C. Crucker and J.J. Gilman, Interscience, New York, (1963).

Good, R.J. J. Adhesion 4 (1972) 133.

Gulbransen E.A. and Hickman J.W. Trans. Amer. Inst. Min. (Metall.) Engrs. 171 (1947) 306.

Horiguchi M., Kurokawa W. and Matsubaguyashi H. Proc. 3rd Int. Tinplate Conf. ITRI, London (1984) No. 29.

Irwin G.R. in "Treatise on Adhesion" ed. R.L. Patrick, Marcel Decker, New York (1967).

Kinloch A.J. J. Adhesion 10 (1979) 193.

Kinloch A.J. J. Mater. Sci. 17 (1982) 617.

Kinloch A.J. and Shaw S.J. in "Developments in Adhesives - 2" ed. A.J. Kinloch, Applied Science, London (1981).

Leroy V., Servais J.P., Habraken L., Belgium C.R.M., Lempereur J. and Cockerill S. Proc. 1st Int. Tinplate Conf. ITRI, London (1976) 399.

Maeda S., Asai T. and Sawairi T. Proc. 2nd Int. Tinplate Conf. ITRI, London (1980) No. 25.

Mecholsky J.J., Freimam S.W. and Rice R.W. J. Mater. Sci. 11 (1976) 1310.

Nagel Soepenberg E., Vriburg H.G. and Spruyt A.C. Proc. 1st Int. Tinplate Conf. ITRI, London (1976) 282.

Okada H. and Yamamoto K. Electrochem. Techn. 6 (1968) 389.

Orowan E. Trans. Inst. Eng. and Shipbuilders, Scotland, 165 (1945).

Pourbaix M. "Atlas of Electrochemical Equilibria in Acqueous Solutions" Pergamon, Oxford (1966).

Rao, C.N.R., Sanna D.D., Vazudevan S. and Hegde M.S. Proc. R. Soc. London A367 (1979) 239.

Rauch S.E. and Steinbicker R.N. J. Electrochem. Soc. 120 (1973) 735.

Rocquet P. and Aubrun Ph. Corrosion-Traitments 16 (1968) 229.

Saijo K., Yoshioka O. and Oyama T. Tech. Rep. Toyo Kahan Co. Ltd. 23 (1976) 17.

Servais J.P., Lempereur J., Renard L. and Leroy V. Br. Corr. J. 14 No. 3 (1979) 126.

Takano H. and Watanabe T. Proc. 2nd Int. Tinplate Conf., ITRI, London (1980) 422.

Tsutsumi T., Ikemoto I., Namikawa T. and Kuroda H. Bull. Chem. Soc. Jpn. 54 (1981) 913.

Vagramyan A.T. and Usachev D.N. Zhur. Fiz. Khim. 32 (1958) 1900.

Wyatt O.H. and Dew-Hughes D. "Metals Ceramics and Polymers" C.U.P., Cambridge (1974).